Second Preliminary Report of African Studies

(Earth Sciences 2)

March 1977

Association for African Studies, Nagoya University
c/o Department of Earth Sciences, Faculty of Science,
Nagoya University, Chikusa, Nagoya 464, JAPAN

Second Preliminary Report

Editor: Kanenori Suwa March 1977

Association for African Studies, Nagoya University
c/o Department of Earth Sciences
Faculty of Science
Nagoya University

The Preliminary Reports of African Studies are printed and distributed privately by the Association for African Studies, Nagoya University.
The papers printed in the Preliminary Reports are generally résumés, while the publication of the full texts is left to the respective authors' choice.
Any reference to this report in a formal list should read:
2nd Prelim. Rep. Afr. Studies, Nagoya Univ.

Contents

The Preliminary Report of African Studies

Introduction

This report covers work done in Africa from the Association for African Studies, Nagoya University and some related work done from the Department of Earth Sciences, Nagoya University during the periods 1975 and 1976.

During the periods 1975 and 1976, some geologists of Nagoya University have performed continuously their field surveys in East Africa as follows.

1975 --- K. Suwa, T. Nureki, Y. Saka, K. Yairi, Y. Yusa (Kenya and Malawi)
1975·1976 -- M.Fujita, S.Miyazaki(Kenya)
1976·1977 -- H.Inoue(Keyna)

In this report, Dr. Suwa discussed the geological and petrological situations of three groups of Precambrian anorthosites and described their characteristic petrographical features. Dr. Nureki and his co-workers surveyed Machakos area and discussed tectonic evolution of the Mozambique belt.

Mr.Yairi discussed fault pattern of the Eastern Rift of Tanzania and lake-floor topography of Lake Malawi in relation to rift-faulting. He also discussed post-Karroo rift-faulting in northern Malawi with Dr. Saka. Dr. Saka surveyed and discussed Karroo System in Livingstonia and Karonga districts of northern Malawi mainly with Mr. Yairi.

Dr. Suwa described and discussed chromian phlogopite found from the Bushveld anorthosite layer and did also contact metamorphic rocks at the north-eastern Bushveld contact aureole with Mr. Suzuki. Dr. Miyakawa described granitoid gneiss of Machakos area with Dr. Suwa. Dr. Aoki described and discussed peridotite nodules from Samburu district with Dr. Suwa. Mr. Fujita surveyed northern half area of the Yatta Plateau and found some interesting evidences. Dr. Shiida described phonolite at the summit of Uhuru Peak, Mt. Kilimanjaro with Mr. Hoshino. Mr. Miyazaki described and discussed vermiculite-like mineral found from Machakos area.

Dr. Ito and his co-workers performed palaeomagnetic studies on Precambrian and Cretaceous kimberlites in South Africa.

Field works were much facilitated by the Office of the President, Kenya; the Mines and Geological Department, Ministry of Natural Resources, Kenya; the Department of Geology, University of Nairobi, Kenya; the Geological Survey Department, Ministry of Agriculture and Natural Resources, Malawi; and the Department of Surveys of the Malawi Government. To all of them I express my sincere thanks for the most esteemed and invaluable assistance.

These works were supported mainly by the grant-in-aid for Scientific Research of the Ministry of Education, Science and Culture of Japanese Government and by the Japan Society for the Promotion of Science, for which I would like to record my sincere thanks.

This report has been edited by Dr. Kanenori Suwa.

ISAO MATSUZAWA
Director
March, 1977

Precambrian Anorthosites and their plagioclases

(Abstract, 1977)

Kanenori SUWA

Department of Earth Sciences, Faculty of Science, Nagoya University

Introduction

Precambrian anorthosites can be divided into three varieties: Group I Bushveld type, Group II Adirondack type, and Group III Fiskenaesset type anorthosites. The emplacement of Precambrian anorthosites may be divided into four periods: 3,500±200 m.y. (Group Ⅲ), 2,200±300 m.y. (Group I), 1,500±300 m.y. (Group Ⅱ), and 1,200±200 m.y. (Group I).

Their plagioclases have respective petrographical characteristics exhibiting their different petrogeneses. In addition to chemical and X-ray properties, the twinning patterns and petrofabrics of plagioclases are examined to clarify their petrogeneses. The petrofabric diagrams for plagioclases on their a-, b- and c-axes can be produced.

Group I anorthosite occurs as layers within stratified intrusions developed under stable cratogenic conditions. The composition of the plagioclase is governed by its position in the sequence and is from labradorite to bytownite. Composition plane (010) is developed subparallel to the cumulate plane in adcumulate layers, whereas it is subperpendicular in heteradcumulate layers. Plagioclase grains are twinned after the albite-Carlsbad, Carlsbad, pericline, and albite laws. First two laws reach 43%. Textural and twinning patterns indicate the igneous origin of this anorthosite.

Group II anorthosite occurs as large independent intrusion with domed roofs. Two major events are recognized for the textural appearance of this anorthosite body. The first is igneous crystallization and a liquid of anorthositic composition has been generated from basic material near the boundary between lower crust and upper mantle. The composition of the plagioclase is governed by the P, T condition of crystallization and is from andesine to labradorite. The second event is deformation and metamorphism. This anorthosite may be reactivated body mobilized partially during the later orogenic cycle to form structure similar to mantled gneiss dome. Initial protoclastic texture is replaced by porphyroclastic texture and in turn emerges as equigranular granoblastic texture. In granoblastic anorthosite, plagioclase grains are mainly twinned after the albite and pericline laws, and petrofabrics of c-axis and composition plane (010) show some regularity.

Group III anorthosite forms layered stratiform sheets occurring as conformable layers in granitic gneiss of the oldest Archaean craton. In this anorthosite, the plagioclase is remarkably calcic, ranging from An 80 to An 96. Textural appearance of plagioclases is considered to be originally similar to that of plagioclases in Group I anorthosite, but at present it is similar to that of Group II anothosite as a result of regional metamorphism and recrystallization. The pericline law is predominant and reaches 64% and this twinning pattern clearly differs from that of Group I and II anorthosites.

2nd Prelim. Rep. Afr. Studies, Nagoya Univ., 3-12, 1977.

Examination of Plagioclase

A. Twinning having the composition plane (010)

Twinning laws having composition plane (010) are albite-, Carlsbad-, albite-Carlsbad-, Ala B-, and albite-Ala B laws.

On the basis of optical data of low- and high- temperature plagioclases, the devised optical method of determining the twinning law having the composition plane (010) was proposed and many diagrams necessary for the determination of the twinning laws were constructed in previous paper (Suwa *et al.*, 1974).

The experimental procedures necessary for the determination of twinning laws, petrofabrics of a- and c-axes consist in measuring the extinction angle, X′∧ trace of (010), in the zone perpendicular to (010) in adjoining twinning lamellae, and recording the variation in the extinction angles. Plagioclase twinned after the albite law produces symmetrical extinction angles, whereas plagioclase twinned after other laws gives rise to asymmetrical extinction angles.

Plagioclases of Group I, II and III anorthosites are of low-temperature form of An 75, 55, and 90, respectively. The twinning laws having composition plane (010) and the orientations of the a- and c-axes can be easily determined in accordance with the procedure described in the paper to which reference has been made.

The principle and the practical examples were described in detail in a previous paper (Suwa *et al.*, 1974).

Up to now, so far as I know, petrofabric diagrams for plagioclase have been made only on the composition plane (010). The petrofabric diagrams for plagioclases on their

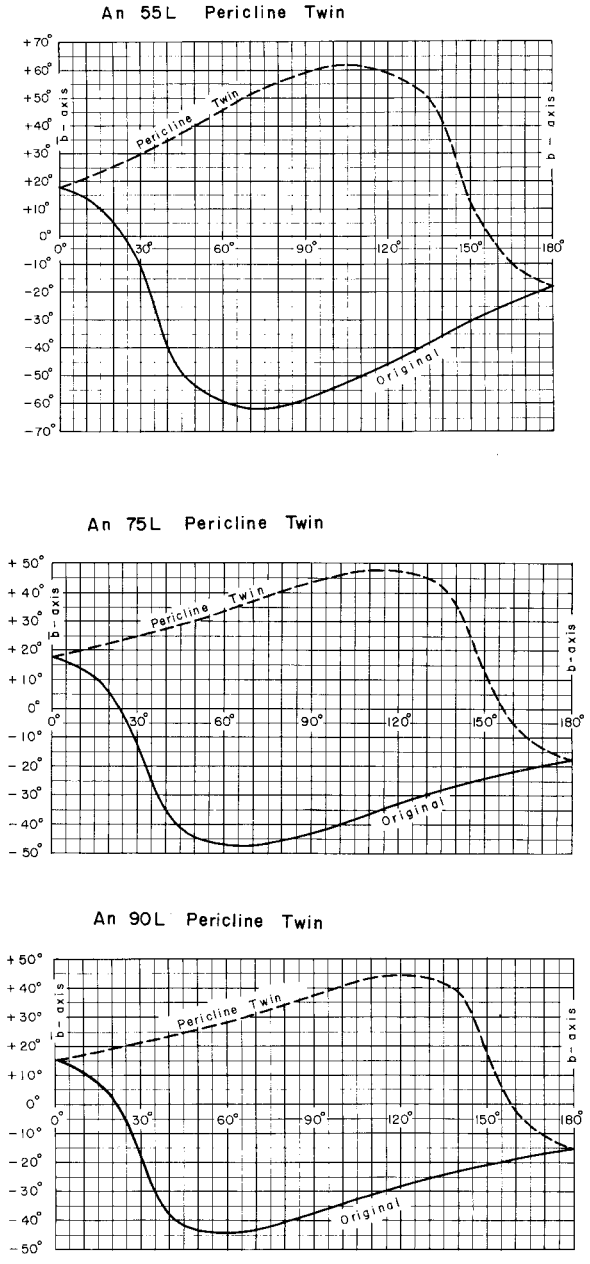

Fig. 1.
Variation curves of extinction angles, X′∧ trace of the rhombic section, in the zone perpendicular to the rhombic section in adjoining twinning lamellae in the low-temperature plagioclases (An 55, 75, and 90) twinned after the pericline law.

a- and c-axes can be produced as shown in Figs.5c and 5b.

B. Twinning having the rhombic section as composition plane

The position of the rhombic section differs appreciably from (001) for compositions near the end-members of the plagioclase group. For compositions of about 20–80% An the angle between both planes is less than 10°; at about 40% An both planes coincide.

When we rotate a plagioclase grain around an axis perpendicular to the rhombic section the extinction angle (δ) varies with the rotation angle θ. Fig. 1 shows the variation curves of extinction angles, X′/\ trace of the rhombic section, in the zone perpendicular to the rhombic section in adjoining pericline twinning lamellae for the low-temperature plagioclases An 55, 75, and 90. Fig. 1 can be produced by using of the revised crystallographic angles α, β, and γ for the low-temperature plagioclases.

Asymmetrical extinction angles are observed in the plagioclases twinned after the pericline law. The experimental procedure necessary for the determination of the b-axis consists in measuring the extinction angle in the zone perpendicular to the rhombic section in adjoining twinning lamellae, and recording the variation in the extinction angle. The orientation of the b-axis can be readily determined by using Fig. 1.

The petrofabric diagram for plagioclases on their b-axis also can be produced as shown in Fig. 5e.

Group I Anorthosite (Bushveld Complex)

As a typical example of Group I anorthosite, I investigated plagioclase grains from the Bushveld Complex, which is an intrusion in the Transvaal System dated at 2,050 m.y.

At Dwars River Bridge, Bushveld, anorthosite belonging to the upper part of the Critical Zone occurs as spectacular alternation of white anorthosite layers(plagioclase adcumulate layers) and black chromite-rich layers (chromite-plagioclase heteradcumulate layers). A sample shows the adcumulate layer to consist of bytownite with small amounts of clinopyroxene, orthopyroxene, chromite and chromian phlogopite, and the heteradcumulate layer to consist of bytownite and chromite with small amounts of clinopyroxene, orthopyroxene and chromian phlogopite (Specimen No. KS-70030818a). (Suwa, 1977b).

Zonal structure is found frequently in the plagioclase grains. The chemical composition of bytownite in the adcumulate layer determined by means of EPMA is An 74.3 (71.0–77.0), Ab 24.6 (22.0–27.6), Or 1.1 (0.6–1.4). The chemical composition of bytownite in the heteradcumulate layer varies considerably: the bytownite in narrow zone (0.005–0.02 mm in width) surrounding the chromite crystal is more calcic than the bytownite in other main parts. The bytownite in contact directly with chromite is of composition An 79.1 (75.1–86.8), Ab 20.6 (13.2–24.4), Or 0.3 (0.0–0.5), and the bytownite in main parts is of composition An 72.7 (69.2–79.2), Ab 26.8 (20.6–30.1), Or 0.5 (0.2–0.7). Chemical, X-ray, and optical data indicate that the bytownite in the adcumulate layers is of the low-temperature form.

Plagioclase grains in the adcumulate layers, so far observed, are twinned according to the albite-Carlsbad law (28/46 = 60.9%), pericline law (11/46 = 23.9%), and albite law (7/46 = 15.2%), and those in the heteradcumulate

layer are twinned according to the pericline law (20/53 = 37.7%), albite law (18/53 = 34.0%), albite-Carlsbad law (12/53 = 22.6%), and Carlsbad law (3/53 = 5.7%).

Fig. 2.
Group I Bushveld type anorthosite, Dwars River Bridge, Bushveld Complex (upper part of the Critical Zone). Specimen No. KS-70030818a. Thin-section prepared perpendicularly to the layering.

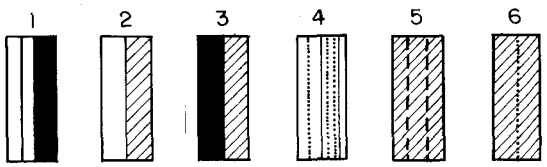

1 : albite twin

2 : Carlsbad twin

3 : albite-Carlsbad twin

4 : pericline twin

5 : albite twin

6 : pericline twin

Fig. 3.
Characteristic twinning laws in plagioclases of anorthosites.

Fig. 3 shows the patterns of characteristic twinning laws in the plagioclases of anorthosites. These patterns are used in Figs. 2, 4 and 6.

As shown in Fig. 2, plagioclase grains in the adcumulate layers are developed with their composition plane (010) subparallel to the cumulate plane, whereas those in the heteradcumulate layers are developed with their composition plane (010) subperpendicular to the cumulate plane. Grain sizes of the plagioclases in both layers are obviously different: plagioclase in the adcumulate layers is of 1–2 mm in length and that in the heteradcumulate layers is of 5–6 mm in length. The grain size of chromite in the heteradcumulate layers is 0.02–0.4 mm in diameter.

Group II Anorthosite (Quebec)

As a typical example of Group II anorthosite, I investigated plagioclase grains from the Quebec anorthosite.

Anorthosite at La Tuque, Quebec Province, Canada, shows beautiful equigranular aggregates of plagioclase grains indicating the recrystallization during emplacement of the anorthosite. The principal mineral of the anorthosite is labradorite with minor amounts of hornblende, biotite, and opaque minerals (Specimen No. KS-72081705).

The chemical composition of the labradorite determined by means of EPMA is An 55.0 (53.5–56.5), Ab 43.5 (42.0–44.5), Or 1.5 (1.0–2.0) and is considered to be homogeneous from the low value of the homogeneity index. Chemical, X-ray, and optical data indicate that the labradorite is of low-temperature form.

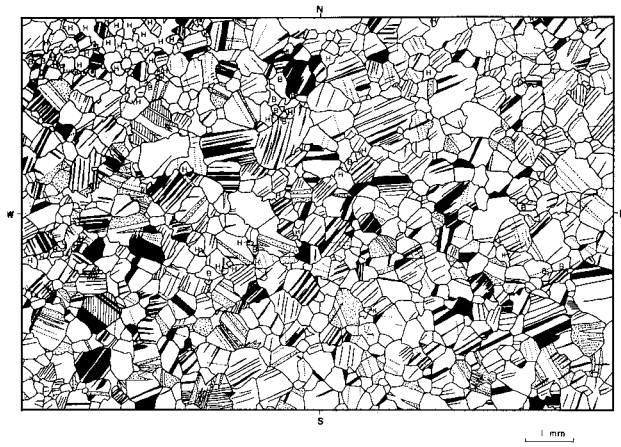

Fig. 4.
Group II Adirondack type anorthosite. La Tuque, Quebec Province, Canada. Specimen No. KS-72081705. Thin-section prepared in the horizontal plane at the outcrop.
Parallel arrangement of the composition plane (010) of the plagioclase grains is distinct and is shown also in Fig. 5a (N, north; S, south; E, east; W, west; B, biotite; H, hornblende).

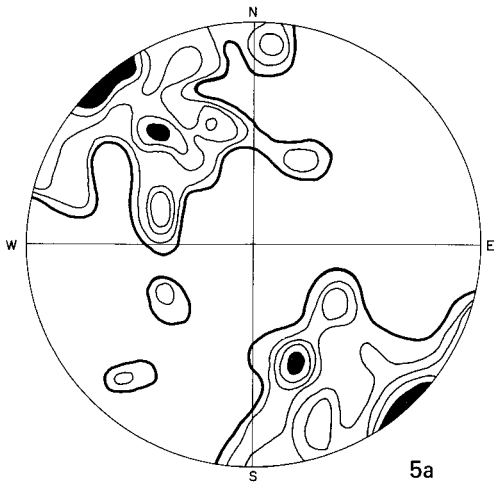

5a

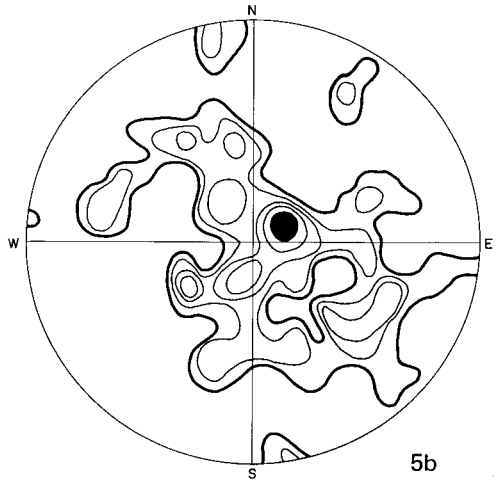

5b

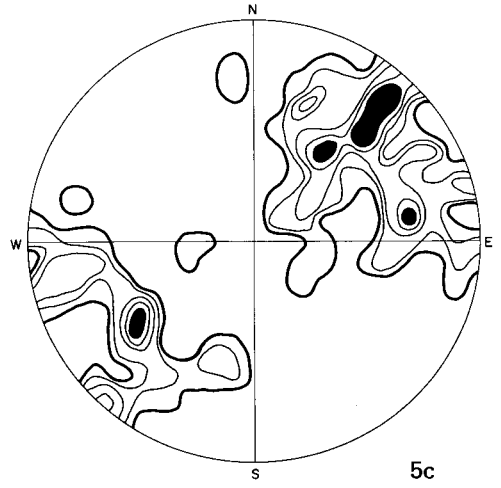

5c

Plagioclase grains in the anorthosite, so far observed, are polysynthetically twinned according to the albite law (132/204 = 64.7%) and the pericline law (70/204 = 34.3%) with rare amounts of the albite-Carlsbad law (1/204 = 0.5%) and the Carlsbad law (1/204 = 0.5%).

The thin-section examined was made in the horizontal plane of the outcrop. As shown in Figs. 4 and 5, plagioclase grains are developed with the composition plane (010) subparallel to the direction of N60°E on the horizontal plane, and the petrofabric pattern of the c-axis is nearly vertical to the horizontal plane.

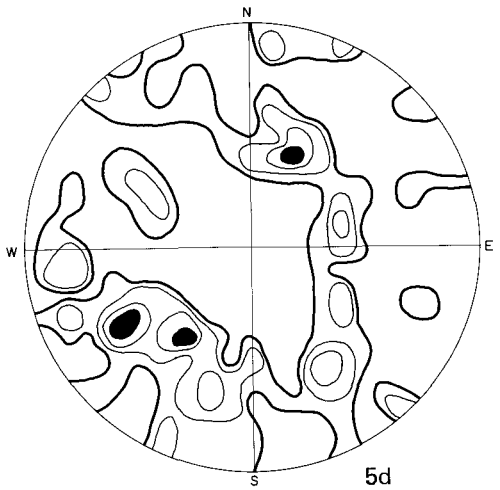

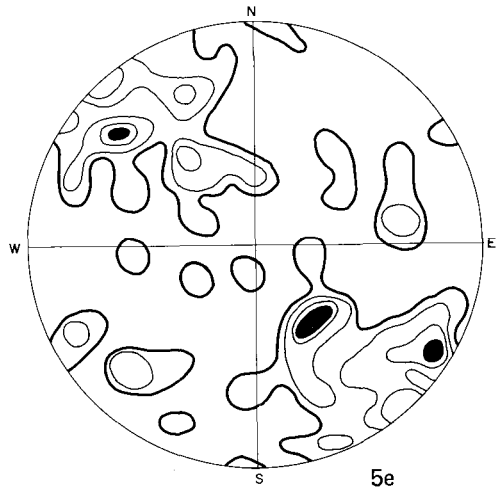

Fig. 5.

Stereographic projections relating to plagioclase of the Group II Adirondack type anorthosite. La Tuque, Quebec Province, Canada, Specimen No. KS-72081705.

5a. One hundred thirty four poles of (010). Contours: > 5-4-3-2-1%.

5b. One hundred thirty four c axes. Contours: > 5-4-3-2-1%.

5c. One hundred thirty four a axes. Contours: > 5-4-3-2-1%.

5d. Seventy poles of the rhombic section. Contours: > 5-4-2-1%.

5e. Seventy b axes. Contours: > 5-4-2-1%.

Group III Anorthosite (Fiskenaesset)

As a typical example of Group III anorthosite, I investigated plagioclase grains from the Fiskenaesset Complex, West Greenland.

Anorthosite examined is from Zone 6 of the Fiskenaesset Complex, in which Group III anorthosite forms extensive layered stratiform sheets with major units of anorthosite, amphibolite, peridotite, and chromitite occurring as conformable layers in granitic gneisses (Windley *et al.*, 1973). The principal mineral of the anorthosite is anorthite with small amounts of hornblende (Specimen No. GGU-132016).

The chemical composition of the plagioclase determined by means of EPMA is An 90.6, Ab 9.4, Or 0.0 (Windley and Smith, 1974). Chemical, X-ray, and optical data indicate that the anorthite is of low-temperature form.

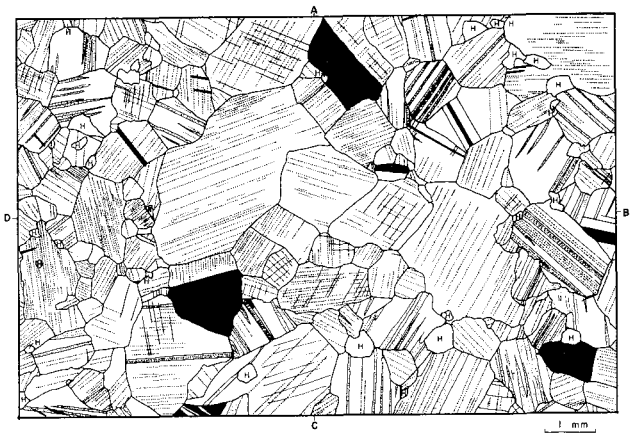

Fig. 6.

Group III Fiskenaesset type anorthosite. Zone 6 of the Fiskenaesset Complex, West Greenland. Specimen No. GGU-132016.

Plagioclase grains in the anorthosite, so far observed, are polysynthetically twinned, exclusively according to the pericline law (70/109 = 64.2%) and the albite law (39/109 = 35.8%). None is twinned after other laws. Whereas the pericline law may occur by itself, the albite law, however, is always found the combination with the pericline law.

To clarify the distinction between the pericline and acline laws, I constructed a diagram showing the variation curves of extinction angles, X'∧ trace of (001), in the zone perpendicular to (001) in adjoining acline twinning lamellae for low-temperature anorthite (An 90). No acline law, however, was found.

Discussion

A. Geological environment of emplacement of anorthosites

Group I Bushveld type anorthosite occurs as layers within stratified basic sheets and lopoliths, which are developed under stable cratogenic conditions. Anorthosite layers occur in the Critical, Main, and Upper Zones in the Bushveld Complex and in the Anorthosite Zone of the Stillwater Complex. No anorthosite layer occur in the lower zone consisting of ultramafic rocks.

There are two Precambrian events forming the basic igneous episodes of the cratons – an earlier episode dating at 2,200±300 m.y. and a later dating 1,200±200 m.y. The former examples are Scourie dyke, Nipissing diabase, Stillwater Complex, Great Dyke, Bushveld Complex and others, and the latter are Post-Jotnian diabases, Gardar dyke swarm, Keweenawan basalts, Duluth gabbro, Bukoban basalt and others. These episodes appear to coincide with periods during which orogenic activity was restricted as a result of widespread stabilization and extension of the cratons. Of considerable interest is the fact that the time of the basic igneous activity coincides with 'lows' in the histograms of isotopic ages of granitic and metamorphic rocks formed in mobile belts (Dearnley, 1966).

Group II Adirondack type anorthosite bodies are limited to Precambrian terrains and they take the form of large intrusions with domed roofs and may reach batholithic proportions. Post-emplacement deformation and metamorphism have occurred in many of the Group II anorthosites. Charnockites, syenites, monzonites, mangerites and iron-titanium oxide concentrations are associated with the Group II anorthosites. Isotope age dating on Group II anorthosites invariably confirms their Precambrian age of 1,500±300 m.y.

Recent studies of the Adirondack anorthosite and of some other masses in the Grenville province suggest that these are reactivated bodies which were partially mobilized during the Grenville cycle to form structures similar to mantled gneiss domes.

Group III anorthosite forms extensive layered stratiform sheets with major units of anorthosite, amphibolite, peridotite, and chromitite occurring as conformable layers in granitic gneisses. Group III calcic anorthosite occurs in the oldest parts of the Archaean craton and is noted for remarkable stratigraphic regularity and persistence along the strike for tens of kilometres. The early Archaean Group III anorthosite has suffered the orogenic effects of one or more periods of regional metamorphism and deformation, with the result that it now occurs as recrystallized tectonic pods and slices.

B. Texture of plagioclase grains of anorthosites

In Group I anorthosite, the composition of the plagioclase is strictly governed by its position in the sequence and the plagioclase is generally more calcic, ranging from labradorite to bytownite. Plagioclase grains in the adcumulate layers are developed with the composition plane (010) subparallel to the cumulate plane, whereas those in the heteradcumulate layers are developed with the composition plane (010) subperpendicular to the cumulate plane. In the adcumulate layers, plagioclase primocrystals crystallizing from the main liquid accumulate first on the cumulate plane and act as seeds for later crystal growth, in which process diffusion between the main and pore space liquids plays an important role, and the resultant crystals are 1–2 mm in length. In the heteradcumulate layers, after the crystallization of chromite, plagioclase begins to crystallize from the pore space liquid and develops to a larger crystals 5–6 mm in length, during this process supercooling may be playing a role.

In Group II anorthosite, the principal mineral is plagioclase ranging from An 35 to An 60. Group II anorthosite is distinguished from Group I anorthosite by its greater homogeneity of composition and very coarse-grained texture. Group II anorthosite becomes emplaced in the plutonic environment, and has been affected to varying degrees during successive deformation and metamorphism. Generation of a liquid of anorthositic composition, with water as an essential component, from basic material under high pressure and relatively moderate temperatures near the boundary between lower crust and upper mantle, has been experimentally confirmed.

Two major events have been recognized for the textural appearance of the Lac Rouvray anorthosite mass by Kehlenbeck (1972). The first is igneous crystallization which terminated with consolidation of the anorthosite mass from its magma. This was followed by the second event, the deformation and metamorphism of this igneous rock. Initial heterogeneity of plagioclase grain size in the protoclastic texture is replaced by a strong bimodal grain size distribution in the porphyroclastic and augen textures, which in turn emerges as nearly equigranular granoblastic texture in the gneissic meta-anorthosite.

The anorthosite at La Tuque, Quebec Province, shows beautiful equigranular aggregates of plagioclase grains indicating the recrystallization during emplacement of the anorthosite and it seems to have reached the final stage of deformation and metamorphism. Some regularities are recognized on the petrofabrics of c-axis and (010) plane.

In Group III anorthosite, the plagioclase is remarkably calcic with most samples lying in the range of An 80 to An 96. Textural appearance of plagioclases in Group III anorthosite is considered to be originally similar to that of plagioclases in Group I anorthosite, but at present that of plagioclases in Group III anorthosite is similar to that of plagioclases in Group II anorthosite as a result of regional metamorphism and recrystallization.

C. Twinning pattern of plagioclase grains of anorthosites

In the Group I anorthosite, plagioclase grains in the adcumulate layers are twinned after the albite-Carlsbad, pericline, and albite laws, and those in the heteradcumulate layers are twinned after the pericline, albite, albite-Carlsbad, and Carlsbad laws. Frequency percentage of the albite-Carlsbad and Carlsbad

laws in both layers reaches 43% in together. This twinning pattern of the plagioclases clearly indicates the igneous origin of the Complex and there is no sign of any metamorphic effect in the later periods (Suwa, 1975).

In the Group II anorthosite, plagioclase grains are polysynthetically twinned after the albite and pericline laws with rare amounts of the albite-Carlsbad and Carlsbad laws. Frequency percentage of the latter two laws reaches only 1% in together. The plagioclase grains twinned after the latter two laws are considered to be relict plagioclase grains from the igneous anorthosite. This twinning pattern of the plagioclases of Group II anorthosite clearly differs from that of Group I anorthosite. The Carlsbad and albite-Carlsbad laws predominate over the albite and pericline laws in the megacrysts from some samples. This twinning pattern obviously corresponds to the textural appearance of Group II anorthosite recognized by Kehlenbeck (1972).

In the Group III anorthosite, plagioclase grains are polysynthetically twinned, exclusively according to the pericline law and the combination of pericline and albite laws. The pericline law is predominant and reaches 64.2% and this twinning pattern clearly differs from that of Group I and II anorthosites.

The frequency percentages of the composition plane (010) in Group I, II, and III anorthosites are 69%, 66% and 36%, respectively.

Table 1 Frequency percentages of the composition plane (010) of plagioclase in various igneous and metamorphic rocks

	An 0-24	An 25-49	An 50-74	An 75-100
Group I anorthosite(1)			69	
Plutonic rocks(2)	91	77	73	
Volcanic rocks (phenocryst)(2)	80	77	80	83
Volcanic rocks (groundmass)(2)	100	91	94	89
Group II anorthosite(1)			66	
Group III anorthosite(1)				36
Granulite(3)		62	69	
Charnockite(4)		63	64	
Schist and gneiss(2)		75	75	33
Hornfels(2)		77	76	65
Paragneiss(5)		89		
Amphibolite(5)		88	87	73
Crystalline schist(6)	100			

(1) This Paper
(2) Gorai (1951)
(3) Suwa (1966)
(4) Naidu (1954)
(5) Suwa (1956)
(6) Tobi (1961)

Table 1 shows the frequency percentages of the composition plane (010) in various igneous and metamorphic rocks. In volcanic rocks, this frequency percentage is high and its variation with An % is very slight. In plutonic rocks and Group I anorthosite, the frequency percentage is higher and it decreases slightly with increase of An %. In Group II and III anorthosites, granulite, and charnockite, the frequency percentage is moderate and it decreases especially in calcic plagioclase.

As shown in Table 1, the frequency percentage of composition plane (010) is very low in calcic plagioclase in Group III anorthosite and metamorphic rocks. It seems reasonable that much pericline twinning results from mechanical deformation.

Acknowledgements—The rock samples from the Fiskenaesset Complex were sent by courtesy of the Geological Survey of Greenland and Dr. B.F. Windley of the University of Leicester, to whom I express my deep gratitude.

References

Dearnley, R. (1966) : Orogenic fold-belts and a hypothesis of earth evolution. In : L. H. Ahrens, F. Press, S. K. Runcorn, and H. C. Urey (Editors), *Physics and Chemistry of the Earth*, **7**, 1-114, Pergamon.

Gorai, M. (1951) : Petrological studies on plagioclase twins. *Am. Miner.*, **36**, 884-901.

Kehlenbeck, M. M. (1972) : Deformation textures in the Lac Rouvray anorthosite mass. *Canad. Jour. Earth Sci.*, **9**, 1087-1098.

Naidu, P. R. J. (1954) : Minerals of charnockites from India. *Schweiz. Miner. Petrog. Mitt.*, **34**, 203-280.

Suwa, K. (1956) : Plagioclase twinning in Ryoke metamorphic rocks from the Mitsue-mura area, Kii peninsula, central Japan. *Jour. Earth Sci. Nagoya Univ.*, 4, 91-122.

Suwa, K. (1966) : On plagioclases in metamorphic rocks from Lützow-Holmbukta area, East Antarctica. *Proc. Japan Acad.*, **42**, 1175-1180.

Suwa, K. (1975) : Plagioclases in anorthosites. *1st Prelim. Rep. Afr. Studies, Nagoya Univ.*, 55-59.

Suwa, K. (1977a) : Precambrian anorthosites and their plagioclases. *Precambrian Research*, **5** (in press).

Suwa, K. (1977b) : Chromian phlogopite in the Bushveld anorthosite, South Africa. *2nd Prelim. Rep. Afr. Studies, Nagoya Univ.*, 133-138.

Suwa, K., Mizutani, S. and Tsuzuki, Y. (1974) : Proposed optical method of determining the twinning laws of plagioclase. *Mem. Geol. Soc. Japan*, **11**, 167-250.

Tobi, A. C. (1961) : Pattern of plagioclase twinning as a significant rock property. *Proc. Koninkl. Nederl. Akad. van Wetenschap.*, **64**, ser. **B**, 576-581.

Windley, B. F., Herd, R. K. and Bowden, A. A. (1973) : The Fiskenaesset Complex, West Greenland, Part 1. *Grønlands Geol. Under Bull.*, **106**, 80pp.

Windley, B. F. and Smith, J. V. (1974) : The Fiskenaesset Complex, West Greenland, Part 2. *Grønlands Geol. Under. Bull.*, **108**, 54pp.

Tectonic Evolution of the Mozambique Belt in Area South-east of Machakos, Kenya

Terukazu NUREKI*, Kanenori SUWA**, Katsumi BIYAJIMA***,
Yukiyasu SAKA**** and Yasuhisa YUSA*****

* Department of Geological Science, College of Liberal Arts, Okayama University
** Department of Earth Sciences, Faculty of Science, Nagoya University
*** Idemitsu Oil Development Company
**** Institute of Earth Science, School of Education, Waseda University
***** Power Reactor and Nuclear Fuel Development Corporation

Introduction

The geology of the southern Machakos district in Kenya was first reported by B.H. BAKER in 1954, who studied mainly the Basement rocks in an extended area including the area now we concern. The geology of the north Machakos-Thika area was also studied and reported by Fairburn in 1963. Recently, Biyajima *et al.* (1975) and Biyajima studied the geology of an area around Mbooni Hill, where Biyajima (1976) was in charge of the petrography of the Precambrian basement rocks and especially of garnet mineralogy.

In 1975 we could work with the aim of knowing the structural details of the Basement rocks in the area bounded by the latitudes 1°30'S and 1°45'S and by the longitudes 37°20'E and 37°30'E. Mbooni (Tututha) Hill is located in the eastern half and Kalama Hill[1)] is located in the western half of the worked area.

After our geological survey we found that a conspicuous dome structure seems to be localized in the Mbooni Hill area, and such dome structure is not found in the Kalama Hill area. Drag folds, folds accompanied by the axial plane cleavage, complicated folds shown by felsic veins or boudins and so on are the characteristic structures in the Kalama Hill area.

Baker considered that Mbooni Hill is composed of granitized paragneisses and migmatites, which were deformed and metamorphosed by only one metamorphic event. His opinions were supported by Fairburn who studied the granitized paragneisses and migmatites in the north Machakos-Thika area. While, Biyajima *et al.* (1975) proposed that the granitoid gneisses in the Mbooni Hill area may correspond to "mantled gneiss dome" of Eskola (1948). Later, Biyajima (1976) modified his opinion because no positive evidence for a mantled gneiss dome can be found.

Their opinions appear to be partly correct but to be misleading in some points especially in interpreting the Mozambiquian metamorphism in the southern Machakos district. The metamorphic history of the district seems to be more complex than the pioneers have considered. In this preliminary report, we are going to take up some structural evidences to believe that at least two sequences of metamorphic events would be lapped over.

1) The name Kalama Hill is now used for convenience' sake to represent the mountain land just on the east-side of a road running from Makaveti to Iiuni, the southern-most part of Kalama Hill being named Iiuni Hill as shown in the Sheet 162/2 (Machakos) on scale of 1 : 50,000.

2nd Prelim. Rep. Afr. Studies, Nagoya Univ., 13-38, 1977.

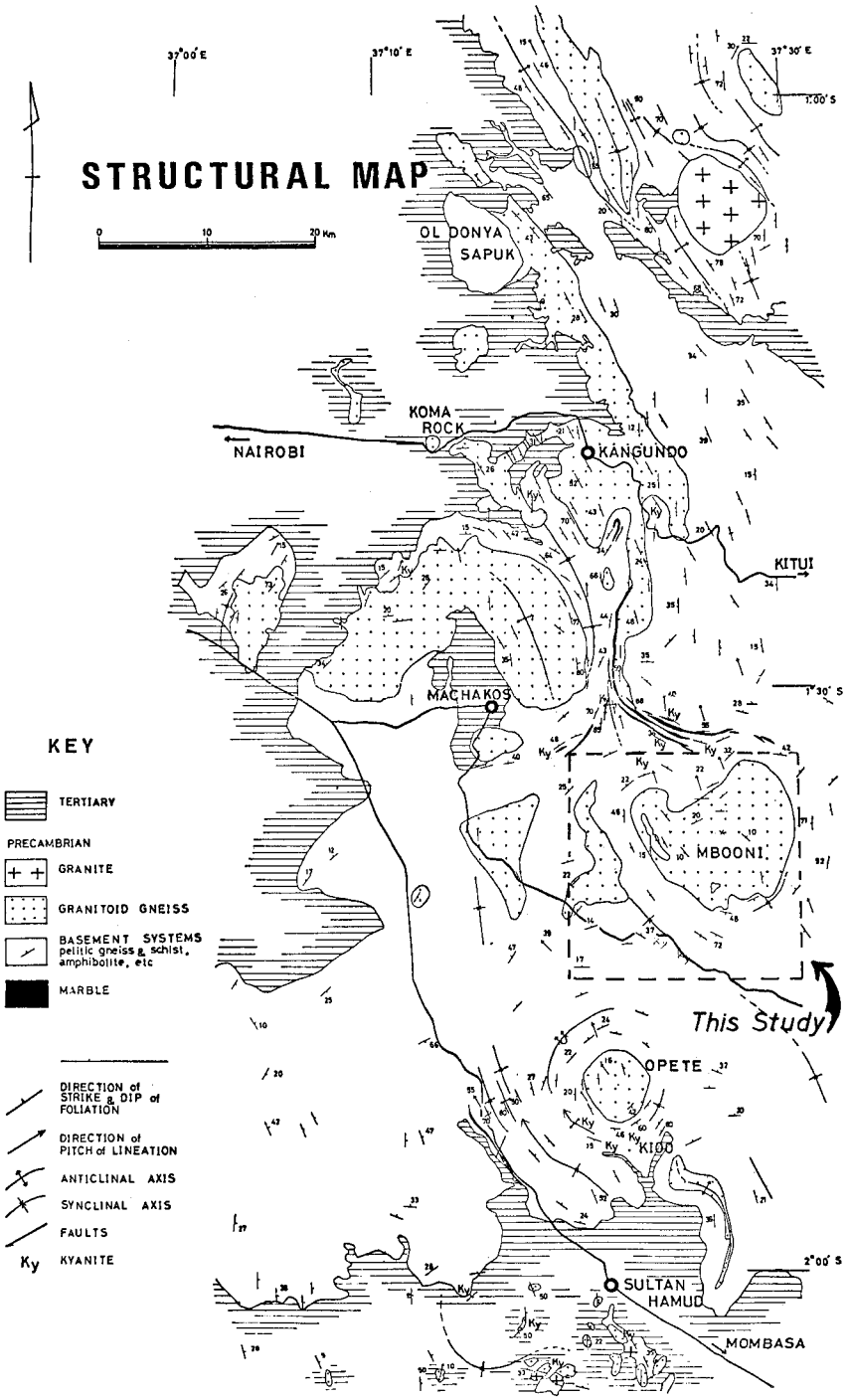

Fig. 1 Structural map of the southern Machakos district (after Biyajima *et. al.* 1975)

General geology

The area south-east of Machakos is occupied by the Precambrian rocks which are represented by paragneisses, granitoid gneisses and other metamorphosed intrusives. These rocks have been considered to be of Archaean age, but now they are considered to be of late Proterozoic.

1. *Precambrian rocks*

A greater part of the foliated paragneisses must be quartzo-feldspathic or psammitic rocks in origin. They have many petrographical characters of the granitoid gneisses, excepting faintly foliated nature of the latter. It is, however, not always possible to distinguish clearly the quartzo-feldspathic paragneisses from the granitoid gneisses, because there are many transitional rock types between the two groups. On the other hand, some of the clearly foliated gneisses are deduced to be orthogneisses which are igneous rocks in origin.

The petrography of all rocks has not been fully examined at present. For convenience the Precambrian basement rocks will be classified into the following headings:

Foliated rocks:

a. Psammitic gneisses (=highly quartzo-feldspathic gneisses):
two-mica gneiss and biotite gneiss; often accompanied by garnet.

b. Pelitic gneisses:
kyanite - staurolite - garnet - biotite gneiss, kyanite-staurolite-garnet-two mica gneiss, kyanite-garnet-two mica gneiss, two mica-garnet gneiss and muscovite-garnet gneiss; often aluminous.

c. Semi-pelitic gneisses (or orthogneisses of intermediate compositions):
biotite quartzo-feldspathic gneiss, hornblende-biotite quartzo-feldspathic gneiss and hornblende quartzo-feldspathic gneiss; rarely accompanied by garnet.

d. Granitoid gneisses (orthogneisses of acid compositions):
two-mica granitoid gneiss and muscovite granitoid gneiss; often accompanied by garnet.

e. Basic gneisses (orthogneisses of basic compositions):
hornblende-plagioclase gneiss, hornblende-biotite-plagioclase gneiss and biotite-plagioclase gneiss; often accompanied by garnet.

Faintly foliated rocks:

Granitoid gneisses (orthogneisses of acid compositions):
biotite granitoid gneiss; often accompanied by garnet.

Unfoliated rocks:

biotite granite, two-mica pegmatite, biotite-kyanite pegmatite and biotite aplite.

As itemized above, a larger amount of the foliated rocks is deduced to be stratified sedimentary rocks and others are perhaps to be igneous rocks in origin. The name "semi-pelite" was first used by Baker (1954). Among the foliated rocks, however, the semi-pelitic gneisses are fairly variable in petrographic characters and possibly in their origin. The senior of us considers that a great deal of the semi-pelitic gneisses is derived from igneous rocks of intermediate compositions. There are so many rock types in the studied area that, at least at the state of knowledge, it is difficult to decide the areal distributions of each gneiss. The names of gneisses which will be used in this report are:

Foliated rocks: psammitic gneisses, pelitic gneisses, semi-pelitic gneisses and basic gneisses.

Fairly foliated rock: granitoid gneiss.

Psammitic gneisses

They are commonly fine-grained and more clearly foliated than the granitoid gneiss. Thin seams rich in mafics are often traceable within a few centimetres. The felsic seams are variable in thickness and straightly extended in general. Some mafic seams show minor folds with or without the axial plane cleavage which is in many cases in parallel to the foliation of the psammitic gneisses.

There are two kinds of psammitic gneisses, one being the biotite gneiss and the other the two-mica gneiss. They are related in mode of occurrence but differ fairly in mineral assemblage from one another. The biotite gneiss is mainly composed of biotite, plagioclase, microcline and quartz, and it is often rich in calcite, sphene and ilmenite. Garnet is found as accessories. Plagioclase and microcline are equivalent in amount, or sometimes the former prevails than the latter. Sometimes leucocratic seams rich in calcite are included in the biotite gneiss. Ilmenite occurs commonly in the core of grains of sphene. The two-mica gneiss is composed of biotite, muscovite, plagioclase, microcline, quartz and often of garnet. Sphene and opaque minerals are not uncommon. Biotite is always larger in amount than muscovite, and microcline more prevails than plagioclase. Calcite is lacking in the two-mica gneiss.

Pelitic gneisses

In this report, kyanite-staurolite-garnet-biotite gneiss, kyanite-staurolite-garnet-two mica gneiss, kyanite-garnet-two mica gneiss, two mica-garnet gneiss and muscovite-garnet gneiss will be treated collectively under the name pelitic gneisses. They are characteristically rich in muscovite and totally grey-coloured. They are in general coarser than the psammitic gneisses. The pelitic gneisses are rather limited into a few localities in distribution (Fig. 2). The foliation surfaces are clearly traceable in many outcrops, but they are often folded and cleaved as the results of complicated folding.

Garnet rarely attains to a few centimetres in diameter. Under the microscope, staurolite, kyanite and quartz appear to coexist stably. All the pelitic gneisses are accompanied by garnet, biotite, plagioclase and quartz, though biotite is very variable in amount. Microcline is found in most pelitic gneisses.

Semi-pelitic gneisses

Biotite quartzo-feldspathic gneiss, hornblende-biotite quartzo-feldspathic gneiss and hornblende quartzo-feldspathic gneiss are included in this category, the hornblende-biotite quartzo-feldspathic gneiss being the most common of all. The semi-pelitic gneisses are commonly medium-grained. The foliated structure is not so distinct as compared with the psammitic and pelitic gneisses. In some exposures we can find folds on small to moderate scale, but in others not. Most of the semi-pelitic gneisses are deduced to be orthogneiss in appearance but some have an appearance of paragneisses.

Quartz is very common in all rock types. Under the microscope, they are lacking in muscovite and have much microcline which often prevails than plagioclase in amount. Sphene and opaque minerals are always found as accessories. Garnet can rarely be found.

Basic gneisses

Most of the basic gneisses are supposed to be intrusive rocks in origin; *i.e.*, they would possibly be sills which were sub-concordantly intruded into the stratified or foliated rocks. The foliated structure is characterized by parallel arrangement of such mafic minerals as hornblende and/or biotite. The basic gneisses are lacking in microcline and always accompanied by epidote and plagioclase. Quartz is found in small amount or perfectly lacking. Hornblede is the most common mafic mineral found to the naked eye, though the amount is varied by addition of biotite. Some of the basic gneisses seem to be totally composed of biotite to the naked eye. Garnet is often associated with hornblende in the hornblede-biotite-quartz-plagioclase gneiss. Actinolite-plagioclase-quartz-epidote gneiss rarely occurs.

Granitoid gneiss

Some of the granitoid gneisses are clearly foliated and found as just like a stratified bed in the column of the psammitic gneisses, but this type of the granitoid gneisses seems to be localized in occurrence. The granitoid gneiss with which we are going to concern in this report is a biotite granitoid gneiss and always shows a faintly foliated nature.

The granitoid gneiss is buff to dirty cream in colour, homogeneous and medium-grained. Biotite, microcline, plagioclase and quartz are the essential constituents of the granitoid gneiss. Muscovite is rather rare in amount. Garnet is often found, and hornblende and clinopyroxene are rarely contained. Small amounts of zircon, sphene, allanite and epidote are ubiquitous. The granitoid gneiss is sometimes accompanied by microcline-perthite and/or microcline-antiperthite which develop to a porphyroblastic crystal. Microcline and plagioclase are nearly equivalent in amount, but the former sometimes prevails. Plagioclase has often sodic rim. Myrmekite can be rarely found.

2. *Distribution and proposed stratigraphy of the gneisses*

In the area south-east of Machakos, the original rocks and their petrographic characters of the gneisses are so complicated that it is not easy to establish a reliable stratigraphy of them. It seems at a glance, however, to be an indisputable fact that most of the rock units are piled up "conformably" on another. We now intend to propose an example of the stratigraphy of gneisses in the area concerned.

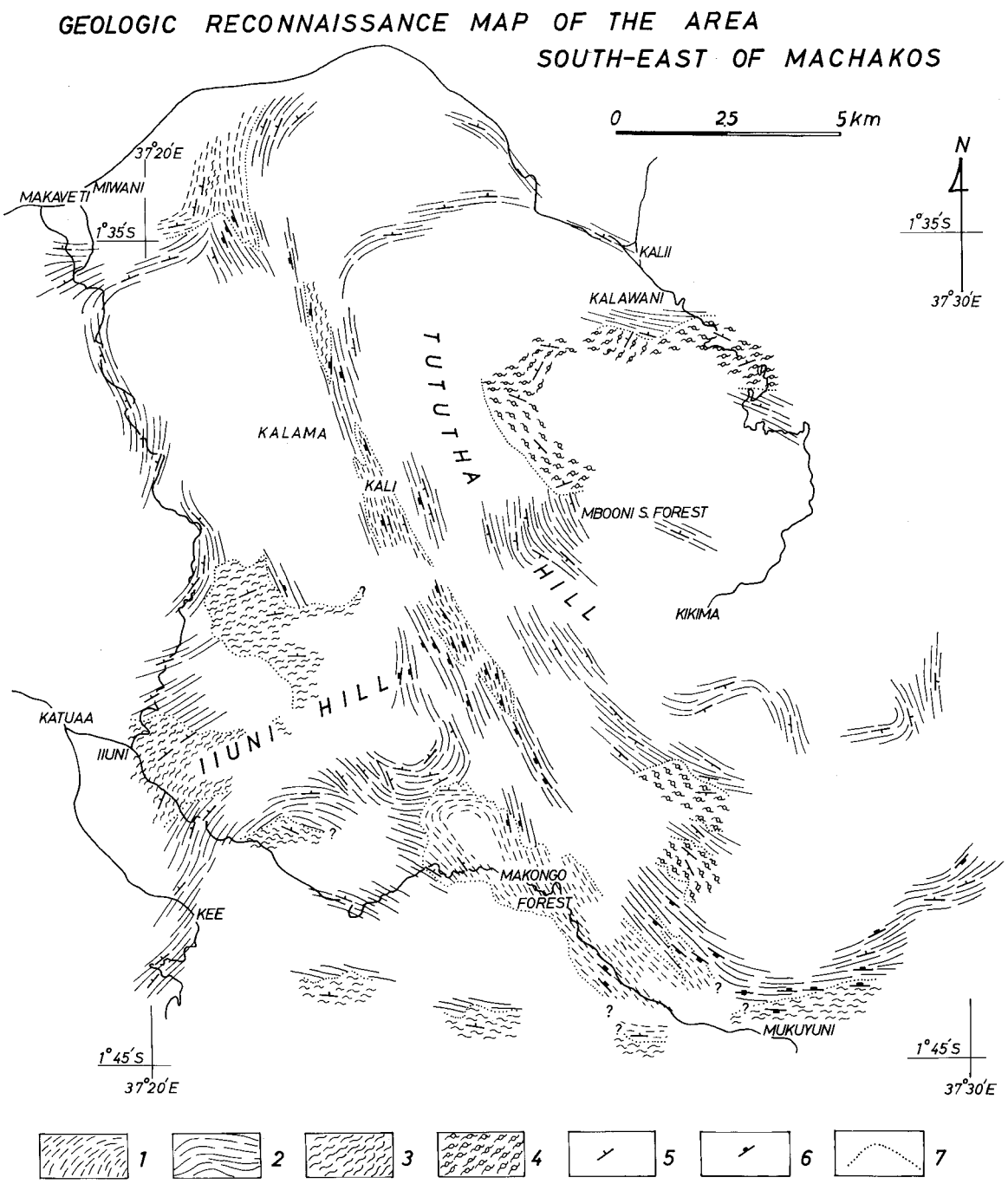

Fig. 2 Geologic reconnaissance map of the area south-east of Machakos. 1: pelitic gneisses, 2: psammitic gneisses, 3: semi-pelitic gneisses, 4: granitoid gneiss, 5: dip (at angles less than 40°) and strike of the foliation, 6: dip (at angles more than 40°) and strike of the foliation, 7: boundaries between the rock units. Each mark in 1—4 is arranged along the general (or deduced) trend of the foliation of gneisses.

The gneisses in the studied area are roughly divided into two stratigraphic formations; one is represented by the granitoid gneiss and the other by the psammitic gneisses. The semi-pelitic gneisses are subsequent in areal distribution.

The Mbooni Hill area is a type locality of the granitoid gneiss (Fig. 2). The upper stratigraphic formations which appear to be laid on the granitoid gneiss are represented by the psammitic gneisses and the pelitic gneisses. We can find another isolated horizon of the granitoid gneiss which is inserted into the psammitic gneisses at the southern part of the Mbooni Hill area.

At the lowland between Mbooni Hill and Kalama Hill, there has been found a horizon of the pelitic gneisses which are perhaps alternated with the psammitic gneisses. The basic gneisses have been often found to occur in or near the horizon of the pelitic gneisses. They are deduced to be subconcordant sheet-like bodies in origin.

The semi-pelitic gneisses prevail in the southern part, near the southern extreme, of the studied area (Fig.2). Another horizon of the semi-pelitic gneisses has been found to occur in the mountain land around Iiuni Hill which is the southern part of the Kalama Hill area. The semi-pelitic gneisses here are often intercalated by the psammitic gneisses. The basic gneisses also occur in or near the semi-pelitic gneisses.

The granitoid gneiss is considered to be orthogneiss, and the senior of us wants to emphasize that most of the semi-pelitic gneisses show in many cases some features which are deduced to be orthogneiss. But, structural as well as stratigraphic features appear, at least on scale of outcrops or of hand-specimens, to be in concordant with the other paragneisses.

The origin of the granitoid gneiss has been considered by some workers to be granitized psammitic gneisses as referred above. However, their opinions seem to be problematic. We would like to propose another origin of the granitoid gneiss by the following reasons. At the first, the last metamorphism would not be attained to such a high grade condition as that under which a granitic melt was produced. In fact, there is no migmatite in the studied area. At the second, the granitoid gneiss has many petrographic features as a layered intrusive mass in origin. At the third, quartz and pegmatite veins and basic dykes are actually lacking in the granitoid gneiss mass, while they are found to occur in many localities outside of the granitoid gneiss mass. These evidences may suggest an intrusive origin of the granitoid mass, which would be intruded into the surrounding gneisses after an emplacement of the basic dykes. The granitoid rock would have suffered a metamorphism later and transformed to the granitoid gneiss.

The psammitic gneisses in the Mbooni Hill area are extended to the Kalama Hill area beyond the lowland between the two Hill areas. In the Kalama Hill area, however, the next stratigraphic horizon lower than the psammitic gneisses is mainly occupied by the semi-pelitic gneisses, the fact being clearly shown at the south of the Kalama Hill area. Geological survey around Kalama Hill is now being done by Mr.Inoue and will be performed by the second of us and his colleagues in this 1977.

The senior of us considers as follows: if the semi-pelitic gneisses are sedimentary rocks in origin, it becomes difficult to explain the fact that the Mbooni Hill area is actually

GEOLOGICAL MAP OF THE MACHAKOS AREA

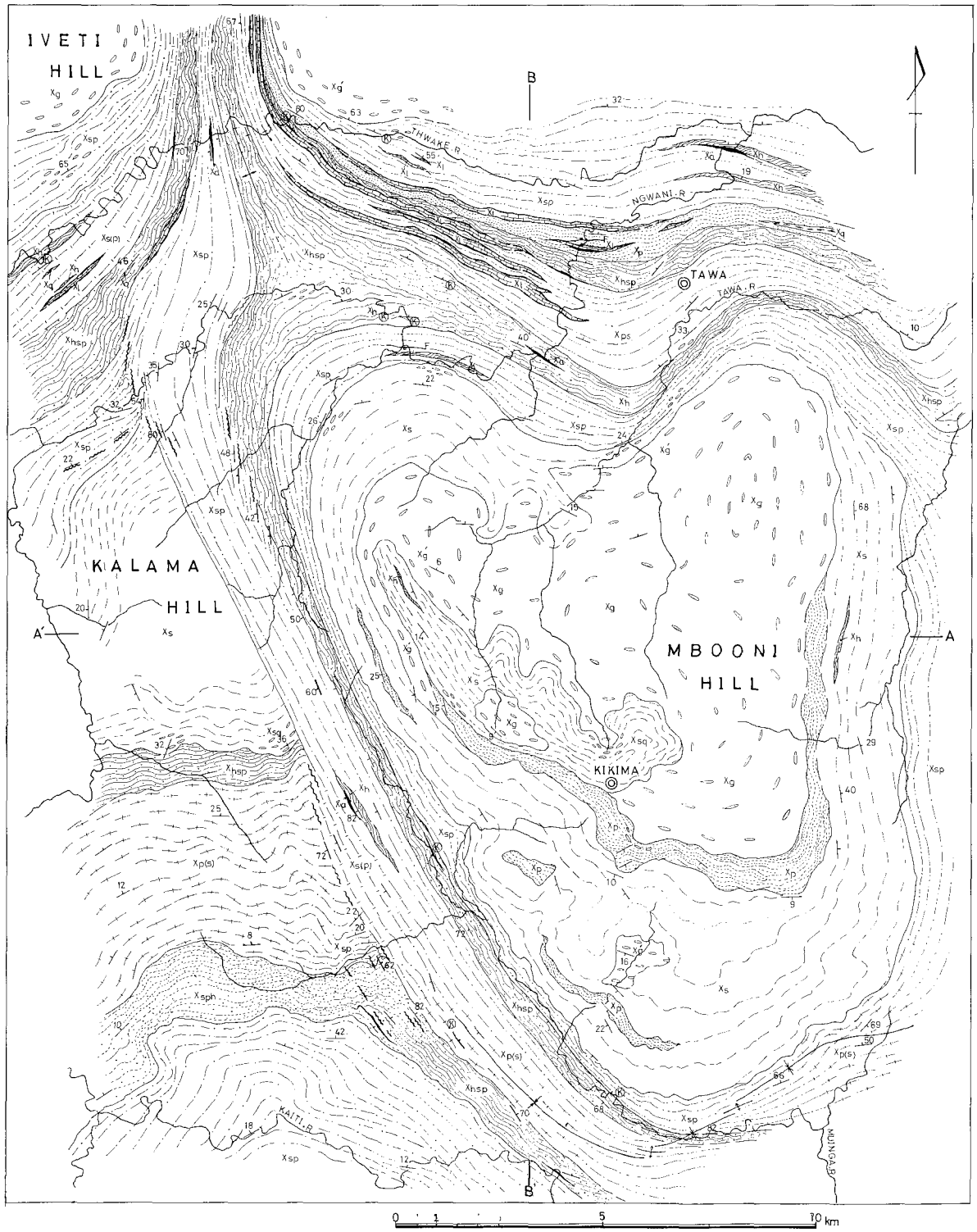

Fig.3A Geological map of the area south-east of Machakos compiled by Biyajima (1976)

KEY


X_g Granitoid gneiss

$X_{g'}$ Migmatitic gneiss


X_p Pelitic schist gneiss and Semi-pelitic gneiss


Migmatitic pelitic and semipeli tic gneiss


X_s Psammitic gneiss

X_{sq} Quartzofeldspathic gneiss


Migmatitic psammitic gneiss


X_h Hornblende gneiss


X_a Amphibolite


X_l Crystalline limestone


X_q Quartzite


X_{sp} Alternation of pelitic schist gneiss and psammitic gneiss in same amounts


$X_{p(s)}$ Ditto (Pelitic gneiss predominates)


$X_{s(p)}$ Ditto (Psammitic gneiss predominates)


X_{sph} Alternation of pelitic schist gneiss, psammitic gneiss with intercalated hornblende gneiss


X_{hsp} Hornblende gneiss with intercalated pelitic and psammitic gneiss


Geological boundary

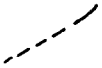
Geological boundary, inffered


Anticline


syncline


Fault


Strike and dip of foliation


Kyanite outcrops in pelitic gneiss

lacking in the semi-pelitic gneisses. If it is allowed to regard both the granitoid gneiss and the semi-pelitic gneisses as orthogneisses, the stratigraphy of gneisses in the studied area becomes fairly simple; that is, we have only one sedimentary formation which is mainly composed of psammitic rocks alternated with subordinate pelitic layers in origin. The senior of us believes that most of the semi-pelitic gneisses may not be sediments but layered intrusives in origin.

The total thickness of the Precambiran gneisses which are cropped out on the surface of the studied area would be more than 1500m but less than 2000m, including the granitoid gneiss and the semi-pelitic gneisses.

3. *Structures*

A simplified structural map of the southern Machakos district is shown in Fig. 1 which is characterized by several dome structures composed of granitoid gneisses. The studied area south-east of Machakos is represented by two domes to the north of the Opete dome.

The general trends of the foliation of gneisses in the studied area are shown in Fig. 2. As have been emphasized by Baker (1954) and Biyajima (1976), the gneisses around Mbooni Hill appear to form a gentle dome structure, as often represented by exfoliation pavements which are in parallel to the foliation of gneisses. Figs. 3A and B show the geological map and the geological profiles of the south-eastern part of the Machakos area complied by Biyajima (1976). At the northern margin of the Mbooni Hill area, the dome structure is clearly shown by the foliation of psammitic gneisses, but it is complicated within the granitoid gneiss at the central part. To the south of Mbooni Hill, however, the dome structure becomes complicated even in the psammitic gneisses.

Near the western and southern margins of the Mbooni Hill area, the foliation of gneisses becomes inclined at moderate to high angles as shown in Fig. 2, and here appears a zone of steeply dipping foliations. Fig. 4 shows the limits of the zone of steeply dipping foliations; the zone is now called by us "Kakalia-Mwea monocline". The monocline runs through the lowland between the two Hill areas.

Going westward over the Kakalia-Mwea monocline, the gneisses in the Kalama Hill area show gently folded structures which may not be a simple dome structure. The foliation of gneisses always inclines northward at low angles. The northern part of the Kalama Hill area appears to be a hemi-dome structure, but the central and southern parts of the Hill area include some gentle anticlines and synclines, they forming an anticlinorium. Thus the Kalama Hill area forms an anticlinorium but does not a dome.

In area along the Kaiti river, to the south of the Kalama Hill area, the foliation of the semi-pelitic gneisses and psammitic gneisses becomes to show a gentle anticline on a larger sclae than that found at Iiuni Hill; that is, the anticlinorium in the Kalama Hill area changes gradually into an anticline, leaving the axes of folds as they were. It is yet unknown whether the anticline may represent the northern wing of a dome or northern crested part of an anticline which has to be found in the area to the south of the studied area. We expect that the anticline may belong to the northern wing of the Opete dome which is already found by Baker (Fig. 1).

GEOLOGICAL PROFILE OF THE MACHAKOS AREA

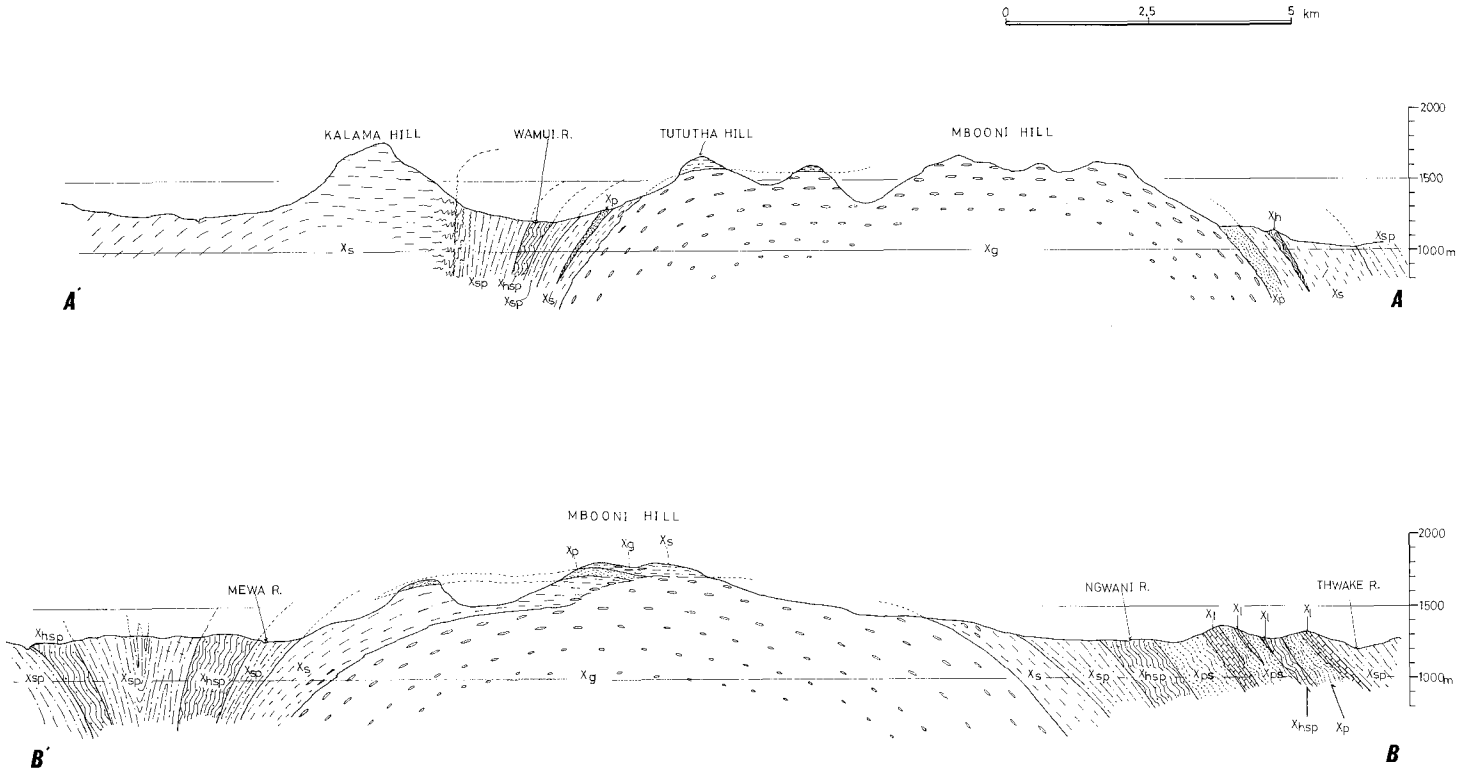

Fig.3B Geological profile of the area south-east of Machakos compiled by Biyajima (1976)

According to Fig. 1, the Kakalia-Mwea monocline is not a special structure which is localized only in the studied area but we have a few examples in the southern Machakos district. A similar structure in the area south-east of the Opete dome has been reported by Baker (1954) who called it the Masokani monocline, which has been traced by him more than 15km from Kioo to the south. Another example will be found at the east of Machakos where Fairburn (1963) has found a zone of steeply dipping foliations, though in his case he has interpreted the structure as a syncline accompanied by steeply closed wings.

It is conceived that the Kakalia-Mwea monocline is one of structural zones which would be locally developed between the antiform structures. These structures seem to be of very significant in the southern Machakos district.

Structural characters of the gneisses

As shown in a former paragraph, structures of the area south-east of Machakos are characterized by two antiforms and a zone of steeply dipping foliations, here called the Kakalia-Mwea monocline, which is placed between the two antiforms. In the antiform area, *i.e.* the Mbooni Hill area and the Kalama Hill area, the foliation of paragneisses is generally inclined at low angles, but the angles become gradually steeper, at more than 40 degrees, in the Kakalia-Mwea monocline.

In the Kalama Hill area and the Kakalia-Mwea monocline, folds on small scale which are accompanied by the axial plane cleavage are locally developed, some of the cleavage being inclined steeply but others being flat or inclined at low angles. The descriptions of the fold-structures will be followed in this paragraph.

1. *The folded area and the Kakalia-Mwea tectonic zone*

Boudinage and folds on every scale are often found to occur in the western half of the studied area. The scope of an area where such structural features have been found is shown in Fig. 4 under the name of "Folded area". The folded area encloses a larger part of the Kakalia-Mwea monocline and the Kalama Hill area. The eastern limit of the folded area runs mostly inside of the Kakalia-Mwea monocline, except the northern part of the studied area where the eastern limit goes outside the monocline (Fig. 4). The western limit of the folded area is more extended to the western outside of the studied area.

The Kakalia-Mwea monocline itself can be regarded as a fold-zone on a larger scale. The monocline is characterized by the foliation of gneisses which is inclined at angles higher than 40 degrees. Here, 40 degrees are only artificially given because the foliation is usually inclined at angles lower than 40 degrees in the studied area (Fig. 2). As shown in Fig. 4, the monocline is running roughly straight in NNW-SSE direction through the lowland between Mbooni (Tututha) Hill and Kalama Hill.

At the south of the Mbooni Hill area, however, the eastern limit of the Kakalia-Mwea monocline abruptly turns from NNW-SSE to ENE-WSW, as if it enclosed the Mbooni Hill area. Then, the monoclinal nature of the monocline disappears near the curve and gradually changes into a synclinal structure. Looking well at Fig. 4, the western limit of the monocline does not run straight, and at the southern extreme it seems to disappear after coming across an area of flat-lying foliations. Thus, the Kakalia-Mwea monocline seems to disappear at the southern ex-

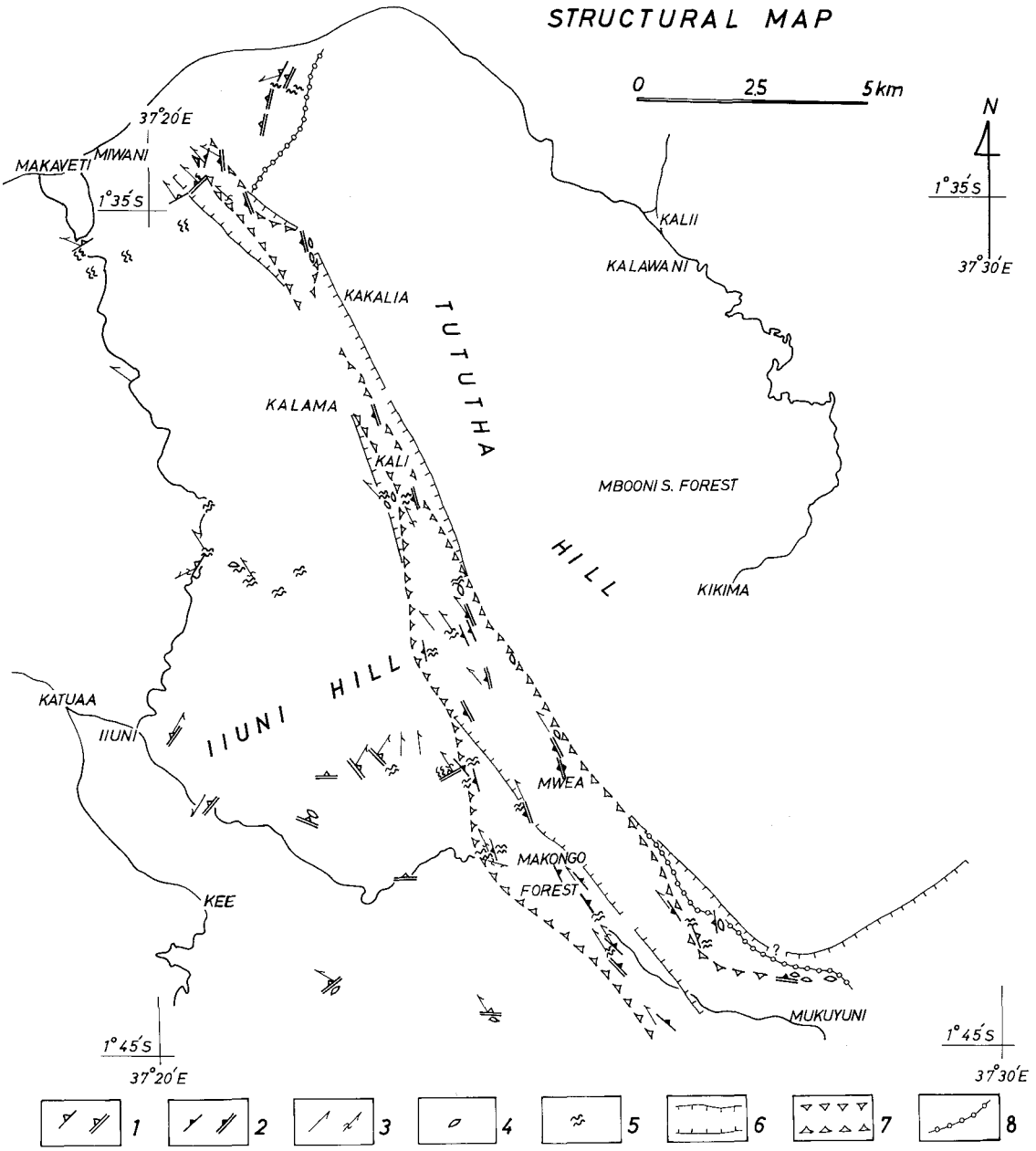

Fig. 4 Structural map of the area south-east of Machakos. 1: dip (at angles less than 40°) and strike of the axial plane cleavage. 2: dip (at angles more than 40°) and strike of the axial plane cleavage. In 1 and 2, the left-hand mark shows the cleavage not parallel to the foliation, and the right-hand mark shows that parallel to foliation, respectively. 3: lineation (left) and axes of folds (right), 4: locations for boudinage, 5: locations for fold-structure which is not accompanied by cleavage, 6: limits of the Kakalia-Mwea monocline, 7: limits of the zone of high angle cleavage, 8: eastern boundary of the folded area. The Kakalia-Mwea monocline and the zone of high angle cleavage are closely related to occur, here called as a whole "Kakalia-Mwea tectonic zone".

treme of the studied area. The northern extreme of the monocline must be extended outside the studied area.

Minor folds are found to occur in a lot of localities, most of them being accompanied by the axial plane cleavage. The axial plane cleavage develops often into shear-fractures, along which a short displacement is recognizable. The axial plane is in many localities in parallel or subparallel to the foliation of gneisses, but in the other localities it is cutting the foliation at high angles.

As shown in Fig. 4, there will be found a limited area where the axial plane of minor folds is usually inclined at angles more than 40 degrees. Again, 40 degrees are only artificially given by judging from the general inclinations of the axial plane of minor folds in the studied area. The limited area can be regarded as a structural zone which is called now "Zone of high angle cleavage".

Of course, the zone of high angle cleavage is included inside of the folded area. According to Fig. 4 the Kakalia-Mwea monocline and the zone of high angle cleavage occur closely to one another. The southern half of the Kakalia-Mwea monocline is enclosed in the zone of high angle cleavage, but conversely the northern half of the latter is enclosed in the former: it is conceived that the Kakalia-Mwea monocline and the zone of high angle cleavage form *en masse* a tectonic zone in the folded area. The tectonic zone is now called "Kakalia-Mwea tectonic zone".

Thus, the areal limits of the Kakalia-Mwea monocline, of the zone of high angle cleavage and of the folded area do not overlap strictly with each other, the fact being of significant for the origin of these variable structures and, accordingly, for the metamorphic history of the area south-east of Machakos.

2. *Boudinage*

In the folded area, there are a lot of exposures where the boudinage is often found. The boudins are found in every exposure where the gneisses, regardless of psammitic or pelitic, are intruded by quartz veins or pegmatite veins. These veins are commonly folded and torn into many boudins.

The gneisses which are accompanied by quartz and pegmatite veins have been called the migmatite by Baker (1954) and Fairburn (1963). Baker (p.10) had clearly shown some sketches of "boudins" as examples representing the migmatite. The gneisses which have been called "migmatite" by them have mineral assemblages of the middle grade now. Unfortunately, there have been found no relic mineral-assemblages which may suggest that the host gneisses would be ever melted in part or would attain to a physical condition of melting. The quartz and pegmatite boudins were perhaps originally "veins", and it is questionable to call them the migmatite.

Figs. 5A and B are sketches of folded quartz veins and boudins. The foliation of the psammitic gneisses, which is in parallel to the axial plane cleavage, is steeply inclined; that is, these boudins were found in the zone of high angle cleavage. They give some impression of ptygmatic veins. The axial plane of the relic folds is in parallel to the foliation surfaces. The quartz veins are clearly torn into boudins in which many cracks are cutting across the long edges of boudins. A displacement along the foliation must be deduced.

Typical boudins are found in Fig. 5C which is also found in the zone of high angle cleavage. This is an example of pegmatite boudins which are in general characterized

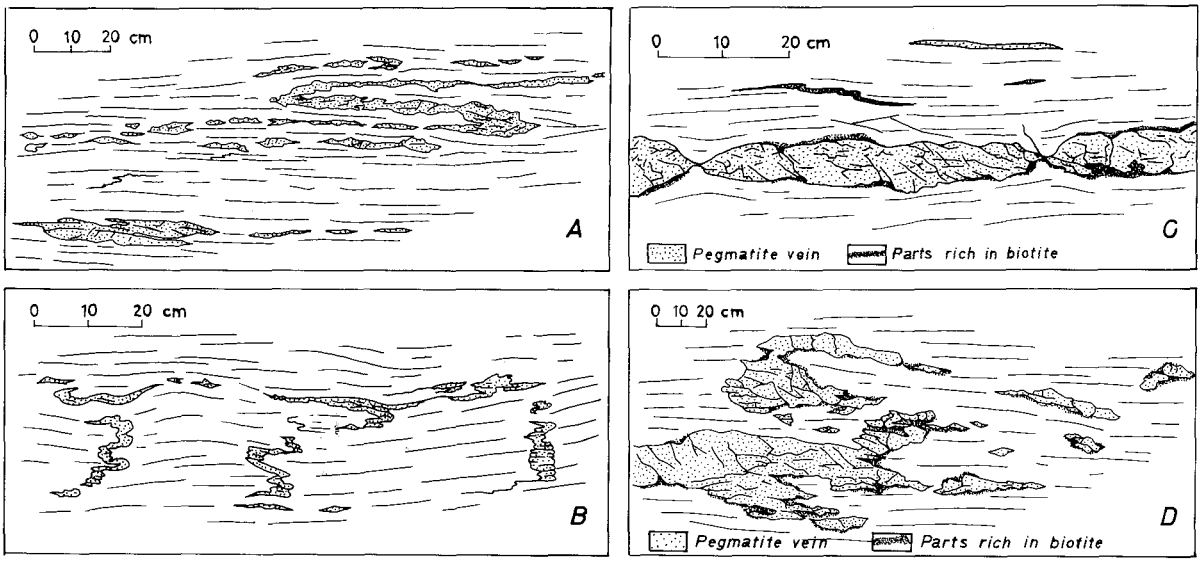

Fig. 5 Examples of the boudinage found in the folded area (reproduced from photographs). A and B: the foliation is inclined at 70° to WSW (in the Kakalia-Mwea tectonic zone); localities: a riverside of the Mwea river; about 500m to N of Mwea. C: the foliation is inclined at 50° to W (in the Kakalia-Mwea tectonic zone); locality: about 1.5km to NW of Kakalia. D: the foliation is inclined at 12° to N; locality: a riverside of the Kaiti river; about 3.5km to WSW of Makongo.

by surrounding, not completely but in part, black bands rich in biotite. The form of boudins, conjugate fracture-systems in the boudins, and a displacement along the fractures are all indicators to be typical boudins. A folded black seam rich in biotite (left upper) may suggest a fold-system which is accompanied by the axial plane cleavage parallel to the foliation.

The boudinage is also often found in the gneisses outside of the zone of high angle cleavage, an example being shown in Fig.5D. Fig. 5D shows folded pegmatite veins and boudins found in the semi-pelitic gneisses. The black bands rich in biotite are also found just as in Fig. 5C, and the axial plane of these folds is in parallel to the foliation of gneisses. Forms of folds and of boudins are, however, not simple but complicated.

Thus, most of the boudins are accompanied by folds, the axial plane of which is always in parallel to the foliation of the gneisses and also, in many cases, to a surface of displacement.

3. *Folds, accompanied by the axial plane cleavage*

Many styles of fold have been found in the folded area. The axial plane of folds is generally cleaved, but the axial plane cleavage is not always visible to the naked eye. The axial plane which is inclined at angles higher than 40 degrees is characteristically

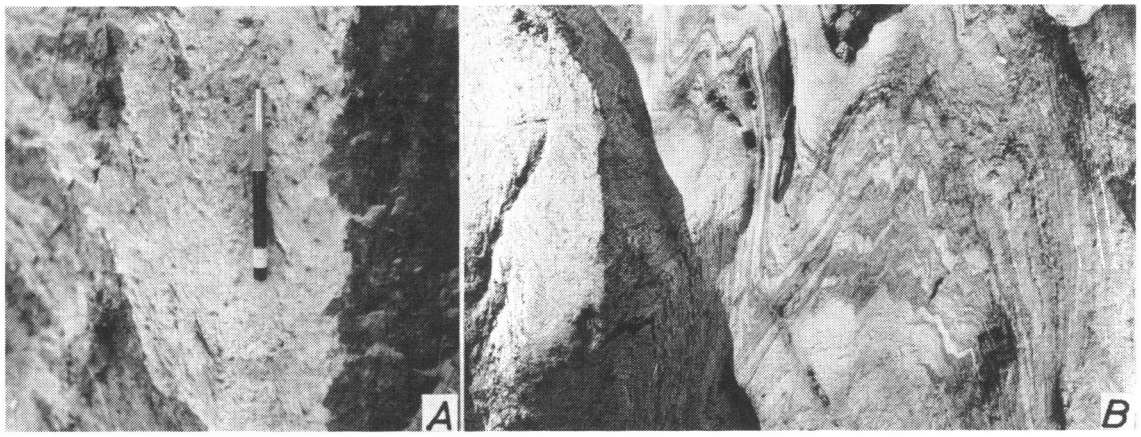

Fig. 6 Shear folds, with the axial plane inclined at high angles (in the zone of high angle cleavage). A: pelitic gneiss at the northern part of the Makongo Forest. B: pelitic/psammitic gneisses at a riverside of the Mukuyu river, a branch of the Mwea river,about 4km to SES of Kali.

limited to occur within the zone of high angle cleavage. In the folded area outside of the zone, the axial plane is usually inclined at angles lower less than 40 degrees.

Two types of fold are shown in Figs. 6A and B as examples common in the pelitic gneisses in the zone of high angle cleavage. They are found in area outside of the Kakalia-Mwea monocline. The wave-length of them is always shorter than 50cm, commonly from a few centimetres to 10cm. The folds in Fig. 6A are found in the pelitic gneiss which is accompanied by kyanite, staurolite and garnet. The rock is strongly cleaved and sheared along the axial plane which stands nearly vertically. The shear folds in Fig. 6B have longer wave-length than those in Fig. 6A, and the axial plane stands also steeply but is not clearly cleaved in appearance.

Figs. 7A and B are examples to show the other types of fold in the pelitic gneisses, which are found in exposures outside of the zone of high angle cleavage.

Folds in Fig. 7A are sharply cleaved and apparently sheared along the foliation of gneisses, now the folds developing to a tectonic *melange*. The foliation is inclined at a low angle. The structure in Fig. 7A is divided into two parts; one is characterized by straight foliation but the other by a lot of relic folds. The former part is quartzo-feldspathic or psammitic gneiss in character, but the latter is characterized by frequent alternation of pelitic gneiss layers with quartzo-feldspathic gneiss layers. The relic folds are represented only by the quartzo-feldspathic gneiss layers which are, in their interior, alternated by attenuated black seams rich in biotite. The original axial plane of the relic folds is now lost by a later shearing, however, it is deduced to be nearly in parallel to the general foliation along which shear movement would take place.

In Fig. 7B, the axial plane is inclined at a low angle and in parallel to the gneral foliation. The axial plane cleavage is clearly

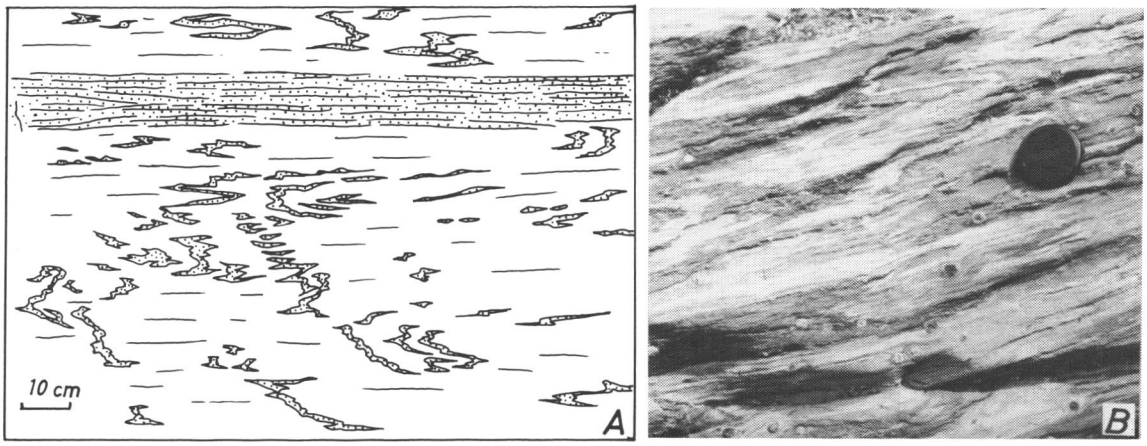

Fig. 7 Shear folds, with the axial plane parallel to the foliation (outside of the zone of high angle cleavage). A: pelitic/psammitic gneisses; the foliation is inclined at 31° to N; locality: a riverside of the Syuuni river, about 3.5km to E of Makaveti. B: pelitic gneiss, with garnet spots; locality: apart about 10m to S from A.

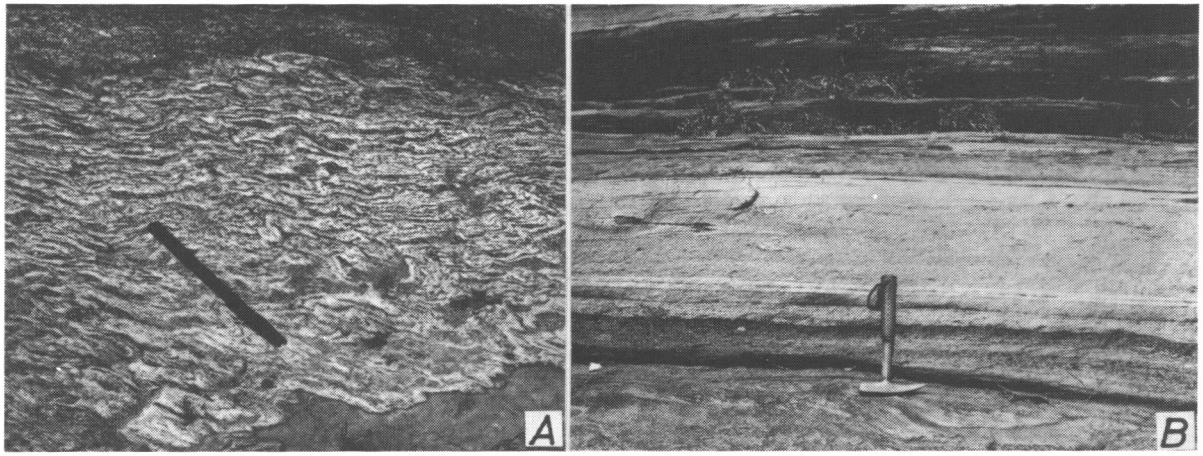

Fig. 8 A: Shear folds in semi-pelitic gneiss which is inserted between psammitic gneiss layers. The axial plane is intersected with the foliation of the surrounding psammitic gneiss at a moderate angle, but no folds have been found to occur in the psammitic gneiss; locality: a riverside of the Syuuni river, about 1.5km to SES of Makaveti (outside of the Kakalia-Mwea tectonic zone). B: intrafolial fold in semi-pelitic gneiss at an exposure very near A. The axial plane is parallel to the foliation of the surrounding gneiss which is inclined at 13° to NW.

found to the naked eye, but shearing along the plane is scarcely recognized. Such examples as shown in Figs. 7A and B are not uncommon over the folded area, especially in localities outside of the Kakalia-Mwea monocline.

In addition, Figs. 8A and B present the other types of fold in localities outside of the zone of high angle cleavage. The folds in Fig. 8A are found in semi-pelitic gneiss layers which are alternated with the psammitic gneiss. In this exposure, only the semi-pelitic layers are folded with the axial plane which is inclined at moderate angles and crosses the foliation of the surrounding psammitic gneiss. The folation of the psammitic gneiss is inclined at a low angle and runs straightly. In Fig. 8B, a semi-pelitic gneiss layer is inserted between the pelitic gneiss layers. The foliation of the pelitic gneiss appears to be straight and shows no fold. On the other hand, one of the quartzo-feldspathic gneiss layers in the semi-pelitic gneiss shows intrafolial folds, the axial plane of which is in parallel to the foliation of the semi-pelitic gneiss but not cleaved. Another quartzo-feldspathic gneiss layer is not folded and appears to have no genetic relation to the intrafolial folds.

Conclusively, the shear folds are commonly found and the flexure folds are actually lacking in the folded area. The origin of these folds is considered to be complicated. It is, however, a general tendency to show that the foliation surfaces of the gneisses took a role of shear surfaces along which displacement had taken place during a metamorphism, though the distance of displacement is variable from place to place. Thus, some folds would be completed by plural tectonic movements but others free from a later movement.

4. *Folded basic dykes*

Origin of the basic gneisses in the studied area is not always easy to decide, some having an appearance of dyke but others appearing just like a tuffaceous beds. In this paragraph, some sheet-like dykes only will be described. Now we have three examples of folded basic dykes, all of which are found in an extended exposure cropped out about 200m along a riverside near Kiatuni, at the western part of the Kalama Hill area. They are shown in Figs. 9A, B and C. All basic dykes in these figures are intruded into a semi-pelitic gneiss. The semi-pelitic gneiss is light coloured and accompanied by epidote, hornblende and felsic minerals. The dykes are black in colour and rich in biotite.

The walls of two sheet-like dykes in Fig. 9A are cutting at low angles the foliation of the surrounding semi-pelitic gneiss. Within the dykes, relic (?) texture which is just like a chilled margin is recognized by changing grain-size of biotite flakes. The foliation of the basic dykes is not clearly found. The surrounding semi-pelitic gneiss does not show any fold structure but includes many small quartzose boudins.

A basic dyke in Fig. 9B includes an island of the semi-pelitic gneiss. The intrusion boundaries of the dyke are cutting the foliation of the wall rock at low angles, though the boundaries are now folded with the axial plane parallel to the surrounding foliation. The foliation of the basic dyke is not clear.

Fig. 9C shows an example of a folded dyke. A relatively thick seam of the semi-pelitic gneiss which is now isolated in the basic dyke clearly represents a fold style, the shear folds. The foliation of the basic dyke is roughly parallel to the axial plane of the fold, and in addition, it appears to be paral-

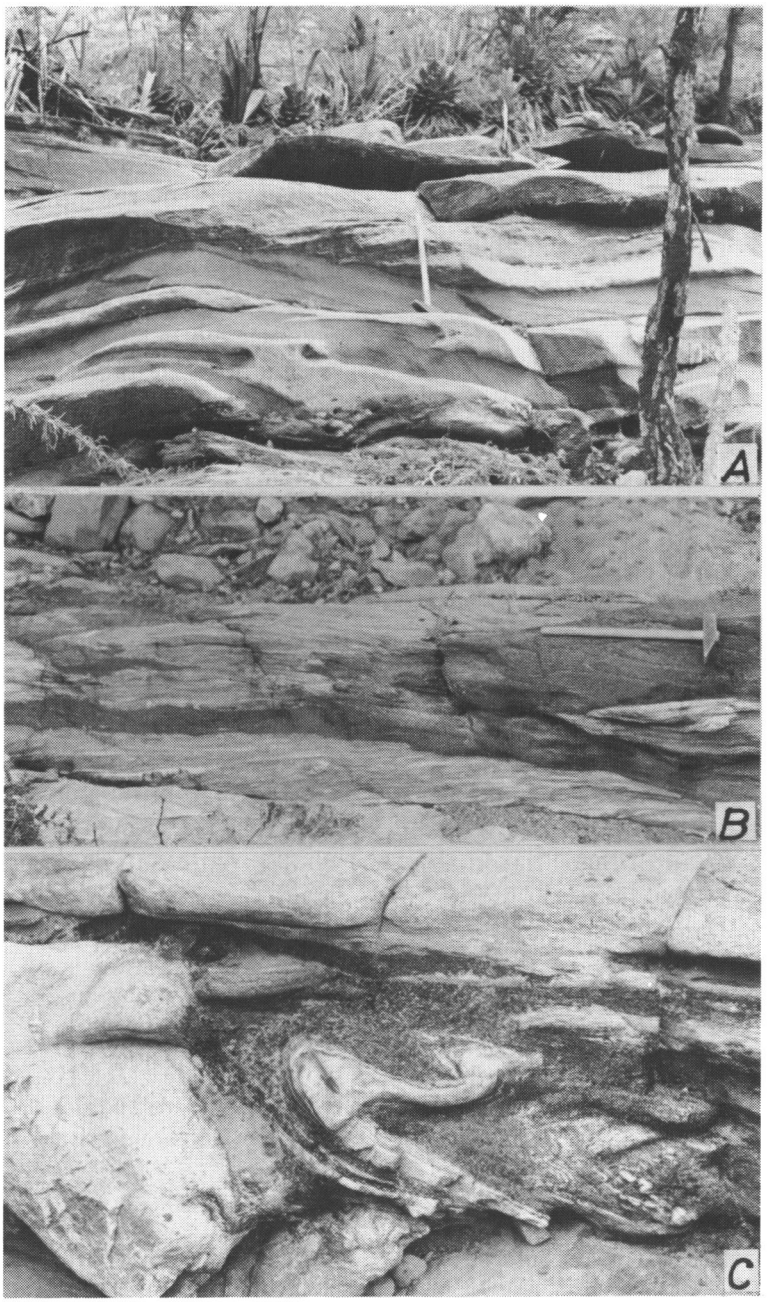

Fig. 9 Folded basic dykes. Three photographs were taken from a long continuous exposure, a riverside of a branch of the Wamui river, about 1.5km to SE of Kiatuni (outside of the Kakali-Mwea tectonic zone).

lel to a shear zone which is found near the upper wing of the folded seam. The axial plane of the isolated semi-pelitic gneiss does not develop to a cleavage in appearance. The foliation of the semi-pelitic gneiss runs straight at the upper side of the folded dyke, but it curves round the crest of the dyke at the left side of the figure. We can find no axial plane cleavage in the surrounding semi-pelitic gneiss.

This example of the folded dyke may suggest at least three phases of event; the first phase is an intrusion of the dyke, the second is a folding, and the last is a shearing movement.

5. *Lineations and axes of folds*

The lineation has been commonly found in the paragneisses, regardless of presence or absence of fold structures. Even in the psammitic gneisses which are lying flat with straight foliation, the lineation is often sharply found. The pelitic gneisses generally present more distinct lineation than that in the psammitic gneisses. The lineation is most frequently measurable in exposures inside of the zone of high angle cleavage.

Perhaps the linear elements would result from various origins, because there have been found many styles of fold in the studied area. Some of the lineation result from intersection of the planar elements such as foliation, cleavage, original bedding and so on, but others may represent axes of minor crenulation. Some axes of folds correspond to the crest of a drag fold, but others are axes of folds which are accompanied by axial plane cleavage. The regional trend of the linear elements and their geometrical relations to the planar elements will be discussed in the next paragraph.

Geometrical relations of the structural elements

The structural features in the studied area may be characterized by the following three structural units: they are,

a: structures of the Mbooni Hill area, where an area of the eastern outside of the Kakalia-Mwea tectonic zone is included,
b: structures of the Kakalia-Mwea tectonic zone, and
c: structures of the Kalama Hill area, where an area of the western outside of the Kakalia-Mwea tectonic zone is included.

Roughly speaking, the Kakalia-Mwea tectonic zone and the Kalama Hill area are the two main structural units in the folded area.

1. *Structures of the Mbooni Hill area and the Kalama Hill area*

As shown in Fig. 2, the Mbooni Hill area is composed mainly of the granitoid gneiss and the psammitic gneisses. The foliation of the gneisses shows gentle waves but, as a whole, represents a dome structure on a larger sclae. π-poles of the foliation surfaces of the gneisses are plotted in Fig. 10A; again, the dome structure is clearly represented in the figure. There are several points which are representing the N-S strike and high dipping angles. They were measured at the eastern margin of the Mbooni Hill area. The lineation has been very difficult to detect either on exfoliated exposures or on fresh surfaces of the gneisses.

The structures of the Kalama Hill area are shown in Fig. 10B in which π-poles of the foliation of gneisses and poles of the lineation are plotted together. Except two π-poles, the foliation surfaces are inclined at low angles toward the north. Distribution of the π-poles suggests the presence of gentle

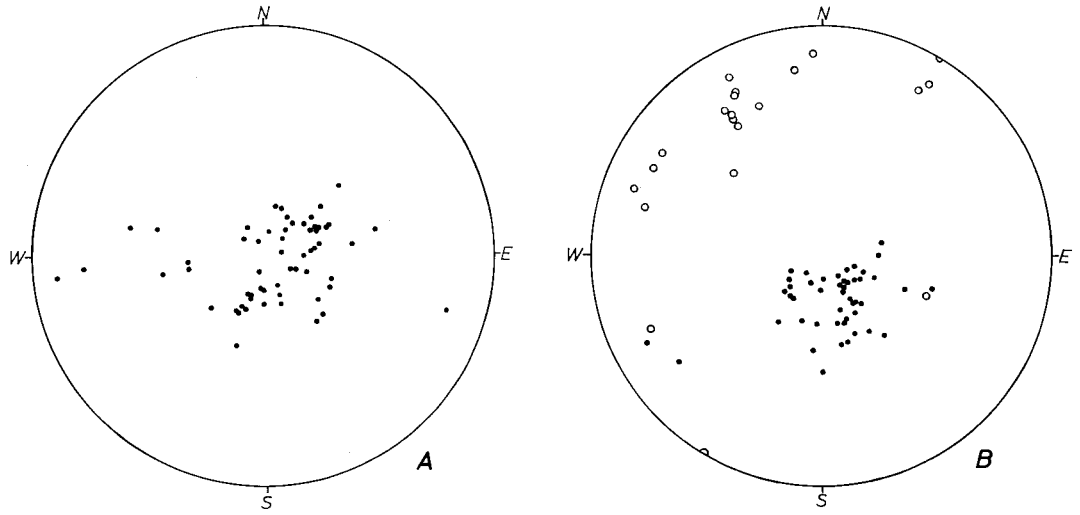

Fig.10 π-pole diagrams for the foliation of gneisses (lower hemisphere projection). A: data were collected at the Mbooni Hill area; 63 π-poles. B: data were collected at the Kalama Hill area; 47 π-poles, along with 20 linear elements (lineation and axes of folds). Solid circles represent π-poles and open circles the linear elements.

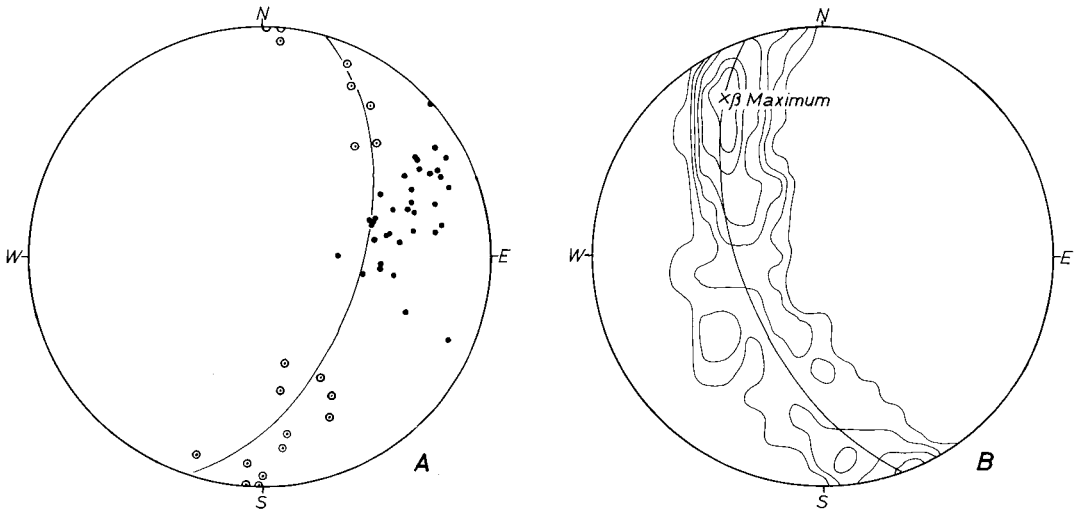

Fig.11 π-pole diagram and β-diagram for the foliation of gneisses in the Kakalia-Mwea monocline(lower hemisphere projection). A: π-poles of the foliation; solid circles: data were collected at the lowland between the Hill areas (36-poles); open circles with dots: data were collected at the southern part of the Mbooni Hill area (18-poles). B: β-diagram for the foliation (random sampling of 24-planes); concentration: $10<-8-6-4-2-1\%$. The β-maximum is trending N30°E and pitching at 20°.

anticlinorium with northerly pitching axes. The lineation is also pitching at low angles, but the trend is variable from WSW, through W, to NNE. The poles appear to be arranged along a great circle; however, we have no definite answer which will make clear a tectonic meaning of the great circle. One of the alternative ideas may be that the lineation would be a remnant structure which was imprinted in the gneisses before formation of the anticlinorium in the Kalama Hill area. Thus, the macroscopic structures in the Kalama Hill area are clearly different from those in the Mbooni Hill area.

2. *Structures of the Kakalia-Mwea tectonic zone*

The Kakalia-Mwea tectonic zone runs through the lowland between the mountainous areas: the Mbooni Hill area and the Kalama Hill area. The scope of the tectonic zone is not shown directly in Fig. 4, because the zone has no sharp tectonic boundaries but is gradational into structures of the surrounding gneisses.

As described in a foregoing paragraph, the eastern limit of the Kakalia-Mwea monocline changes its trend from NNW-SSE to ENE-WSW at the south of the Mbooni Hill area. The trend of the western limit of the monocline seems, on the other hand, to go nearly straight by keeping the NNW-SSE trend. It has not been known whether the monocline curves its general trend from NNW-SSE to ENE-WSW or goes straight by keeping its trend in NNW-SSE. Supposing that the latter is the case, the monocline is expected to disappear soon at the outside of the studied area. Then, ENE-WSW trend may belong to the other structure than to the monocline.

Fig. 11A is a π-diagram for the foliation of gneisses in the Kakalia-Mwea monocline. In this figure the foliation surfaces which were measured at the south of the Mbooni Hill area are plotted by different marks from those measured at the lowland. The π-poles which were collected at the lowland are crowded in a limited area in Fig. 11A, but the other π-poles are distributed along a great circle. The latter fact may suggest the presence of a fold-system which appears to be the other structure than the monocline, but more positive evidences will be required to explain the fold-system.

A β-diagram for the foliation surfaces which were measured at the lowland shows a complete great circle girdle with one conspicuous maximum concentration (β-maximum in Fig. 11B). The β-maximum pitches to N30°W at 20 degrees, and the monocline-structure is suggested in the figure.

In the folded area, the foliation surfaces are often in parallel to the axial plane cleavage. Fig. 12A shows a π-diagram for the axial plane cleavage in the zone of high angle cleavage, many foliation surfaces being plotted on the figure for the cleavage surfaces. Fig. 12B is a β-diagram for the axial plane cleavage in the zone of high angle cleavage. The concentration of the β-axes is conspicuous in Fig.12B but a complete girdle does not appear. The β-maximum pitches to N34°W at 22 degrees; it is very close to the β-maximum in Fig.11B.

The lineation and axes of folds in the folded area are plotted together in Fig.13, in which the β-maximum areas for the foliation (Fig.11B) and those for the cleavage (Fig. 12B) are also reproduced to show a geometrical relation of the linear elements to

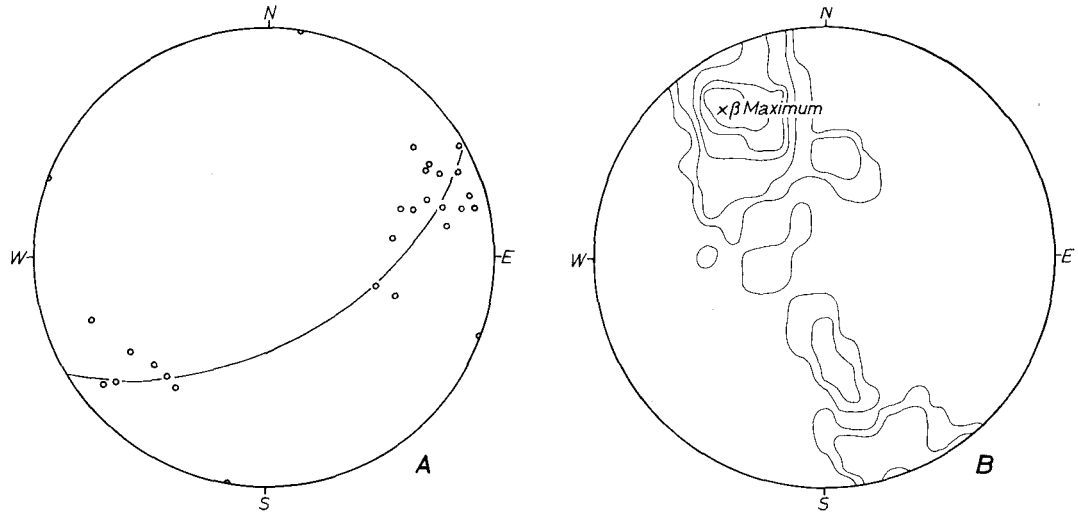

Fig.12 π-pole diagram and β-diagram for the axial plane cleavage, data being collected at the zone of high angle cleavage (lower hemisphere projection). A: π-poles of the cleavage (26-poles). B: β-diagram for cleavage (random sampling of 22-planes); concentration: $14 < -10-6-3-1\%$. The β-maximum is trending N34°E and pitching at 22°.

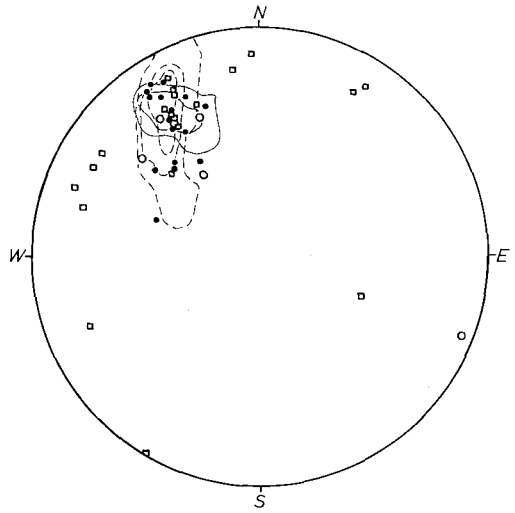

Fig.13 A composite diagram for the linear elements and the β-maximum areas, data being collected at the folded area (lower hemisphere projection). The β-maximum area are reproduced from Fig.11B (dashed line) and Fig.12B (line); solid circles: the lineation poles at the Kakalia-Mwea tectonic zone (16-points); open circles: axes of folds at the Kakalia-Mwea tectonic zone (5-points); open squares: the linear elements at the Kalama Hill area (20-points).

the planar elements. It is deduced that no trouble will be caused in regarding all the linear elements as one linear element. In Fig.13, all the β-maximum areas are found very near to each other, and most of the linear elements are distributed in and near the β-maximum areas. It is suggested by Fig. 13 that the Kakalia-Mwea monocline would be developed at the same time as the zone of high angle cleavage; that is, the Kakalia-Mwea tectonic zone would be completed during one tectonic event or perhaps during one metamorphism. In addition, it is deduced that the folds in the Kalama Hill area would have a different origin from those in the tectonic zone.

The position of the Kakalia-Mwea tectonic zone is sandwiched between the Mbooni Hill area and the Kalama Hill area. Originating in difference of some mechanical characters of rocks, the tectonic zone would have been strongly compressed by competent blocks of the both sides during a tectonic event.

Tectonic evolution of the area south-east of Machakos

Based on the structural characters, the studied area can be divided into three units, *i.e.* the Mbooni Hill area, the Kakalia-Mwea tectonic zone and the Kalama Hill area, which are arranged in order from the east to the west. Many folds on every scale have been found in the last two units.

The Mbooni Hill area shows a dome structure, but the Kalama Hill area shows an anticlinorium which may correspond to the northern wing of the Opete dome. The geometrical relations between the structural elements in the Kalama Hill area can hardly be explained by a single tectonic event.

Of interesting are the structures of the Kakalia-Mwea tectonic zone which are characterized by development of the boudinage, high dip-angles of the foliation and the axial plane cleavage. After geometrical examinations of the structural elements, the tectonic zone would possibly be completed during a tectonic event later than that during which an anticlinorium of the Kalama Hill area was formed.

In his study on the Machakos area, Baker (1954) considered one sequence of events that resulted in the regional metamorphism and granitization; however, such complicated fold-structures as pointed out in the foregoing paragraphs can not be explained by one sequence of events. While, Biyajima *et. al.* (1975) and Biyajima (1976) proposed two sequences of metamorphic events. Two phases of geosynclinal sedimentation prior to each metamorphic event are considered. The interpretation by Biyajima *et al.* (1975) is based on their proposal for "mangled gneiss dome" of the Mbooni Hill area, and the interpretation by Biyajima (1976) is based on his proposal for two different directions of tectonic compression during the metamorphism. The two phases of sedimentation are, however, difficult to prove at the state of knowledge. Provided that the two sedimentary phases could be considered in the Machakos area, they would be a supracrustal event which possibly took place at a far upper horizon than that of the paragneisses cropped out in the studied area.

Especially, the senior of us would like to propose a metamorphic history of the studied area, the proposition being summarized in Table 1. The chronologic ages of these geologic events in Table 1 have not been clarified. It has been believed however that

Table 1 Proposed metamorphic history of the Mozambique belt in area south-east of Machakos, Kenya.

Sedimentation	Igneous activity	Folding	Metamorphism
	Granitoid minor intrusives	Second folding (Kakalia-Mwea tectonic zone)	Second metamorphism (medium grade)
	Quartz- and pegmatite-veins		
	Granitoid rocks	First folding (formation of domes)	First metamorphism
	Basic dykes Intermediate rocks		(?) Boundary of medium/high grade)
Psammitic and pelitic rocks	("semi-pelitic")	?	?

the Archaean (or early Proterozoic ?) rocks in the studied area were regionally metamorphosed during the Mozambiquian orogeny.

The first metamorphism would have taken place after the intrusion of basic dykes into the surroundings. The metamorphism was accompanied by the first folding. Most of fold structures found in the Kalama Hill area, and perhaps some of those in the Kakalia-Mwea tectonic zone, appear to be originated from the first folding. Folds accompanied by the axial plane cleavage were possibly formed in an earlier phase of the folding, and they were followed by gentle open folds on moderate scale with increasing temperatures of the metamorphism. The compressive force in the earlier phase would be kept powerfully in E-W or ENE-WSW direction but would become weak with increasing temperatures later, and at last viscous upwelling of the paragneisses occurred.

Emplacement of the layered granitoid rocks which now fill the core of the Mbooni Hill area may correspond to one of the late-kinematic igneous activities, when the surrounding rocks were kept fairly plastic yet. Then, the Mbooni Hill area appears to be risen to a level upper than the Kalama Hill area where the rocks were possibly left without conspicuous updoming. A primitive form of the Kakalia-Mwea monocline would appear during the late-kinematic phase. Quartz and pegmatite veins represent the postkinematic minor intrusives.

The highest grade to which the first metamorphism would attain is unknown in the studied area, because there are no relic minerals to be indicative. We tentatively consider that the highest part of the first metamorphism would be near the boundary of medium/high grade (Winkler, 1974).

Later, the second metamorphism would take place in the present area, and its physical condition attained to the epidote-amphibolite facies or the medium grade; that is, the highest grade during the metamorphism is supposed to be too low to cause a partial melt of any rock. The second metamorphism was accompanied by the second folding. The layered granitoid rocks in the Mbooni Hill area were transformed into orthogneisses, and the other gneisses were recrystallized by the second metamorphism. Compared with the first folding, the second folding seems to take place in a less extensive area, the Kakalia-Mwea tectonic zone being developed in a limited position between the two antiform areas. The gneisses of the Hill areas would behave like a competent mass during the second folding. No minor folds would be newly formed in gneisses of the Hill areas, except for folds originated in a later regional shearing (Fig.4).

In the Kakalia-Mwea tectonic zone, different fold-styles seem to be originated from differences in competency of rocks. The pelitic gneisses which were laid at low angles would be selectively folded and cleaved along the axial plane during an early phase of the folding, but later the cleavage was transformed into the shear-surface. While, the psammitic gneisses were possibly free from the early folding due to their competent nature. Shearing is deduced to be especially active in a later phase of the second folding. The boudinage in the gneisses is one of typical structures formed during the folding. The compressive force was possibly powerful in E-W or ENE-WSW direction in the early phase but gradually turned into NNW-SSE in the later phase of the folding.

Conclusively, the metamorphic history of the area south-east of Machakos probably began with the geosynclinal sedimentation of detritus materials, and at least two sequences of metamorphic events must be considered during the Mozambiquian orogeny.

Acknowledgements – We greatly acknowledge the assistance given by the Mines and Geological Department of Kenya during our stay in Kenya. The field work was made possible by the Grant-in-Aid for Overseas Scientific Researches from the Ministry of Education, Japan, to which we express our thanks.

References

BAKER, B.H. (1954): Geology of the southern Machakos district. *Report No.***27**, *Geol. Surv. Kenya.*

BIYAJIMA, K., SUWA, K. and MIYAKAWA, K. (1975): Mantled gneiss dome in the Mozambique belt around the Machakos area, Kenya. *1st Prelim. Rep. African Studies,* 6-13.

BIYAJIMA, K. (1976): Petrological study on the Mozambiquian metamorphic rocks in the Machakos area, Central Kenya. Master's thesis in Nagoya University, Manuscript (in Japanese).

ESKOLA, P. (1948): The problem of mantled gneiss domes. *Q. J. G. S.,* **104**, 461-476.

FAIRBURN, W.A. (1963): Geology of the northern Machakos – Thika area. *Report No.***59**, *Geol. Surv. Kenya.*

WINKLER, H.G.F. (1974): *Petrogenesis of metamorphic rocks.* Springer-Verlag.

Fault Pattern of the Southern Part of the Eastern Rift, Tanzania

Kenji YAIRI

Department of Earth Sciences, Faculty of Science, Nagoya University

Introduction

The main part of the Eastern Rift or Gregory Rift Valley traverses central and southern Kenya, trending approximately north-south. It is characterized by a series of graben structures 40 to 65 km wide and by the extensive Neogene volcanism (Baker and others, 1972). The Eastern Rift rapidly changes its character southward in Tanzania, where Neogene faults diverge and result in a chain of asymmetrical faulted troughs trending northeast-southwest; the outline of the individual trough forms a circular arc, the troughs being arranged en echelon as a whole. Major marginal faults defining the northwest of the troughs form a zigzag or en echelon pattern. In the southern segment of the Eastern Rift, fault patterns are recognized as a distinctive geomorphological manifestation of the fracturing of basement rocks without any modification of Neogene volcanism, this matter providing a particularly preferable condition for the study on the fault pattern. The objects of this paper are to show a possible mechanism of the formation of en echelon, arcuate and zigzag fault patterns and to estimate the direction and amount of crustal extension across the segment according to the method proposed by Yairi (1974, 1975a), which is based on the geometry of en echelon faulting.

Geological setting

The East African Rift System is divisible into the Eastern and Western Rifts, which conjoin in the Mbeya Crux; the investigated area, between lat. 3°S. and 6°S., forms a

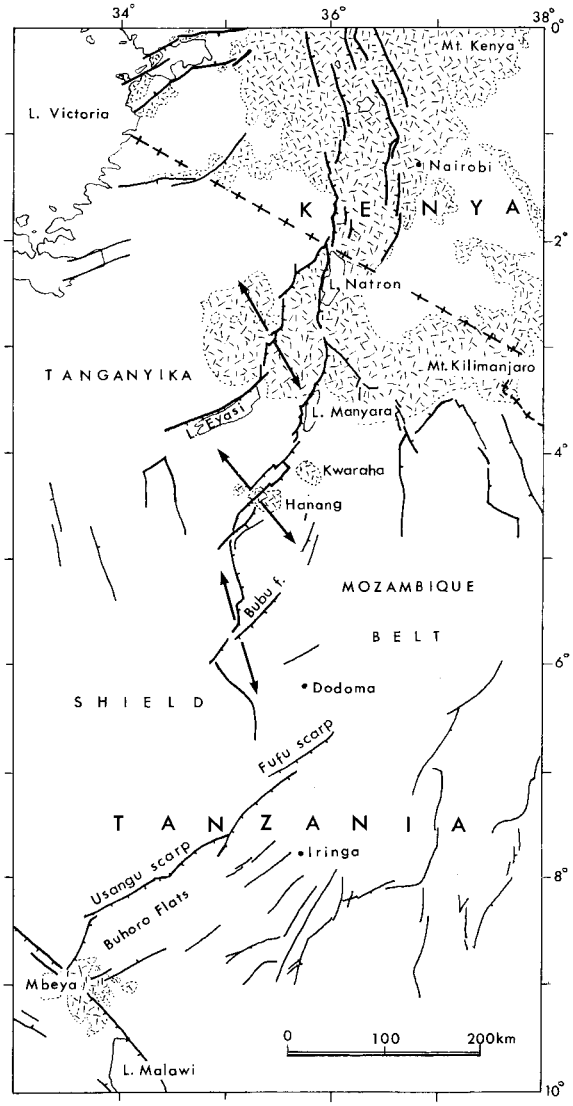

Fig. 1

Fault pattern and crustal extension across the southern part of the Eastern Rift. Faults are after King (1970), Baker (1971), Baker and others (1972), and the present work; arrows indicating the direction of crustal extension.

2nd Prelim. Rep. Afr. Studies, Nagoya Univ., 39-50, 1977.

southern part of the Eastern Rift (Fig. 1). The area is occupied mainly by the Precambrian basement complex, which includes part of the Tanganyika shield (probably older than 3200 m.y.) and of the late Proterozoic-early Paleozoic Mozambique orogenic belt (McConnell, 1974). The Precambrian basement is covered by extensive superficial deposits and some volcanic rocks of Neogene age. Unlike Tertiary volcanic rocks are well developed in Central Kenya, such a volcanism is here limited to the small areas of Kwaraha and Hanang volcanic fields.

In the area from Lake Manyara to Hanang, the rift-faulting is thought to be of Plio-Pleistocene age based on its relation to the Neogene volcanic sequences (*e.g.*, Pickering, 1965; Orridge, 1965). At the south, in the area from Kwa Mtoro to Bahi depression, the faulting occurred after the formation of the Kilimatinde Cement, which is the youngest formation in the area and considered to be of Miocene to Pliocene age (Lounsberry and others, 1967). The faulting indicates tension stress (*ibid.*) and almost all of the faults are considered to be of normal as well as those of the main part of the Eastern Rift in Central Kenya (Baker and others, 1972).

En echelon pattern and estimation of crustal extension

Unlike well-defined, normal grabens found in the central part of the Eastern Rift, its extension southward in Tanzania, between lat. 3°S. and 9°S., is characterized by a chain of asymmetrical faulted troughs trending northeast-southwest and arranged en echelon. A broad zone comprising these troughs follows the eastern margin of the Tanganyika shield adjoining to the Mozambique orogenic belt on the east (McConnel, 1972, 1974). This zone can be considered as an unstable, mechanically weak zone to be fractured in rifting. En echelon rift-faulting is attributable to the second order strain state reorientated in the weak zone, the trend of which is rather oblique than normal to the direction of the regional horizontal extension (Yairi, 1975a). Based on the geometry of en echelon pattern, the direction of crustal extension across the southern part of the Eastern Rift can be estimated by the method of Yairi (1975a).

As can be recognized in Fig. 1, in this region there are four main arcuate elements arranged en echelon, each of which is 200–300 km in length: Lake Eyasi, Lake Manyara-Hanang, Bubu, and Usangu-Fufu. The row of en echelon pattern of these elements, which follows the weak zone, also forms a gently curved line sweeping from N-S in the north to NNE-SSW in the south. The directions of extension obtained from RE-angle (row-element angle) and en echelon pattern ("backhand writing m" type) are shown by arrows in Fig. 1: N30°W-S30°E, N40°W-S40°E and N15°W-S15°E for the Lake Eyasi, the Lake Manyara-Hanang, and the Bubu elements, respectively.

Each trough designated here an element is bounded on the northwest by several linear fault scarps of 10 to 20 km in length. The outline of the fault scarps is zigzag in a plane view and appears to consist of the alternation of NE- and NW-trending faults. As will be mentioned later, however, this zigzag feature is originally attributed to en echelon arrangement of NE-trending faults, its pattern being "backhand writing m" type. A typical example is well recognized near Lake Manyara, where faults trending N34°E to N42°E form a row trending N26°E (Fig. 2). The direction of the extension across the Lake Manyara region is estimated to be N40°W-S40°E. This direction agrees well with the result (Fig. 1) obtained by using en echelon pattern of different order.

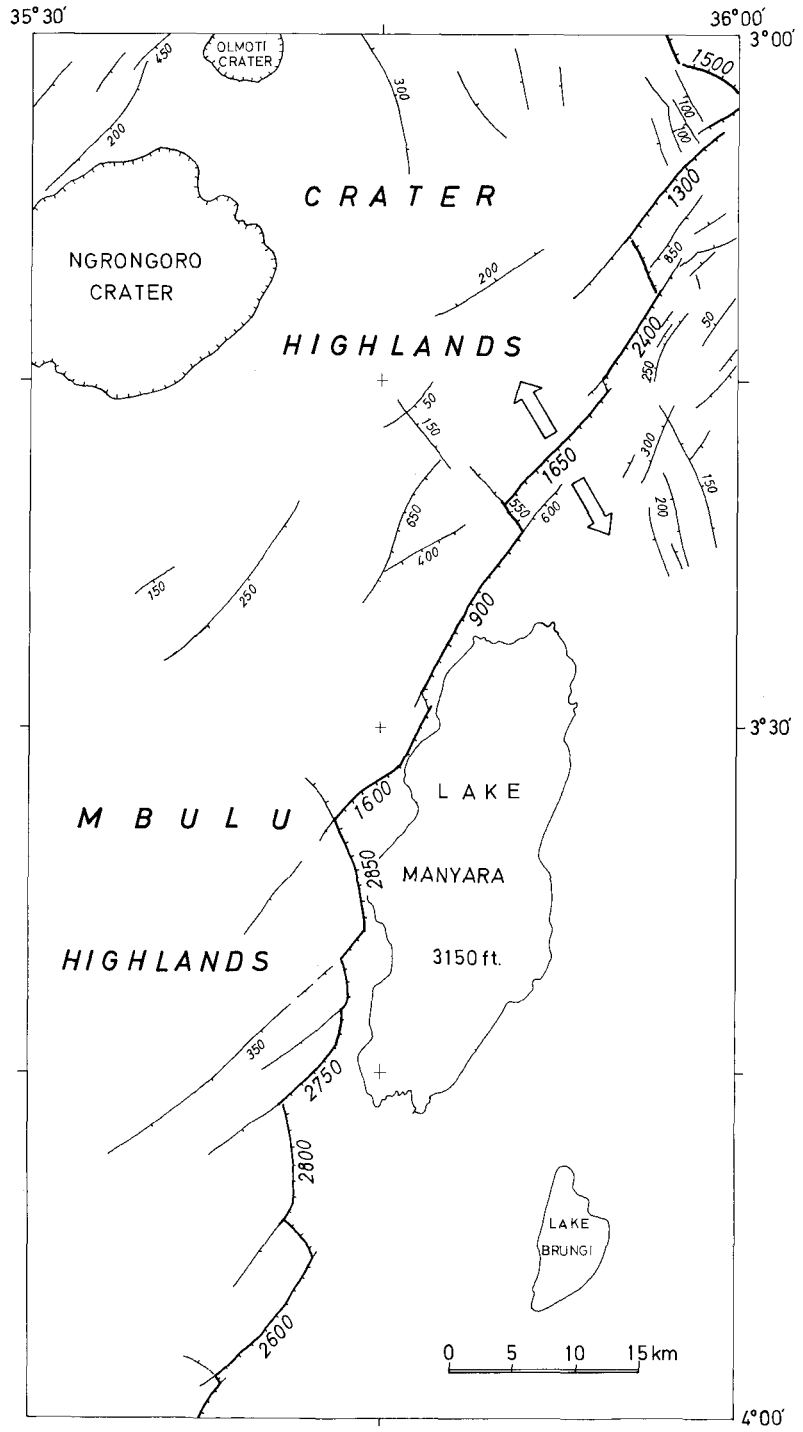

Fig. 2

Zigzag fault pattern along the Lake Manyara depression. Faults are after Orridge (1965), Pickering (1965), and the present work based on topographic maps at a scale of 1 : 50,000 (53/1, 53/2, 53/3, 53/4, 69/1, 69/2, 69/3, and 69/4). Open arrows indicate the direction of crustal extension, fault throws shown in feet on downthrow sides.

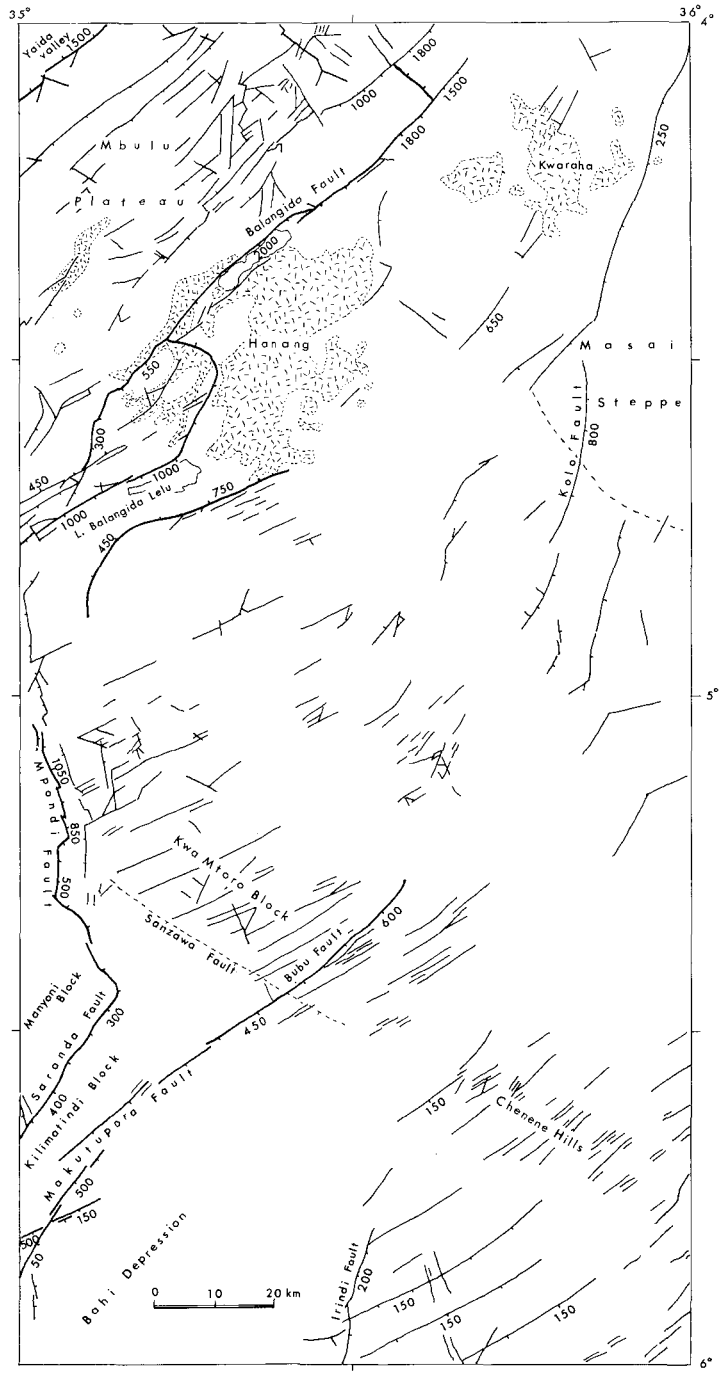

Fig. 3

Fault pattern between lat. 4°S. and 6°S. Faults were compiled from Thomas (1966a, 1966b), Mudd and Orridge (1966), Selby and Mudd (1965), Fozzard (1960, 1961), Lounsberry and others (1967), and Julian and others (1963). Fault throws are shown in feet on downthrow sides.

A striking feature in the region between lat. 5°S. and 6°S. is fault swarms trending ENE-WSW on the Kwa Mtoro Block and Chenene Hills (Fig. 3); they suggest the crustal extension of the same direction as obtained for the Bubu element in Fig. 1. Overall inspection of the southern part of the Gregory Rift leads to the conclusion that the crustal extension was in the direction of the NW-SE to NNW-SSE during Neogene rifting.

In Figs. 2 and 3 are given minimum throws along faults, which are estimated mainly from topographic reliefs. Total throws between rift floor and the plateau to the northwest are 3000 feet between lat. 3°S. and 4°S., 2000 feet between lat. 4°S. and 5°S., and 1000 feet between lat. 5°S. and 6°S. The amount of the crustal extension seems to decrease gradually toward the south, though more detailed investigation is required to quantify the amount exactly.

Zigzag fault pattern

Attention here is focussed on the mode of formation of the zigzag pattern, as seen in plan, of fault escarpments. As shown in Figs. 2 and 3, the Lake Manyara depression and its southern extension are bounded on the northwest by a series of well-preserved fault scarps. The outline of the escarpments is zigzag in plan, and is suggestive of an alternation of NE- and NW-trending faults. Usually the NE-trending lineaments are much higher in continuity, 10 to 20 km long, and are more uniform in orientation than the NW-trending ones which never exceed 5 km in length. Based on evidences mentioned below, it is proposed that the main NE-trending faults arranged en echelon were formed at first and then modified by the subsidiary NW-trending faults, to result in the formation of the zigzag pattern of the fault scarps.

Fig. 4-a shows a simplified topographic map of an area near the southwestern corner of Fig.3, where contour lines are smoothed out by burying valleys less than 1 km in width on topographic maps on a scale of 1;50,000 (sheets of 123/3, 123/4, 142/1 and 142/2 in Tanzania). Fig.4-b shows east-west topographic profiles of the same area drawn at equal intervals, on which the arrangement of faults shown by shade is superimposed. The northwestern margin of the Bahi depression is stepped fault scarps trending northeast, which are known as the Saranda fault and the Makutupora-Bubu fault (Fozzard, 1961; Lounsberry and others, 1967). The fault scarps comprise closely spaced scarplets arranged subparallel or en echelon. Throws of the scarplets diminish toward both ends of individual faults. There is not always developed the NW-trending fault in a zone of offset between two faults disposed en echelon or overlapping one another, and the offset zone is rather characterized by monoclinal flexure. The development of a subsidiary fault trending northwest is expected in the flexure zone with the growth of throwing along the main faults. The zigzag pattern of fault scarps found in the region of Lake Manyara is considered to represent the most progressive phase of faulting. A schematic model is given to show the successive phases of zigzag faulting (Fig. 6). The subsidiary fault should follow the line of the maximum curvature in the flexure zone, the shape of which is dependent on the degree of overlapping at the offset of two faults arranged en echelon as shown in Fig. 7, and consequently, the trend of subsidiary fault is destined to become variable.

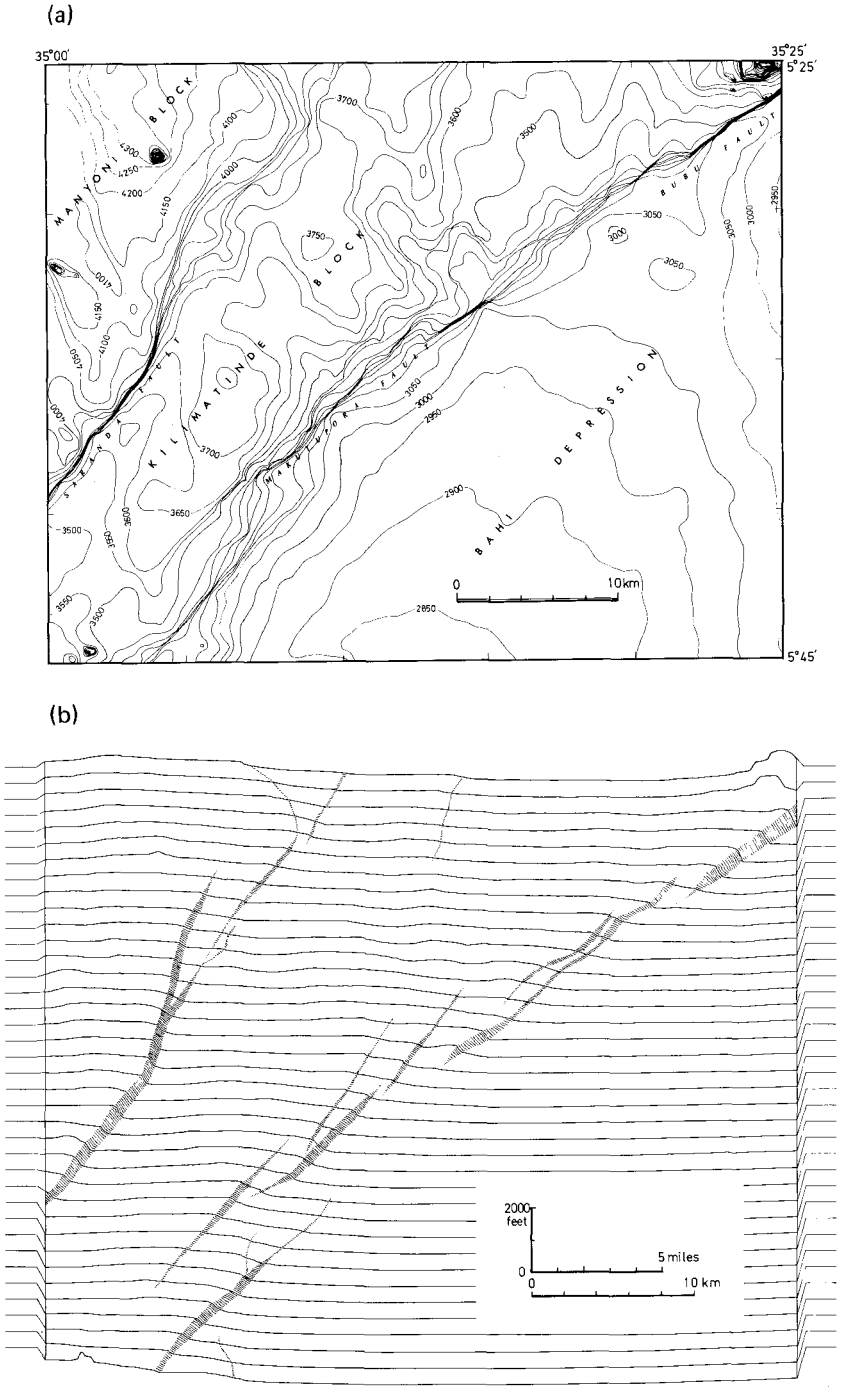

Fig. 4

Simplified topographic map (a), and east-west profiles (b), of the northern area of Bahi depression (see text). Parallel lines of both sides of the figure (b) show the base levels 4000 feet high.

Near the Derakuta Hill we can see a zigzag faulting of a typical intermediate type between the Lake Manyara type of a progressive phase and the Makutupora-Bubu type of an embryonic phase (Fig. 5). Across the NW-trending escarpment which links two NE-trending ones arranged en echelon, the summit level continuously decreases its height toward northeast from the plateau side to the Derakuta Hill. This feature is strongly suggestive of the original flexure of landsurface preceding the generation of the escarpment.

Paying attention to the pattern of rift depressions on a larger scale as shown in Fig. 1, NW-trending depressions about 100 km long can be also interpreted to be subsidiary ones developed in offset areas between two NE-trending depressions arranged en echelon. A good example is shown by the Mpondi fault zone between the Lake Manyara-Hanangu depression and the Makutupora-Bubu fault demarcating the northwest of the Bahi depression *(see also* Fig.3)

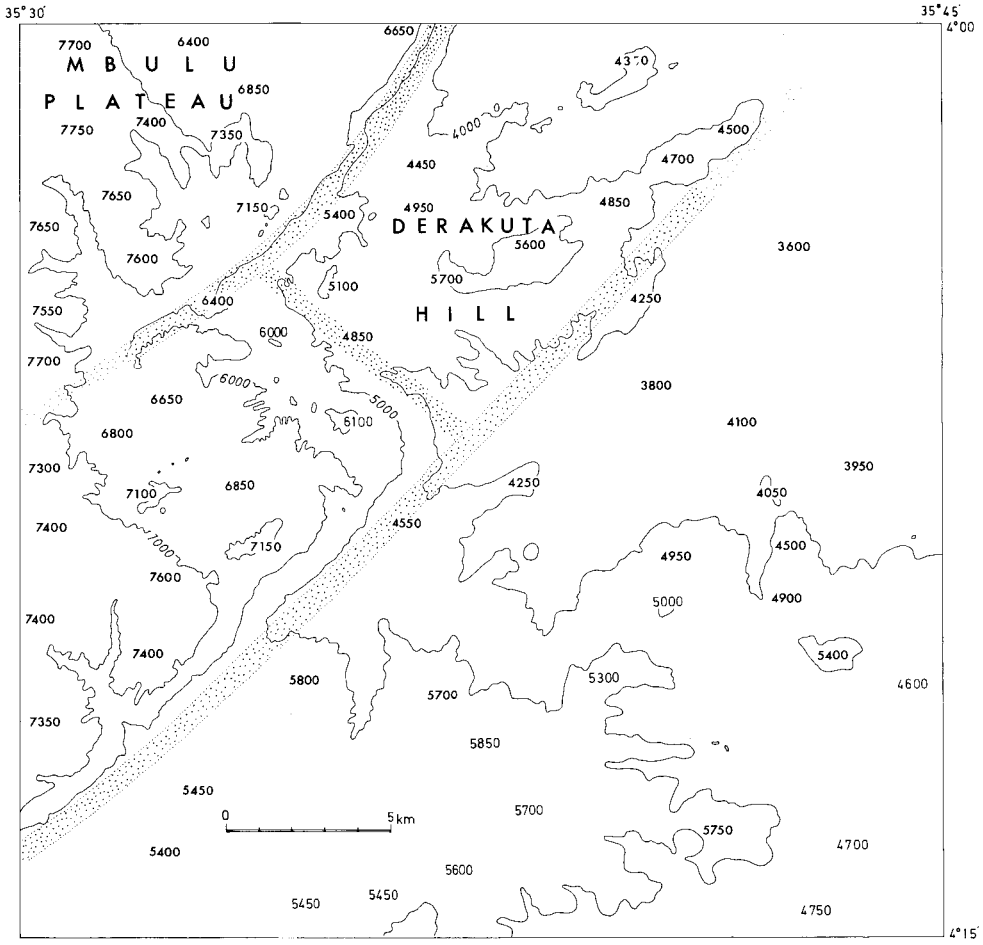

Fig. 5

Topographic map of the Derakuta Hill area. The figures indicate heights of isolated summits considered as remnants of a planar erosion surface, dotted area showing distinctive escarpment zones.

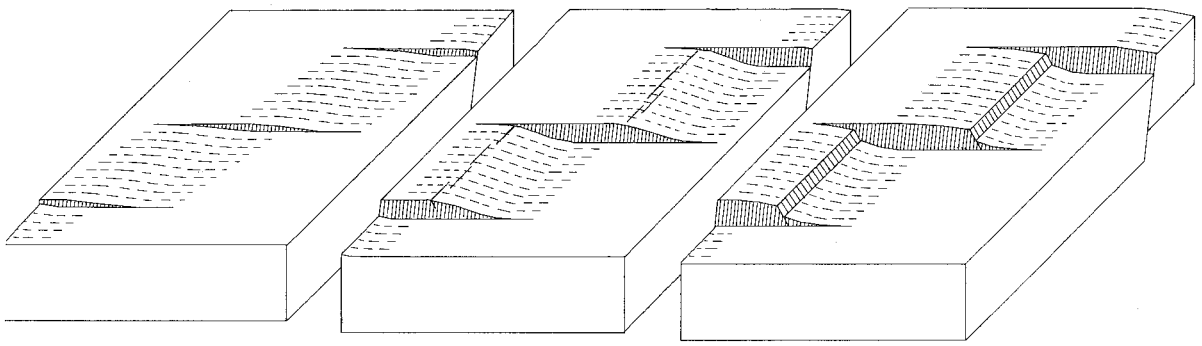

Fig. 6
Schematic model showing process of zigzag faulting.

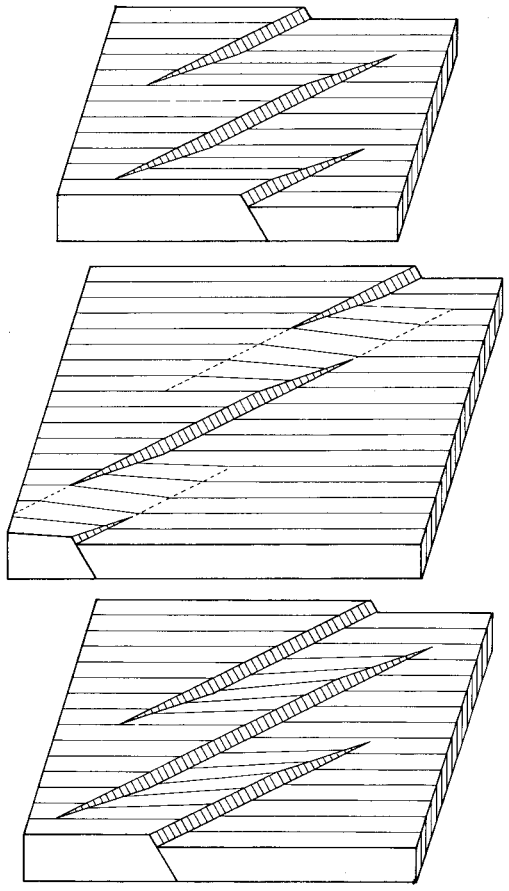

Fig. 7
Schematic models showing the feature of flexure zone developed at the offset between faults arranged en echelon.

Arcuate fault pattern

As shown in Fig. 1, not only the marginal faults of individual rift depressions but the zone comprising them arranged en echelon form gentle arcuate outlines convex to the southeast. Based on geomorphological studies in the Basin and Range province of the western United States, Moore (1960) confirmed that boundary faults of tilted blocks are generally curved in plan and are convex toward the direction of tilting, and he suggested that such arcuate pattern had a close analogy with the spoon-shaped sliding surface seen in landslides. This is not the case for the southern part of the Eastern Rift. Main marginal faults of asymmetrical rift depressions are not convex but rather concave toward the tilting. The arcuate pattern of the individual depressions seems to reflect the arcuate pattern of a major fractured zone comprising them. The following geometrical consideration is developed to explain that extension fractures occurring in a mechanically weak zone forming a circular arc always form minor arcs convex to the same direction as the former.

Let us suppose a mechanically weak zone to be placed between two rigid plates under the horizontal tension stress field as shown in Fig. 8-a. When the weak zone trends rather oblique than normal to the direction of the

horizontal extension, a formula, $\phi = 90°-2\alpha$, is obtained from the geometry of en echelon pattern, where ϕ is the angle between the trend of weak zone and the direction of the horizontal extension, and α, defined as RE-angle, is the angle between en echelon fractures and their row (Yairi, 1975a).

As illustrated in Fig. 8-b, let us suppose that a weak zone forms a circular arc given by a circle C_1 of the radius R with center at point O_1; the axis O_1X is chosen in the direction of the horizontal extension. We draw the circle C_e passing through a point P_1 on the circle C_1, where the center of the circle C_e is situated at the intersection of the line O_1X and the circle C_1, O_e. Let the tangents to the circles C_1 and C_e at the point P_1 be r_1 (row-1) and e_1 (element-1), respectively; let the angles between e_1 and r_1, and between r_1 and O_1X be α_1 and ϕ_1, respectively. Then, as is evident from Fig.8-b, we find the relationship $\phi_1 = 90°-2\alpha_1$; that is, e_1 indicates the trend of fractures to occur at point P_1. Similarly, we draw the circle C_2 with the same radius as the circle C_1 passing through a point P_2 on the circle C_e, the point P_2 being close to the point P_1; where the center of the circle C_2 is situated on the O_1X. Let the tangents the circles C_2 and C_e at the point P_2 be r_2 and e_2, respectively. Then we get the relationship $\phi_2 = 90°-2\alpha_2$, where the angles between e_2 and r_2, and between r_2 and O_1X be α_2 and ϕ_2, respectively; that is, e_2 indicates the trend of fracture at the point P_2.

The result represents that fracturing originated from the point P_1 grows up toward the point P_2 along the circle C_e, where the circle C_e is convex toward the convex side of the arcuate weak zone designated here as C_1 or C_2.

The geometrical consideration mentioned above is confirmed by the following simple

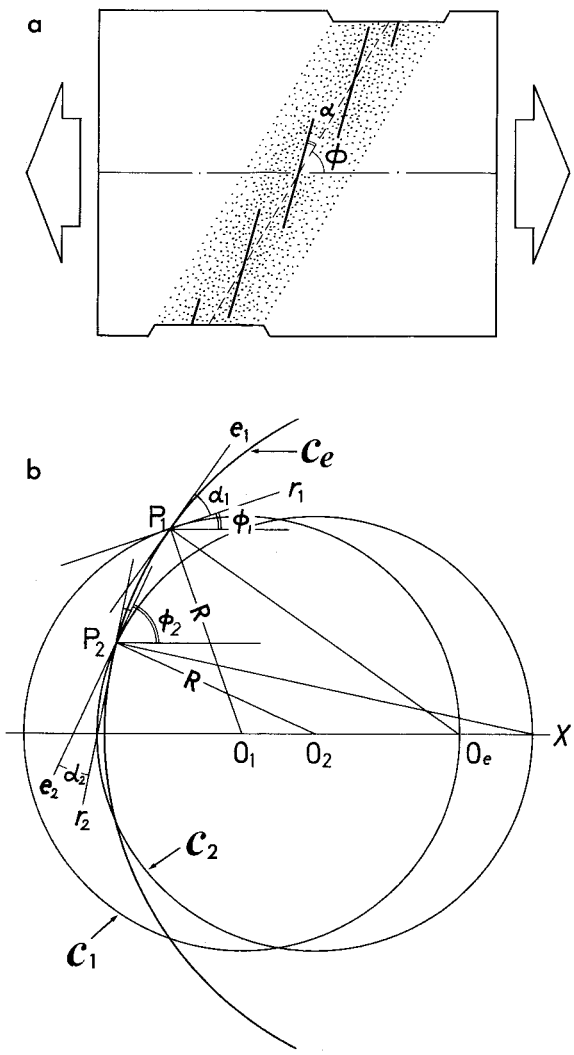

Fig. 8.
Geometry of arcuate fault pattern.

experiment. A model layer made up of powdered sugar is set on two boards with the arcuate joining line which could be pulled apart in opposite directions. Sliding the underlying boards apart, the layer is brought under tension, and as a result, minor arcuate extension fractures convex to the convex side of the arcuate joining line are developed (Fig. 9).

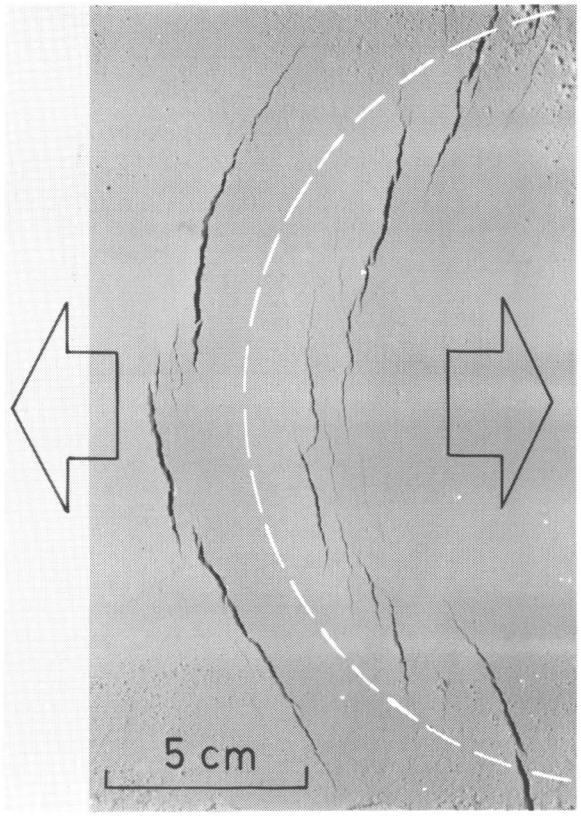

Fig. 9.

Arcuate fracture pattern on model surface. White broken line forming a circular arc shows the joining line of two boards overlain by a model layer, two boards pulled in opposit direction as indicated by open arrows (see text).

Discussion and conclusion

The fault pattern in the southern part of the Eastern Rift between lat. 3°S. and 6°S. is studied. The region is characterized by a belt comprising asymmetrical faulted troughs arranged en echelon; each trough forms a gentle arc and marginal faults bounding the trough on the northwest show the zigzag pattern in a plane view. The belt follows the western margin of the Tanganyika shield and must have played an important role as an unstable, mechanically weak zone under the regional horizontal crustal extension in the Neogene rifting. In this paper, it is emphasized that the pattern of rift depressions and their marginal faults must have been strongly controlled by the shape of the pre-existing weak zone.

The main part of the Eastern Rift in Kenya is marked by a series of normal grabens with uniform width of 40–65 km along the crest of topographic culmination, Kenya domal uplift, and by extensive Neogene volcanism closely related to the uplift and faulting. However, its southern extension in Tanzania is characterized by a belt comprising sparsely spaced faults splayed over the less uplifted broader zone a few hundred km wide, where the faults are not accompanied by significant volcanism. The above character strongly suggests that the latter region is still in a younger stage of rifting than the former; this is already discussed by Degens and others (1971) and supported by the result of the present investigations that the amount of the crustal extension tends to decrease gradually toward the south.

In applications of the plate tectonics theory to the Eastern Rift, a WNW-ESE extension across the main part of the Eastern Rift has been inferred from earthquake mechanisms (Fairhead and Girdler, 1971, 1972) and gravity anomalies (Searle, 1970). The WNW-ESE extension is supported by geometry of en echelon faulting (Yairi, 1975). The present conclusions show a NW-SE to NNW-SSE crustal extension across the southern segment of the Eastern Rift. From these results, a pole of rotation between two plates, which are demarcated by the Eastern Rift and its southern extension, is supposed to be situated far southwest, possibly near Lake Rukwa in Southwest Tanzania.

The uniform direction of tilting of the rift floors is worthy of special mention, though mechanically unsolved. In contrast to normal grabens at the advanced stage of rifting, splay

faults and asymmetrical grabens seem to be a feature characteristic of the embryonic stage of rifting. It is difficult to interpret that the asymmetrical feature of grabens have occurred under the horizontal extension resulted from a "relative" movement of plates; an "absolute" movement should be taken into account, for example, gravity sliding of the lithospheric plate along an inclined upper surface of the underlying asthenosphere.

The principal conclusions of this study are as follows:

1. The direction of the crustal extension across the Eastern Rift region in Tanzania was determined, according to the method of Yairi (1974, 1975a) (Fig. 1). The result points to the direction of N40°W-S40°E in the Lake Manyara region. The amount of the extension tends to decrease gradually toward the south as estimated from fault throws of 3000 feet at lat. 3°S. and 1000 feet at lat. 6°S.

2. The zigzag pattern of marginal faults is considered to be originally attributed to en echelon arrangement of NE-trending faults, which is modified by subsidiary NW-trending ones at the later stage of faulting. A schematic model showing the progressive phases of the zigzag faulting is illustrated in Fig. 6; some examples are shown in Figs. 4 and 5.

3. Generally the major marginal faults of rift depressions form circular arcs convex to the southeast. Their arcuate pattern reflects the arcuate shape of the zone which comprises all the depressions arranged en echelon. The arcuate zone is also convex to the southeast. A mechanism of the formation of arcuate fault pattern is discussed on the basis of the geometrical consideration (Fig. 8) and the experimental result (Fig. 9).

Acknowledgments—The author is indebted to Emeritus Prof. Dr. Isao Matsuzawa of Nagoya University for his encouragement. Thanks also are extended to Prof. Dr. Takeshi Uemura of Niigata University, Dr. Yukiyasu Saka of Waseda University and Mr. Mamoru Adachi of Nagoya University, for their kindness in critically reading this manuscript and offering constructive suggestions.

References

BAKER, B. H. (1971): Explanatory note on the structure of the southern part of the African rift system. *Tectonics of Africa, Unesco*, 543-548.

BAKER, B. H., MOHR, P. A. and WILLIAMS, L.A.J. (1972): Geology of the eastern rift system of Africa. *Geol. Soc. America, Spec. Paper*, **136**, 67pp.

DEGENS, E.T., VON HERZEN, R.P. and WONG, H.K. (1971): Lake Tanganyika: water chemistry, sediments, geological structure. *Naturwissenschaften*, **58**, 229-241.

FAIRHEAD, J.D. and GIRDLER, R.W. (1971): The seismicity of Africa. *Geophys. J. R. Astr. Soc.*, **24**, 271-301.

FAIRHEAD, J.D. and GIRDLER, R.W. (1972) The seismicity of the African rift system. *Tectonophysics*, **15**, 115-122.

FOZZARD, P.M.H. (1960): Quarter degree sheet No. 124, "Kelema", 1:125,000. *Geol. Surv. Tanganyika.*

FOZZARD, P.M.H. (1961): Quarter degree sheet No. 123, "Kwa Mtoro", 1:125,000. *Geol. Surv. Tanganyika.*

JULIAN, W., LOUNSBERRY, W., TAMURA, A., VAN LOENEN, R. and WRIGHT, M.P. (1963): Quarter degree sheet No. 143, "Meia Meia", 1:125,000. *Geol. Surv. Tanganyika*

KING, B.C. (1970): Vulcanicity and rift tectonics in Africa. *In: Clifford, T.N. and Gass, I.G., eds., African magmatism and tectonics.* Edinburgh, Oliver and Boyd, 263-283.

LOUNSBERRY, W.A., VAN LOENEN, R.E. and HASLAM, H.W. (1967): Quarter degree sheet No. 142, "Bahi", 1:125,000. *Geol. Surv. Tanganyika.*

MCCONNELL, R.B. (1972): Geological development of the rift system of eastern Africa. *Geol. Soc. Am. Bull.*, **83**, 2549-2572.

MCCONNELL, R.B. (1974): Evolution of taphrogenic lineaments in continental platforms. *Geol. Rundsch.*, **63**, 389-430.

MOORE, J.G. (1960): Curvature of normal faults in the Basin and Range province of the western United States. *U.S. Geol. Surv. Prof. Paper*, **400B**, 409-411.

MUDD, D.C. and ORRIDGE, G.R. (1966): Quarter degree sheet, No. 85, "Babati", 1:125,000. *Geol. Surv. Tanganyika.*

ORRIDGE, G.R. (1965): Quarter degree sheet, No. 69, "Mbulu", 1:125,000. *Geol. Surv. Tanganyika.*

PICKERING, R. (1965): Quarter degree sheet, No. 53, "Ngorongoro", 1:125,000. *Geol. Surv. Tanganyika.*

SEARLE, R.C. (1970): Evidence from gravity anomalies for thinning of the lithosphere beneath the rift valley in Kenya. *Geophys. J. R. Astr. Soc.*, **21**, 13-31.

SELBY, J. and MUDD, G.C. (1965): Quarter degree sheet No. 104, "Kondoa", 1:125,000. *Geol. Surv. Tanganyika.*

THOMAS, C.M. (1966a): Quarter degree sheet, No. 103, "Balangida Lelu", 1:125,000. *Geol. Surv. Tanganyika.*

THOMAS, C.M. (1966b): Quarter degree sheet, No. 84, "Hanang", 1:125,000. *Geol. Surv. Tanganyika.*

YAIRI, K. (1974): En echelon pattern of the East African Rift System. *Jour. Afr. Studies,* **14**, 21-46 (in Japanese with English abstract).

YAIRI, K. (1975a): Geometry and mechanics of en echelon faulting with applications to the East African Rift System. *1st Prelim. Rep. Afr. Studies, Nagoya Univ.*, 29-38.

YAIRI, K. (1975b): Fault pattern and crustal extension of the Kavirondo rift valley in relation to a bifurcating rift model. *1st. Prelim. Rep. Afr. Studies, Nagoya Univ.*, 39-43.

Preliminary Account of the Lake-floor Topography of Lake Malawi in Relation to the Formation of the Malawi Rift Valley

Kenji YAIRI*

* Department of Earth Sciences, Faculty of Science, Nagoya University

Introduction

Lake Malawi is the second deepest of the African lakes, next to Lake Tanganyika. The lake level is in a height of 474 m above sea level and the deepest part of the lake floor reaches a depth of 706m below lake level. The highest level of the uplifted plateaus surrounding the Lake stands at heights 2000 m to 2500 m above sea level. The northern half of the Lake is demarcated by precipitous escarpments and the lake side has practically no littoral except at river mouths. Genetically these geomorphological features are closely related to the formation of the Malawi Rift Valley, which forms a part of the East African Rift System (Dixey, 1956).

In this paper is outlined the lake-floor topography as read from bathymetric charts of Lake Malawi available to the writer, and its close relation to the formation of the rift valley is discussed briefly based on the geological data on the rift fault pattern.

Bathymetric charts of Lake Malawi

Lake Malawi has played an important role in the transport by ship; the 620-ton motor vessel "Ilala II" cruises regularly between Monkey Bay in the south and Kambwe, north of Karonga, in the north. On this account, navigation charts mapped at various scales are ready for public and private use in the Department of Surveys, Malawi. They were originally published by the Director of the Federal Department of Trigonometrical and Topographical Surveys, Rhodesia and Nyasaland (1963). The following sixteen sheets of bathymetric chart are available at present: "Lake Nyasa" at a scale of 1:625,000; "Lake Nyasa" containing three sheets at a scale of 1:250,000; 12 sheets at various scales ranging from 1:72,000 to 1:3960 which cover most of imporatant harbors.

Most of the charts are based on the sounding data along lines at an interval of about 5 km in the larger scaled-charts and at about 50 m in the smaller scalled-ones. The measurements of depth are plotted at the sounding points on the charts in fathom (1 fathom = 6 feet = 1.829 m). The charts are intended only to show the general trend of contours of the Lake, and contoured mostly at an interval of 50 fathoms, except near the lakeshore where they are contoured at intervals of 3 to 10 fathoms.

The seasonal variation in the level of the Lake is reported to be as large as one fathom (Pike, 1972). The long-term fluctuation in the lake-level, which has been recorded since 1896, has attained to 3 fathoms ranging from 1538 feet, the lowest level recorded, to over 1556 feet, the highest (*ibid.*). The present lake level is at a relatively higher level in the range of the long-term fluctuation. On the navigation charts the lake-level is reduced to a height of 1546.5 feet above mean sea level.

For the purpose of the present study, all contours were redrawn at intervals of 10 to 20 fathoms, occasionally at 2 fathom-intervals at need. Based on these revised bathymetric charts (Fig. 2 to 18), characteristic features of the lake-floor topography are described be-

2nd Prelim. Rep. Afr. Studies, Nagoya Univ., 51-69, 1977.

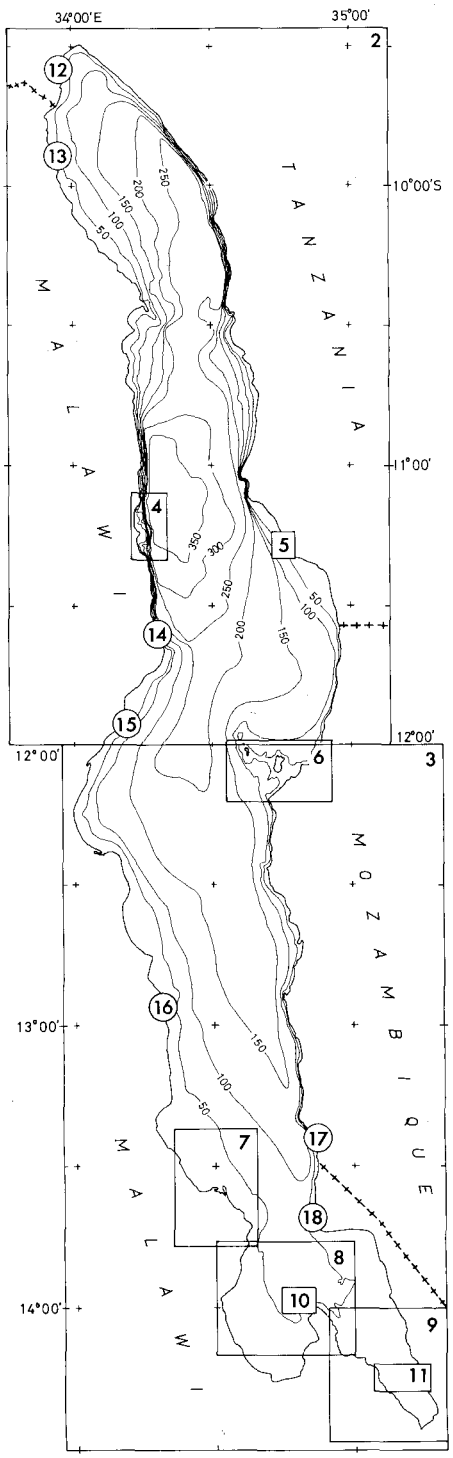

Fig. 1
Bathymetric chart of Lake Malawi (contour interval: 50 fathoms). Location number corresponds to the number of text-figure.

low. In each description, N.C. and numbers in the parentheses succeeding the number of text-figure represent the sheet numbers of original navigation charts from which each text-figure was compiled.

Fig.1, 2 and 3 (N.C. 13, 14, 15 and 16), Lake Malawi:

Lake Malawi is 570 km in the north-south elongation and about 50 km, up to 90 km in the central part, in width. The Lake Malawi basin is typically asymmetrical in the east-west underwater profile (Pike, 1972). In the northernmost part, the axis of the basin elongated in the direction of NW-SE is largely shifted toward the eastern shore, where the steep underwater slope is the continuation of the escarpment along the Livingstonia Mountains Fault. On the other hand, between lat. 11°S. and 11°30'S., the deepest part flanked by the steep underwater slope on the west runs closely adjacent to the escarpments bounding the Vipya and Kandoli mountains. To the south of lat. 12°S. the basin axis jumps again to near the eastern lakeshore. In short, the lake-floor tends to tilt toward either side of the lakeshores.

The Lake Malawi basin appears to be composed of a series of semi-closed sub-basins of much smaller scale which are elongated in the direction of NNW-SSE. Each sub-basin is separated by a sort of topographic barrier which is expressed as a swell on the lake-floor. Thus, three sub-basins are distinguishable at least: the northern, central and southern sub-basins. The northern sub-basin is separat-

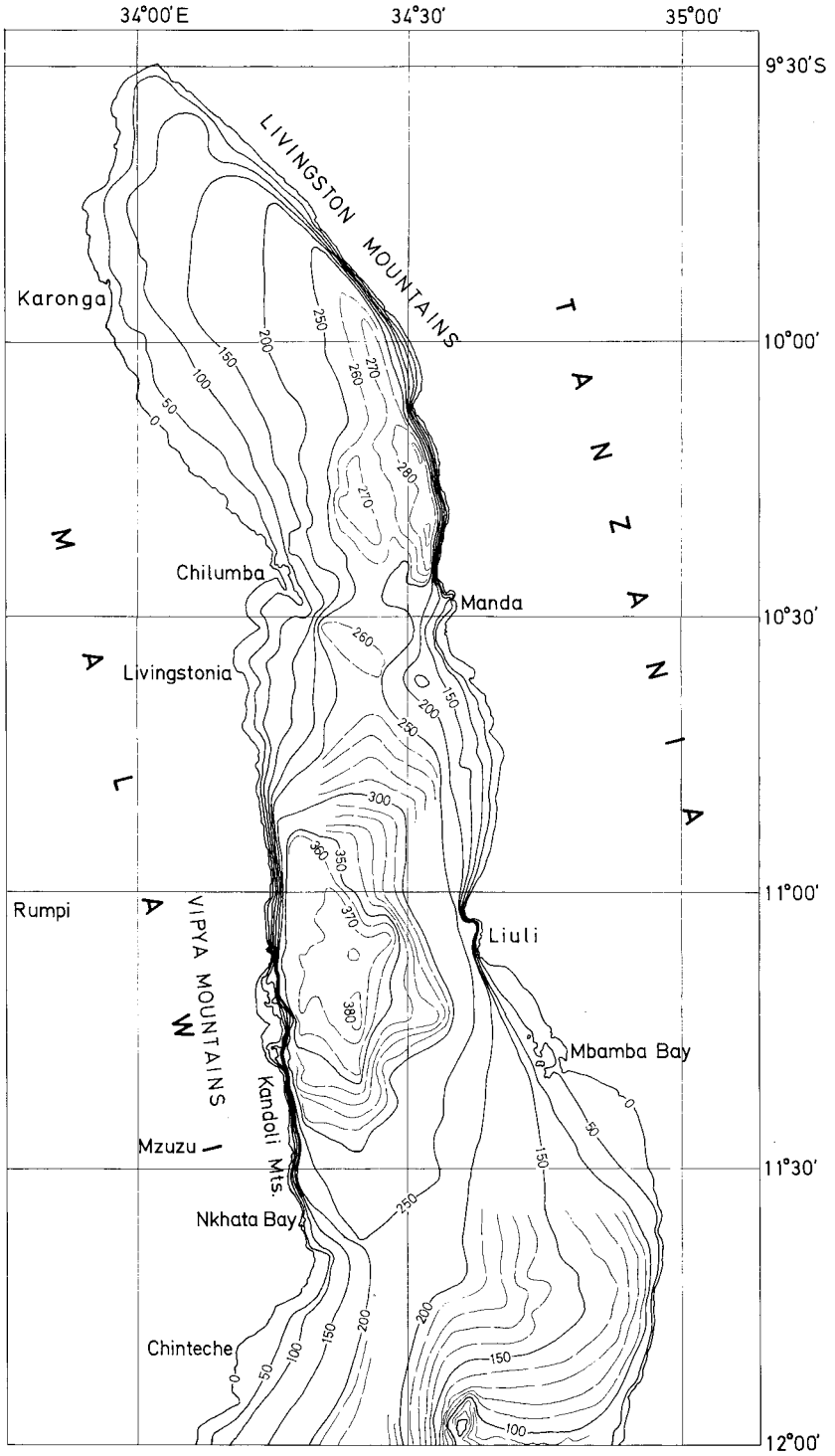

Fig. 2
Bathymetric chart of Lake Malawi North (contour interval: 50 fathoms, partly 10 fathoms).

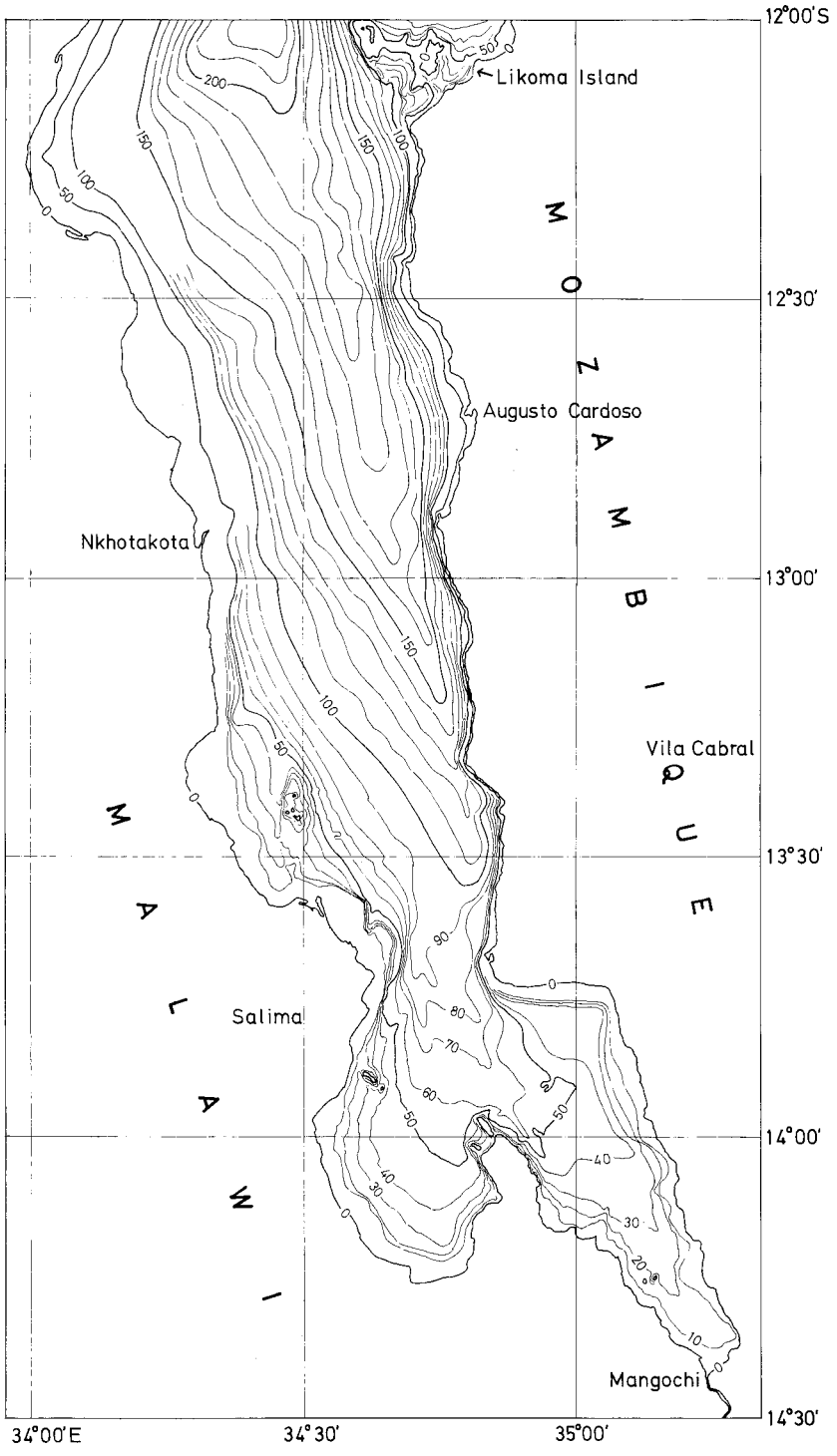

Fig. 3

Bathymetric chart of Lake Malawi South (contour interval: 10 fathoms, partly 50 fathoms).

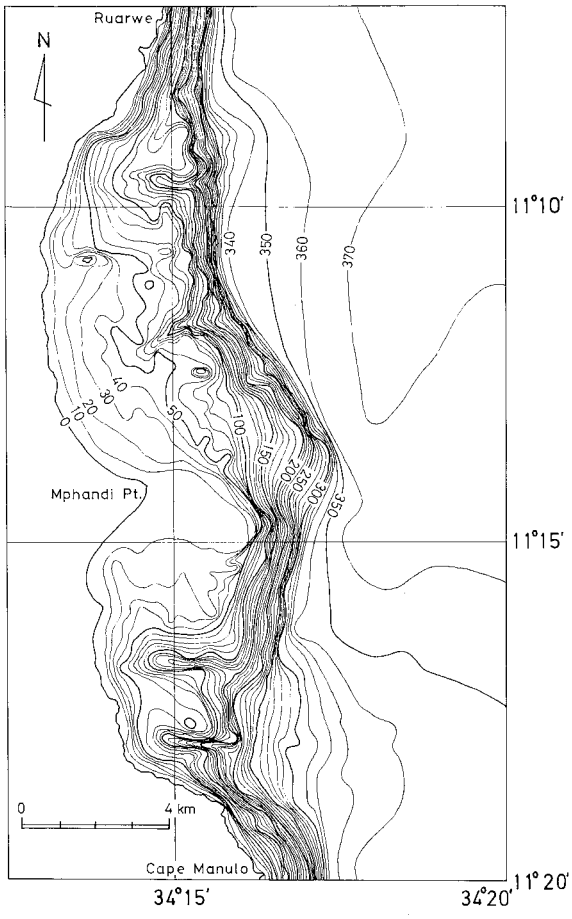

Fig. 4

Bathymetric chart of Ruarwe to Cape Manulo (contour interval: 10 fathoms).

ed from the central sub-basin by a barrier extending from Chilumba toward the southeast, and the latter sub-basin is separated from the southern one by a barrier extending from Nkhata Bay to Likoma Island.

Fig. 4 (N.C. 8), Ruarwe to Cape Manulo:

In this chart covering a part of the western margin of the central sub-basin, three distinctive topographic units are recognized: a relatively flat, gentle slope zone descending from the lakeshore down to a depth of 100 fathoms; a steep slope zone between 100 and 330 fathoms; an extremely flat lake-floor below a depth of 330 fathoms. The formation of the steep slope zone must be attributed to the major rift faulting.

A striking feature of the slope zones is the submerged valley which frequently cuts into both of the gentle and steep slope zones. The upper reaches of these underwater valleys can be traced into the valleys on the land without exception. They bear a close resemblance to the submarine canyons found in the sea floor. To the east of the area shown in the chart, Malawi lake attains its greatest depth, 386 fathoms (706 m).

Fig. 5 (N.C. 4), Mbamba Bay;

The underwater topography of the eastern margin of the central sub-basin is complicated near Mbamba Bay because of the disposition of Ngkuyo Island, Ngkuyo Reef and Rhoades Bank, which seem to be submerged inserbergs. A steep slope zone trending NNW-SSE is recognizable along the lakeshore extending from Tumbi Point to the western slope of Mbamba Hill, and may be attributed to the major rift faulting. Below a depth of 90 fathoms bathymetric contours represent the general trend of NNW-SSE of the central sub-basin.

Fig. 6 (N.C. 9), Likoma Islands:

As pointed above, the central sub-basin is separated from the southern sub-basin by a line linking Likoma-Chisumulu Islands and Nkhata Bay to the northwest across the Lake. Along the western slope of a series of rises represented by Chisumulu Island is presumed a fault trending NNW-SSE.

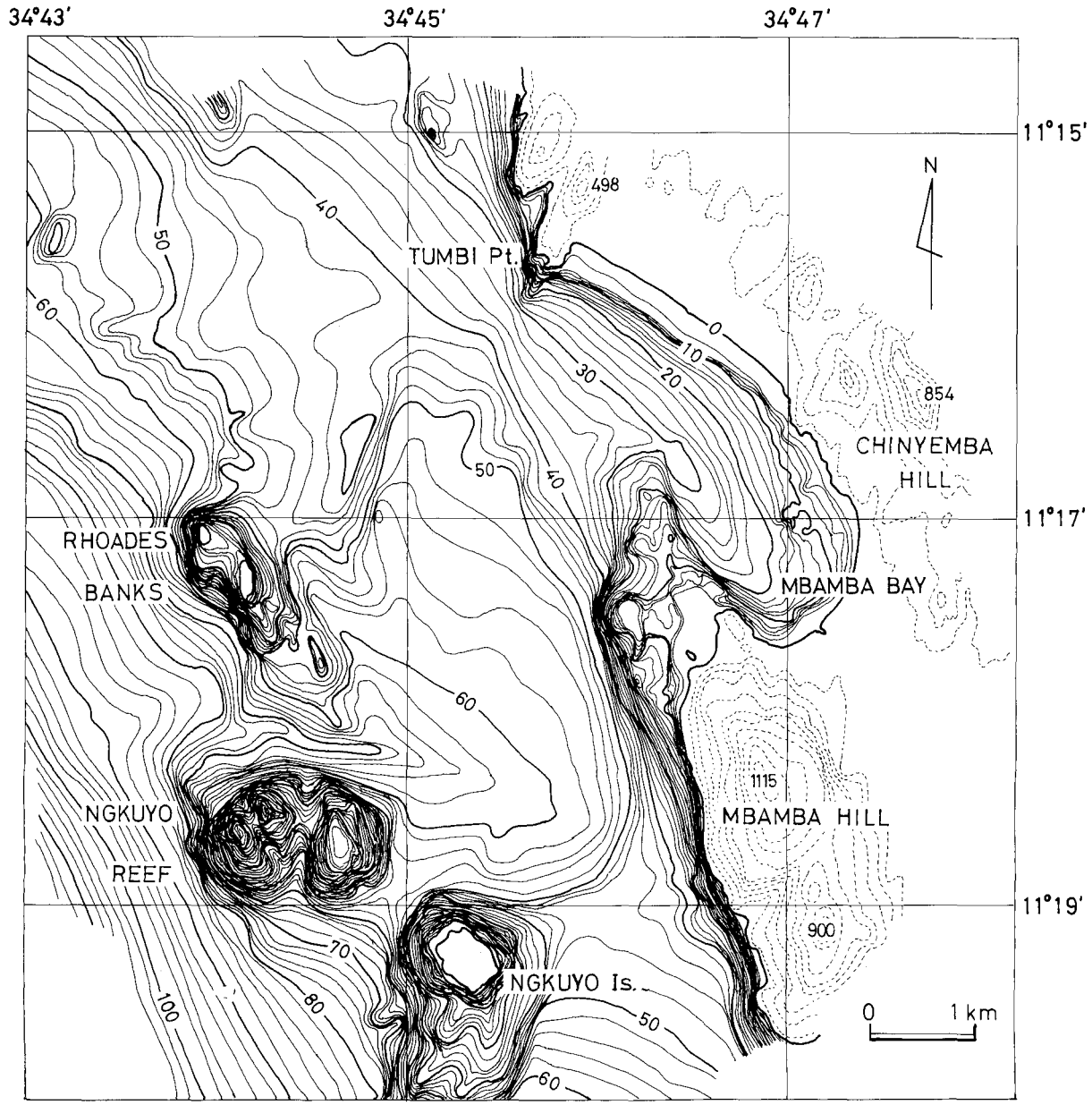

Fig. 5

Bathymetric chart of Mbamba Bay and its environs (contour interval: 2 fathoms). Heights on the land are in feet, contours shown by dotted lines.

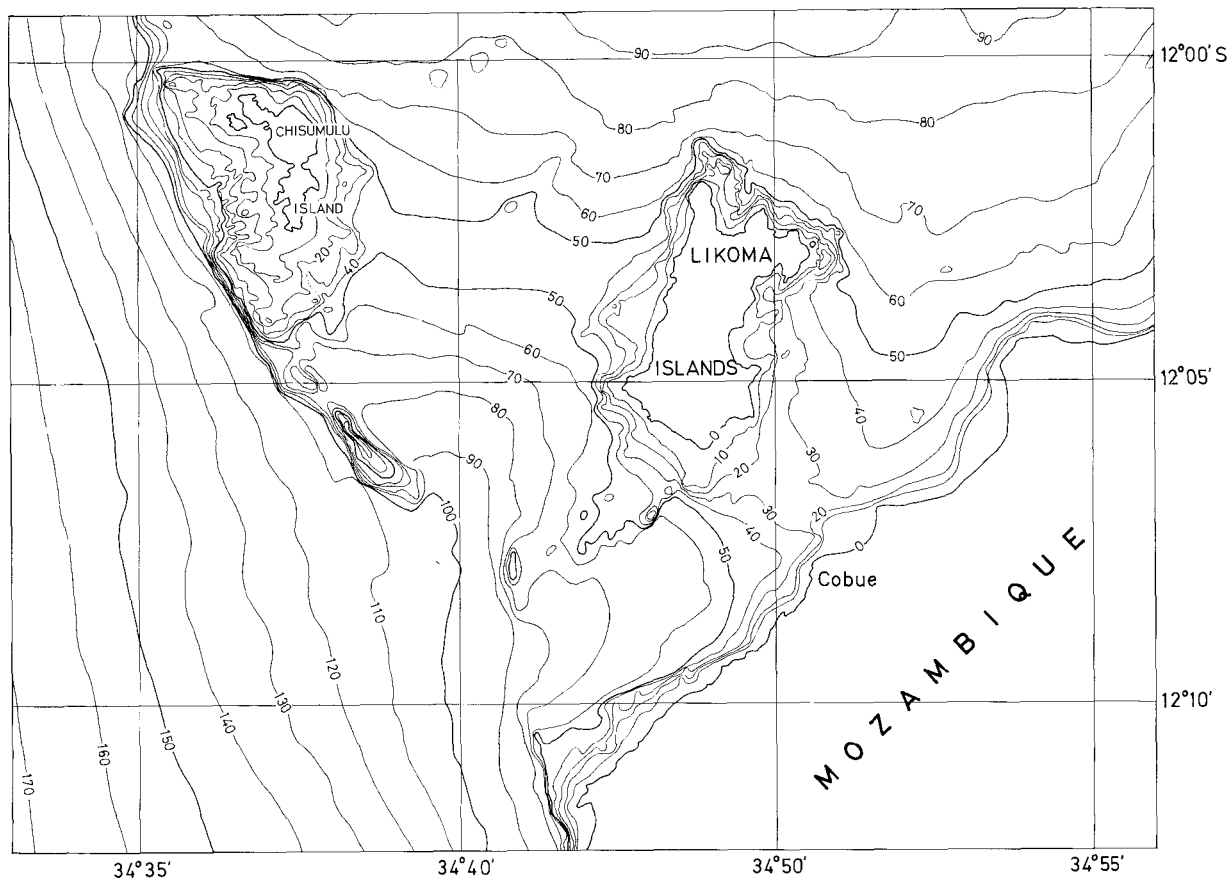

Fig. 6
Bathymetric chart around Likoma and Chisumulu Islands (contour interval: 2 fathoms).

Fig. 7 (N.C. 10), Mbenji Island:

A series of steep slopes can be seen on the lake-floor not so far from the shore: NS-trending slope on the west of Mbenji Island, WNW-trending one on the north of Sungu Point and NS-trending one on the east of Senga Bay. They are probably topographic manifestations of fault movements. Mbenji Island seems to be on a faulted and uplifted block tilting toward the east, which is bounded on the west by a gently curved, NS-trending fault downthrown to the west. This fault truncates apparently the general trend of the lake slope of NNW-SSE, and may be an expression of a younger phase of rift-faulting.

Fig. 8 (N.C. 6), Chipoka to Monkey Bay:

The Nankumba Peninsula is bounded on the both sides by distinctive steep underwater slopes trending NW-SE. The trends of the slopes appear to follow closely the geological faults on the land, one of which is known as Lisangadzi Fault (Dawson and Kirkpatrick, 1968). The Nankumba Peninsula is considered to form a horst structure in the rift depression together with Nangoma and Maleri Islands to the northwest. Zimbawe Rock and Mumbo Island seem to be sumberged inserbergs (*see* Fig.10).

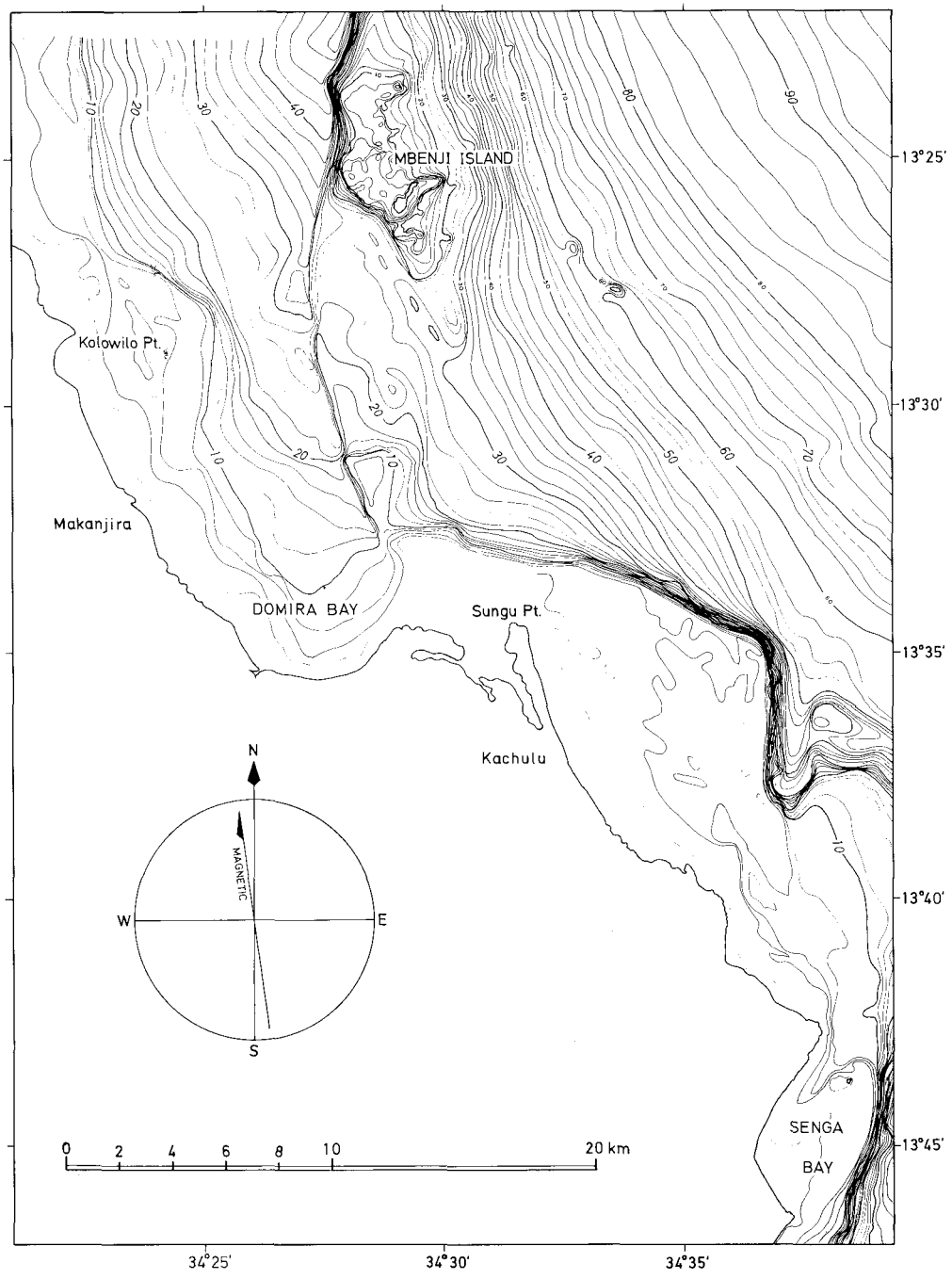

Fig. 7
Bathymetric chart of Mbenji Island to Senga Bay (contour interval: 2 fathoms).

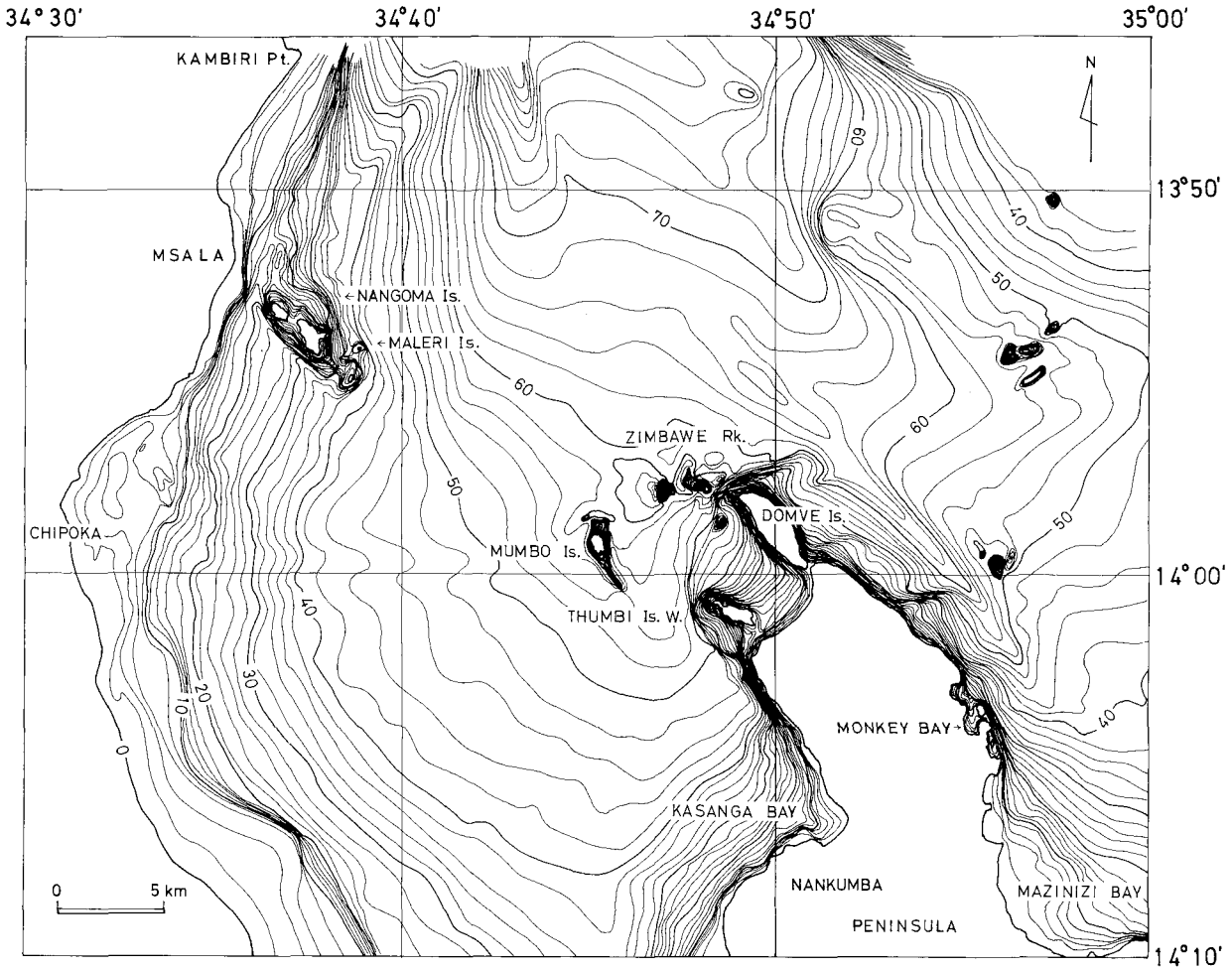

Fig. 8

Bathymetricchart of Chipoka to Monkey Bay (contour interval: 2 fathoms).

Fig. 9 (N.C. 7), Monkey Bay to Mangochi:

The striking feature read from this chart is a relatively shallow and flat lake floor, though it is slightly disturbed by the disposition of submerged inserbergs such as Boadzulu Island and its surroundings (*see* Fig. 11). On the land east of the Lake are confirmed two sub-parallel faults trending NNW-SSE; one follows approximately the eastern shoreline and the other, Namizimu Fault, runs about 8 km east of the former (Holt, 1961). The Namizimu Fault is one of the major rift faults forming the eastern wall of the Malawi Rift Valley. The outlet of Lake Malawi to the Shire River originates at the southern end of the lake to the north of Mangochi.

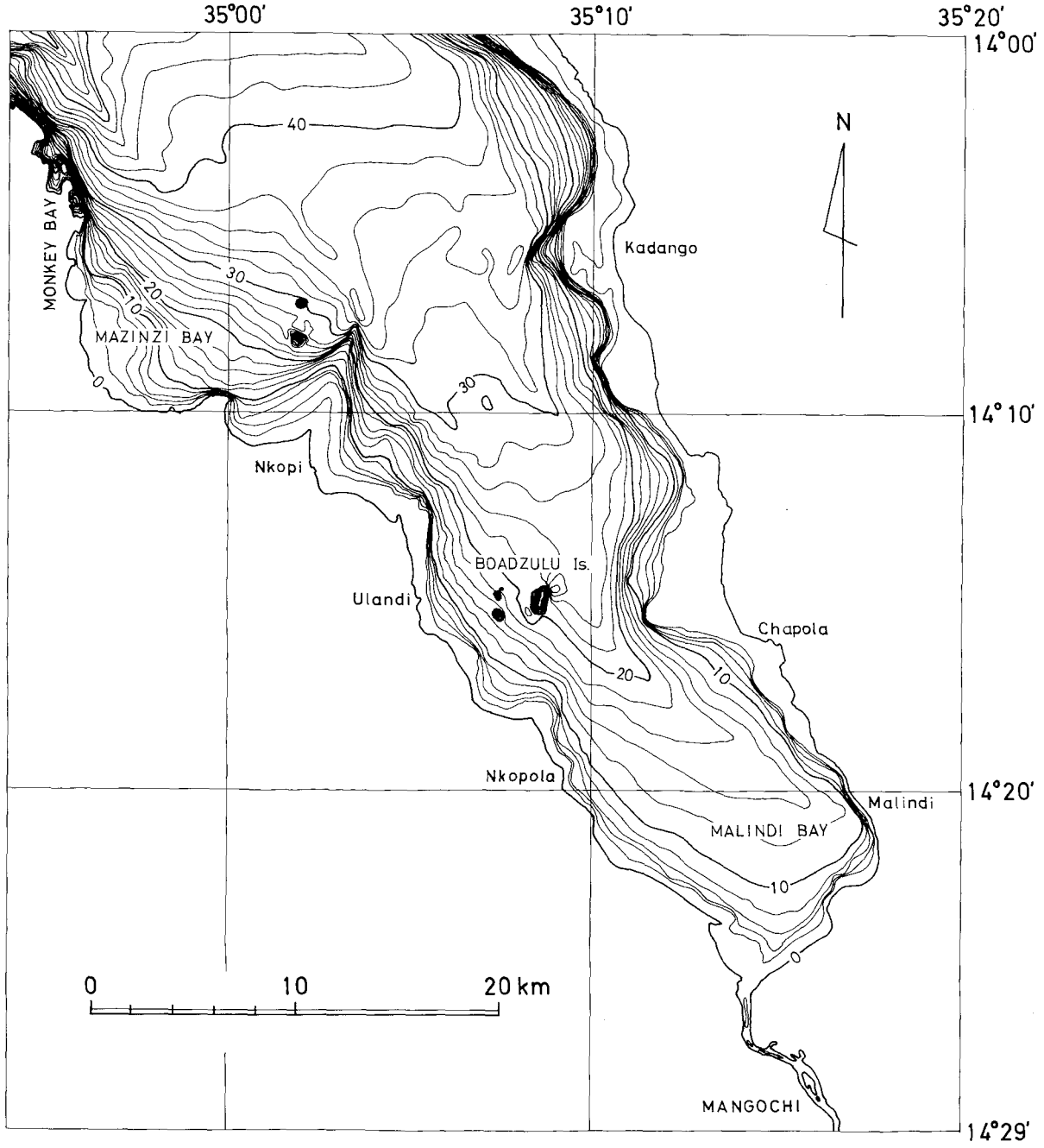

Fig. 9
Bathymetric chart of Monkey Bay to Mangochi (contour interval: 2 fathoms).

Fig. 10 and 11 (N.C. 6 and 11), Mumbo Island, Zimbawe Rock and Boazulu Island:

We can find a characteristic underwater topography around these islands or reef, which are considered to be submerged inserbergs as suggested already; that is, the inserberg is moated by a depression deeper than the surrounding lake-floor. The contours of the depression appear to be disposed concentrically centering around each inserberg. It is considered, though still a matter of conjecture because of scarcity of sounding data, that these concentric features of underwater topography is indicative of the ring struture of quartz-syenites enclosing granites, which is developed extensively in the Nankumba Peninsula (Dawson and Kirkpatrick, 1968). Holt (1961) regards the Boadzulu Island as an eroded remnant of a fault block as already pointed out in the explanation of Fig. 9.

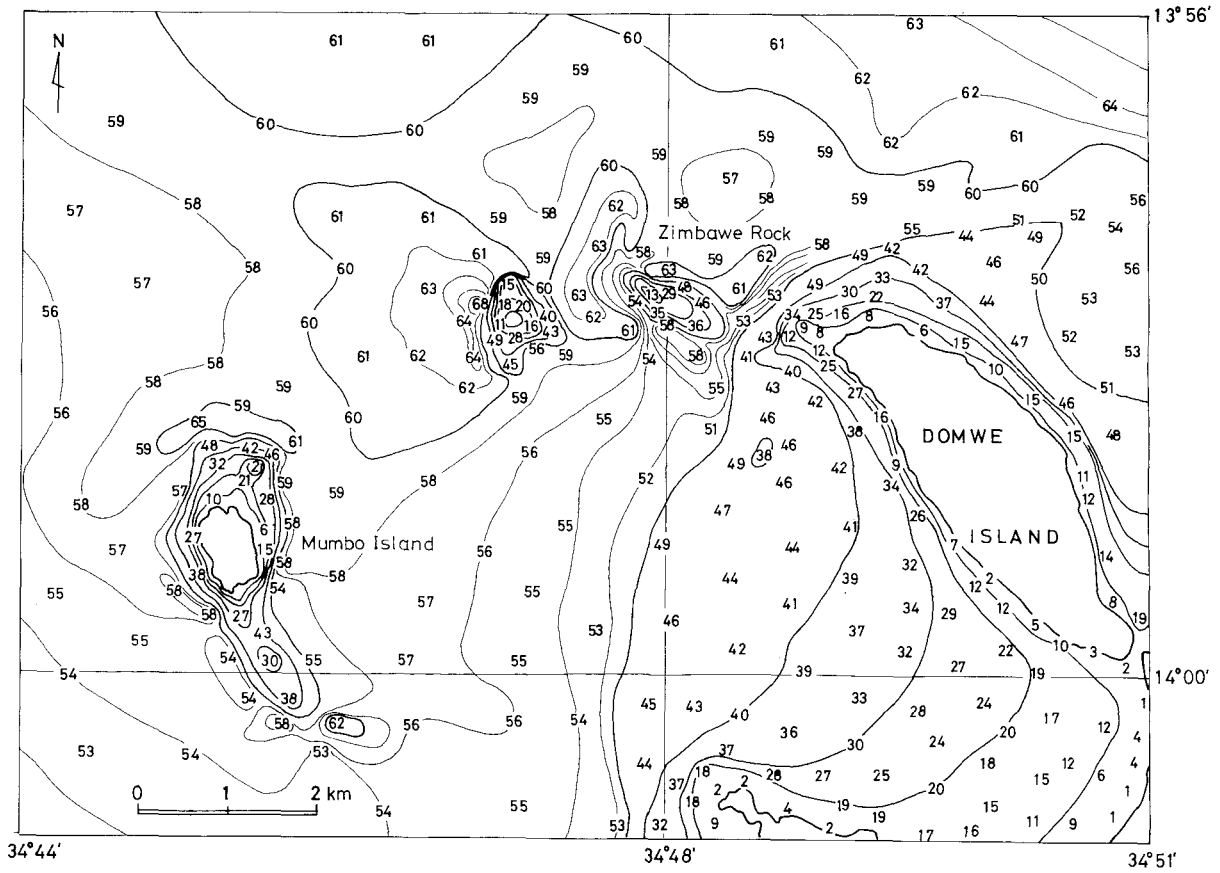

Fig. 10

Bathymetric chart around Mumbo Island and Zimbawe Rock (contour interval: 2 fathoms, partly 10 fathoms).

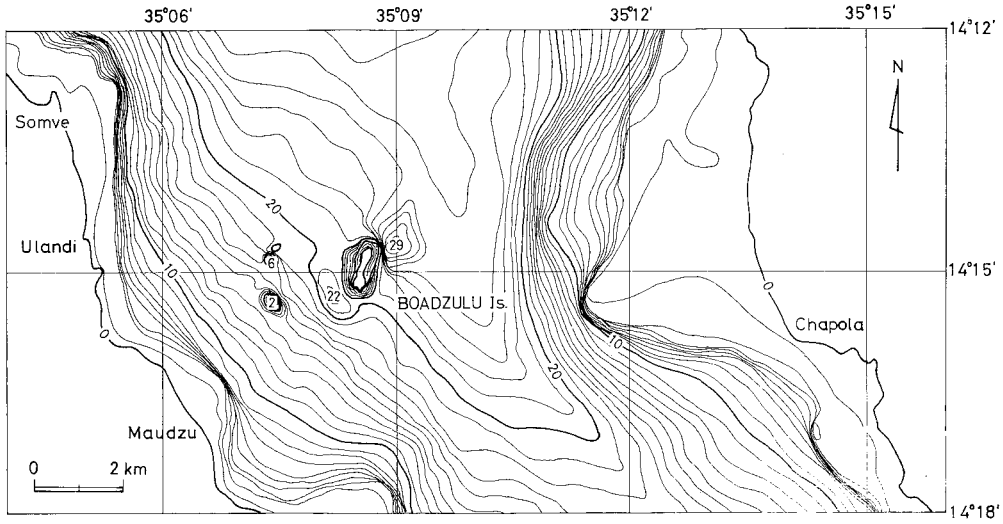

Fig. 11
Bathymetric chart around Boadzulu Island (contour interval: 1 fathom).

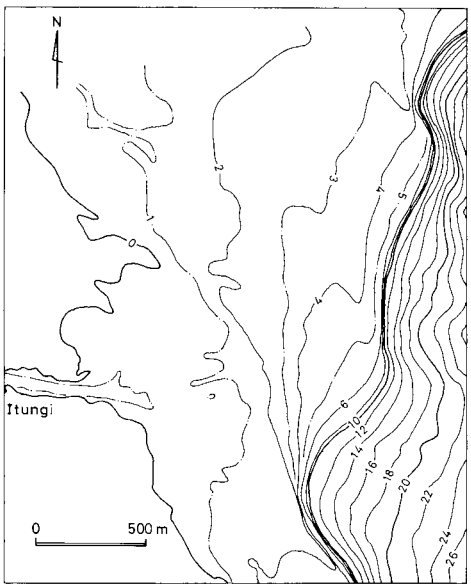

Fig. 12
Bathymetric chart near the shore of Itungi (contour interval: 2 fathoms, 1 fathom above 6 fathoms).

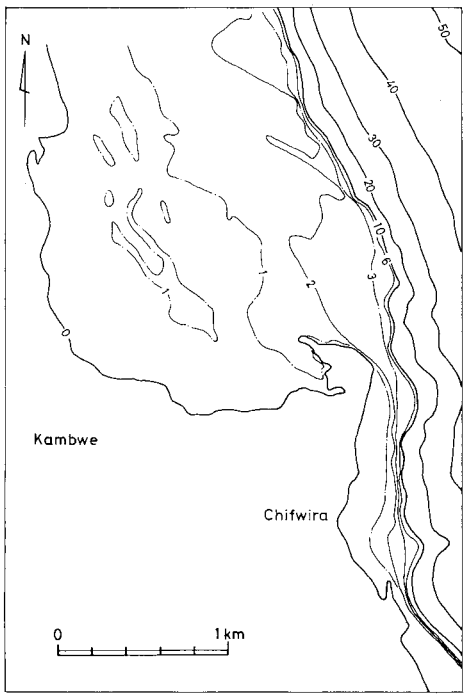

Fig. 13
Bathymetric chart near the shore of Kambwe (contour interval: 10 fathoms, 1 fathom above 3 fathoms).

Figs. 12, 13, 15, 16 and 18 (N.C. 1, 2, 5 and 11), Itungi, Kambwe, Bandawe, Nkhotakota, Makanjira Point:

These charts at relatively larger scales provide a detailed underwater profile to be drawn close to the shore. A feature common to all the charts is an abrupt change of slope inclination between a very flat surface along the shore and a lake slope descending from a few kilometers off the shore toward the basin axis. The inflection line between the two slopes lies in a depth of 3 fathoms or so, never exceeding 5 fathoms. This depth corresponds to the range of the long-term fluctuation of lake-level; the inflection line on the lake slope must show an ancient shoreline.

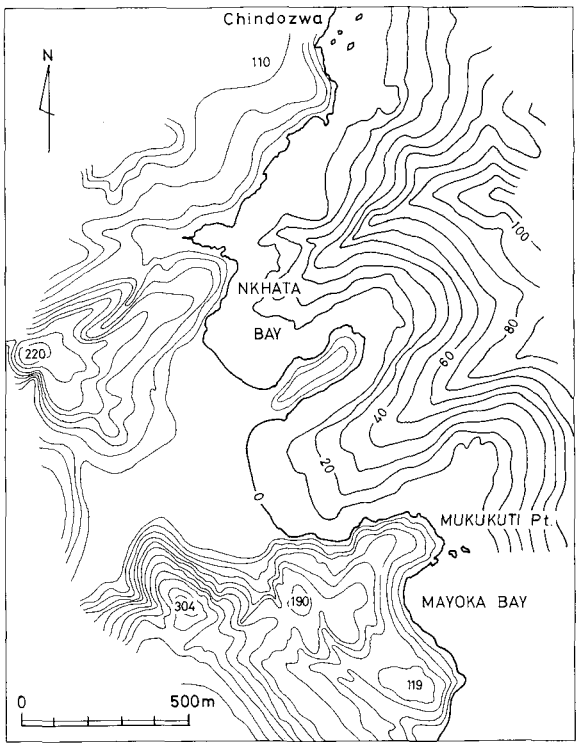

Fig. 14

Bathymetric chart of Nkhata Bay and its environs (contour interval: 10 fathoms). Heights on the land are in feet, contours shown by fine lines.

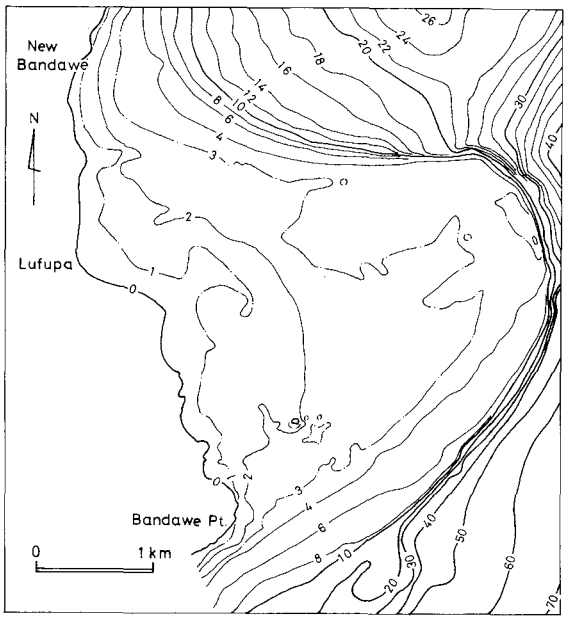

Fig. 15

Bathymetric chart near the shore of Bandawe (contour interval: 2 fathoms, 1 fathom above 4 fathoms).

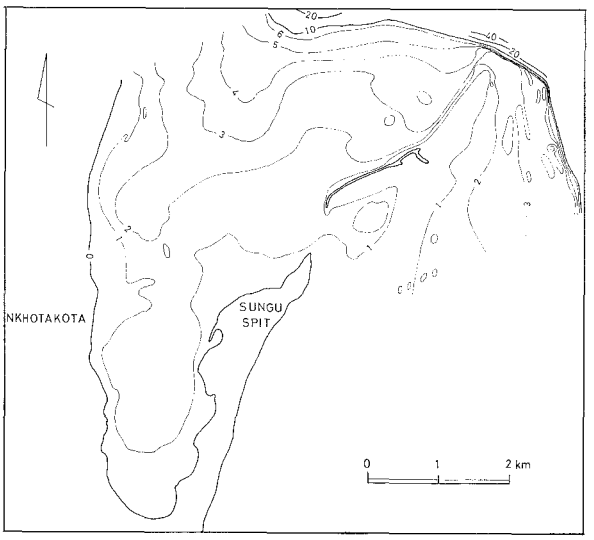

Fig. 16

Bathymetric chart near the shore of Kkhotakota (contour interval: 10 fathoms, 1 fathom above 6 fathoms).

Fig. 14 (N.C. 3), Nkhata Bay:

There can be seen typical submerged valleys on the lake slope of the Nkhata Bay area. The upper reaches of the underwater valleys are traceable into valleys on the land.

Fig. 17 (N.C. 12), Meponda:

The chart shows the development of linear steep slope below lake level, which demarcates a part of the eastern margin of the southern sub-basin. Along the steep slope is presumed a NW-trending fault.

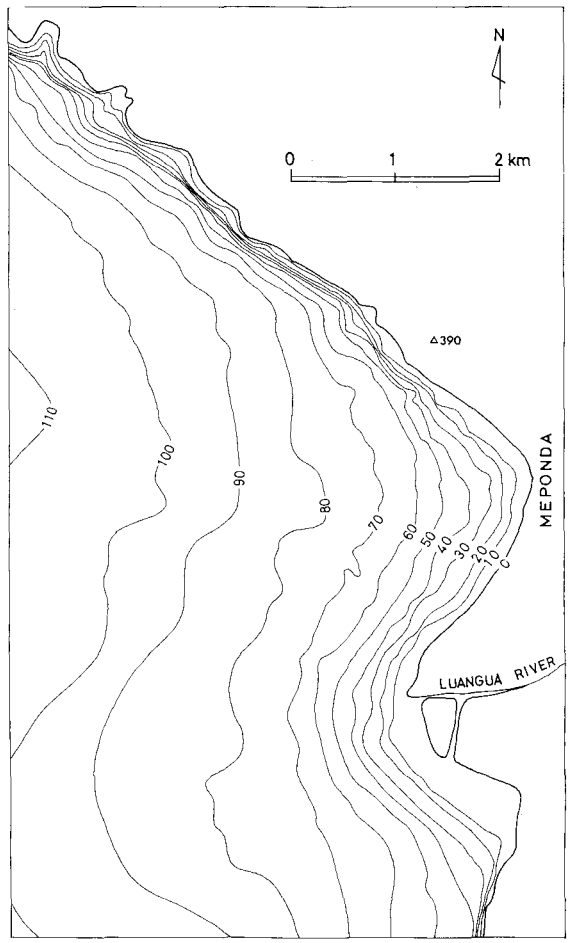

Fig. 17

Bathymetric chart Meponda and its environs (contour interval: 10 fathoms).

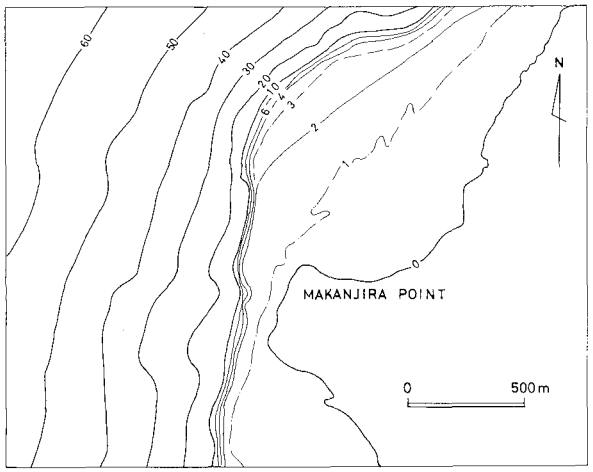

Fig. 18

Bathymetric chart near the shore of Makanjira Point (contour interval: 10 fathoms, 1 fathom above 4 fathoms).

The Malawi Rift Valley

The northern two-thirds of the Malawi Rift Valley are occupied by Lake Malawi as shown in Fig. 19, in which the distribution and trends of the major rift faults are superimposed according to Geological Map of Malawi (Bloomfield, 1966), Provisional Geological Map of Malawi (Carter and Bennett, 1973), and the present study. The present outline of the Lake is strongly controlled by the trend of the rift-faults, though most of them are now submerged beneath the Lake.

Based on the descriptions of bathymetric charts given above, some characteristics of the lake-floor topography are summarized as follows:

1) The Lake Malawi basin comprises a series of semi-closed sub-basins, each of which is elongated in the direction of NNW-SSE.

2) Each sub-basin displays an asymmetrical profile in the east-west direction, that is, it is bounded on one side by a prominent marginal steep slope.

3) The central part of the lake-floor shows a distinctive flatness, gently tilting toward one side. Generally the boundary between the flat lake-floor and the marginal steep slope is sharp.

4) Cutting into the marginal steep slope can be seen submerged valleys upper reaches of which are traceable into the valleys on the land.

5) A characteristic topography bearing a close resemblance to those of inserbergs on the land can be seen on the lake-floor saved from burial by sediments.

6) Most of submerged escarpments, along which faults are presumed, trend NW-SE to NNW-SSE except those which trend N-S along the western lakeshore between lat. 10°45′ and 11°30′S.

In considering the influence of tectonic movements on the lake-floor topography, modificatory effects by sedimentation should be taken into account, though we have no information concerning sediments on the lake bottom. It is uncertain whether the asymmetrical basin structures are tectonic or sedimentary in origin. Several topographic features mentioned above, for example 2), 4), and 5), however, seem to provide the justification to consider that there has been little modification of the tectonically originated lake-floor by sedimentation. Thus, the asymmetrical basin structures characterized by unilateral tilting of the lake-floor may safely be attributed to the major faults on one side and to monoclinal flexures or minor faults on the other. The same reason applied to regard that the formation of basins associated with faulting took place in a relatively younger phase of tectonic movements, probably in the Neogene age.

As is evident from Fig. 19, there exists a close parallelism between major rift-faults evidenced geologically and those revealed from the lake-floor topography. By combining these evidences derived independently, the outline of the basin structures can be defined more clearly. The Lake Malawi basin comprises four semi-closed sub-basins which, represented by a dotted area in Fig. 19, are elongated in the direction of NNW and arranged en echelon. The southern sub-basin as termed above is composed of two sub-basins partly overlapping one another. One more sub-basin or graben structure is postulated to the south of Lake Malawi. It is a portion of what has been the Shire Rift Valley (McConnell, 1972), where the rift floor is accentuated by an extensive erosion of the Shire River and by NW-trending faults

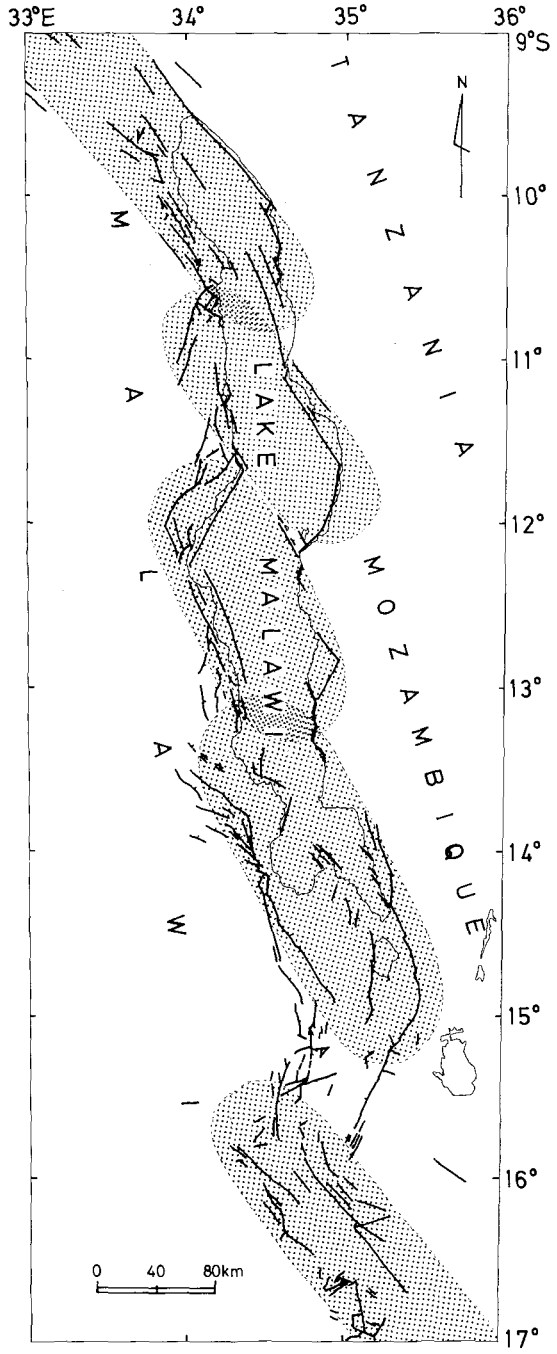

Fig. 19

The Malawi Rift Valley and its fault pattern. Faults compiled after Bloomfield (1966), Carter and Bennett (1973), and the present work. Dotted, extent of sub-basin or graben structures.

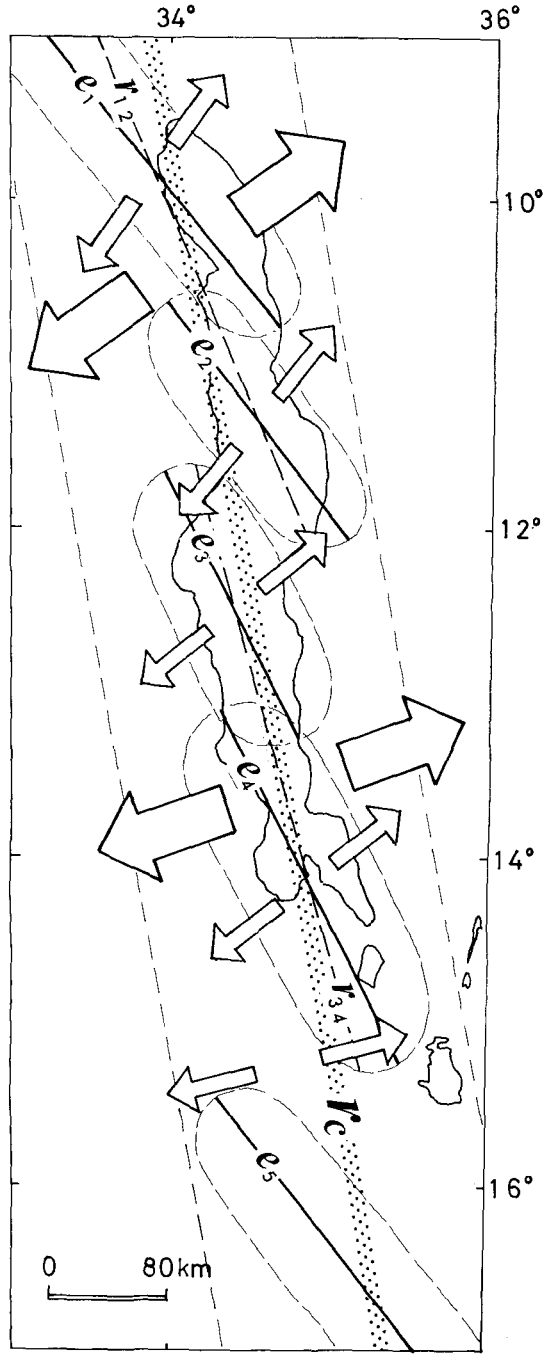

Fig. 20

Crustal extension across the Malawi Rift Valley (*see text*).

such as the Thyolo Fault (Habgood and Holt, 1973) and Mwanza Fault (Habgood, 1963) which bound the Shire valley on the east.

Brock (1966, 1972) points out that the irregularities in the configuration of the Lake, including two radical kinks in the central part, suggest five or six crustal prisms. Each crustal prism is approximately identical, at least in size, to the semi-closed sub-basins described here.

Generally individual basin structure is bounded by major faults on the northeast and southwest, but its northwestern and southeastern margins are not always defined by faults. It is considered that NE-trending faults bounding occasionally the basins on the northwest and southeast may be attributed to subsidiary faults which may have occurred in a progressive phase of the deepening of the basins.

Under an assumption that these basin structures are products of tension tectonics caused by the horizontal extension of crust, which is applied to the Gregory Rift Valley in Kenya and Tanzania (Yairi, 1975ab, 1977), we can estimate the direction of the horizontal extension across the Malawi Rift Valley according to the method of Yairi (1974, 1975) based on the geometry of en echelon faulting. The following terminology is here used for en echelon pattern: the term row expresses the orientation of the belt which comprises en echelon structures, the individual structural units are termed elements, and the angles between the row and the elements are abbreviated to RE-angles (Yairi, 1975).

In Fig. 20 the longitudinal axes of five elongated sub-basins or graben structures are illustrated as five elements; e_1, e_2, e_3, e_4, and e_5 from north to south. The row through all the five elements is not a straight line, but it seems that the row of e_1 and e_2, designated $r_{1,2}$, and that of e_3 and e_4, $r_{3,4}$, are arranged en echelon together with one more element e_5. A common row through these newly defined three elements, $e_{1,2}$ ($=r_{1,2}$), $e_{3,4}$ ($=r_{3,4}$), and e_5, represents a straight line, being designated r_c. Thus, the directions of crustal extension are obtained from RE-angles and en echelon pattern ("Italic m" type; *see* Yairi, 1975). The results are shown by arrows in Fig. 20; large open arrows represent the results obtained from $e_{1,2}$ and $e_{3,4}$ with reference to r_c; small arrows from e_1 and e_2 to $r_{1,2}$, and e_3 and e_4 to $r_{3,4}$, respectively.

The directions of extension revealed from smaller scale rows and elements are more or less normal to the NW-trending rift-faults parallel to the axis of individual sub-basin structure, while those from larger scale ones are normal rather to the principal axis of row, r_c. These facts suggest that en echelon arrangement of the semi-closed sub-basin structures may have been controlled by a regional stress field originated by the horizontal crustal extension, approximately N60°E-S60°W in trend, and that the rift-faulting may have been taken place under a local stress state reorientated in a zone to be fractured along the margin of the individual sub-basin.

In the offset area intervened by e_4 and e_5, the boundary faults of the rift valley show en echelon pattern of "backhand writing m" type, especially on the western wall, where the elements trend slightly east of north and their row does NNE. The geometry of the pattern postulates the crustal extension across this segment to be in the direction of ENE-WSW, which is in good concordance with that for the element $e_{3,4}$ immediately to the north.

The belt, about 180 km in width, which involves all basin structures arranged en

echelon, must have played an important role as an unstable, mechanically weak zone between two relatively rigid plates when the rifting took place. The belt trending N10°W, represented by r_c, is approximately parallel to the general trend of the late Proterozoic-early Paleozoic Mozambique orogenic belt, and intimates the existence of the "perennial deep lineament" proposed by McConnell (1972).

Summary

1. In order to clarify the tectonic influence of the formation of the Malawi Rift Valley on the lake-floor topography, the bathymetric charts of Lake Malawi are newly contoured on the basis of sounding data available to the writer (Figs.1 to 18). The underwater topography seems to manifest directly the tectonic reliefs free from little modifications by sedimentation. This feature is strongly suggestive of the origin by a young tectonic movements.

2.From the rift-fault pattern obtained geologically as well as that shown by underwater topography, it is concluded that the Lake Malawi basin consists of four semi-closed sub-basin structures elongated in the direction of NNW and arranged en echelon. The Malawi Rift Valley, as generally termed, comprises these four basin structures and a graben structure along the Shire River (Fig. 19).

3. Each basin or graben structure has a typically asymmetrical east-west profile, which is originated tectonically; major faults trending NNW to NW define the basins or grabens either on the northeast or on the southwest. On the other hand, the NE-trending faults bounding occasionally the basins on the northwest and southeast may be attributable to subsidiary faulting which may have occurred at the progressive phase of the deepening of the basins.

4. Based on the geometry of en echelon faulting, the directions of crustal extension across the Malawi Rift Valley are obtained as shown in Fig. 20. The regional extension is in the direction of ENE-WSW.

Acknowledgements—The author wishes to thank Dr. Yukiyasu Saka of Waseda University for his kindness in critically reading this manuscript and offering constructive suggestions. The author wishes to express his thank to the Government of Malawi for permission to use the navigation charts of Lake Malawi for the purpose of the present study.

References

BLOOMFIELD, K. (1966): Geological map of Malawi; scale 1: 1,000,000. *Geol. Surv. Malawi*.

BROCK, B.B. (1966): The rift valley craton. *Geol. Surv. Canada Paper,* **66-14**, 99-123.

BROCK, B.B. (1972): *A global approach to geology.* A.A. Balkema, Cape Town, 365pp.

CARTER, G.S. and BENNETT, J.D. (1973): Provisional geological map of Malawi; scale 1:1,000,000. *Geol. Surv. Malawi.*

DAWSON, A.L. and KIRKPATRICK, I.M. (1968): The geology of the Cape Maclear Peninsula and lower Bwanje Valley. *Bull. Geol. Surv. Malawi,* **28**, 71pp.

DIXEY, F. (1956): The East African Rift System. *Bull. Suppl. Geol. Miner. Res.*, **1**, 77pp.

HABGOOD, F. (1963): The geology of the country west of the Shire River between Chikwawa and Chiromo. *Bull. Geol. Surv. Nyasaland*, **14**, 60pp.

HABGOOD, F. and HOLT, D.N. (1973): The geology of the Thyolo area. *Bull. Geol. Surv. Malawi*, **22**, 24pp.

HOLT, D.N. (1961): The geology of part of Fort Johnston District east of Lake Nyasa. *Rec. Geol. Surv. Nyasaland*, **1**, 23-39.

MCCONNELL, R.B. (1972): Geological development of the rift system of eastern Africa. *Geol. Soc. Am. Bull.*, **83**, 2549-2572.

PIKE, J.G. (1972): Hydrology. *In: Agnew, S. and Stubbs, M. (Eds.): Malawi in maps.* University of London Press, 34-35.

YAIRI, K. (1974): En echelon pattern of the East African Rift System. *J. Afri. Studies*, **14**, 21-46 (in Japanese with English abstract).

YAIRI, K. (1975a): Geometry and mechanics of en echelon faulting with applications to the East African Rift System. *1st Prelim. Rep. Afr. Studies, Nagoya Univ.*, 29-38.

YAIRI, K. (1975b): Fault pattern and crustal extension of the Kavirondo rift valley in relation to a bifurcating rift model. *1st Prelim. Rep. Afr. Studies, Nagoya Univ.*, 39-43.

YAIRI, K. (1977): Fault pattern of the southern part of the Eastern Rift, Tanzania. *2nd Prelim. Rep. Afr. Studies, Nagoya Univ.*, 39-50.

Karroo System to the West of Karonga, Northern Malawi

Yukiyasu SAKA* and Kenji YAIRI**

* Institute of Earth Science, School of Education, Waseda University
** Department of Earth Sciences, Faculty of Science, Nagoya University

Introduction

In northern Malawi the Precambrian to early Paleozoic crystalline rocks, the Malawi Basement Complex, are covered by the Karroo sediments of Permo-Triassic period, the Dinosaur Beds of late Jurassic to early Cretaceous period and the lacustrine deposits which, separated by unconformities into several beds, range in age presumably from Miocene to recent (Carter and Bennett, 1973) (Fig.1).

Of the Karroo rocks distributed in northern Malawi, those of the Nkana area and the Livingstonia area were investigated in detail in prospect of the occurrence of the coals (Bloomfield, 1957 and Cooper and Habgood, 1959, respectively). The others have not so far received such a serious attention because of their relative inaccessibility and supposed inferior quality of the coals. Recently, Thatcher (1974) and Kemp (1975) gave concise reviews of the Karroo and the post-Karroo System lying between lat. 10°S and 11°S supplemented by the photogeological interpretation by Stephens (1963, unpublished report).

The distribution and the mutual relationship of the Phanerozoic sedimentary covers in northern Malawi are summerized as follows:

The distribution of both the Karroo and the post-Karroo deposits, with the exception of the recent deposits which occupy the lowlands along the western shore of Lake Malawi, is restricted to isolated basins or troughs where they rest on the basement complex unconformably and are overlain in turn with successive unconformities by the younger deposits. The shape of the basin or trough is largely controlled by the major post-Karroo faults. This is especially the case for the basins lying between lat. 10°S and 10°30'S, where nearly all the basins are narrow and elongate troughs bounded on the east by faults downthrowing to the west and trending parallel to the Malawi Rift System. On the west of the basin, the trough is demarcated in most cases by unconformities below either the lowermost part of the beds trapped in the trough or some higher horizons which overstep the underlying beds.

Such a closely associated occurrence of the Karroo and the post-Karroo deposits within narrow troughs controlled by the faults of the Rift trend is strongly indicative of the genetic relationship between the episodic Rift faulting and the successive generation of sites in which the clastics accumulated.

The succession for the Karroo System in northern Malawi is given in Table 1. The K subdivisions of the Karroo System established by Stockley (1931) in the Ruhuhu area, Tanzania are juxtaposed for the purpose of comparison. The whole or a segment of the sucession shown in Table 1 occurs in each basin showing a local variety in the lithology.

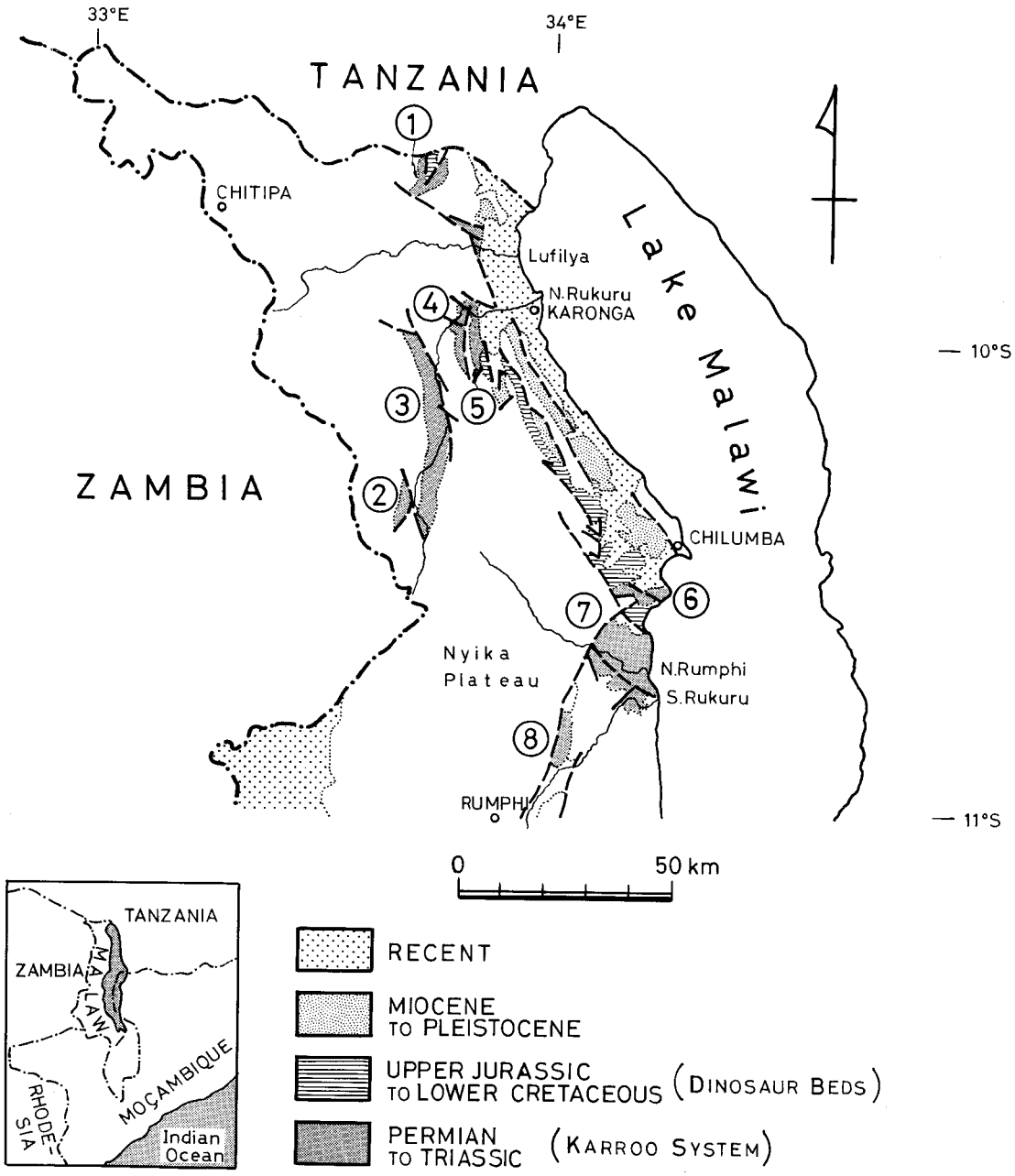

Fig. 1 Distribution of the Karroo Beds and the post-Karroo Beds in northern Malawi (after Carter and Bennett, 1973). 1: Nkana area, 2: Nthalire area, 3: North Rukuru area, 4: Kasikisi area -- Mwankenja Basin West, 5: Mwesia area -- Mwankenja Basin East, 6: Lion Point area, 7: Livingstonia area, 8: Henga Valley area.

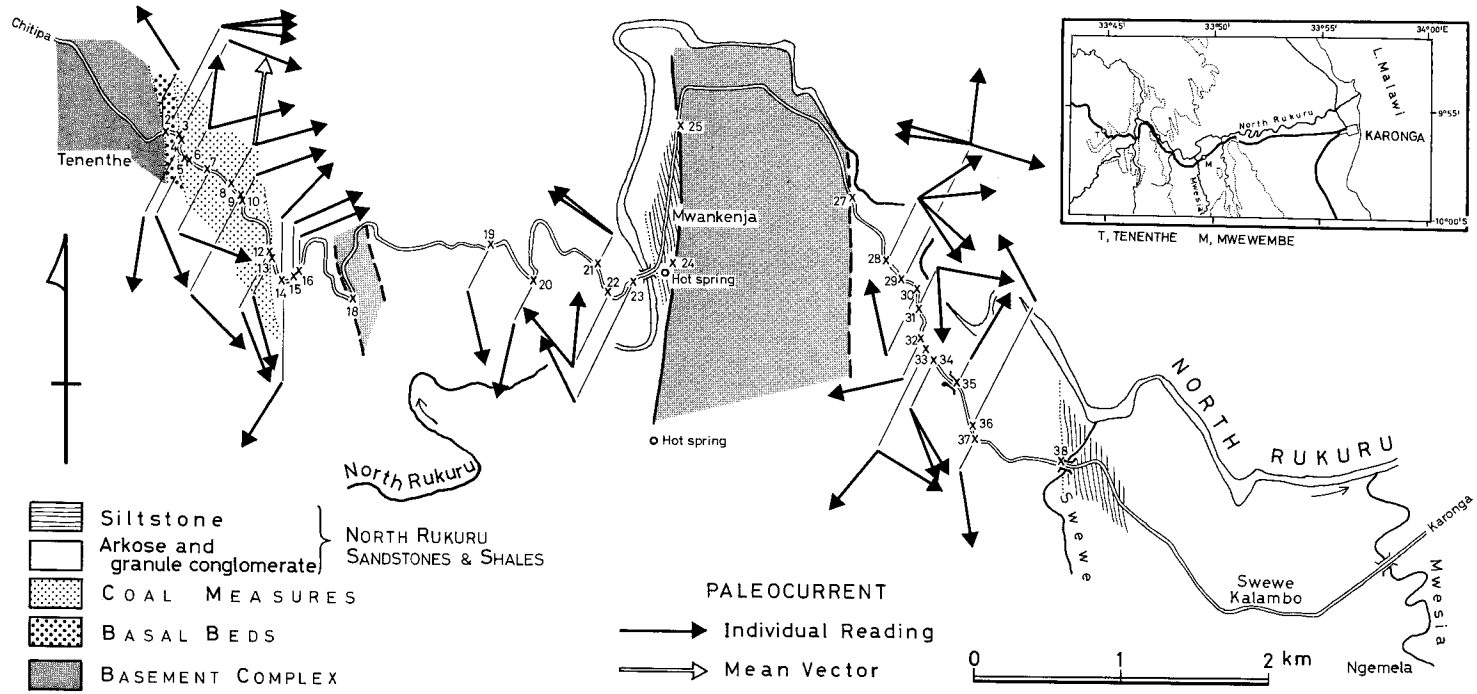

Fig. 2 Route map along the Karonga-Chitipa road between Swewe Kalambo and Tenenthe.

Table 1 The Karroo succession in the North Nyika area and in the Ruhuhu coalfield, Tanzania

		North Nyika Area (Thatcher, 1974)			Ruhuhu, Tanzania (Stockley, 1932)	
System	Group	Formation	Lithology	Thick-ness(m)	Formation	Thick-ness(m)
KARROO	STORMBERG				K8. Manda Beds and Upper Bone Beds	134
	(?) UPPER BEAUFORT				K7. Kingori Sandstones	370
	LOWER BEAUFORT	Mwesia Beds	Pale grey mudstones, marls and limestones Dark brown ferruginous sandstones	290 91	K6. Lower Bone Beds	92
		North Rukuru Sandstone and Shales	Purple shaly mudstones Alternation of arkose and shale	91 460-823	K5. Ruhuhu Beds	213-305
	ECCA	Coal Measures	Carbonaceous shales, sandstones and coal seams	0-61	K4. Upper Coal Measures K3. Intermediate mudstones and Sandstones K2. Lower Coal Measures	102 137 137
	DWYKA-ECCA	Basal Beds	Conglomerates and sandstones	0-21	K1. Basal Beds	515

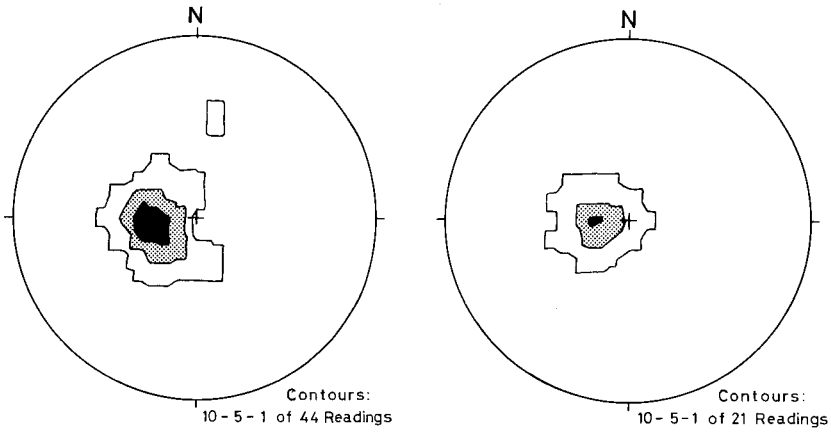

Western Zone Eastern Zone

Fig. 3 Equal-area projection (from the lower hemisphere) of bedding poles.

The Karroo System to the west of Karonga

A motor road extending from Karonga follows the lowest reaches of the North Rukuru as west as Mwankenja about 21 km west of Karonga, and the road, leaving the North Rukuru from here, leads to Chitipa and further to Nakonde, Zambia. Along this road the Karroo rocks of the Mwankenja Basin are well exposed between Tenenthe 3.5 km west and Swewe Kalambo 4 km east of Mwankenja (Fig.2). The area of the Karroo rocks is splitted into the western and eastern parts by a N–S trending strip of gneisses 1.5 km in width near Mwankenja. The Karroo beds, striking essentially N–S, dip at about 20° to the east in the eastern zone and 30° to the east in the western, respectively (Fig.3). The situation and the lithofacies of these Karroo beds justify to connect the eastern zone with the Mwesia Basin and the western zone with the Kasikisi Basin, both belonging to the Nyika map area (Thatcher, 1974).

The writers' informations came from the observations made merely along the Karonga-Chitipa road, and are too fragmental to lead to any systematic account of the geology of the Karroo System of these two zones. Moreover, no precise estimate of the thickness of each formation could be obtained because of the inconstant attitudes of strata and the supposed displacement of strata along numerous minor faults.

Western zone

This zone is the northern extent of the Kasikisi Basin and has been termed the Mwankenja Basin West (Kirkpatrick, 1965, unpublished report). It is bounded on the east by the major post-Karroo fault. On the west the sediments lie unconformably on the basement metamorphics. The Karroo System consists chiefly of coarser clastics with occasional intercalations of mudstones and micaceous or carbonaceous sandstones. Owing to the general eastwards inclination of beds, successive upper horizons occur from the west to the east along the road.

Basal Beds. The westernmost outcrop of the Karroo rocks along the road lies at point 2 in Fig.2. The basement rocks cropping out immediately to the west of point 2 consist of biotite-(hornblende)-quartz gneiss which belongs to Chambo Gneisses. The gneissosity has a trend of WNW-ESE, characteristic of the Misuku Belt which extends northwestwards into Tanzania, where it is termed the Ubendian Belt. Although the contact between the Karroo System and the Chambo Gneisses is not seen, it is of no doubt that the former rests on the latter unconformably. The lowermost part of the Karroo System consists of white, partly mottled in chocolate brown, medium grained arkoses, succeeded by conglomerates chocolate or purple in colour. Pebbles and cobbles contained in conglomerates are mostly of quartzites and attain a maximum diameter of 10 cm. They are subangular to subrounded in shape, the larger one being more rounded. These conglomerates are regarded to belong to the Basal Beds and not to the basal conglomerate of the North Rukuru Sandstones and Shales which are reported to overstep the Basal Beds in the Nthalire and the North Rukuru Basin (Thatcher, 1974), because the beds correlatable to the Coal Measures intervene between the conglomerates and arkoses characteristic of the North Rukuru Sandstones and Shales to the east.

The main rock type of the Basal Beds is very coarse grained sandstones and granule conglomerates which grade upwards to the Coal Measures.

Coal Measures. Coarse to very coarse grained arkoses and granule conglomerates are predominant with frequent intercalations of pebble conglomerates, flaggy carbonaceous sandstones, flaggy micaceous sandstones with or without carbonaceous materials and fine grained sandstones with mud laminae. Coal seams rarely interstratified with micaceous or carbonaceous sandstones are thin and impersistent. Cross lamination, mostly of tabular type, is abundant in arkoses. Upwards gradation of lithofacies from conglomerate or arkose through micaceous sandstone, carbonaceous sandstone to coal seam, commonly seen in the Karroo System of the Livingstonia area (Saka and Yairi, 1977), is not ascertained to be present because of lack of the exposure in which all of these rocks occur together. Observed predominance of the coarser clastics in the Coal Measures may be in part due to the preferred survival against weathering and subsequent higher likelihood of exposure of these rocks along the road laid out on the gentle rolling mountain surface.

North Rukuru Sandstones and Shales. No sharp boundary between this formation and the underlying Coal Measures is seen. The lithofacies of the main part of the present formation is represented by medium to very coarse grained arkoses and granule conglomerates buff and chocolate in colour, with much lessor amounts of flaggy micaceous sandstones, flaggy carbonaceous sandstones and siltstones. Calcareous nodules are contained in profusion in the upper half of the arkose facies. Bedding is well developed. Tabular cross lamination is abundant in coarser facies.

The uppermost horizon of the North Rukuru Sandstones and Shales is occupied by much finer clastics which are exposed along the linear western foot of the N–S trending ridge near Mwankenja. There the sequence is as follows:

TOP
Alternation of greyish white, calcareous silt-to fine grained sandstone, 10 to 50 cm bedded and greenish grey to green siltstone, splitting finely and 15 cm bedded
Dark grey, massive, fine to medium grained sandstone with intercalation of abundant calcareous nodules
Greenish grey to green siltsone
Light grey to greenish grey nodulifer-
ous siltstone without sandy
BOTTOM intercalation

Neither external nor internal sedimentary structures are developed. These beds are correlatable to the "Purple shaly mudstones" which occupy the upper part of the North Rukuru Sandstones and Shales. The overall lack of purplish tint is considered to be resulted from weathering.

Between point 18 and the bend of the road about 0.5 km to the north are seen only isolated blocks of gneisses. A narrow strip consisting of gneisses is supposed to intervene between the Karroo System as in the case of the Kasikisi Basin. Its western boundary is considered to be a fault. On the east, the strip is considered to be bounded not by unconformity but by a fault. The fact in support of this view is the complete lack of basal conglomerates and carbonaceous sandstones immediately to the east of the presumed strip of gneisses.

Eastern zone

The eastern zone, termed the Mwankenja Basin East by Kirkpatrick (1965), is the northern extremity of the Mwesia Basin in the Nyika map area. The Karroo System in the Mwesia Basin is reported by Thatcher (1974) to have the succession more complete than elsewhere in the Nyika map area ranging from the Basal Beds upwards to the Mwesia Beds of the Lower Beaufort Series. The eastern half of the present zone is, however, covered by the recent deposits along the North Rukuru and the Mwesia. As in the case of the western zone, successive younger beds crop out towards the east because of their gentle monoclinic structure facing to the east.

North Rukuru Sandstones and Shales. There is no outcrop, along the road, where the contact between the basement to the west and the Karroo System to the east is seen. Along the presumed boundary, isolated blocks of various sizes both of the basement rocks and of the Karroo rocks are scattered intermingled with one another. Blocks of the Karroo rocks consist exclusively of very coarse grained arkoses and granule conglomerates, identical with those of the North Rukuru Sandstones and Shales widely distributed to the east. Lack of the Basal Beds and Coal Measures near the western margin of the zone can be accounted for in either of the following two ways: 1) The North Rukuru Sandstones and Shales rest with unconformity on the basement complex directly. They overstep the underlying beds which accumulated in a series of unconnected depressions of the pre-Karroo surface at the initiating stages of the deposition of the Karroo System (Fig.4a). 2) The Basal Beds and the Coal Measures do exist under the North Rukuru Sandstones and Shales

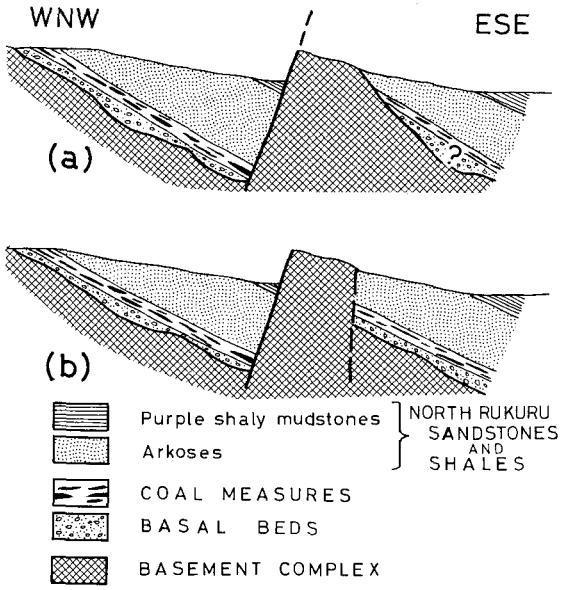

Fig. 4 Schematic profiles to account for the lack of the Basal Beds and the Coal Measures along the western margin of the eastern zone. Explanation in text.

which are faulted against the basement to the west (Fig.4b). Judging from the widespread overstep of the North Rukuru Sandstones and Shales seen in every basin and the poor development of the lower beds in the Mwesia Basin (Thatcher, 1974), the former view is considered to be true.

There are found little differences in the lithofacies between the North Rukuru Sandstones and Shales in the present zone and those in the western. Very coarse grained arkoses and granule conglomerates buff and chocolate in colour are predominant except in the upper third of the succession exposed along the road. Tabular cross lamination is well developed. Towards the top, chocolate-coloured granule conglomerates become to overwhelm the other rocks. To the east of point 38, coarser rocks are succeeded by the alternation of white calcareous sandstone and white siltstone. It is correlatable to the finer facies exposed along the eastern margin

of the western zone and, therefore, to "Purple shaly mudstones".

Eastern marginal faults of the basins

Western Zone. A major fault scarp is seen at point 24 in Fig.2. It strikes N20°E and dips at 58° to the west. The foot wall consists of mylonitized gneisses associated with cemented fault breccia (Fig.5). The hanging wall is not seen concealed by talus deposits derived from the foot wall. The fault plane is smooth and even but bears no features indicative of the direction of relative displacement along the fault. To the north of point 24, the boundary of the "Purple shaly mudstones" and the basement gneisses is obviously represented by the marked change in the colour of the surface soils on and along the road: The former is indicated to underlie by the white soils and the latter by the brown. A straight line of demarcation between two kinds of soils can be detected to run in the direction of N15°W, when viewed from a certain height. These facts, supplemented by the N–S trending contour lines and the alignment of hot springs marked on the Karonga map (1:50,000. Sheet 0933D3), attest that the eastern boundary of the western zone is a normal fault trending essentially N–S and downthrowing to the west. No abrupt change of the bedding attitudes is observed near the faulted eastern margin. Any conglomeratic facies suggestive of the syndepositional movement along the eastern boundary fault is not developed unlike the case of the southern boundary fault of the Nkana Basin (Bloomfield, 1957).

Eastern zone. It is of no doubt that the eastern boundary fault of the Mwesia Basin (Thatcher, 1974) reaches the extent into the present area. Neither the fault itself nor the uppermost horizon faulted against it is exposed, being masked by the recent deposits.

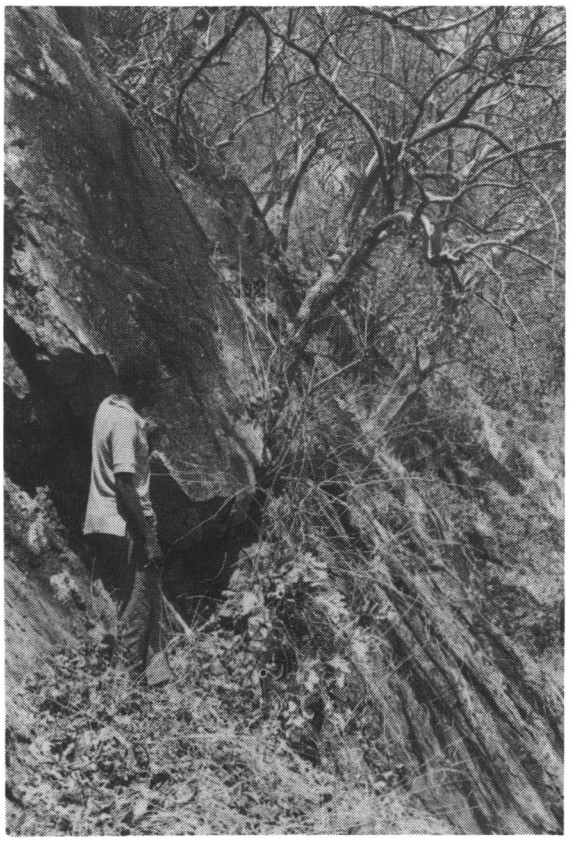

Fig. 5 Western boundary fault of the strip of the basement gneisses which intervenes in the Karroo area, point 24, Mwankenja. Viewed from the south. Hammer for scale.

The Karroo System now separated into the western and the eastern zone by intervening basement complex is considered to have been originally deposited in a single basin, although the accumulation of the lower divisions may have been restricted to several unconnected minor basins. The duplicated

occurrence of the same horizon in the western and the eastern zone is attributable to the repitition due to the fault movement which brought about the intervening basement complex.

Sedimentary structures

Cross lamination, as defined below, is the only sedimentary structure that was observed to occur in the Karroo beds along the road.

Concerning the stratification, there are too many terms each of which has been differently understood and used by different authors, resulting in the complete lack of the standardization of the nomenclatures. In this paper, the terms listed below are tentatively defined as follows:

Stratification: a general term that describes the property of layering in sedimentary rocks.
Bedding: a plane that forms the upper and the lower boundary of a single sedimentary unit designated a single bed.
Lamina: a layer, parallel or diagonal to the bedding, within a single bed; independent of scale.
Lamination: a plane that separates the individual lamina.
Cross lamina: Lamina, diagonal to the bedding, ranging the total or major part of the thickness of a single bed.
Micro cross lamina: Lamina diagonal to the bedding; restricted to only a portion of the thickness of a single bed.

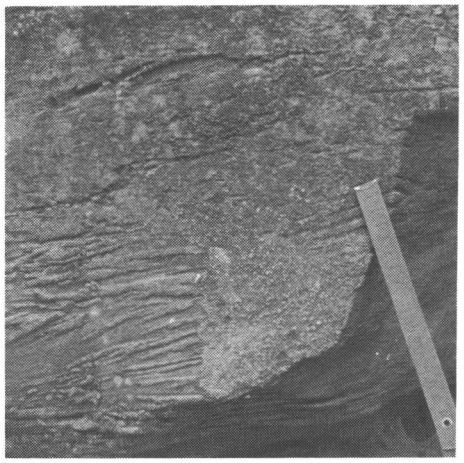

Fig. 6 Micro cross laminae of tabular type in medium grained arkose, North Rukuru Sandstones and Shales, point 14, western zone. Note that each lamina tends to turn up near the lower boundary. In the upper fifth of the photo is another set of micro cross laminae. Length of a segment of scale is 18cm.

Micro cross lamina

Thinly stratified micro cross lamina occurs in the finer facies except the "Purple shaly mudstones". It is much less abundant than is cross lamina. The scarcity of micro cross lamina may be in part attributable to the low likelihood of exposure of the finer facies and to the inferior conspicuousness of the laminae on the weathered outcrops. Most of micro cross laminae are of trough type, occurrence of planar micro cross laminae being exceptional (Fig.6). No ripple cross laminae in which the entire ripple form is preserved are seen. Micro cross laminae occupy a portion of a single bed, overlain and underlain by likewise thinly stratified parallel laminae. Because so few examples were found, generalization of the mode of occurrence within a single bed cannot be obtained. The succession of laminae of different kinds in a single bed is suggestive of the changing flow regime in the course of the deposition.

Fig. 7 Upper boundary of tabular type cross laminae in very coarse grained to granule conglomeratic arkose, Coal Measures, point 9, western zone. Bedding dips gently to the right.

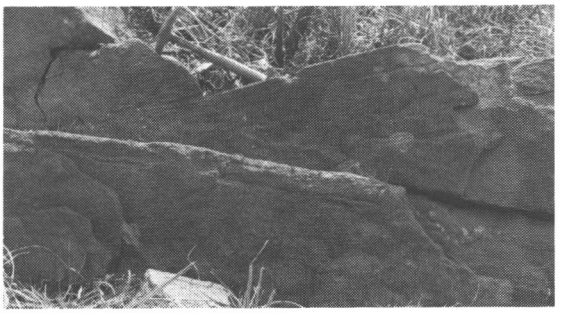

Fig. 8 Lower boundary of tabular type cross laminae in very coarse grained arkose, North Rukuru Sandstones and Shales, point 21, western zone.

Cross lamina

Large scale cross laminae are abundant in coarse grained arkoses and granule conglomerates. They are mostly of tabular type. Individual forset is straight and truncated at the upper boundary of the bed (Fig.7). Where the laminae approach the lower boundary, they rarely tend to turn up (Fig.8). As many authors point out, difficulty in distinguishing the tabular from the trough type of cross lamina occurs in outcrops which provide only two-dimensional sections. Theron (1967) reports very large scale cross laminae of trough type from the Beaufort Series in South Africa, which appear to be typical tabular type cross laminae when only small part is viewed. In the present area, however, little difficulty is encountered, because the beds are not so thick and can be easily viewed in three dimensions. Lamination is generally clear, although there are some examples in which only faint traces of cross laminations are visible in the otherwise structureless bed. The thickness of each lamina is widely variable from 1 cm to as large as 20 cm, 5 – 10 cm being most abundant. Angles of inclination of laminae are variable,

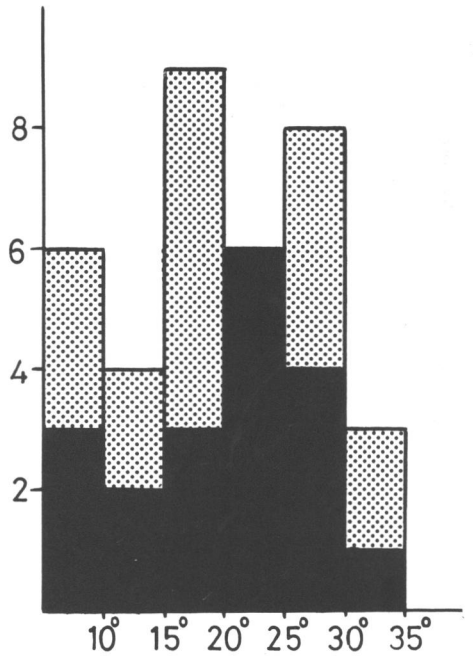

Fig. 9 Distribution of inclination angles of cross laminae. Black: western zone, stippled: eastern zone.

in the order of 5 – 30 degrees; the mean value is about 22 degrees (Fig.9). There appears to be no systematic relationship between the inclination angle of the lamina and the thickness of the lamina or the grain size. The cross laminae shown in Fig.10 occur in very coarse grained to granule conglomeratic arkoses, purple in colour, consisting mainly of angular to subangular grains of quartzite cemented by much lessor amounts of matrix. Although the lamination is not so clearly discernible, the individual lamina is distinct because of grading within a lamina. The coarsest grains occur at the bottom of a lamina succeeded by an upwards decrease in grain size up to the horizon where the next grading starts. As Kuenen and Menard (1952) stressed, a sudden and short-lived supply of the unsorted clastics is necessary for the formation of a graded deposit irrespective of the sedimentation environments. The graded cross laminae are considered to have the same origin as the avalanche-front cross-stratification as Picard and High (1973) report from the ephemeral stream deposits. They result from clastics slumping down the lee face of a bar or a delta under their own weight. Slumping takes place at successive intervals of time during which deposits accumulate at the lee edge of the delta or bar. Consequently each lamina is straight and sharply abuts against the bottom at the angle of repose. The observed maximum angle of inclination is as high as 36°. The same origin may be possible for the other tabular type cross laminae.

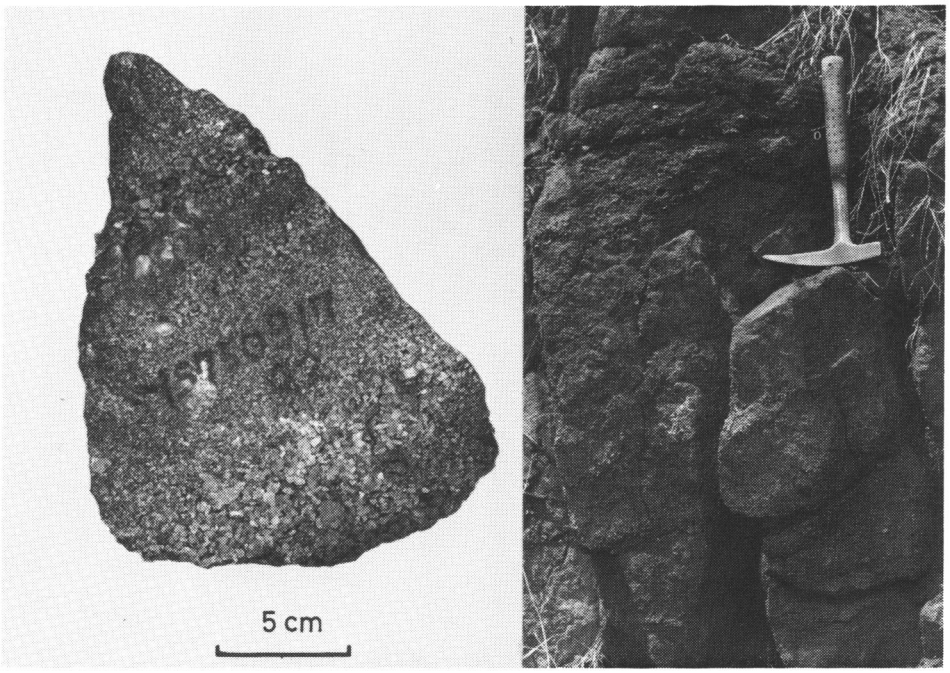

Fig.10 Graded cross laminae, granule conglomeratic arkose, North Rukuru Sandstones and Shales, point 22, western zone. The photograph on the left is a close up of the section below the hammer shown on the right.

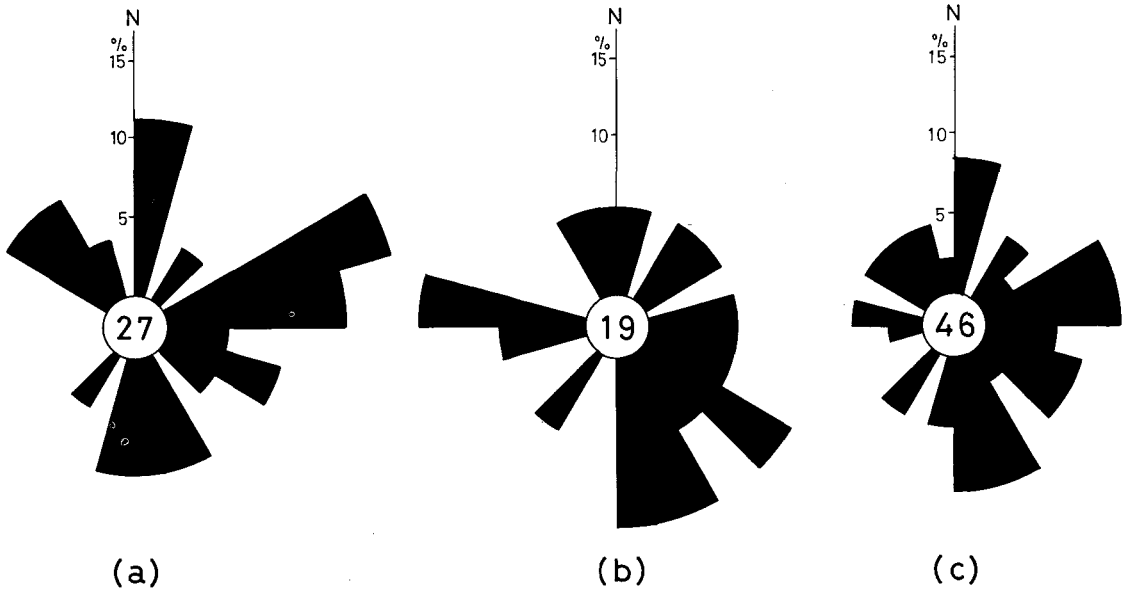

Fig.11 Rose diagrams showing the paleocurrent directions of the Karroo beds. The numbers of readings are shown in the circles.
(a) Western zone, (b) eastern zone, (c) whole area.

Consideration

The lithology and the angularity of pebbles and sand grains of the Karroo beds are, as they have been considered to be, indicative of the proximity of the source area consisting of the basement complex. According to the informations available to the writers, it seems that no systematic paleogeographic basin analysis has so far been carried out for the Karroo basins in terms of the paleocurrent based on the current indicators. Such an abundant occurrence of the cross laminae in the coarser facies of the Karroo beds promises in all probability a fruitful result of the paleocurrent analysis. The readings of the azimuth of the forsets, *i.e.*, the bearing of the maximum dip direction of the forsets, generally show more or less lower consistency than those of the linear current indicators. This result partly from the original inconsistency of current directions and partly from the difficulty of defining the true dip direction, especially of trough type cross laminae.

Paleocurrent readings of 46 were taken at 31 localities along the Karonga-Chitipa road (27 readings at 21 localities in the western zone; 19 readings at 10 localities in the eastern). Paleocurrent directions at each locality are shown in Fig.2 and are grouped into 15° class intervals in rose diagrams of Fig.11. More than two readings obtained from the same single bed are expressed by the mean vector as one reading. Nearly all the readings are tilt compensated except those of forsets dipping in the same direction as the tectonic

tilt, because the azimuth of forsets can be appreciably altered by even a slight tectonic tilt of a cross laminated bed.

The paleocurrent directions are widely scattered, lacking any prominent preferred orientations both in the western and the eastern zone. It can be said that the clastics were supplied from almost all directions. Most broadly speaking, however, the sectors of the rose diagrams are somewhat more distinguished on the eastern half than on the western. Although the current direction indicated by the azimuth of forsets is merely a local one which is not always directly away from the source area, a slight predominance of the easterly current over the westerly suggests that the main provenance from which the clastics were derived was situated to the west of the Karroo basin. It cannot be decided whether the poor consistency of current directions is ascribed to the small numbers of readings obtained only along one route or it is inherent in the Karroo basin where currents changed the flow directions from place to place and from time to time. The paleocurrent analyses on the Beaufort Series (Theron, 1967) and on the Stormberg Series (Botha, 1967), both in South Africa, suggest that the latter is the case.

References

BLOOMFIELD, K. (1957): The geology of the Nkana coalfield, Karonga District. *Bull. Geol. Surv. Nyasaland Prot.,* **8.,** 36p.

BOTHA, B.J.V. (1967): The provenance and depositional environment of the Red Beds stage of the Karroo System. In: UNESCO, *Gondwana Stratigraphy,* 763-771.

CARTER, G.S. and BENNETT, J.D. (1973): The geology and mineral resources of Malawi (2nd. revised ed.). *Bull. Geol. Surv. Malawi,* **6,** *62p.*

COOPER, W.G.G. and HABGOOD, F. (1959): The geology of the Livingstonia coalfield. *Bull. Geol. Surv. Nyasaland Prot.,* **11,** 51p.

KEMP, J. (1975): The geology of the Uzumara area. *Bull. Geol. Surv. Malawi,* **41** (in press).

KIRKPATRICK, I.M. (1965): Unpublished Geol. Surv. Dept. Rep., IMK/21.

KUENEN, Ph.H. and MENARD, H.W. (1952): Turbidity currents, graded and non-graded deposits. *J. Sed. Petrol.,* **22,** 83-96.

PICARD, M.D. and HIGH, L.R.Jr. (1973): *Sedimentary structures of ephemeral streams, Development of sedimentology,* **17,** Elsevier, Amsterdam, 223p.

SAKA, Y. and YAIRI, K. (1977): Sedimentary structures of the Karroo System in the Livingstonia area, northern Malawi. *2nd. Prel. Rep., Afr. Studies, Nagoya Univ.,* 89-107.

STEPHENS, E.A. (1963): Unpublished repot.

STOCKLEY, G.M. (1932): The geology of the Ruhuhu coalfield, Tanganyika Territory. *Quart. J. geol. Soc. Lond.,* **88,** 610-622.

THATCHER, E.C. (1967): The geology of the Nyika area. *Bull. Geol. Surv. Malawi,* **40,** 90p.

THERON, J.C. (1975): A paleocurrent analysis of a portion of the Beaufort Series, Karroo System. In: UNESCO, *Gondwana Stratigraphy,* 725-738.

Note on the Karroo System and the Probable Dinosaur Beds near the Lion Point, Karonga District, Northern Malawi

Yukiyasu SAKA

Institute of Earth Science, School of Education, Waseda University

Introduction

In the southern extremity of Karonga District, a small faulted block consisting of the Karroo System forms a gentle hill on the Lakeshore Plain. The hill, bounded on the west by the NW–SE trending Livingstonia Escarpment downthrowing to the northeast, descends gradually towards the east to run out into Lake Malawi at the Lion Point. On the northern and the southern side of the faulted block, the Dinosaur Beds crop out and are considered to underlie the recent lacustrine deposits.

The Lion Point area was mapped photogeologically by Stephens (1963, unpublished report) and slight modifications to the margin of the Karroo area were given by Kemp (1975). According to Kemp, the stratigraphy of the Karroo System of the Lion Point area is summerized as follows:

K3 arkoses, overstepping the carbonaceous mudstones (K2) and basal conglomerates (K1), cover directly the basement gneisses with unconformity along the northwestern margin of the area. Light brown mudstones distributed at and near the head of the Point are correlatable with the K5 Beds and are considered to be downfaulted against the K3 Beds to the west. Since the original descriptions by Dixey (1928) no additional work has been carried out on the Dinosaur Beds.

The road which descends the precipitous Livingstonia Escarpment turns northwards at Khondowe on the Lakeshore. From here, a new road runs on the eastern side of the road shown in the Livingstonia map (1:50,000, Sheet 1034C1); the latter road is no more a motor road because of heavy deterioration. Where the new road crosses the above mentioned hill, a part of the K5 and K3 Beds and the basal part of the beds correlatable to the Dinosaur Beds are well exposed in the cuttings along the road (Fig.1).

The boundary fault which, as inferred by Kemp (1975), demarcates the K5 Beds to the east and the K3 Beds to the west is considered to run between the cutting 2 and the cutting 3. To the northwest of this fault, the beds correlatable to the Dinosaur Beds (hereafter designated "Dinosaur Beds") cover the K3 Beds which are exposed in the cuttings of lower positions and along the stream courses. Both the Karroo beds and the "Dinosaur Beds" dip as a whole to the northeast at low angles never exceeding 30 degrees.

2nd Prelim. Rep. Afr. Studies, Nagoya Univ., 83-88, 1977.

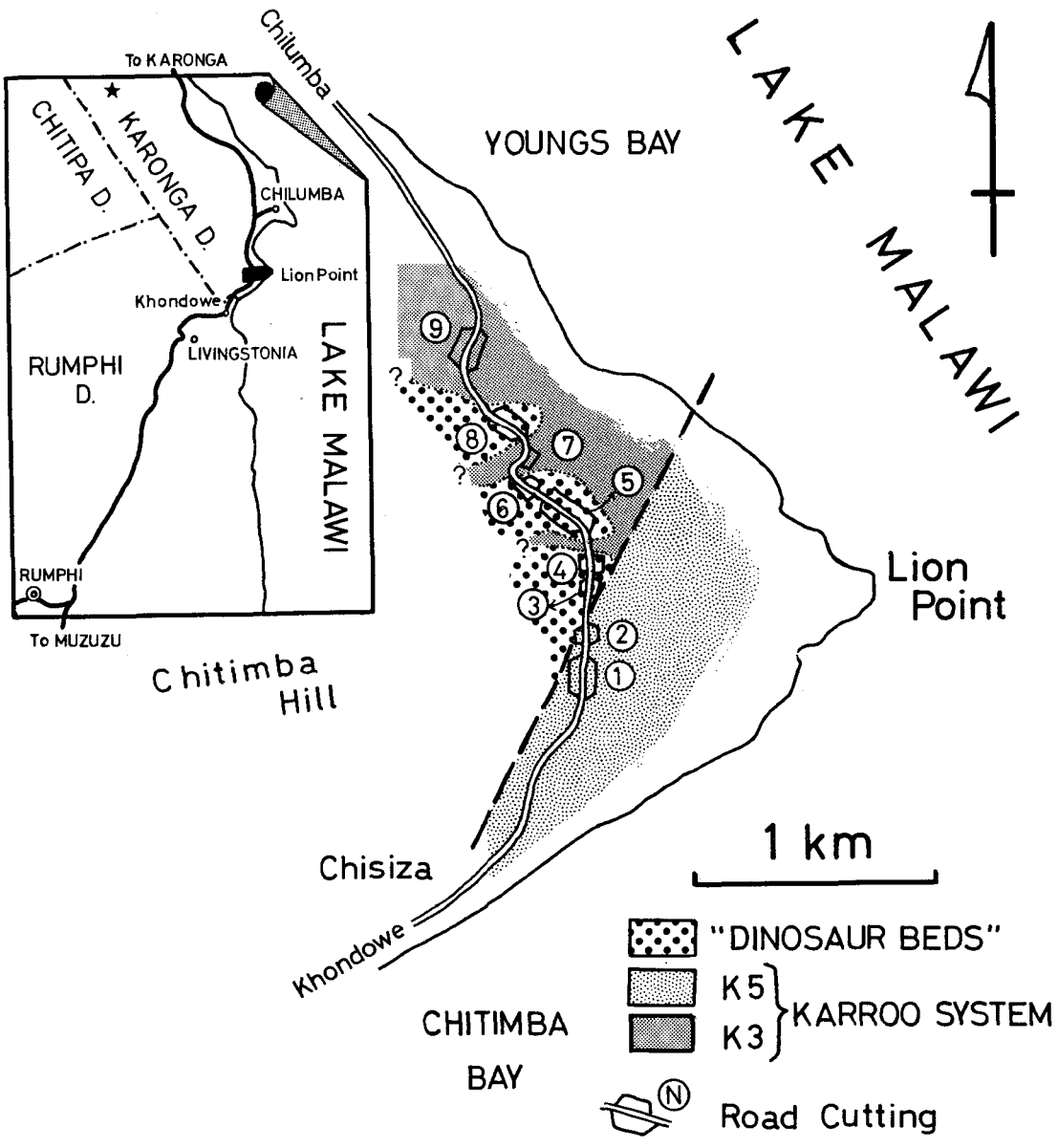

Fig. 1 Sketch map of the Lion Point area, Karonga District. Road cuttings are referred by the numbers encircled.

Karroo System

K3 Beds

Fine grained sandstone and mudstone in alternation are exposed in the cutting 7 and along the stream course between the cuttings 4 and 5. Judging from the lithology, the stratigraphic situation of this sequence is considered to correspond to the intermediate horizon between the middle division (chocolate-coloured and green mudstones, exposed in the cutting 9) and the lowest division (pink arkose and sandstone, not exposed along the road) of the K3 Beds in the Livingstonia area (Cooper and Habgood, 1959). Buff and yellow fine grained sandstones, 5 – 30 cm bedded, alternate with greyish blue to greyish white mudstones of similar thickness (Fig.2). Bedding is very sharp and neither gradation from sandstone to mudstone nor graded bedding in a single sandstone bed is observed. Several sets of beds are involved in the gentle slump structure of a constant thickness of about 50 cm, in which the sandstone bed shows the pull-apart structure and forms a slump fold indicative of the slumping towards the north (Fig.3). The contorted beds are truncated sharply by the overlying mudstone bed.

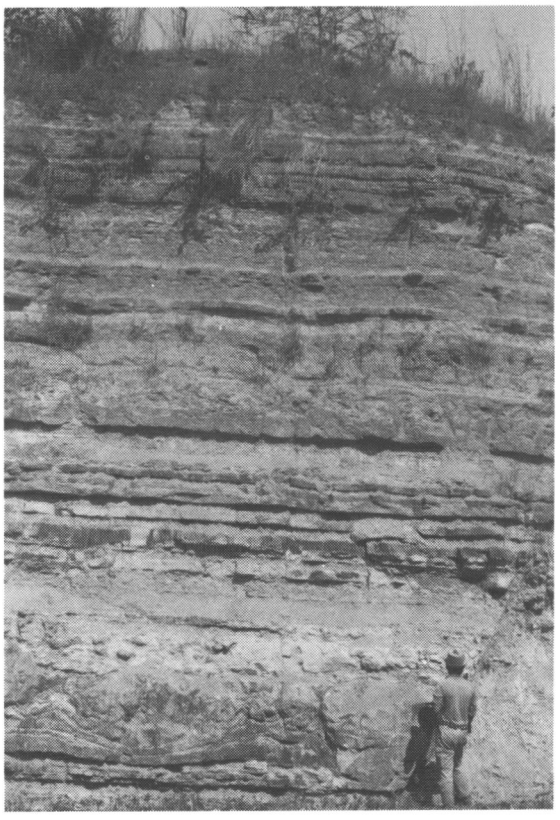

Fig. 2 Alternation of sandstone and siltstone of the K3 Beds, Cutting 7.

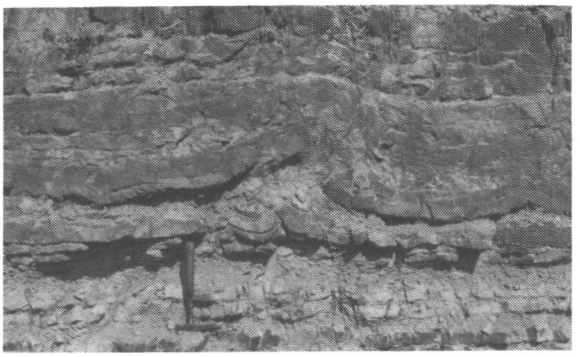

Fig. 3 Slump structure developed in the alternation of sandstone and mudstone of the K3 Beds, Cutting 7.

Chocolate-coloured and green mudstones typical of the middle division of the K3 Beds are exposed in the northernmost cutting (9). Thickness of the individual chocolate-coloured or green layer is variable, ranging from several milimeters to 15 cm or more. Although the contrast between the green and the chocolate-coloured layer is striking on the outcrop, close inspection reveals that the boundary of them is in most cases neither sharp nor straight, but is rather wavy or rugged and more or less blurred. There are many examples

in which the tint of chocolate grades upwards into that of green in the distance of one centimeter or so (Fig.4). In some cases, indistinctly bounded green bands alternate with similar chocolate-coloured bands to make up a unit demarcated by the relatively sharp upper and lower boundary surfaces (Fig.5). These features demonstrate that a single bed is not always represented by a particular colour. Besides the sinusoidal stratification shown by most layers, small scale slump structures (Fig.4), convolute laminations and flame structures (Fig.5) are abundant, suggesting the unstability of these fine grained sediments after the deposition.

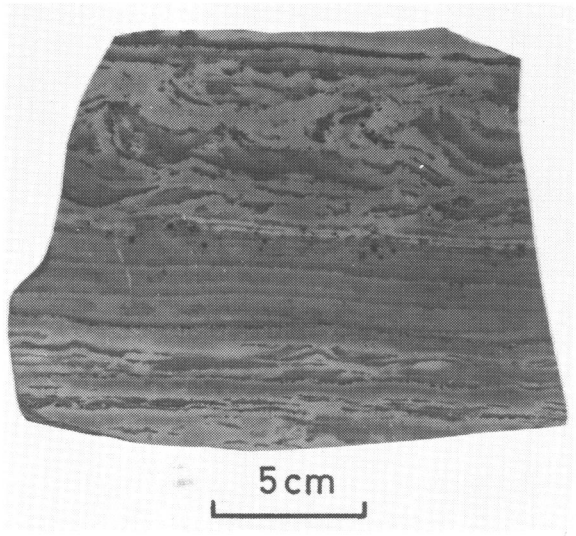

Fig. 4 Chocolate-coloured and green mudstones from the cutting 9. Dark: chocolate-coloured mudstone, light: green mudstone. Slump structures are in the upper half and in the lower fourth. Note the grading from chocolate-coloured to green mudstone below the upper slumped unit.

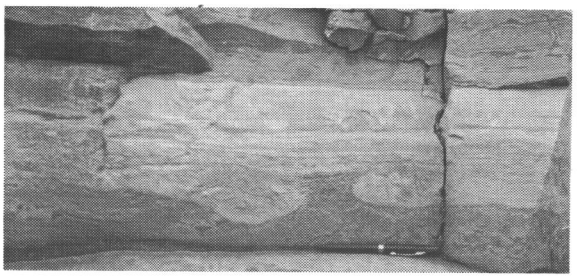

Fig. 5 Flame structure in the chocolate-coloured and green mudstones of the K3 Beds, Cutting 9. Pen is 14cm long.

K5 Beds

The Karroo rocks exposed in the cuttings 1 and 2 are correlatable to the lower series (yellow mudstones) of the K5 Beds. They consist mainly of well bedded siltstones grey to pale yellow in colour, with intercalations of very fine grained sandstones. Sedimentary structures are rare. Sandstones intercalated in siltstones do not show graded bedding. Only a few examples were found to occur: micro cross laminae, as defined by Saka and Yairi (1977), indicative of the currents towards the northwest ~ west and wave ripple marks with the wave length of 1 cm yielding the NE–SW trend of wave oscillation. Because of the small numbers of readings of current indicators, no conclusions regarding the paleocurrent pattern are possible (Fig. 7A).

"Dinosaur Beds"

On the northwestern side of the estimated fault, the K3 Beds are overlain by the beds of friable purple grits, the facies of which is distinctly different from that of the underlying K3 Beds. They consist of angular sand

grains, 1 to 2 mm in diameter, cemented imperfectly by much lessor amounts of mud. Subangular to angular pebbles and cobbles of quartzites and gneisses are contained inhomogeneously in the grits. Some of them resemble the facetted gravels in shape. Cross lamination becomes progressively more prominent from the southeast to the northwest. The grits exposed in the cutting 3 are free from cross lamination, while those in the cutting 8 are characterized by the development of large scale cross laminae of a typical tabular type (Fig.6).

Fig. 6 Large scale cross laminae of tabular type, "Dinosaur Beds", Cutting 8.

Although no paleontological evidences could be found, the purple grits are correlatable, on the basis of the lithology, to the basal part of the Dinosaur Beds which are distributed along a strip of the Lakeshore Plain and the South Karonga Scarp Zone (Dixey, 1928). The contact between the "Dinosaur Beds" and the Karroo Beds is seen at the southeastern edge of the cutting 8. The "Dinosaur Beds" above and the Karroo Beds below the essentially planar surface of unconformity lie apparently parallel to one another, striking N70°E at the dip of 6° to the northwest. There is no development of a basal facies in the "Dinosaur Beds" immediately above the unconformity, as in the case at Mwakasyunguti, one of Dixey's type localities about 50 km northwest of the Lion Point (approximate location is shown by an asterisk at top center of the inset in Fig.1).

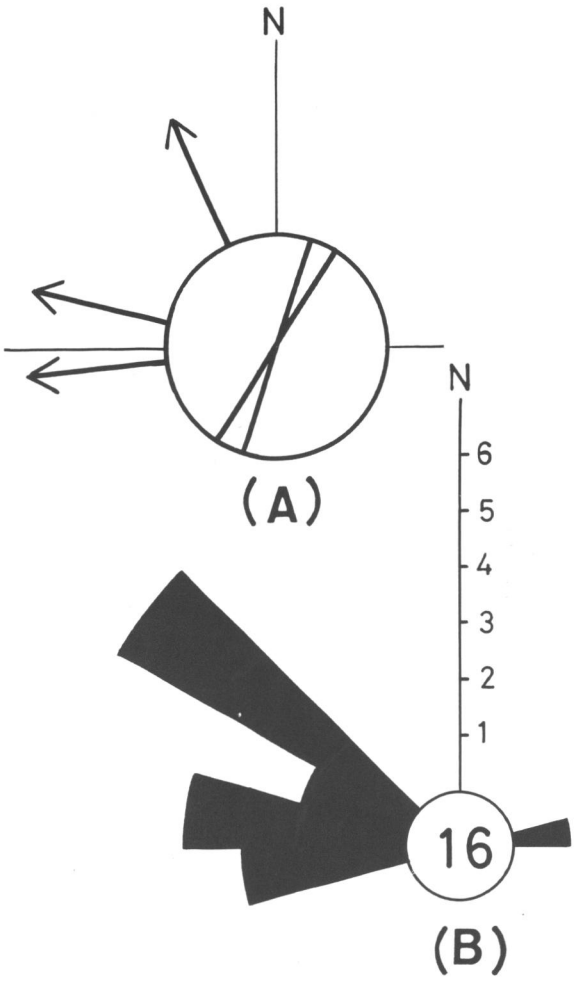

Fig. 7 Paleocurrent directions.
(a) K5 Beds of the Karroo System. Inside of circle: 2 readings of wave ripple marks, outside of circle: 3 readings of micro cross laminae.
(b) "Dinosaur Beds". 16 readings of cross laminae.

Paleocurrent directions indicated by the azimuth of forsets are shown in Fig. 7B. Although the numbers of readings are by no means sufficient enough to discuss the general paleocurrent system of the "Dinosaur Beds", the prevalence of the currents towards the northwest ~ west is noteworthy. Even if the current pattern restored here was a local one in the whole sedimentary basin of the Dinosaur Beds, it demonstrates that at least some portions of the clastics of the "Dinosaur Beds" were derived from the provenance located somewhere in what is now Lake Malawi. The existence of the hinterland to the east is postulated regardless of the sedimentary conditions of the "Dinosaur Beds"; fluviolacustrine or eolian as suggested by the facetted gravels contained in the purple grits.

Acknowledgements – The writer wishes to thank Mr. K.Yairi of Nagoya University for his co-working in the field.

References

KEMP, J. (1975): The geology of the Uzumara area. *Bull. Geol. Surv. Malawi,* **41** (in press).

DIXEY, F. (1928): The Dinosaur Beds of Lake Nyasa. *Trans. roy. Soc. S. Afr.,* **16,** 55-66.

COOPER, G.C. and HABGOOD, F. (1959): The geology of the Livingstonia coalfield. *Bull. Geol. Surv. Nyasaland Prot.,* **11,** 51p.

SAKA, Y. and YAIRI, K. (1977): Karroo System to the west of Karonga, northern Malawi. *2nd. Prel. Rep., Afr. Studies, Nagoya Univ.,* 70-82.

Sedimentary Structures of the Karroo System in Livingstonia Area, Northern Malawi

Yukiyasu SAKA* and Kenji YAIRI**

* Institute of Earth Science, School of Education, Waseda University
** Department of Earth Sciences, Faculty of Science, Nagoya University

Introduction

Of the Karroo System distributed sporadically in northern Malawi, the Karroo System in the Livingstonia area has long received attentions owing to the occurrence of the coals. Detailed investigation which involved drill-hole programme clarified the quality and quantity of the coals as well as the stratigraphy, lithology and geological structures of the area. The result of this work is summarized in a comprehensive description and an excellent geological map (Cooper and Habgood, 1959). Recently the margin of the Karroo area was slightly modified by Kemp (1975) as mapped photogeologically by Stephens (1963, unpublished report).

Outline of geology

The Karroo geology in the Livingstonia area is reviewed briefly below according to Cooper and Habgood (1959).

The Karroo beds are entirely separated from the surrounding basement complex by major faults (Fig.1). The general succession given below is correlated on grounds of lithology with the K subdivisions of the Karroo sequence in the Ruhuhu Coalfield, Tanzania (Stockley, 1932) directly across Lake Malawi to the east.

Correlation	Division	Thickness (m)
K7	Chiweta Grits	46
	(unconformity)	
K6	Chiweta Bone Beds	260
	(unconformity)	
K5	Calcareous Siltstones	120
	Yellow and Khaki Mudstones	(top not seen) ca. 300
K3	Intermediate Beds;	
	hard arkosic siltstones	18
	chocolate-coloured and green mudstones	90
	yellow and pink arkoses and sandstones	ca. 145
K2	Coal Measures	30–107
K1	Basal Beds: green flaggy siltstones and pink arkoses with basal conglomerate	up to 76 (possibly much more)

2nd Prelim. Rep. Afr. Studies, Nagoya Univ., 89-107, 1977.

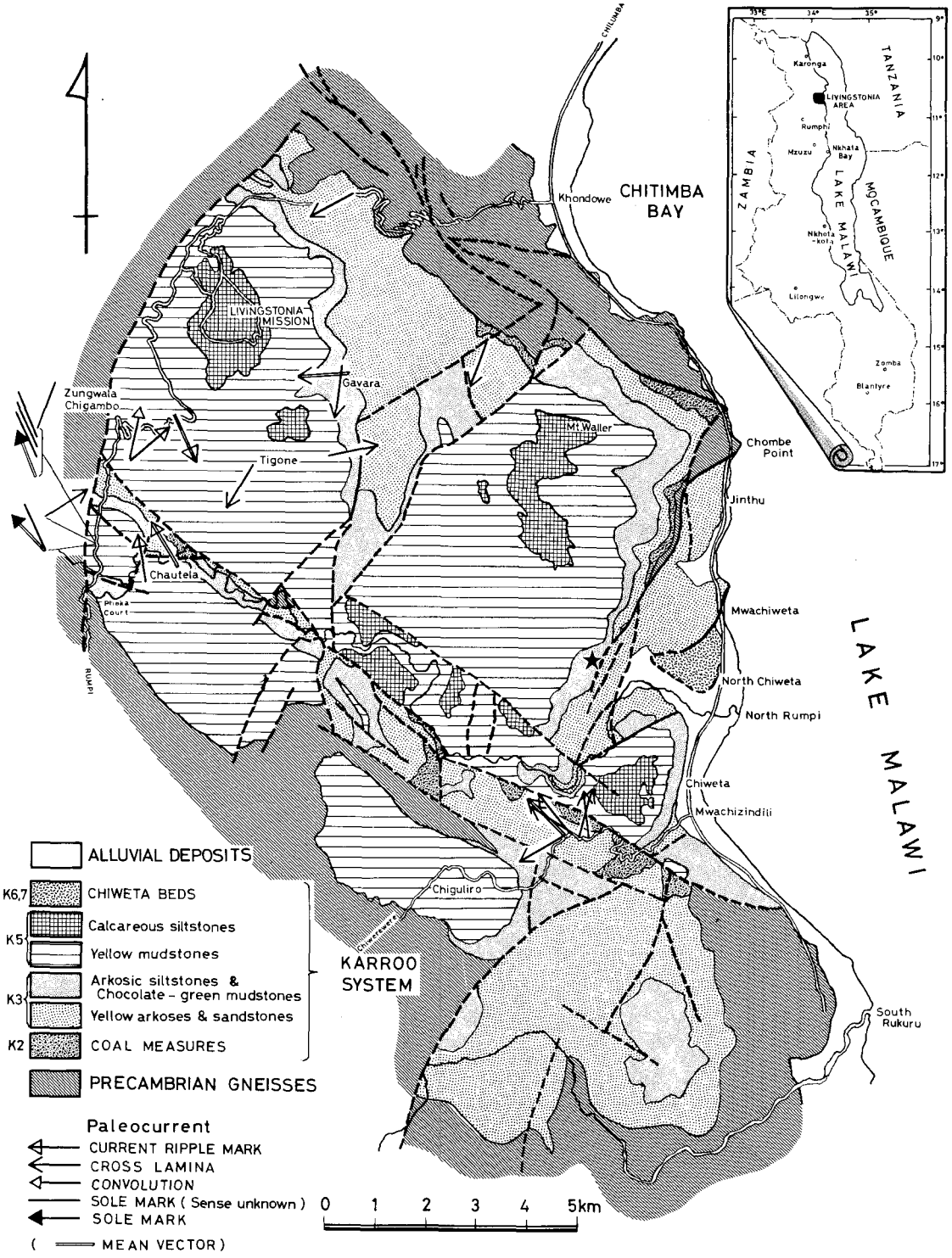

Fig. 1 Geological map of the Livingstonia area (after Cooper and Habgood, 1959). Paleocurrent directions are superimposed.

The Basal Beds (K1) and the Coal Measures (K2) are poorly exposed and the lithology is best known from drill-hole cores. The K2 Beds consist mainly of carbonaceous shales and siltstones with intercalations of feldspathic sandstones, coarse arkoses and coals or shaly coals. The Upper Coal Measures (K4) are not developed except thin and impersistent beds of carbonaceous mudstone which occur near the top of the K3 Beds. The K5 Beds overstep the K3 Beds in places and rest directly on the basement gneisses. The Chiweta Beds occupy a small down-faulted block near the mouth of the North Rumpi. The K6 Beds consist mainly of purplish mudstones the lower and the middle division of which include beds of nodular limestone and marly conglomerate. The K7 Beds consist of purplish grits.

The Karroo beds dip as a whole to the southwest as a result of the regional tilting of the basement which accompanied the major post-Karroo faulting. Drag on the beds along the major faults caused local increases and reverses in dip especially along the western margin of the area and to the south of the North Rumpi. Besides major faults, numerous minor faults and joints are developed throughout the area. Most of them trend essentially parallel to the major faults which control the tectonic feature of the Livingstonia Karroo area. The faulting and jointing mechanism and its relationship to the Rift faulting are examined on the basis of the structural analysis of these fractures by Yairi and Saka (1977).

Sedimentary structures

Owing to the poor communications within the Karroo area, the field work was restricted to only along the motor roads surrounding the area and footpaths around the Livingstonia Mission. On this account, the present investigation contributed no modifications to the stratigraphy and the mapping of the Livingstonia Karroo area. Sedimentological inspection of the Karroo beds, although restricted in place and horizon, revealed that there were developed several kinds of sedimentary structures suggestive or in some cases diagnostic of the depositional mechanism and environments. The sedimentary structures, especially those with directional properties, are of fundamental importance to the basin analysis (Potter and Pettijohn, 1963).

Apart from the scientific interest, the systematic basin analysis of the Karroo basin brings about a practical bearing in estimating where and how much the coals are available, inasmuch as the coals greatly owe their accumulation to the paleogeographical conditions.

This paper is intended to describe some sedimentary structures and to point out their usefulness for the basin analysis. It is beyond the scope of this paper to present an atlas of the sedimentary structures developed in the Livingstonia Karroo area or to reconstruct the paleogeography of the Karroo basin based on them. Sedimentary structures which disclose directional properties only when mapped are not treated here. To describe the property of layering the terms defined by Saka and Yairi (1977) are to be used.

Ripple mark

Ripple marks, both symmetrical and asymmetrical in a cross-section, are common in the finer grained facies; fine grained sandstones and siltstones of the K5 and K6 Beds. Crests are relatively straight, continuous and subparallel to each other, suggesting that the current directions were transverse to them

(Fig.2). Wave lengths are rather uniform in every set, ranging from as small as 1cm up to 10cm. Amplitudes of crests are of the order of milimeter. It is rare that all the bedding surface exposed is ornamented by ripple marks. Covering only patches of the bedding, marks become extinct rapidly in the transverse direction and much less rapidly in the trend direction (Fig.2,c). Ripple cross lamination genetically connected with ripple marks is not seen with the naked eye in the ripple marked stratum probably because of homogeneity and fineness of sediment.

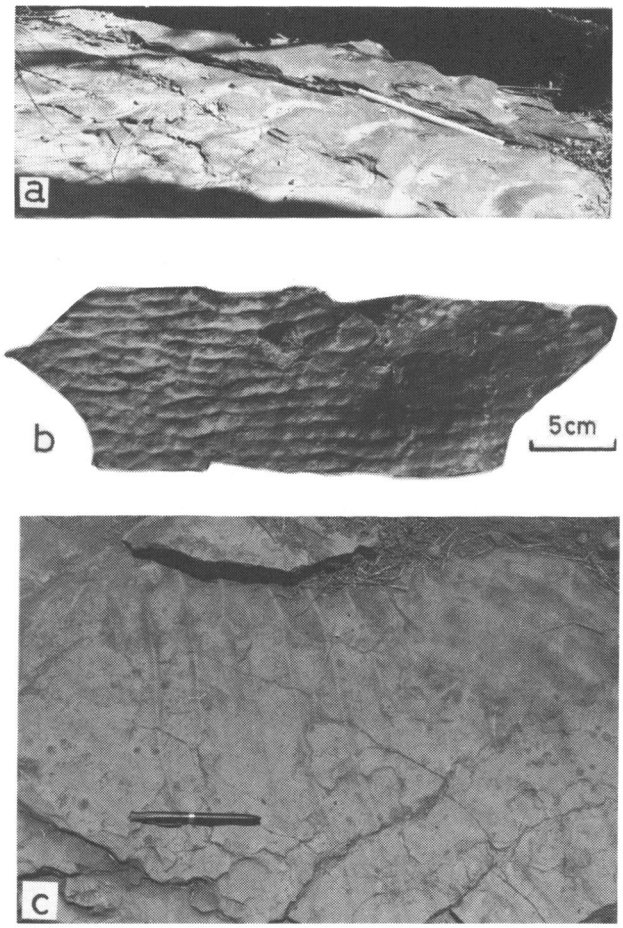

Fig. 2 Ripple mark

a. Asymmetrical ripple marks on yellow sandstone of K5 Beds. Current from left to right, parallel to ruler 30cm in length. Chautela.
b. Symmetrical ripple marks on 3cm-bedded siltstone, buff in colour, of K6 Beds. North Chiweta.
c. Asymmetrical ripple marks on greenish white, very fine grained sandstone of K6 Beds. Note that ripple marks occupy only a patch of bedding. Pen is 13.5cm long. North Chiweta.

Fig. 3 Asymmetrical ripple marks, as seen from above, on micro cross laminated siltstone of K6 Beds. Current from upper left to lower right for ripple marks and from top to bottom for micro cross laminae of trough type. Note the disparity of current directions between two structures. North Chiweta (Sketch by Y.S.)

The current readings of asymmetrical ripple marks are shown in Figs.16 and 17. Fig. 3 shows asymmetrical ripple marks developed on the upper surface of a micro cross laminated bed of siltstone. The down-current direction indicated by ripple marks is S10°E, while that indicated by micro cross laminae is S50°W, yielding a disparity of as large as 60°. The siltstone, though easily splitting into lamellae 1mm or so in thickness, forms a single bed. The discordance of the current directions read on and within a single bed may be attributable either to the change of the current direction in the course of the deposition of a bed or to the workings of two different currents independent from one another; one deposited the micro cross laminated bed, the other reworked the superficial materials to build up ripple marks.

It is of no doubt that ripple marks are products of bed load transport of sediment. They have, however, inferior directional significance, because many examples have been known which trend parallel or diagonal to the main current direction (Picard and High, 1973).

Micro cross lamina

Although micro cross laminae were observed only in mudstones of the K6 Beds, their actual occurrence may be common in the fine grained facies more or less interbedded in the coarse grained facies of the other Beds. Homogeneity of lithology and inferior likeli-

hood of exposure of the fine grained rocks may reduce apparently the occurrence of this structure.

Micro cross laminae are mostly of trough type. Those of tabular type are rare and ripple cross laminae are not seen. They occur in a single bed in either of the following two modes.

i) One or a few sets, as defined by McKee and Weir (1953), of micro cross laminae occupy a portion of a single bed, the rest of which is structureless or parallel laminated.

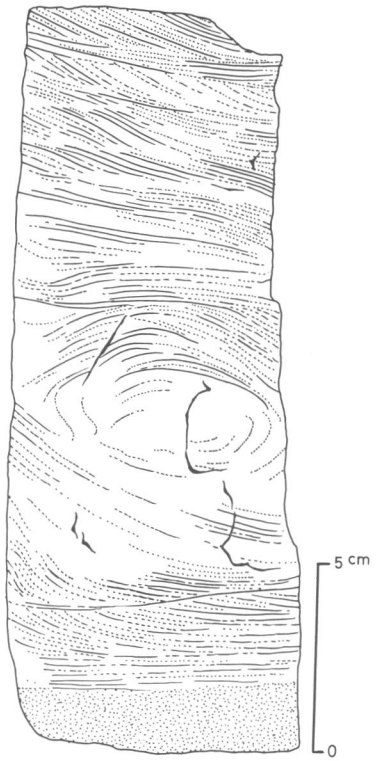

Fig. 4 Sequence of sets of micro cross laminae, parallel laminae and convoluted laminae seen in greyish white, very fine grained sandstone of K6 Beds. Mwachiweta. (Sketch by Y.S.).

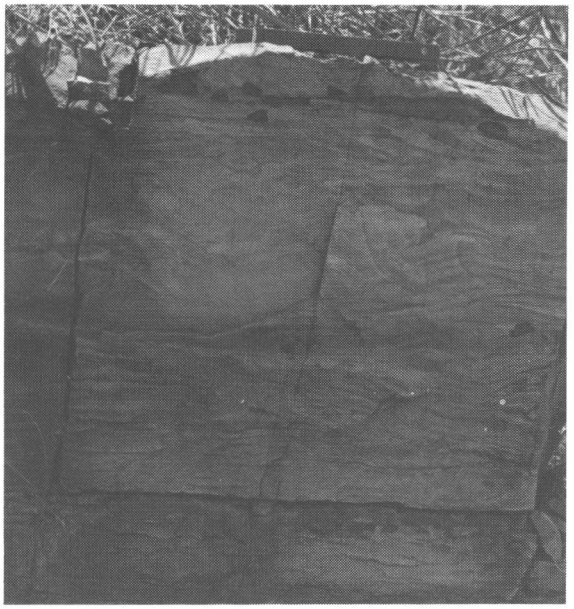

Fig. 5 Micro cross laminae above and below weakly convoluted laminae (middle) in greyish white, very fine grained sandstone of K6 Beds. Note a cut surface inclining to the right above the basal set of parallel laminae. Eighteen-centimeter ruler for scale. Mwachiweta.

ii) Several sets of micro cross laminae occupy the greater part of a single bed: Each set is truncated by an overlying set of micro cross laminae or of parallel laminae. Occasionally a few sets of convoluted laminae of various thicknesses are accompanied. In general, the sequence of sets in a single bed is as follows (in ascending order): Parallel laminae → micro cross laminae → convoluted laminae → micro cross laminae (intercalating parallel laminae) (Fig.4). A small-scale cut-and-fill structure was observed in one sample in which the basal set of parallel laminae are interrupted discordantly by the overlying set of cross

laminae (Fig.5). The latter set shows the sudden coarsening of sediment at somewhat rugged cut face. Such a regular sequence of laminae of different kinds in a single bed is strongly suggestive of the subsequently changing flow regime of the sediment-laden currents during one depositional episode.

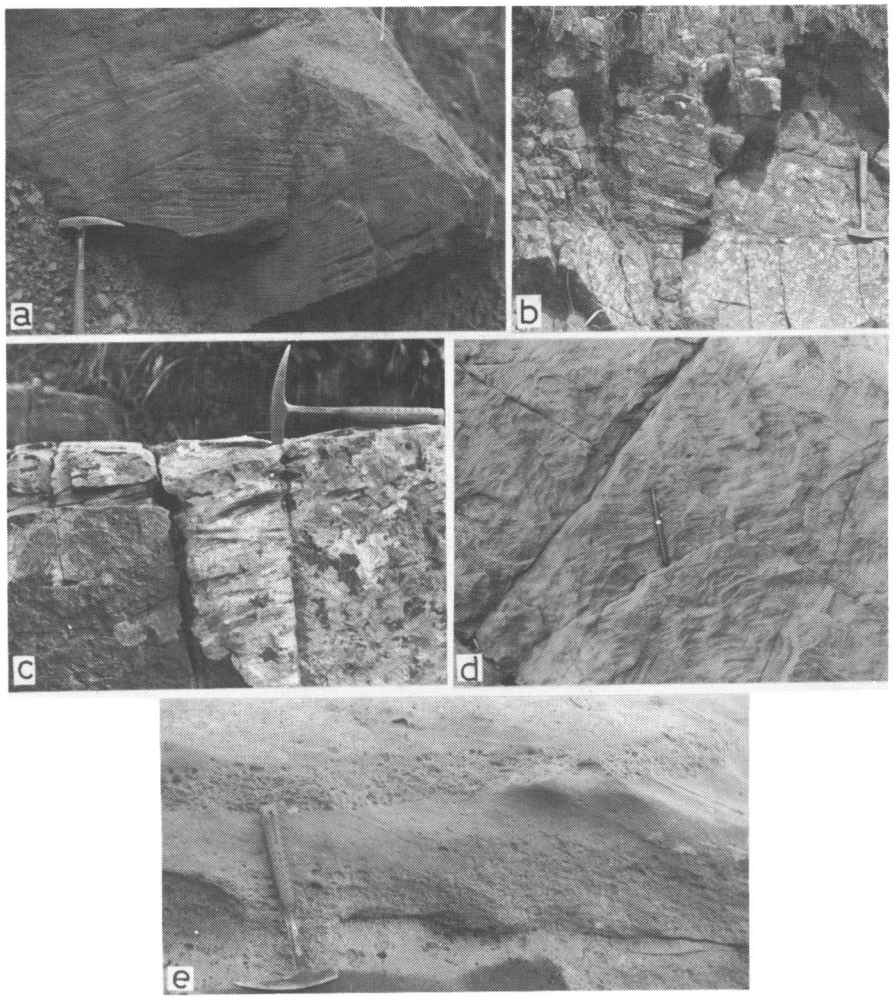

Fig. 6 Cross laminae of tabular type in arkosic sandstones of K3 Beds.

a. Set of cross laminae intercalated between sets of parallel laminae. Along the road between Chiguliro and Mwachizindili.
b. Set of cross laminae developed between massive sandstones below and above. *Ibid.*
c. Thin-stratified cross laminae. Gavara.
d. Plan view of cross laminae shown in c. Note that lamination is straight. Pen is 13.5cm long.
e. Concentration of pebbles in the lower part of cross laminated bed. Mwachiweta.

Cross lamina

Cross laminae are abundant in coarse arkoses of the K3 Beds and rarely observed in the K5, K6 and K7 Beds. In general, the cross laminated bed occurs isolatedly, being intercalated in structureless or parallel laminated beds (Fig.6, a and b). Thick sequence of cross laminated beds is seen only along the lakeshore at Jinthu where 20 to 50cm bedded, very coarse grained arkoses typical of the K3 Beds are well exposed.

Cross laminae of tabular type exceed those of trough type in abundance. Lamination is distinct (Fig.6, a) or indistinct (Fig.6, b). Thickness of individual laminae is variable ranging from 2 or 3mm to 10cm (Fig.6, c and d). Cross lamination of tabular type is straight, sharply abutting against the planar bottom and truncated by the upper bedding surface. The cross laminae shown in Fig.6, a, being exceptional, are concave-downward near the top and concave-upward near the base, taking a somewhat sinusoidal figure. Inclination of laminae is variable ranging from 15° to 30°. Those inclining at moderate angles between 20° and 25° predominate (Fig.7).

Fig.6, e shows cross laminae developed in coarse grained arkoses of the K3 Beds at Mwachiweta. Angular pebbles of dark greenish siltstone derived by contemporaneous erosion are concentrated in the lower part of a bed. "Conglomerate division" grades upward into "sandstone division", in which cross lamination is distinct, by rather abrupt decrease in sizes and amounts of pebbles. In the "conglomerate division", though lamination is invisible, its extension can be traced in the regular arrangement of long axes of pebbles. The cross lamination cited here may be referred to the avalanche-front cross-stratification reported by Picard and High (1973).

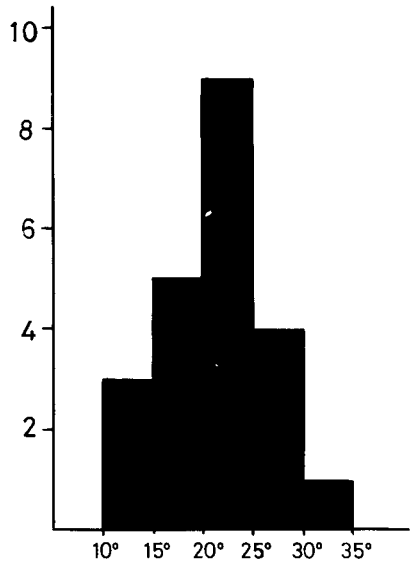

Fig. 7 Distribution of inclination angles of cross laminae developed in K3 Beds at Mwachiweta.

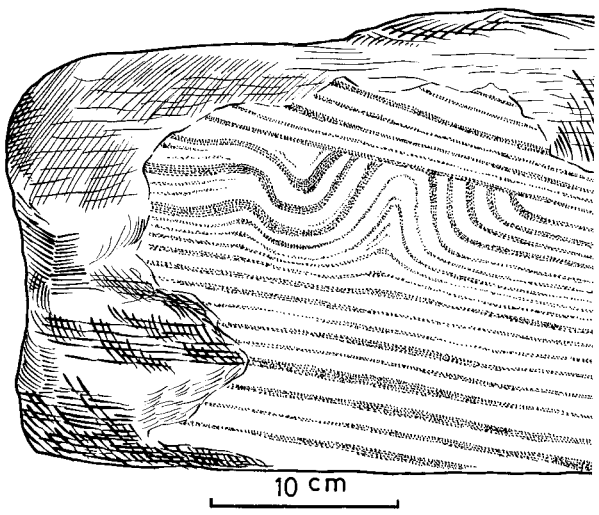

Fig. 8 Slumping of cross laminae in yellow, fine grained sandstone of K5 Beds. Tigone (Sketch by Y.S.).

Slumped cross laminae were found in a fine grained sandstone bed, 45cm in thickness, of the K5 Beds at Tigone. The slumped division, 6.5cm in thickness, is interstratified between cross laminae of tabular type dipping to the southwest at 12 degrees. The disturbed laminae are sharply truncated at the top, while their lower boundary is transitional to the undisturbed laminae below (Fig. 8). Contortion of laminae may be attributable to the superficial slumping on the front of a growing bar induced by some shocks, most probably by earthquake.

The paleocurrent directions indicated by cross laminae are shown in Figs.15, 16 and 17. The readings from a single set are fairly consistent. For example, consistency ratios of 98.9%, 99.8% and 91.6% are obtained for the cross laminae given in Fig.6, b, d and e, respectively.

Current mark

To the north of Phoka court, the siltstone facies characteristic of the lower division of the K5 Beds contains flysch sequences, the total thickness of which is about 10m. Sandstone beds, 5 to 15cm in thickness, alternate rhythmically with mudstone beds several centimeters in thickness (Fig.9). These flysch sequences bear many of the sedimentary features such as graded bedding and current marks diagnostic or suggestive of turbidites. Graded bedding, which Murphy and Schlanger (1962) designated the only valid criterion for recognition of turbidites, is observed in every sandstone bed. The complete succession of internal sedimentary structures, T_{a-e} of Bouma (1962), is not developed. Only the lowermost division (graded interval, T_a) (Fig.10, b) or lower two divisions (graded interval and lower interval of parallel lamination, T_{a-b}) (Fig.10, a) constitute a bed.

Fig. 9 Flysch-type alternation of graded sandstone and mudstone interbedded in the lower division of K5 Beds. Hammer for scale in right middle. North of Phoka court.

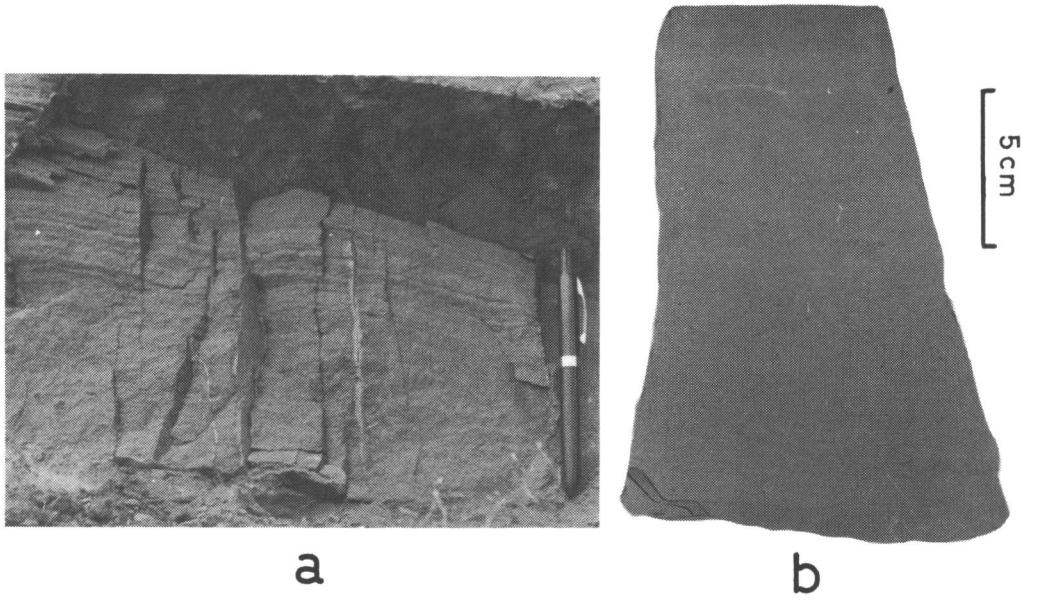

Fig.10 Graded bedding of sandstone in turbidite sequences intercalated in K5 Beds. North of Phoka court.
a. Sandstone bed with laminated top and graded base.
b. Structureless graded sandstone with flat top and loaded base. Note a mud plume in the basal part (traced in ink to enhance visibility).

Current marks recognized on the lower surface of graded sandstone beds are flute, bounce, groove marks and longitudinal ridges and furrows, all of which have been best known from marine turbidites of various ages and also from artificial turbidites made by flume experiments. Recently, Adachi (1975) reported occurrence of sole marks such as flute, furrow and groove marks from the Karroo System (Upper Triassic Mazeras Sandstones) to the northwest of Mombasa, Kenya.

Flute marks occur closely crowded. They are deviating in shape from a typical mark. Conical type and bulbous type, as defined by Dzulynski and Walton (1965), are recognized (Fig.11, a and b). Only one bounce mark was found on the sole surface ornamented by flute marks of conical type (Fig.11, c). It is 5cm long and has a width of 5mm at the middle point of the welt. Observed two groove marks are shown in Figs.11, c and 12, b. The one (Fig.11, c) is margined on both sides by fine and sharp ditches several milimeters in depth. The thickness of the groove mark is 1cm from the bottom of the ditch. The other (Fig.12, b) occurs on the surface marked by numerous moulds, irregular in shape and various in size, of problematical origin. Of these moulds, those strongly elongated trend parallel to the groove mark and are regarded as delicate bounce marks. The groove mark has a width of 10mm and a

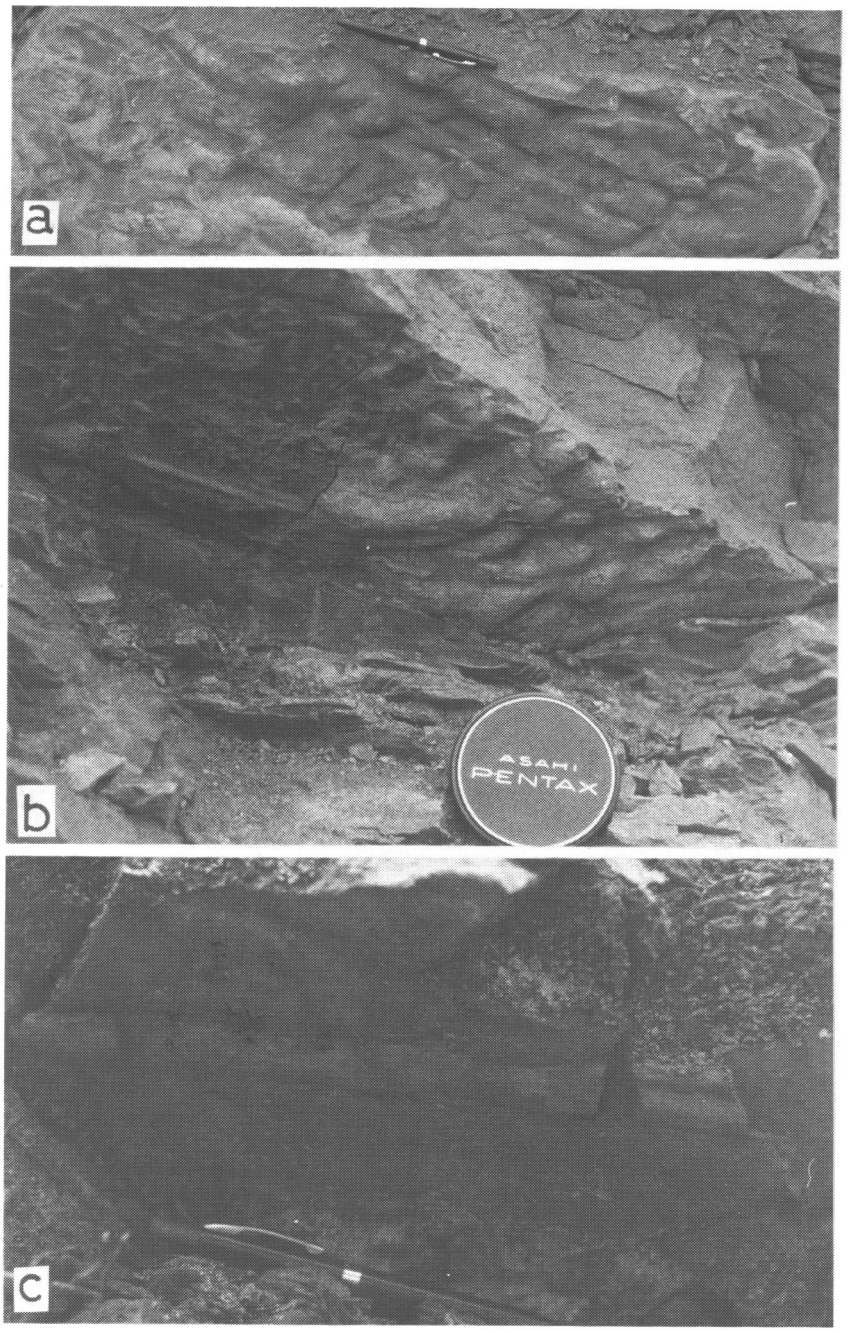

Fig.11 Sole marks on the lower surfaces of graded sandstones interbedded in K5 Beds. North of Phoka court.

a. Swarm of flute marks somewhat irregular in shape. Current from right to left. Pen is 13.5cm long.
b. Bounce mark (left middle) and flute marks (right middle). Cap of camera lens for scale is 5cm in diameter.
c. Groove mark bounded on both sides by sharp ditches.

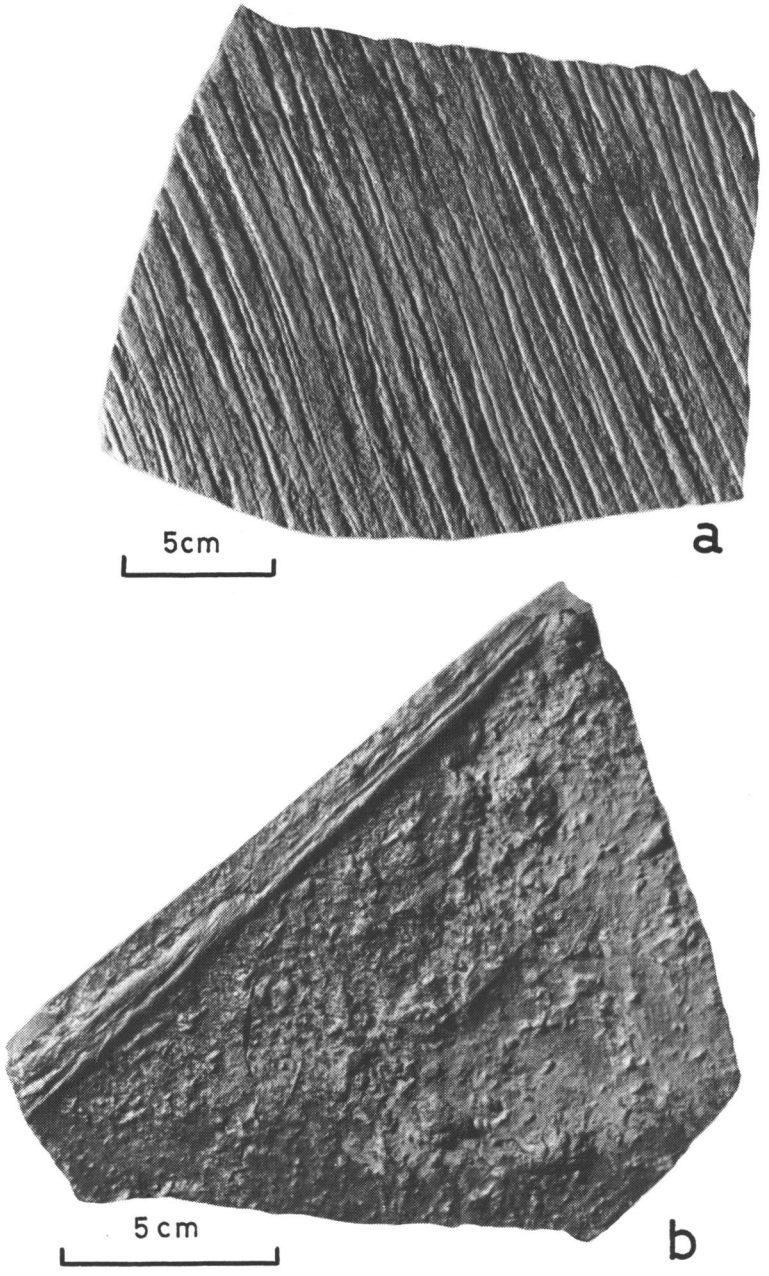

Fig.12 Sole marks of graded sandstones of K5 Beds. North of Phoka court.

a. Longitudinal ridges and furrows on the lower surface of 10cm-bedded fine grained sandstone.

b. Groove mark with minor striations and irregular moulds of problematical origin.

depth of 1.5mm. It is accompanied by minor striations parallel to the margins. Longitudinal ridges and furrows are developed occasionally (Fig.12, a). Flat topped ridges, 15-20mm in width, are separated by sharp furrows 1mm± in width. Ridges are parallel or subparallel and continuous, although they show appreciable change in width and occasionally coalesce. The joining of ridges is in both directions. Trends of ridges occurring on different surfaces are consistent. A consistency ratio of 99.98% are obtained for three samples occurring close to each other.

Load marks without any directional significance are common.

Paleocurrent readings of these current marks are shown in Fig.16. They are fairly consistent with the consistency ratio of 94.4% and mean vector of S18°E → N18°W.

Graded bedding is seen also in some horizons of the lower division of the K5 Beds at Chiguliro. There, more or less micaceous sandstones 10cm to 20cm in thickness alternate with shaly siltstones 1cm to 10cm in thickness. Sandstone beds occasionally show graded bedding or have a graded base and a laminated top. Although no sole marks were found, they can safely be referred to turbidites.

Detailed investigations are required to reveal the distribution and to fix the stratigraphic position of turbidite sequences within the lower half of the K5 Beds, for they not only provide many clues useful to basin analysis but serve as marker beds.

Deformational structure

Besides the slumped cross laminae and load marks described above, slump structures and convoluted laminae are listed up as deformational structures seen in the present area.

Unlike the structures formed by currents which were not always directly away from the hinterland, slump structures are excellent indicators of the paleoslope-direction, though only a local one, inasmuch as they are products of gravity-generated movement of sediment. Only one sample of slump structures was found in siltstones of the K6 Beds at North Chiweta(Fig.13,a). The base of slumped zone cuts the underlying beds. Lamination of slumped beds in part abutts against the base. These features demonstrate that the sliding was not of décollement type. The undulation of slumped beds is most marked near the base, where thickening of beds is recognized, and diminishes gradually upwards.

There is a controversy on the origin of convoluted laminae. The directional significance of convoluted laminae is, therefore, evaluated in largely varying degrees. For this reason, only convoluted laminae with distinct polarity and undoubtedly indicative of the paleoslope-direction were taken into account. Convoluted laminae are common in fine grained rocks of the K5 and K6 Beds. The convolutions usually occupy the center of a bed, dying out both upward and downward to grade into the parallel laminations (Fig.13, b). In white siltstones of the K6 Beds is occasionally found the chaotic crumpling of laminae, though not so well visible because of homogeneity of sediment, suggestive of great mobility of silt materials just after deposition (Fig.13, c).

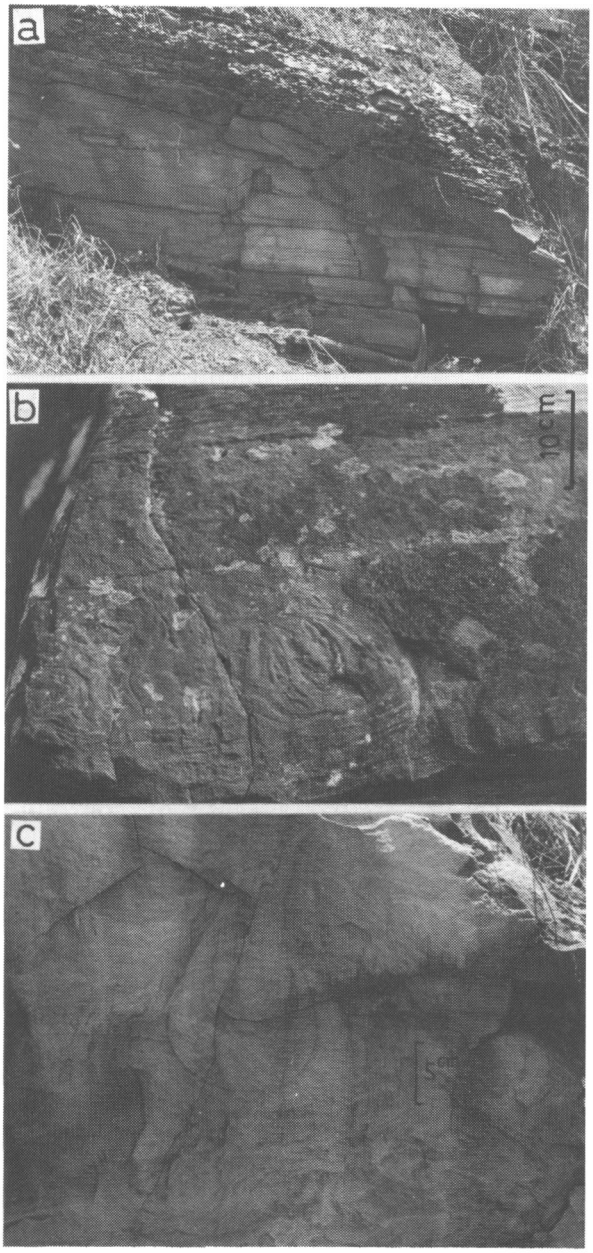

Fig.13 Deformational structures

a. Slump structure seen in siltstones of K6 Beds. North Chiweta.
b. Convoluted laminae in very fine grained sandstone, buff in colour, of K5 Beds. 1km southeast of Zungwata Chigambo.
c. Convoluted laminae in white siltstone of K6 Beds. Scale is marked on outcrop surface. North Chiweta.

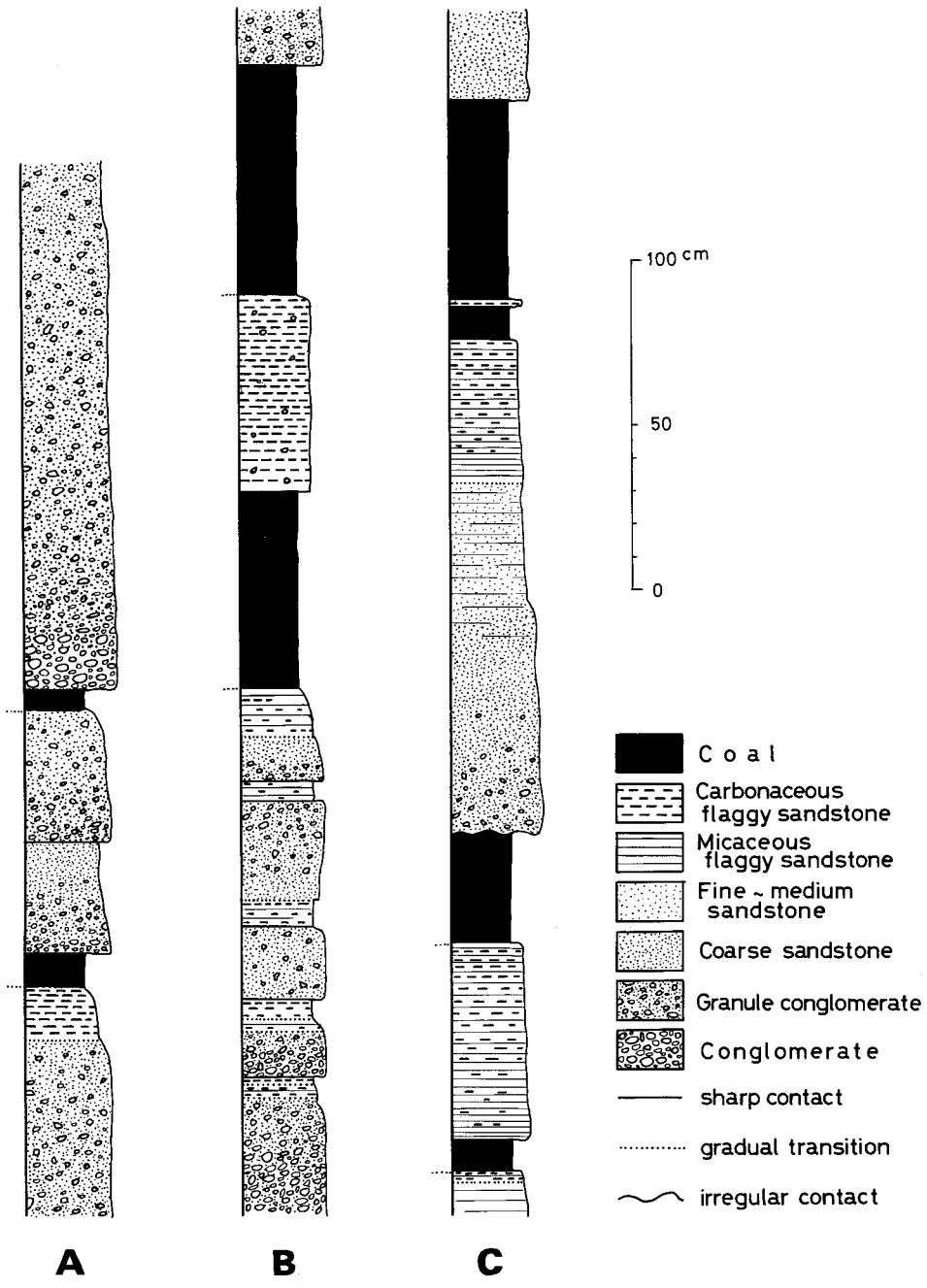

Fig.14 Hemi-cyclic sequences of sediments developed in K3 Beds. Along the road between Chiguliro and Mwachizindili. See text for explanation.

Cyclic sediments

A systematic upward gradation of lithofacies is occasionally developed in the coarse grained facies of the K3 Beds (Fig.14). The integral sequence is as follows:

Top	Coal Seam	
	Carbonaceous flaggy sandstone	Amount of carbonaceous material increasing upward
	Micaceous flaggy sandstone	Lamination more distinct upward
	Massive arkose	
	Granule conglomeratic arkose of conglomerate	Granule and pebble increasing in size and amount downward
Bottom		

The upper and the lower boundary of the sequence is sharp and sometimes erosional, while each lithofacies grades into the overlying one without distinct boundary. The sequence is usually incomplete: It may be interrupted at any horizon and the lower divisions may be missing. The intervening divisions may be absent to bring the otherwise separated divisions into contact with one another by a somewhat sharp boundary. The thickness of a sequence is widely variable ranging from only several tens centimeters to more than 2m.

These sequences reflect the hemi-cyclic sedimentation. To make use of them for basin analysis, several parameters are required to be mapped independently or in combination; *e.g.*, thickness of the sequence or individual division, frequency of occurrence of a given division, maximum grain size in the lower division and so on.

Consideration

Paleocurrent readings are plotted on the geological map (Fig.1) and in the rose diagrams (Figs.15, 16 and 17). Because of small numbers of readings, no paleocurrent pattern sufficient to reconstruct the paleo-

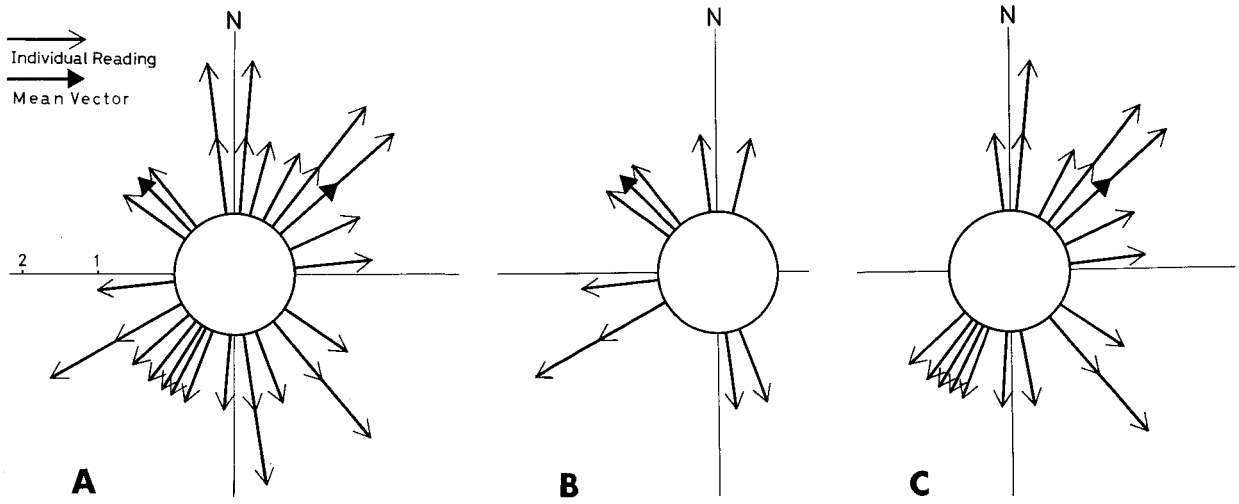

Fig.15 Current-rose diagrams of K3 Beds based on cross laminae. A. All observations plotted. B. Those taken in lakeshore area excluded. C. Only those taken in lakeshore area plotted.

geography of the Karroo depositional basin can be integrated.

There is, however, an observable tendency that most of paleocurrents are directed to the center of the Karroo area, or more strictly to say, to the inside of the area, except to the north of Phoka court and along the lakeshore. The centripetal pattern of the paleocurrent directions may exclude the possibility that the original basin of the K3 Beds covered far much wider area than the present Karroo area does, the latter being only a fragmental relic of the former. The north-northwestward paleocurrents seen to the north of Phoka court, probably of turbidity currents as suggested by sedimentary structures, suggest that the basin extended to this direction beyond the present boundary fault.

The current rose diagram of cross laminae in the K3 Beds along the lakeshore (Fig.15, C) makes a mirror image of that of the main part to the west (Fig.15, B). A sector of perfect blank of readings is contained in both diagrams showing widely scattered directions; a slight west of north to southwest in the former diagram, northeast to southeast in the latter, respectively. Such a paleocurrent pattern of the K3 Beds is strongly indicative of the hinterland of the K3 Beds being situated between the lakeshore area and the main area. The hinterland, originally a ridge on the pre-Karroo surface, may have been a barrier separating the main Livingstonia basin from the basin to the east when the K3 Beds were deposited. The approximate position and trend of this barrier may be represented

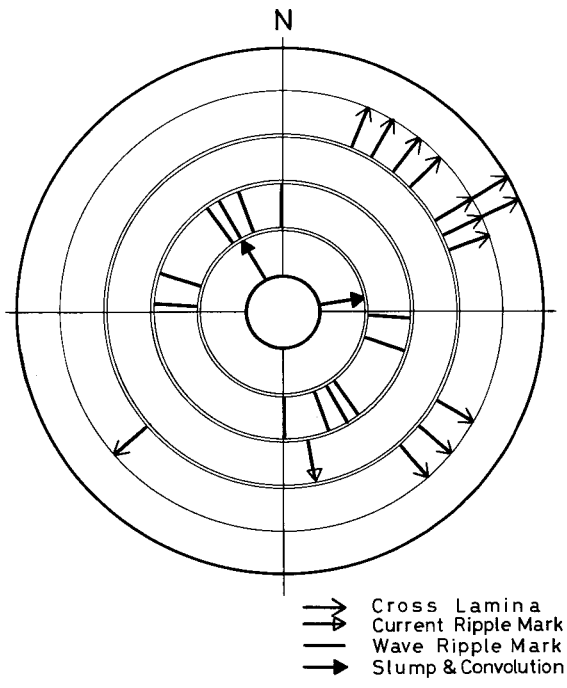

Fig.16 Current-rose diagram of K5 Beds. Numbers of circles correspond with those of readings.

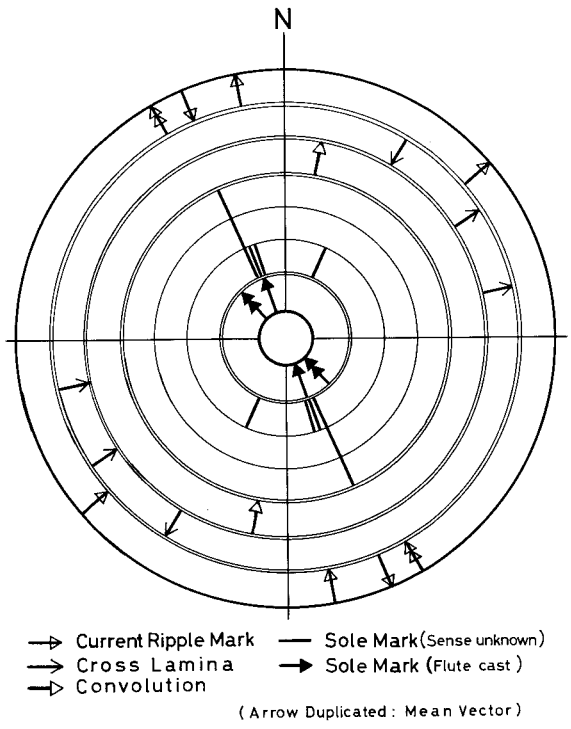

Fig.17 Current-rose diagram of K6 and K7 Beds. Numbers of circles correspond with those of readings.

by a slice of basement gneisses which is expressed on the geological map (Cooper and Habgood, 1959) as a tectonic inlier intervening in the Karroo System (Fig.1). It extends from the Chombe Point south-southwestward for about 3.5km. At the point marked by an asterisk on Fig.1, a ridge of the basement is ascertained beneath the Karroo beds by drilling: The K1 Beds as well as the greater part of the K2 Beds are lacking and the uppermost part of the K2 Beds rests directly on the basement (Cooper and Habgood, 1959). Although Cooper and Habgood give no remark on the extent of the ridge, it is of no doubt that this is the south-southwestern extension of the ridge now represented by the inlier.

It has been known that the K3 Beds were deposited after the relief of the pre-Karroo surface had been concealed beneath the K1 and K2 Beds. It is concluded that the main Livingstonia Karroo basin remained unconnected, at least in its northern part up to the later stage of the K3 Beds, with the basin to the east which is considered to have been situated in what is now Lake Malawi.

The general change of lithofacies of the Karroo System ranging from the K1 Beds up to the upper division of the K5 Beds demonstrates the subsequent increase in depth and distality of the depositional site. It is of interest that cross laminae are abundant in the relatively shallow and proximal facies (the K3 Beds), while the turbidites are intercalated in the relatively deep and distal facies (the K5 Beds). At the K3 stage, when the basin was still narrow and shallow, the deltaic sedimentation was one of the major mechanisms to fill up the basin. Within the main part of the basin enlarged on the beginning of the K5 stage, the deltaic sedimentation was replaced by another mechanism which involved the emplacement of clastics by turbidity currents. Turbidity currents may have started from slumping at the advancing front of delta which is supposed to have occupied the near-shore side of the finer grained facies now characteristic of the K5 Beds. The environmental model tentatively cited here closely resembles the model which explains the occurrence of turbidites found in the glaciolacustrine sequence of the Dwyka Series in northeastern India (Banerjee, 1966). Turbidite origin of glaciolacustrine sediments is also suggested for the Pleistocene sediments in northwestern Pennsylvania, U.S.A., based on the examination of sedimentary structures (Harrison, 1975).

Acknowledgements – We wish to thank Professor Emeritus Isao Matsuzawa of Nagoya University for his encouragement. Field work was much facilitated by Mr. V.H.B. Gondwe of Ministry of Agriculture and Natural Resources of Malawi (already retired), Mr.J.H.Dean and Dr.M.J.Crow of Geological Survey Department of Malawi, Mr.Yoshihide Nakai and other staffs of Japan Overseas Cooperation Volunteers, to whom we express our deep gratitude. Thanks are also extended to the staffs of the Livingstonia Mission and people in Livingstonia, who gave us warm hospitality during our stay in Livingstonia.

References

ADACHI, M. (1975): Sole markings from the Mazeras Sandstones (Upper Triassic), northwest of Mombasa, Kenya. *1st. Prel. Rep., Afr. Studies, Nagoya Univ.,* 21-25.

BANERJEE, I. (1966): Turbidites in a glacial sequence : A study from the Talchir Formation, Raniganj Coalfield, India. *Jour. Geol.,* **74,** 593-606.

BOUMA, A.H. (1962): *Sedimentology of some flysch deposits – A graphic approach to facies interpretation.* Elsevier, Amsterdam, 168p.

COOPER, W.G.G. and HABGOOD, F. (1959): The geology of the Livingstonia coalfield. *Bull. Geol. Surv. Nyasaland Prot.,* **11,** 51p.

DZULYNSKI, S. and WALTON, E.K. (1965): *Sedimentary features of flysch and greywackes, Developments in sedimentology,* **7,** Elsevier, Amsterdam, 274p.

HARRISON, S.S. (1975): Turbidite origin of glaciolacustrine sediments, Woodcock Lake, Pennsylvania. *Jour. Sed. Petrol.,* **45,** 738-744.

KEMP, J. (1975): The geology of the Uzumara area. *Bull. Geol. Surv. Malawi,* **41,** (in press).

McKEE, E.D. and WEIR, G.W. (1953): Terminology for stratification and cross-stratification in sedimentary rocks. *Bull. Geol. Soc. Amer.,* **64,** 381-390.

MURPHY, M.A. and SCHLANGER, S.O. (1962): Sedimentary structures in Ilhas and Sao Sebastiao Formation (Cretaceous), Reconcavo Basin, Brazil. *Bull. Amer. Assoc. Petrol. Geol.,* **46,** 457-477.

PICARD, M.D. and HIGH, L.R.Jr. (1973): *Sedimentary structures of ephemeral streams, Developments in sedimentology,* **17,** Elsevier, Amsterdam, 223p.

POTTER, P.E. and PETTIJOHN, F.J. (1963): *Paleocurrents and basin analysis.* Springer, Berlin, 296p.

SAKA, Y. and YAIRI, K. (1977): Karroo System to the west of Karonga, Northern Malawi. *2nd. Prel. Rep., Afr. Studies, Nagoya Univ.* (in press).

STEPHENS, E.A. (1963): Unpublished report.

STOCKLEY, G.M. (1932): The geology of the Ruhuhu Coalfield, Tanganyika Territory. *Quart. J. geol. Soc. Lond.,* **88,** 610-622.

YAIRI, K. and SAKA, Y. (1977): Tectonic notes on the Livingstonia area, northern Malawi; in relation to post-Karroo rift faulting. *2nd. Prel. Rep., Afr. Studies, Nagoya Univ.,* 108-132.

Tectonic Notes on the Livingstonia Area, Northern Malawi, in Relation to the Post-Karroo Rift-Faulting

Kenji YAIRI* and Yukiyasu SAKA**

* Department of Earth Sciences, Faculty of Science, Nagoya University
** Institute of Earth Science, School of Education, Waseda University

Introduction

Sedimentary rocks of the Karroo System are well preserved in the Livingstonia area of Northern Malawi as a downfaulted trough surrounded by Basement Complex gneisses. Cooper and Habgood (1959) described the geology of the Livingstonia Coalfield in detail, and the regional geology of its environs was summarized by Carter and Bennett (1973), Thatcher (1974) and Kemp (1975).

In August and September in 1975, we carried out field investigations to throw light on the Karroo sedimentology and post-Karroo tectonics in the areas shown in Figs. 7, 17 and 18 (Fig. 1). Sedimentary structures of the Karroo System are described in separate articles of this volume (Saka and Yairi, 1977ab; Saka, 1977). In this paper, we describe fault and joint patterns developed in the Karroo System and Basement Complex, and discuss their close relation to the formation of the Malawi Rift Valley. For convenience a few data taken in the Karonga (Fig. 17) and the Nkhata Bay area (Fig. 18) are treated here.

The Malawi Rift Valley forms a southern part of the East African Rift System (Dixey, 1956; McConnell, 1972, 1974), and is still active at the present day as inferred from the seismic activity (Fairhead and Girdler, 1969). The birth of the Malawi Rift Valley, however, is a matter of controversy. Dixey considered that the rifting was fundamentally caused by a stress system that had been effective since Precambrian time and also showed that many of the features of the Malawi trough dated back in the early Cretaceous time (Dixey,

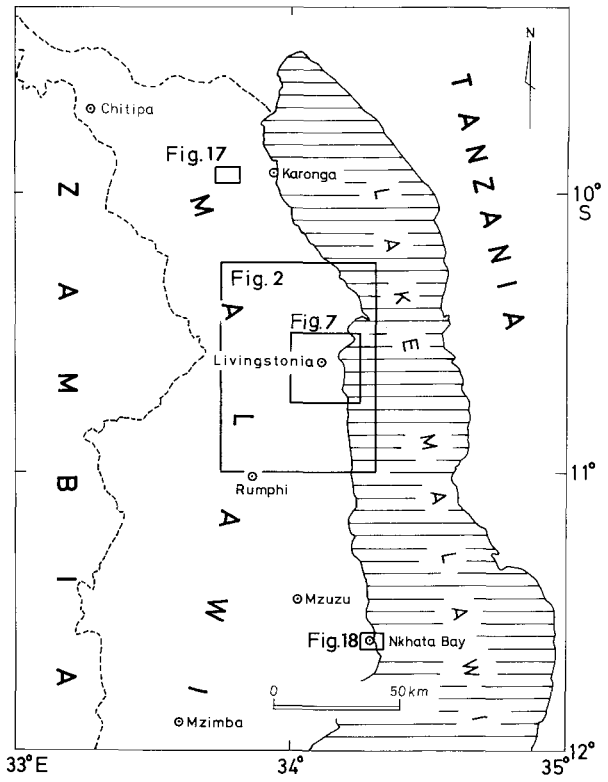

Fig. 1 Index map of the investigated area. Detailed locality maps are given in Figs. 2, 7, 17 and 18 shown by insets.

2nd Prelim. Rep. Afr. Studies, Nagoya Univ., 108-132, 1977.

Table 1 Five principal erosion surfaces in Malawi (Lister, 1967). Average heights of the erosion surfaces in the Livingstonia area and its environs shown in Fig.2 are listed in feet in the right column.

Gondwana	Jurassic	8500–8000
Post-Gondwana	early- and mid-Cretaceous	8000–6500
African	late-Cretaceous to early-Miocene	4500–4000
Post-African	late-Miocene and Pliocene	3000–2000
Quaternary	end-Pliocene to present day	1800–1600

1939, 1956). As for Northern Malawi, Thatcher (1974) noted that major rift-faultings took place during the middle Cretaceous time after the sedimentation of the Upper Jurassic–Lower Cretaceous Dinosaur Beds, and that further episodes of the rift-faulting occurred at the close of the African and post-African erosion cycles, respectively, and were followed by successive younger phases of uplift and faulting during Pleistocene to Recent (Table 3). In Central Malawi, the main rift-faulting is considered to have occurred in Jurassic-Cretaceous times by Bloomfield and Garson (1965) and Walshaw (1965); while the rift-faulting is believed to have occurred in Miocene time by Dawson and Kirkpatrik (1968), Thatcher (1968) and Walter (1972). It is of great importance to know the timing of the initiation and development of the rift-faulting after the Karroo sedimentation.

Geomorphology

The geomorphology of the Livingstonia area and its environs is here outlined. For this purpose a summit level map (Fig. 2) was prepared by using six sheets of topographic map at a scale of 1 : 50,000 (1033B4, 1033D2, 1033D4, 1034A3 &A4, 1034C1 and 1034C3). The area is divided into the following topographic units: high-level plateaus, low-level wide valleys, lakeshore plains, and steep linear escarpments making steps between these relatively flat surfaces. These features reflect the influence of successive periods of rift-faulting on land forms developed during the major erosion cycles since Jurassic (Lister, 1967). The geomorphological development of Malawi has been described in terms of the five principal erosion cycles listed up in Table 1 (Lister, 1967; Dixey, 1937; King, 1963), though one more ancient surface is represented by the basal contacts of the Karroo System and the underlying Basement Complex (Thatcher, 1974).

The Gondwana surface is best displayed on the undulated crestlines on the Nyika Plateau, where the original planation was dissected by subsequent erosion cycles, chiefly of the post-Gondwana. It stands at a height over 8000 feet above sea level as the highest peaks such as Nganda (8552 ft.) and Vitumbi (8292 ft.). The basal contact of the Dinosaur Beds, which occur in a narrow belt along the lakeshore at Lion Point and northward, probably represents a fossil Gondwana surface (Lister, 1967; Thatcher, 1974).

The post-Gondwana surface is developed on the northern and the southern margin of the Nyika Plateau and is characterized by

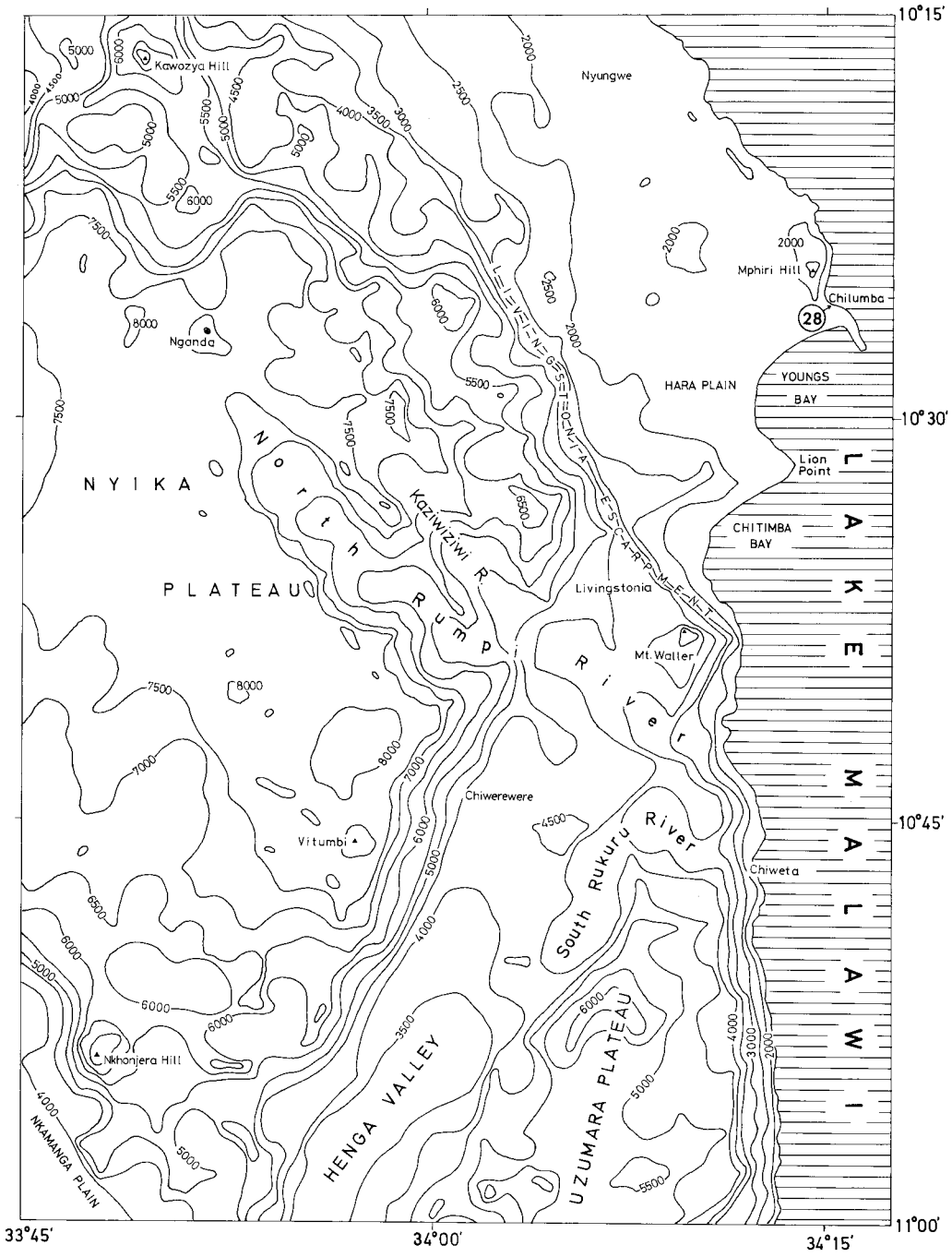

Fig. 2 Summit level map of the Nyika Plateau and Livingstonia area (contours: 500 feet intervals). Contour lines are smoothed out by burying valleys less than 2km in width on topographic maps at a scale of 1 : 50,000.

broad valleys which cut into the higher Gondwana surface. A number of hill summits in the North and South Nyika Foot-hills (Thatcher, 1974) are probably remnants of this surface. Uzumara Plateau which stands at a height over 6000 feet may have been formed during the post-Gondwana cycle, though it is dissected by valleys formed by the subsequent African cycle of erosion.

The African surface, which is most extensively developed in Malawi and characterized by a mature peneplanation, is well developed in the Nkamanga Plain at the southwestern corner of Fig. 1 and in the area from the Henga Valley to the Livingstonia Hills. It forms a flat-bottomed valley floor at the Henga Valley and well-preserved flat summits on the Karroo sediments at Livingstonia Hills, where the surface is particularly well displayed on the Mount Waller or Chombe Hill (4501 ft.) and on the Livingstonia Hill (4500 ft.). The deep dissection of the African cycle of erosion penetrates into the post-Gondwana surface. The dissections along the North Rumpi River, the North and South Nyika Foot-hills, and the margin of Uzumara Plateau probably took place during this cycle. The base of the Sungwa Beds (Table 3), which occur to the north of the present area, may represent a fossil African erosion surface (Thatcher, 1974).

The African surface of the Livingstonia Hills is abruptly truncated on the east by the Livingstonia Escarpment. Between the foot of the escarpment and the lakeshore, the post-African surface is well preserved on the hill summits of 2000 to 3000 feet in elevation. The post-African erosion is considered to have been promoted by the down-faulting of a portion of the African surface (Kemp, 1975). This erosion cycle also penetrates the major valley floor formed by the African cycle of erosion.

The Quaternary cycle of erosion has taken place together with the deposition of alluvium and lacustrine sediments since the close of the post-African cycle, and is well displayed on the Lakeshore Plain which stands at heights of 1600 to 1800 feet. Although the dissection by this cycle disappears to be buried in the summit level map of Fig. 2, youthful Quaternary erosion does progress along the crest of the rift valley escarpment. This erosion notches the crest and face of the scarp and sometimes continues headwards for several miles into the valleys formed by older cycles of erosion (Lister, 1974). The South Rukuru River has captured the drainage system of the Henga Valley which, once flowed southwest, now flows to the northeast draining into Lake Malawi.

The Nyika Plateau is bounded on the northeast, southeast and northwest by distinctive linear escarpments, which are called the Livingstonia, East Nyika and West Nyika Escarpments, respectively (Thatcher, 1974; Kemp, 1975). As shown in Fig. 2, the Livingstonia Escarpment trending northwest cuts sharply the East Nyika Escarpment trending northeast. The former NW trend, on this account, may represent a younger phase of the post-Karroo movements compared with the latter NE trend.

The Livingstonia Escarpment (Fig. 3), which marges northward with the South Karonga Scarp Zone (Fig. 4) (Thatcher, 1974), extends southward swinging to the southwest to the east of the Mount Waller, then trending slightly east of south passing Chiweta to Nkhata Bay (*see* Figs. 1 and 2). North of Nkhata Bay, the Lake is directly flanked by steep escarpments bounding the eastern

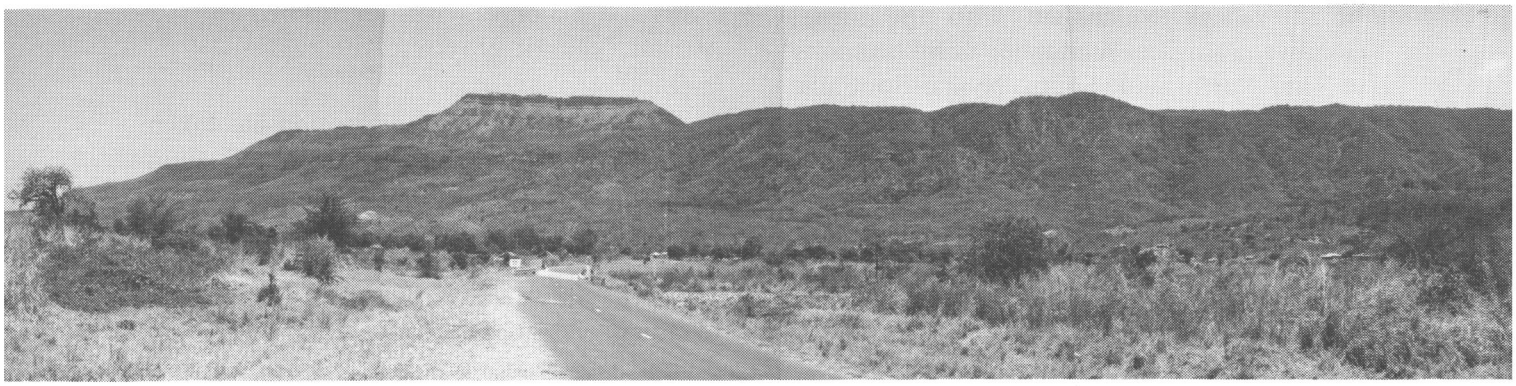

Fig. 3 Mt. Waller and Livingstonia Escarpment viewed from khondowe village.

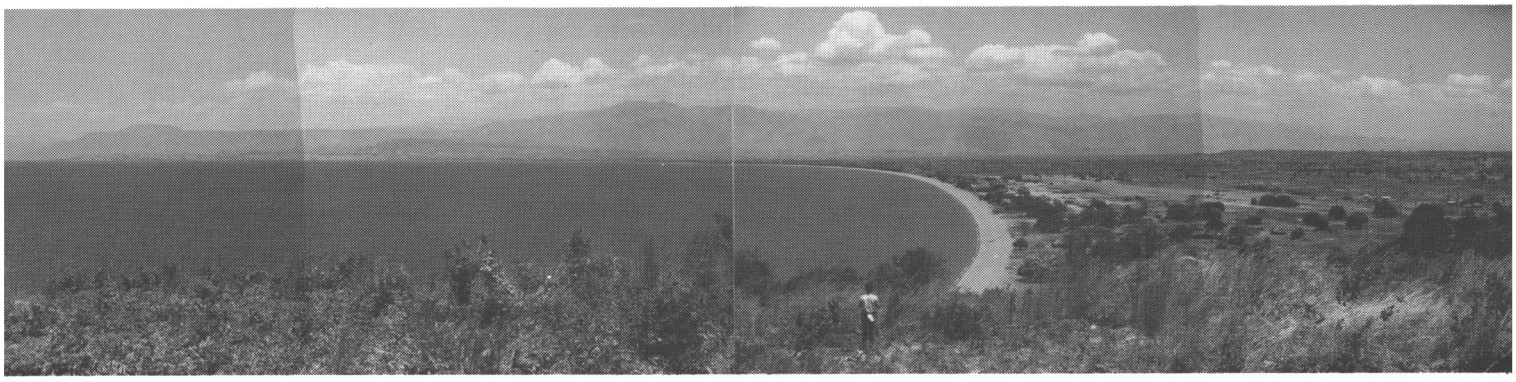

Fig. 4 Livingstonia Escarpment (left) and South Karonga Scarp Zone (right) as seen from Chilumba north of Youngs Bay.

margin of the Kandoli Mountains and practically no littoral zone is developed except at river mouth (Fig. 6). The escarpments maintain their linearity and steepness in the underwater profile across the Lake, which falls as deep as 2000 feet below lake level only two miles off the shore near lat. 11°S. (Yairi, 1977). The extensive rift-faulting must played a decisive role to give rise to the present geomorphology, the shape of the Lake and impressive escarpments rising from the lakeshore (Hopkins, 1973).

The northwest-trending faulting typically represented by the Livingstonia Escarpment, though it is somewhat deviated in trend in the area from Chiweta to Nkhata Bay, demarcates the African and post-African surfaces. On the west of the Livingstonia Escarpment, several subparallel step-faults of this trend have broken down the post-Gondwana surface promoting its deep dissection (Thatcher, 1974). The post-African deep dissection cutting into the valley floor of the North Rumpi, which is a product of

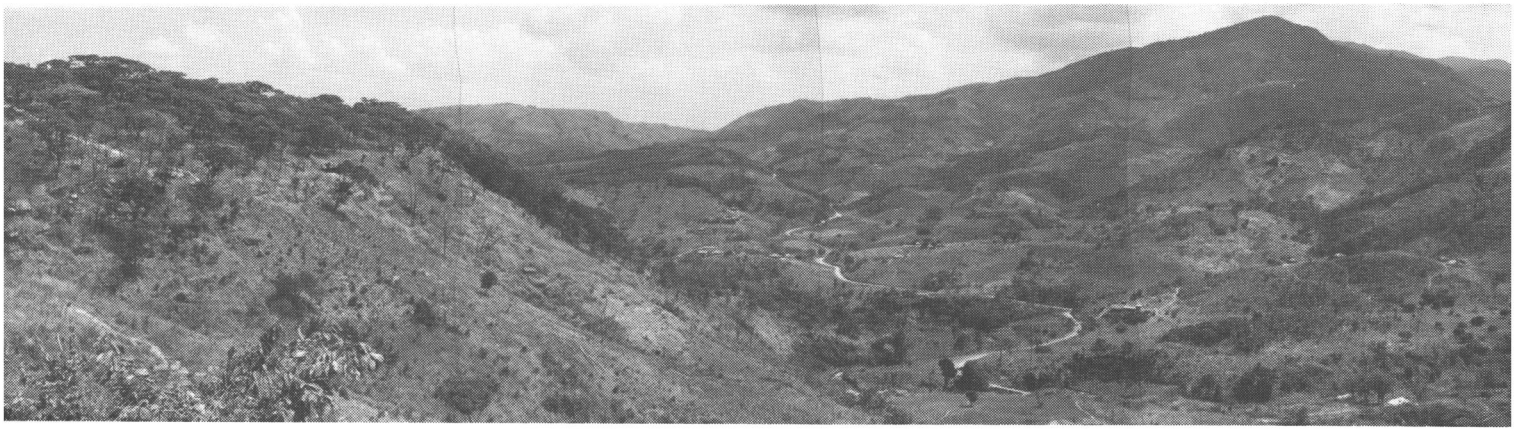

Fig. 5 East Nyika Escarpment photographed from a point 3 km southwest of the Livingstonia Mission. The Henga Valley Fault runs along a foot hill of the rugged mountains consisting of the Basement Complex (right). Note the flat-topped hills of the Karroo System (left).

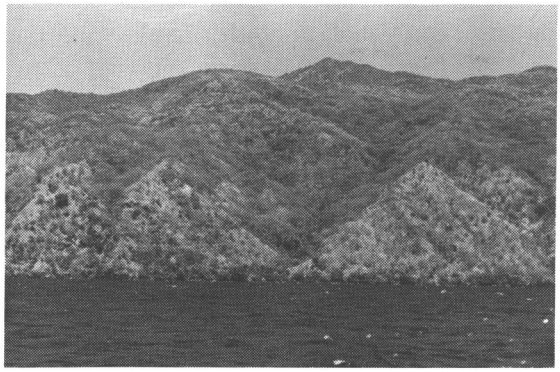

Fig. 6 Escarpment with prominent terminal facets flanking Lake Malawi to the north of Nkhata Bay; the lake side has practically no littoral.

the African cycle of erosion, may have followed the fracture system of the same trend.

On the other hand, the northeast faulting demonstrated by the East Nyika Escarpment (Fig. 5) is developed between the post-Gondwana with the Gondwana residuals and African surface. The formation of a flat-bottomed open valley of 10 km in width extending from the Henga Valley to Livingstonia is probably related to the faulting of this trend, and it can be a sort of graben structure which might define the present distribution of the Karroo sediments. Thatcher (1974) pointed that the main Karroo boundary faults were formed prior to the development of the Gondwana erosion surface, *i.e.* in the Jurassic, as the surface appears to be continuous across them.

From the geomorphological evidence outlined above, we provisionally consider that

Table 2 General succession of the Karroo System in the Livingstonia area (Cooper and Habgood, 1959).

K7	Chiweta Grits	150 ft.
	(unconformity)	
K6	Chiweta Bone Beds	850 ft.
	(unconformity)	
K5	Calcareous siltstone	+400 ft. (top not seen)
	Yellow and khaki mudstones	±1000 ft.
K3	Hard arkosic siltstone	60 ft
	Chocolate and green calcareous mudstones	+300 ft.
	Yellow and pink arkose and sandstone	±475 ft.
K2	Coal Measures with sandstones	100 - 350 ft.
K1	Green flaggy siltstones and pink arkoses with basal conglomerate	0 - 250 ft. +

the main phase of the movement of the NW-trending faults is intimately related to the Middle Miocene event after the close of the African cycle of erosion, and that of the NE-trending ones to the Lower Jurassic event prior to the Gondwana erosion cycle, though the latter faults were undoubtedly rejuvenated after the close of the post-Gondwana cycle of erosion. The former NW trend is designated here for convenience as R(Rift)-trend and the latter NE trend as K(Karroo)-trend. The time-relationship between these two major trends will be discussed later.

Structure

General structure

Sedimentary rocks of the Karroo System are well developed in the area, extending southward from Livingstonia, known as the Livingstonia Coal Field. Here are no additional remarks to the stratigraphy described in detail by Cooper and Habgood (1959); the general succession and distribution of the Karroo System in the Livingstonia Coal Field are summarized in Table 2 and Fig. 7 according to them.

As shown in Fig. 7 the Karroo System and the Basement Complex are generally in fault-contact and the unconformable relations between them can be seen only at a few places on the Livingstonia Escarpment (Cooper and Habgood, 1959). The post-Karroo faulting appears to be normal and to have occurred in two main direction, NW-SE and NE-SW (*ibid.*). These two trends correspond to the R- and K-trends designated above, respectively. To the R-trend are referable a fault zone along the Livingstonia Escarpment west of Kondowe and a fault zone along the North Rumpi extending from the north of Phoka Court to the south of Chiweta. The K-trend is well shown by the western marginal fault along the East Nyika Escarpment, Henga Valley Fault by Kemp (1975), and by faults bounding the faulted block of the Mount Waller on the northwest and southeast.

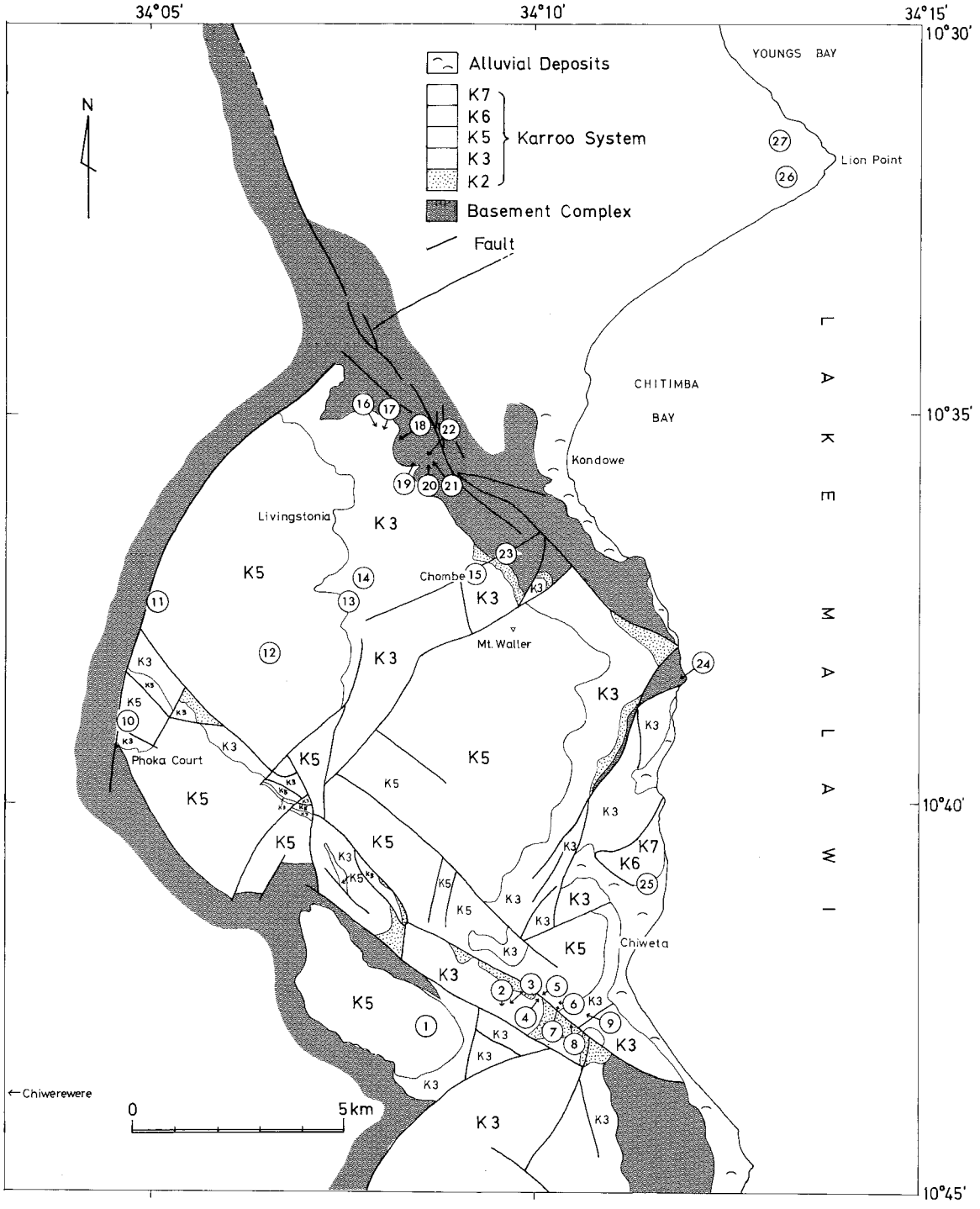

Fig. 7 Geological map of the Livingstonia Coal Field (simplified after Cooper and Habgood, 1959). Locality points in the present study are shown by the number encircled.

In the Livingstonia and Mt. Waller areas, the Karroo System consisting largely of K3 and K5 beds is gently tilted toward the southwest as a whole with an angle of a few degrees. Along the Henga Valley Fault, the beds strike northeast and dip at the angles of 20°±, sometimes over 70°, to the southeast; this local variation of bedding attitude can be attributed to a sort of drag on the beds by the faulting (*see* Fig. 13). In a narrow zone along the North Rumpi, the Karroo sediments are so disorganized by the faults of R-trend that the attitude of the beds exhibits a great complexity; the beds generally strike northeast and dip varying angles up to 20°, rarely 40° to 60°, to the northwest or southeast.

The Chiweta Beds (K6 and K7), originally described by Dixey (1926), occur in a small downfaulted block on the lakeshore north of Chiweta, where the beds dip to northeast at about 15°. To the west of Lion Point, although not shown in Fig. 7, the Karroo sediments (K5, K3, K2 and K1) occur in a faulted block bounded on the west by the Livingstonia Escarpment Fault and on the south by the extension of the Henga Valley Fault (Kemp, 1975).

Description of representative localities

Field works were carried out mainly along three roads crossing faults or fault zones of R- and K-trends: (1) the main road leading from Rumpi through Phoka Court, Livingstonia and Kondowe to Karonga, a part of which is well known as the escarpment road with 22 hairpin bends following the Livingstonia Escarpment; (2) the road from Chiwerewere 9 km south of Phoka Court to Chiweta; and (3) the lakeshore road from Kondowe to Chiweta.

The points of representative localities to be described below are shown in Fig. 7 for the Livingstonia area (Locs. 1 to 25) and the Lion Point area (Locs. 26 and 27), in Fig. 2 for the Chilumba area (Loc. 28), in Fig. 17 for the Karonga area (Locs. 29 to 33), and in Fig. 18 for the Nkhata Bay area (Locs. 34 and 35), respectively.

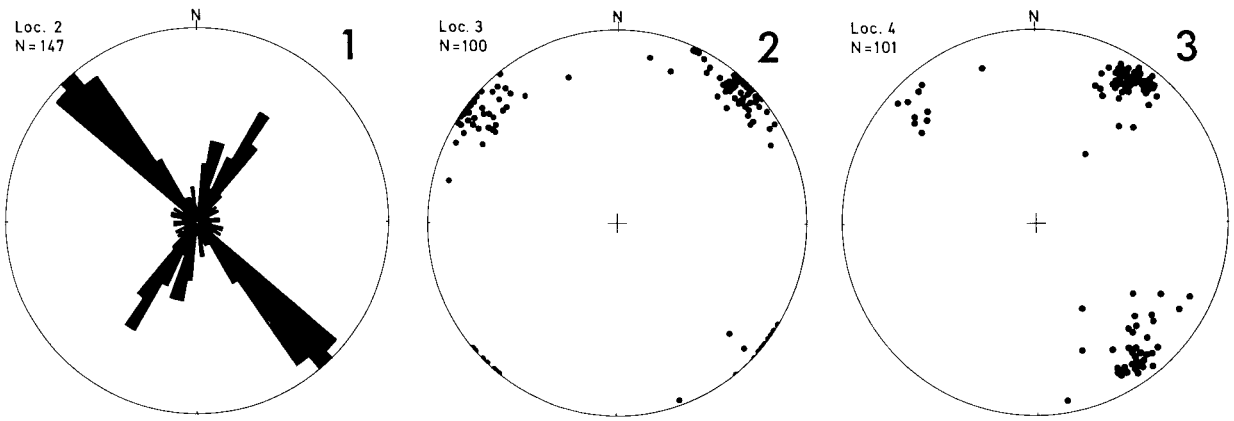

Fig. 8 Equal area projection of poles to beddings, joints, faults, and foliation planes of the Karroo System and Basement Complex. Plotted on upper hemisphere. Locality point and the number of reading are shown on top left of the primitive circle (open circle: bedding plane or foliation plane; solid circle: joint plane; star: fault plane). In Figs.8-1 and 8-11, strikes of joint planes are shown by rose diagrams since almost all of them are nearly vertical.

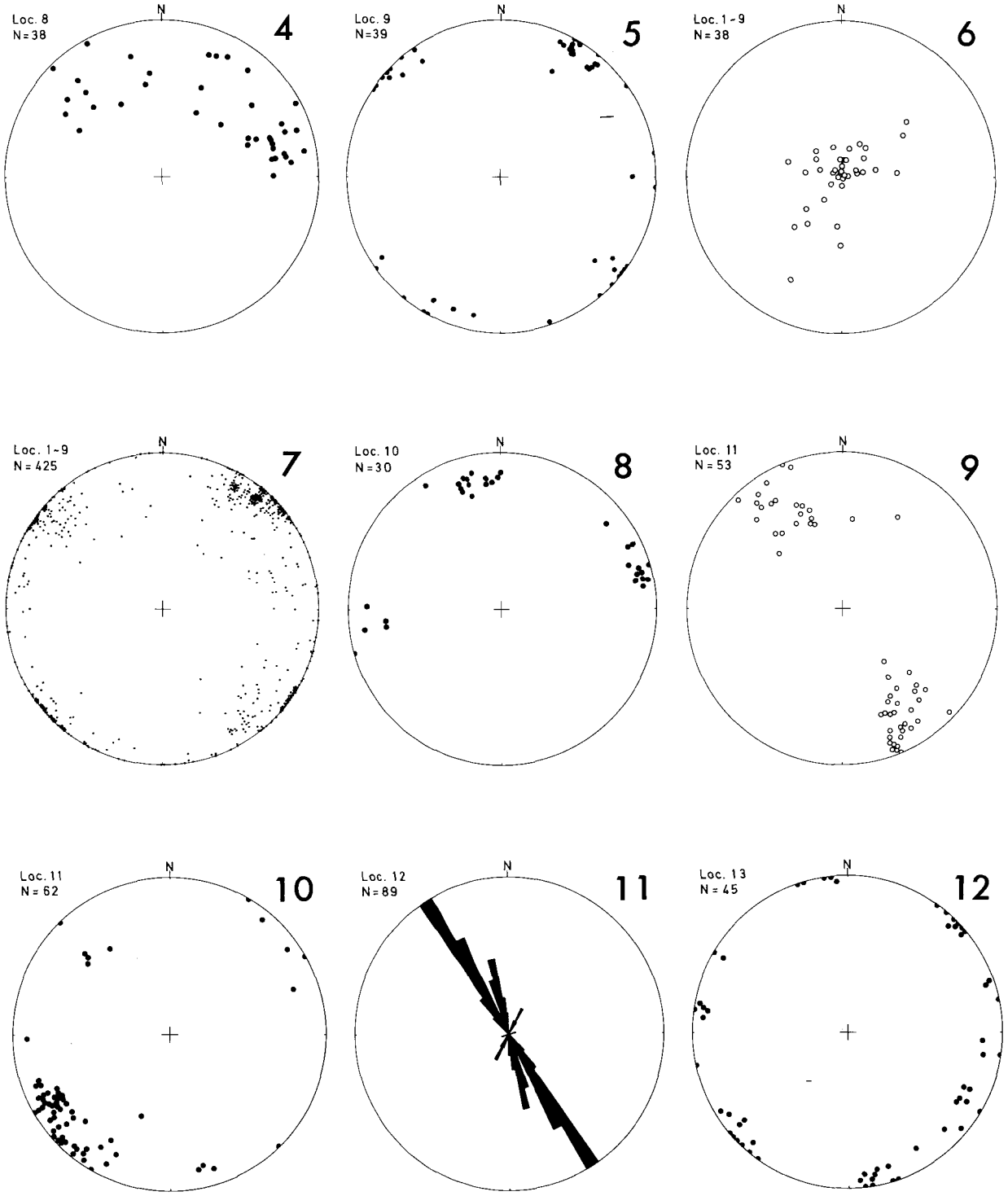

Fig. 8 (continued)

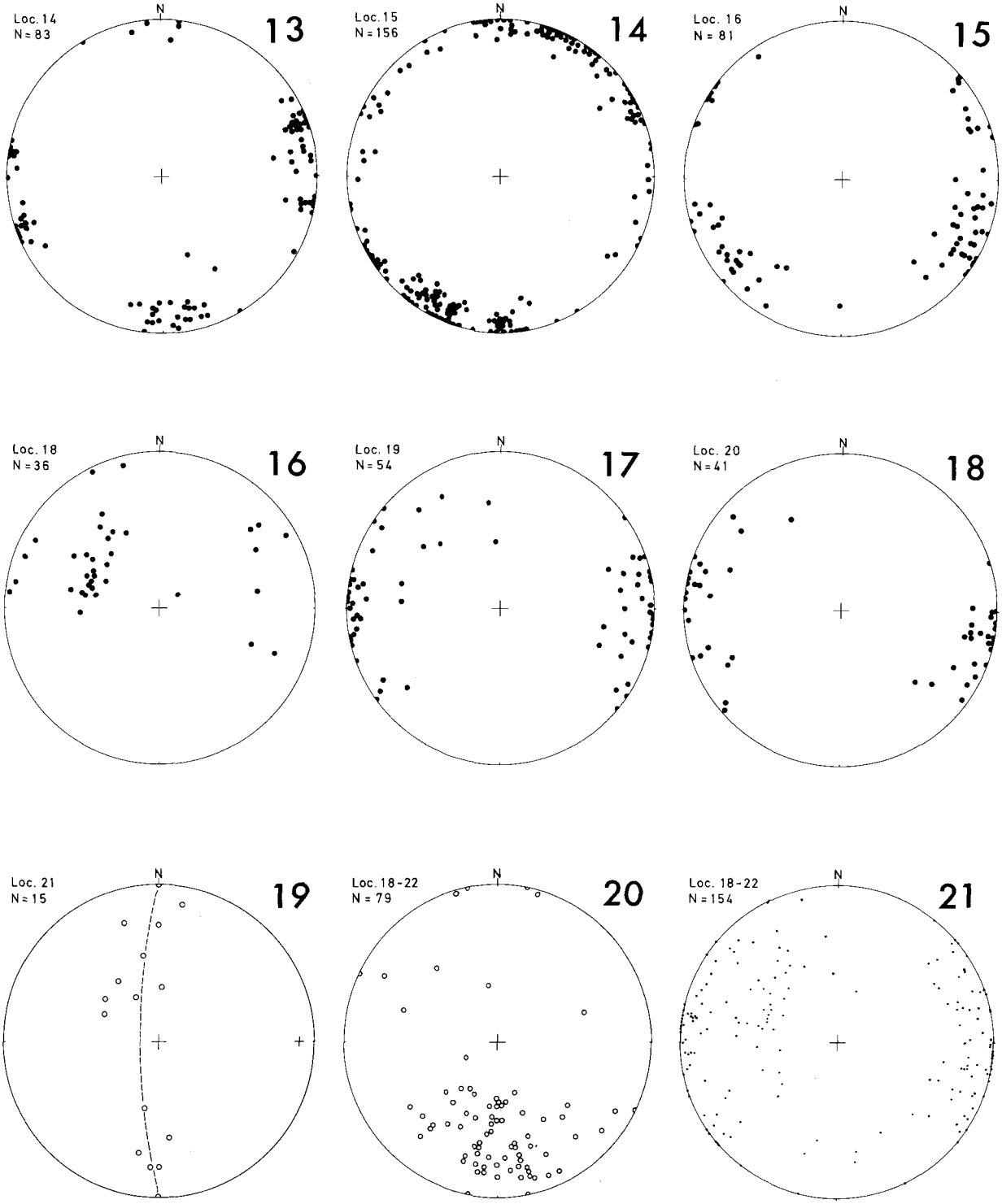

Fig. 8 (continued)

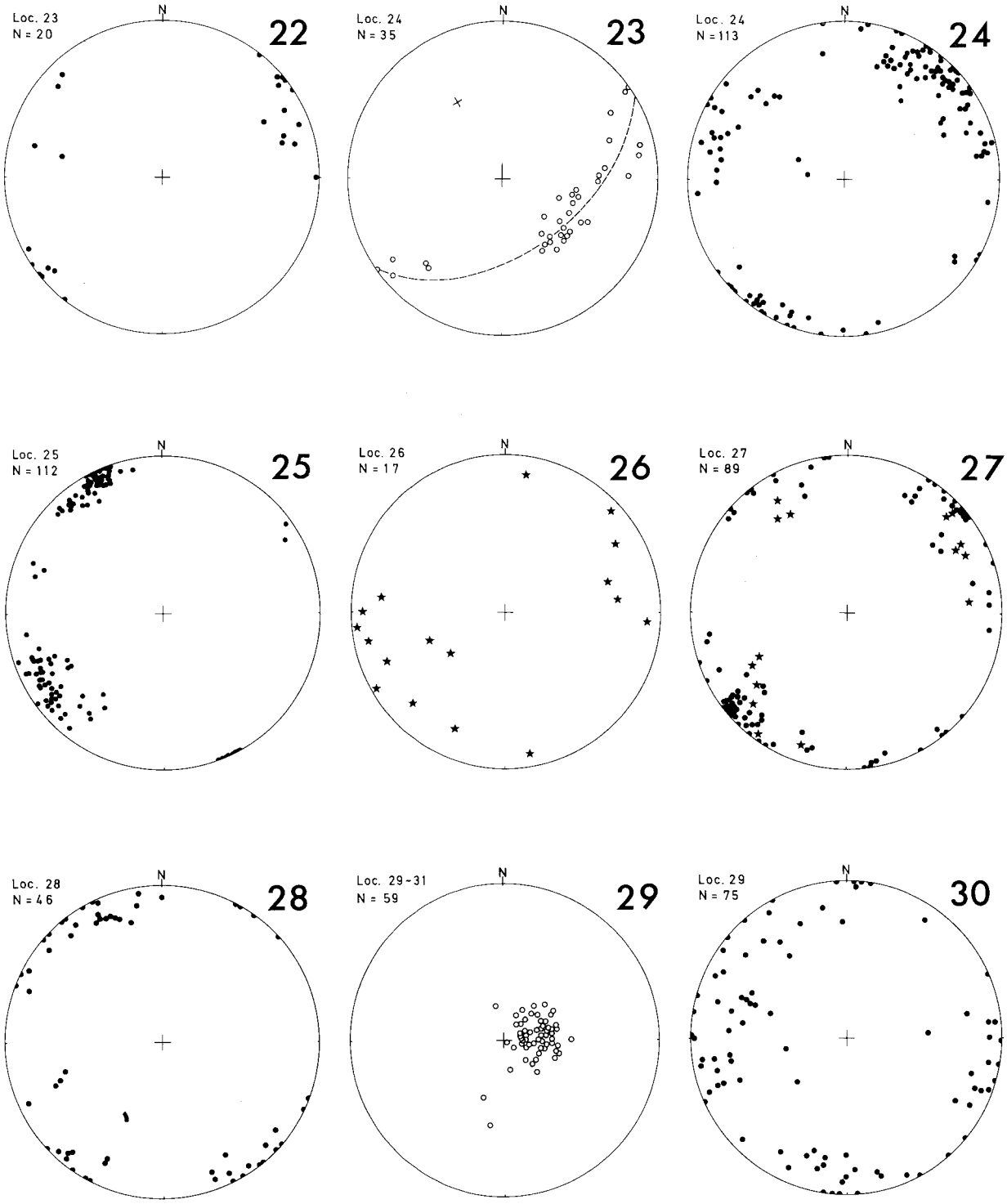

Fig. 8 (continued)

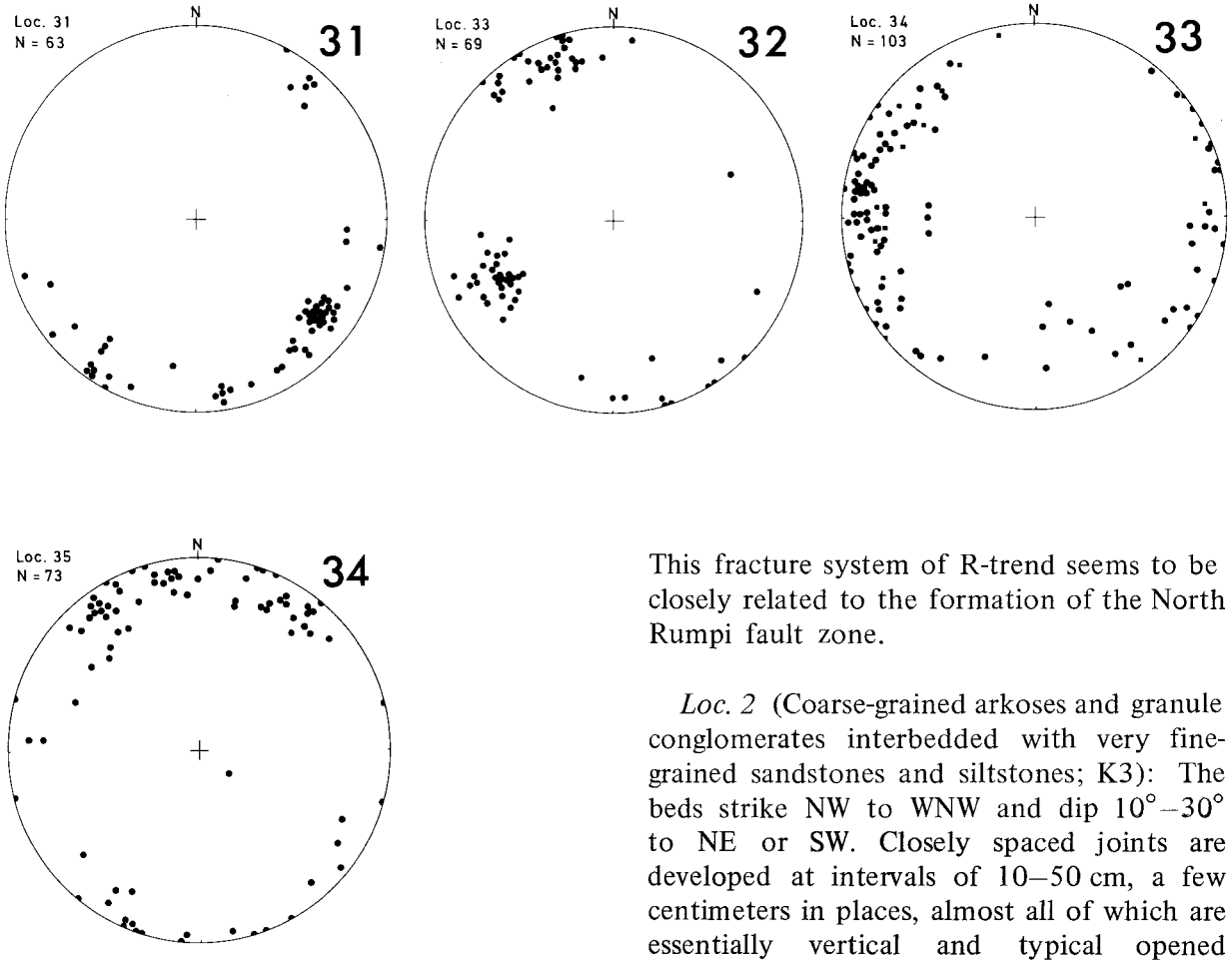

Fig. 8 (continued)

Loc. 1 (Alternation of 1–5 m thick, massive, fine- to medium-grained micaceous sandstones and 1–2 m thick, bedded siltstones; correlative with K5): The beds lie nearly horizontally, sometimes dipping 4°–20° to SW. They are displaced by NW-trending minor normal faults with downthrows of a few to several tens centimeters to NE, one of which shows the strike and dip of N24°W · 74°E. Nearly vertical and subparallel joints of this trend occur associated with faults. This fracture system of R-trend seems to be closely related to the formation of the North Rumpi fault zone.

Loc. 2 (Coarse-grained arkoses and granule conglomerates interbedded with very fine-grained sandstones and siltstones; K3): The beds strike NW to WNW and dip 10°–30° to NE or SW. Closely spaced joints are developed at intervals of 10–50 cm, a few centimeters in places, almost all of which are essentially vertical and typical opened fractures. Fig. 8–1 shows the distribution of trends of joints by a rose diagram; preferred orientations both in N40°W ~ N45°W (R-trend) and N10°E ~ N40°E (K-trend).

Loc. 3 (Massive coarse-grained arkoses with intercalations of coal seams and coaly and micaceous sandstones grading from pebbly conglomerates near the base; K3): Two normal faults with dip slips cut the beds (N42°W·24°SW). The attitudes of fault planes are N44°W·80°SE (R-trend) and N48°E·80°SE (K-trend), and their throws are 150 cm and 25 cm, respectively. The K-trending

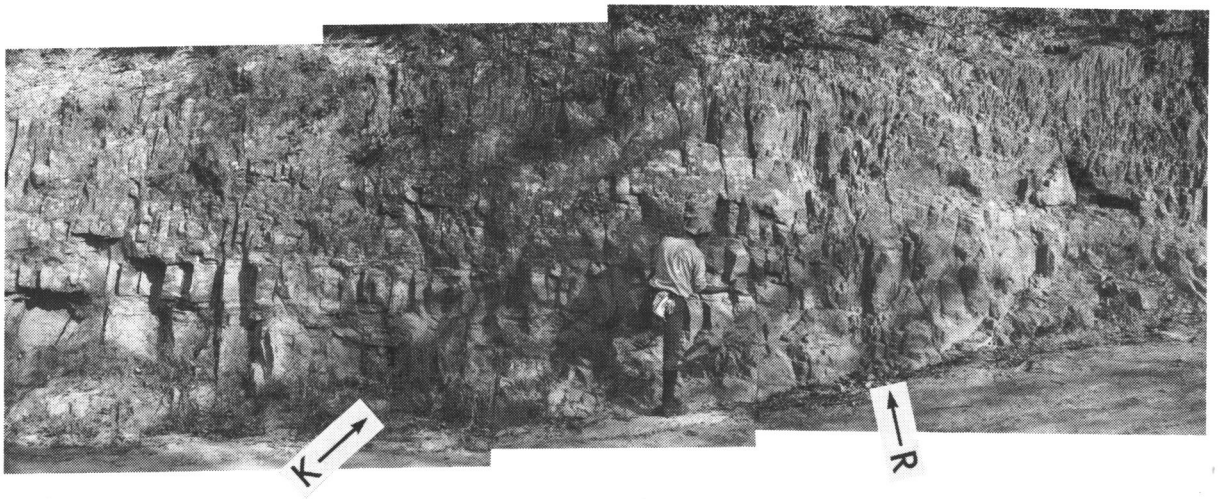

Fig. 9 Faults and joint swarm cutting the K3 beds. Loc. 3. K and R denote K- and R-trending faults, respectively.

Fig.10 Joint swarm cutting the K5 beds. Loc. 4. Note onion structures by weathering.

fault appears to be displaced by the R-trending one (Fig. 9). Nearly vertical joints are closely developed forming a swarm. Attitudes of joints are concentrated in N35°–50°E·70°–90°NW (K-trend) and N35°–55°W·75°–90°NE (R-trend) (Fig. 8-2). The R-trending joints have relatively sharp and extensive planes compared with the K-trending ones (Fig. 9). The joints of R-trend cut sharply, sometimes displace slightly, those of K-trend. Some joints of R-trend cut occasionally pebbles contained in the lower division of the beds.

Loc. 4 (Greenish yellow massive siltstones of K5): Closely spaced joints of R-trend are well developed at intervals of a few to ten centimeters, point-maximum of them being in N50°–60°W·70°–85°NE. Joints of K-trend are less spaced and their orientations are considerably scattered (Fig. 8-3). The striking feature is development of onion structures upon weathering, shapes and dimensions of which are notably controlled both by trends and spacings of the joints (Fig. 10).

Loc. 5 (Greenish and dark grey massive siltstones with intercalations of 50 cm thick bedded shale, K5): The strike and dip of the bed is N54°W·39°SW, though it is sometimes variable because of drag on the beds along faults. The bed is displaced by minor normal faults with downthrows of 20–30 cm to NW or SE; strikes and dips of N60°E·60°NW, N54°E·70°SE, N68°E·56°SE and N50°E·70°NW are obtained for four faults. The former two and the latter two are considered to be conjugate sets of faults, respectively, and to be formed under the stress state of N30°W-S30°E horizontal tension.

Loc. 6 (Massive siltstones interbedded with irregularly shaped, fine arkosic sandstones about 1 m in thickness; K5): The beds dips gently to NW, and is displaced by a sharp-cut fault of N52°W·80°SW (R-trend), along which no drag on the bed can be seen. The bed is cut also by closey spaced joints parallel to the fault.

Loc. 7 (Greenish yellow massive siltstones of K5): Closely spaced joints, nearly vertical in attitude, of R- and K-trends are typically displayed at this locality; the R-trending joints are developed at intervals of 7–8 cm and the K-trending at an interval of 2 cm (Fig. 11). The fragmentation of the bed by the joints is prominent especially in weathered parts. This fact shows that some crypto-joints have been actualized only when exposed to weathering.

Loc. 8 (Alternation of very coarse-grained sandstones grading downward into granule conglomerates and micaceous sandstones, interbedded with 20–100 cm thick coal seams; referable to the Coal Measures of K2): The beds (N86°W·26°S) are cut by joints with various trends and inclinations (Fig. 8–4).

Loc. 9 (Alternation of bedded siltstones and very coarse-grained sandstones; probably K3): The beds (N8°E · 13°NW) are cut by nearly vertical joints of R-trend; the joints of R-trend are in the direction of N50°–60°W and those of K-trend in N35°–55°E (Fig. 8-5).

Fig. 8-6 shows the point diagram of poles to bedding planes of the Karroo sediments exposed between Loc. 1 and 9 along the Chiwerewere-Chiweta road. Though the beds

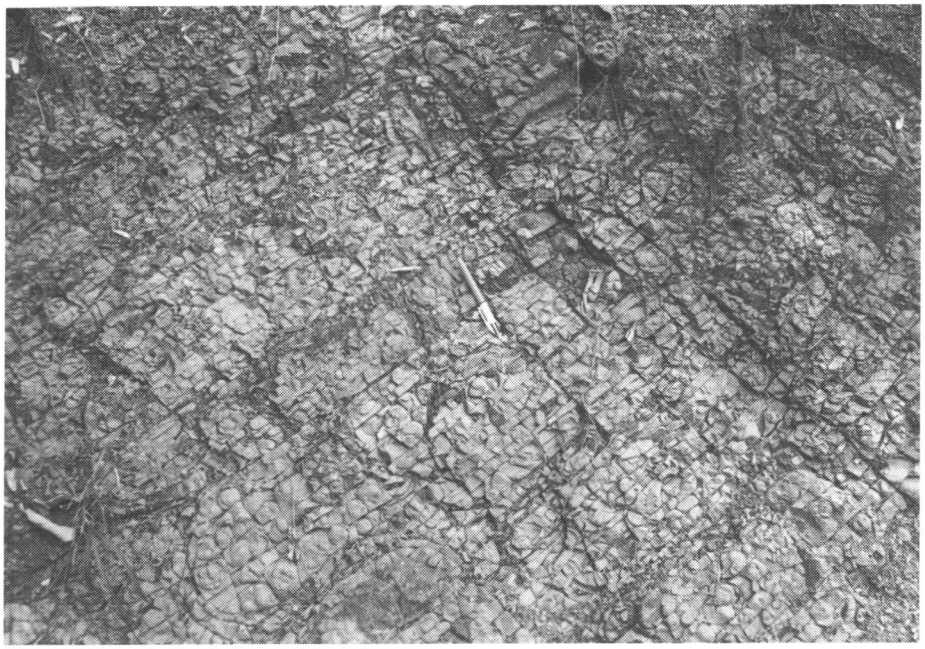

Fig.11 Closely spaced K- and R-trending joint swarms found in the K5 beds. Loc. 7.

Fig.12 Gently folded structure of the K5 beds. Loc. 10.

are widely variable in attitude, the poles appear, as a whole, to be aligned on a nearly vertical great circle of NE-trend. This suggests that tectonic disturbance of beds were to some extent caused by the faulting of NW-trend along the North Rumpi, *e.g.*, by drag and tilt of the beds along the R-trending faults. Fig. 8-7 shows a point diagram of all joints measured along the same road; both K- and R-trends are clearly distinguished.

Loc. 10 (Fissile bedded mudstones of K5): The bed shows a gently folded structure with a wavelength of 200 cm and an amplitude of 60 cm, the fold axis plunging 20° to S70°E (Fig. 12). The strikes and dips of the northern and southern limbs of an anticline are N16°W·20°NE and N64°E·24°SE, respectively. Nearly vertical joints cutting the folded structure trend in preferred orientations of N10°–20°W and N70°–90°E (Fig. 8-8), but it is uncertain whether these orientations are referable to the R- or K-trends because of a clockwise deviation from the typical R- and K-trends.

One kilometer northward from this locality, the K5 beds show a wide variety of strikes ranging from NNW to NE and eastward dips from 20° to 52°. The variety of bedding attitudes may be attributed to the similar flexure or folding as seen at Loc. 10. A striking tectonic feature observed at these locality is that the K5 beds dip to the east only in a narrow zone of 1 km in width along the Henga Valley Fault in marked contrast to overall gentle southwest-dipping in the Livingstonia area. Consequently the K5 beds form an asymmetrical syncline which appears to be ascribed to the Henga Valley faulting.

Loc. 11 (Bluish grey bedded siltstones of K5): The beds dip steeply to NW or SE, and form a complicated folded structure with nearly horizontal axial planes. Fig. 8-9 shows a projection of poles to bedding planes, from which the horizontal fold axes trending N60°E are postulated. This trend is approximately parallel to the Henga Valley Fault of K-trend. The parallelism of the two structural elements is strongly indicative of some genetic relationship between the folding and faulting. From the pattern of the folded structure it is considered that the folding may be attributed to a sort of gravitational flexure by dead load of the steeply inclined beds dragged by the steep fault as shown schematically in Fig. 13.

These folded beds are cut by subparallel joints of R-trend (Fig. 8-10) obviously later in origin than the folding. The K5 beds, 20 m north of this locality, show typical onion structures with diameters of 5–30 cm, shapes and dimensions of which are strongly controlled by nearly vertical joints of R-trend and bedding planes (N40°E·26°SW).

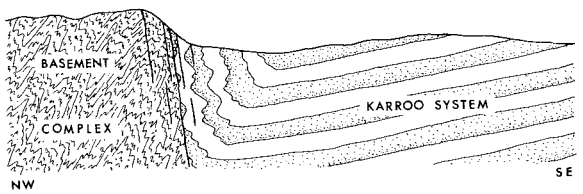

Fig.13 A schematic NW-SE cross-section across the Henga Valley Fault.

Loc. 12 (Thick bedded, yellow fine-grained sandstones of K5): Nearly vertical joints of R-trend are well developed at an interval of 30 cm cutting the beds which gently dip to NW, though some joints of K-trend are recognized (Fig. 8-11). The R-trending joints generally show good continuity, and occasionally appear as steep cliffs on the hill top near Tigone village.

Loc. 13 (Chocolate-coloured and green mudstones with intercalations of coarse-grained arkoses; K3): Joints show some variety in orientation but appear to be concentrated in the trends of N30°–50°W (R-trend), N10°–40°E and N70°–90°E (Fig. 8–12).

Loc. 14 (Medium-grained arkoses with cross lamina, K3): Preferred orientations of nearly vertical joints can be seen in the direction of N20°W, N10°E and nearly E-W (Fig. 8-13).

Loc 15 (Micaceous coarse grained sandstones, chocolate-coloured siltstones, and granule conglomerates with an intercalation of thin coal seam, K3): The beds generally dip 4°–12° to N, occasionally 18°–22° to NE or NW. Closely spaced and nearly vertical joints are developed. Preferred orientation of them (R-trend), though widely variable, is approximately parallel to this segment of the Livingstonia Escarpment Fault (Fig. 8-14).

Loc. 16 (Massive coarse-grained sandstones and granule conglomerates interbedded with thin bluish grey siltstones, K3): The beds are displaced by two normal faults; one has a downthrow of 3.5 m and the attitude of N30°W·80°NE, the other a downthrow of 1 m and the attitude of N40°E·80°SE. The former one, possibly the latter, too, is considered to be associated with the Livingstonia Escarpment faulting. The distribution of poles to joint planes (Fig. 8-15) are concentrated in two maxima: N20°–45°W (R-trend) and N20°–35°E (K-trend).

Loc. 17 (Alternation of sandstones and mudstones, K3): Two normal faults are observed, one, N30°E·82°SE (K-trend) in strike and dip, has a downthrow of 2 m to SE.

Loc. 18 (Muscovite schists of the Basement Complex with dominant foliation of N80°W·68°S): Joints projected on the Fig. 8-16 make a weak maximum around a point representative of N20°E·40°NW, that is, considerably lower dip than that of the joints developed in the Karroo System.

Loc. 19 (Muscovite gneisses of the Basement Complex with dominant foliation of N82°E·32°S): Joints, though showing a wide variety of orientation, have a tendency to strike N-S and dip steeply to E or W (Fig. 8-17).

Loc. 20 (Muscovite schists of the Basement Complex with dominant foliation of N86°E·32°S): Most of joints strike nearly NNE and dip steeply to E or W (Fig. 8-18).

Loc. 21 (Amphibolites of the Basement Complex): The amphibolites show a minor folded structure with a wavelength of 2 m. Poles to foliation planes plotted on Fig. 8-19 describe a great circle which defines the fold axis plunging 10° to W.

Loc. 22 (Amphibolites of the Basement Complex with dominant foliation of N88°E · 32°S): A vertical fault striking N28°W (R-trend), probably accompanied by the Livingstonia Escarpment faulting, cuts sharply the amphibolites.

Fig. 8-20 shows the distribution of poles to foliation planes of the Basement rocks exposed from Loc. 18 to 22 along the escarpment road. Fig. 8-21 is a scatter diagram of poles to joint planes cutting the same Basement rocks.

Loc. 23 (Muscovite gneisses of the Basement Complex with dominant foliation of N80°W·60°S): Nearly vertical joints of R-trend are developed (Fig. 8-22).

Loc. 24 (Muscovite gneisses of the Basement Complex): The gneisses make a typical cylindrical fold (Fig. 14) with the axis plunging 45° to S30°E as obtained by the π-diagram of Fig.8-23. Distinct striations can be seen on some slickensided faults; plunges of them are 48° to S56°W on a fault plane of N86°E · 66°S, 56° to N40°E on N4°E · 72°E, and 65° to N56°E on N18°W · 72°NE. The directional concordance recognized between the latter two and dip-slippings of R-trending faults strongly suggests a rejuvenation along the pre-existing fault planes. Fig. 8-24 is a scatter diagram of poles to joint planes cutting the gneisses; the R-trending joints are predominant over the K-trending ones.

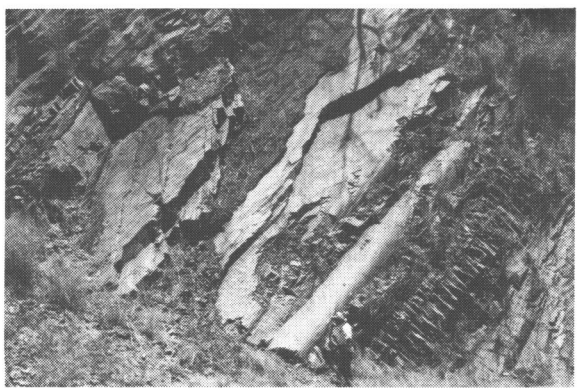

Fig.14 Cylindrical fold found in the Basement Complex. Loc. 24.

Loc. 25 (Alternation of bluish grey siltstones and yellowish grey, very fine- to coarse-grained sandstones, K6 and K7): Joints cutting the beds which strike N30°–50°E and dip 8°–18° to E are well developed with high concentrations around both the K- and R-trends (Fig. 8-25).

Loc. 26 (Well bedded, grey to pale yellow siltstone with intercalations of very fine-grained sandstones; K5): The beds strike approximately E-W and dip 6°–14° to N except along faults. Most of numerous faults well developed at an interval of a few meters are of normal dip-slip type with throws of 10-200 cm (Fig. 15). In Fig. 8–26 are plotted 17 poles to fault planes; they form two groups, though not so dense, representative of NW-strike and NE-dip and NW-strike and SW-dip. Regarding the two groups of the faults as a conjugate set of faults, we can reconstruct a paleo-stress field with a horizontal tension in the direction of N30°E–S30°W. Drag along the faults causes the beds to strike NNW and dip 16°–30° to NE. The faults as well as joints are sometimes filled by calcite veins.

Loc. 27 (Alternation of fine-grained sandstones and mudstones; K3): There are observed conjugate sets of NW-trending normal faults, the dip-slip along which is confirmed by striations on the slickensides; faults downthrowing to NE about 300 cm and those to SW several tens centrimeters (Fig. 16). Joints as well as minor faults with a displacement of a few centimeters are also well developed as shown in Fig. 8-27, where both R- and K-trends are distinguishable. Some of them are filled by calcite veins.

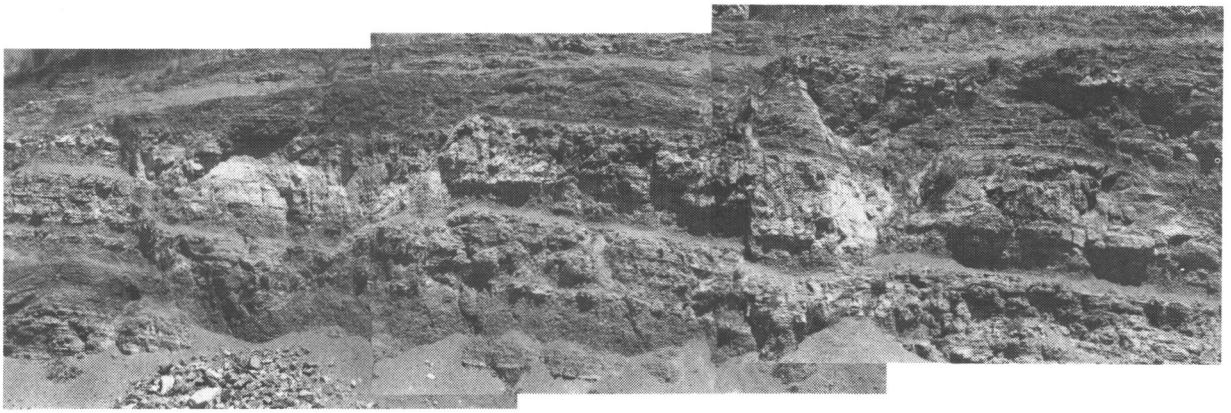

Fig.15 Conjugate sets of normal faults (R-trend) cutting the K5 beds. Loc. 26.

Fig.16 Conjugate sets of normal fualts (R-trend) cutting the K3 beds. Loc. 27.

Loc. 28 (Amphibolites with pegmatite veins; the Basement Complex): Fig. 8-28 shows a scatter diagram of poles to joint planes cutting the amphibolites, whose foliations strike NNW to NNE and dip 34°–52° to E; both R- and K-trending joints are predominant.

Loc. 29 (medium- to very coarse-grained arkoses and granule conglomerates; the lower part of the North Rukuru Sandstones and Shales, referred to K3 (Thatcher, 1964)): The joints cutting monoclinal structure of the beds dipping 10°–30° to E (Fig. 8-29) are measured for a distance of 3 km containing this locality, to yield only a very scattered pattern without any preferred orientation (Fig. 8-30).

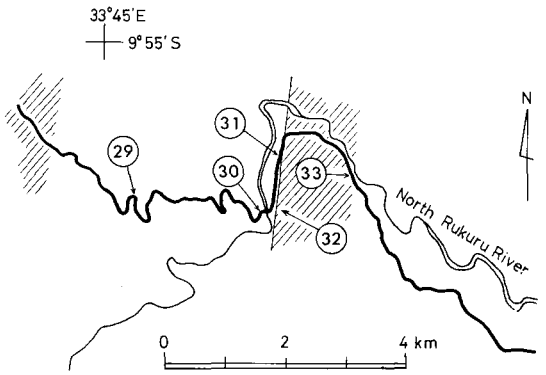

Fig.17 Locality-point map along the Karonga-Chitipa road (see Fig.1).

Loc. 30 (Thick bedded, coarse-grained sandstones of the North Rukuru Sandstones and Shales): The beds striking N58°W and dipping 18°NE are cut sharply by several faults; dip-slip striations are observed on the slickensided faults. Fault planes measured are N24°E·70°SE, N24°E·78°SE and N4°W·84°W in attitude, the former two being referable to the K-trend.

Loc. 31 (Alternation of greyish white, calcareous, fine-grained sandstones and greenish grey, fissile siltstones; uppermost horizon of the North Rukuru Sandstones and Shales): The beds strike N48°W and dip 24° to NE. A scatter diagram of poles to joint planes cutting the beds (Fig. 8-31) shows that both R- and K-trending joints are predominant; some joints are filled with calcite.

Loc. 32 (Eastern marginal faults of the Western Zone of the Karroo-basin to the west of Karonga; *see* Saka and Yairi (1977) in this volume): There can be seen, adjacent to the undisturbed Basement Complex, a major sheared zone striking N20°E and dipping 58° to NW, which consists of mylonitized gneisses with cemented fault breccias. The faulting must be closely related to a movement which caused the monoclinal westward tilting of the Karroo beds.

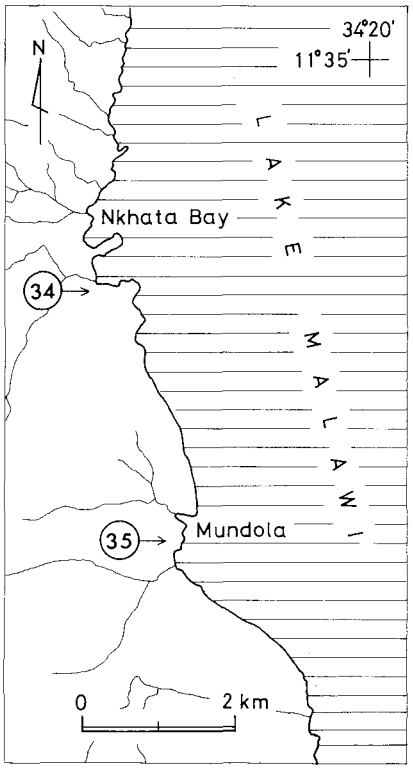

Fig.18 Locality-point map in the Nkhata Bay are(see Fig.1).

Loc. 33 (Quartzie of the Basement Complex): In a distribution pattern of joints (Fig. 8-32) can be seen two preferred orientations, one trending ENE and nearly vertically dipping (K-trend) and the other being N30°W·60°SW in attitude (Fig. 8-32). Possibly the latter represents the schistosity of the quartzites.

Loc. 34 (Augen gneisses of the Basement Complex with dominant foliation of N26°W·70°NE): Approximately N-S trending joints appear to predominate in the joint pattern widely variable in orientation (Fig. 8-33).

Loc. 35 (Augen gneisses of the Basement Complex with dominant foliation striking NNE and dipping 50°–80° to SE): A scatter diagram of poles to joint planes (Fig. 8-34) shows that nearly E-W trending joints are predominant.

Post-Karroo faulting

From the tectonic evidences mentioned above, it is confirmed that two kinds of fault movements, the R- and K-trends, affected all over the sequences of the Karroo System in and around the Livingstonia area, and that a series of joint system is developed closely following the trends of the major faults. The fault system of either trend is characterized by conjugate sets of normal faults, which demonstrate that the K-trending faults occurred under the NW-SE horizontal tension and the R-trending under the NE-SW horizontal tension (Locs. 5, 26 and 27).

It is of much importance to know the time-relationship between the K-trending faulting and R-trending one. Unfortunately, however, evidences which testify it are not common except a few cases recognized at Loc. 3, where the R-trending faults appear to be preceded by the K-trending ones. A folded structure with horizontal axial planes, observed at Loc. 11 along the Henga Valley Fault of K-trend, may be attributed to a tectonic movement soon after deposition. The marginal faults of K-trend bounding the Western Zone of the Karroo-basin, west of Karonga (Loc. 32; *see* Saka and Yairi, 1977) may also be attributed to such an earlier tectonic movement. As the Karroo sedimentary basins are believed to have been tectonic in origin (Cooper and Habgood, 1959; Shrooder, 1972; Drysdall and Kitching, 1963), the faulting of the K-trend may date back in origin as old as a relatively earlier stage of the Karroo sedimentation; though the K-trending faultings are considered to have taken place repeatedly during and after the Karroo sedimentation.

Closely spaced, nearly vertical and subparallel joints of the R-trend, on the other hand, are most extensively developed over the area independently of the lithology and pre-existing structures. They cut the folded structure associated with the faulting of the K-trend as observed at Loc. 11. The R-trending faults and joints are best expressed on the topography of the present area as linear escarpments and a series of subparallel drainage system. These facts may indicate that the R-trending structures were formed during a relatively younger stage of the tectonic movement. As pointed out in a separate article in this volume (Yairi, 1977), the formation of the Malawi Rift Valley has been intimately related with a NW-SE or R-trending, as designated here, taphrogenesis, which defined the present outline of the Lake Malawi trough.

Table 3 Karroo to Recent geological history of the Nyika area (after Thatcher, 1974)

Division of time m.y.	Deposition	Tectonic incident	Erosion cycle
Recent	Alluvial deposits	Uplift	Quaternary
0.01	Dwangwa Gravels	Uplift and rift-faulting	
Pleistocene upper	Chitimwe Beds		
Pleistocene middle	Chiwondo Beds	Uplift and faulting	
Pleistocene lower		? Rift-faulting	
1.8			
Pliocene			Post-African
5			
Miocene upper	? Sungwa Beds		
Miocene middle		Faulting	
Miocene lower			
22.5			African
Paleogene			
65			
Cretaceous upper		Major rift-faulting	Post-Gondwana
Cretaceous middle			
Cretaceous lower	Dinosaur Beds		
141			
Jurassic upper		Uplift and minor faulting	Gondwana
Jurassic middle			
Jurassic lower		Major faulting	
195			
Triassic			
230			
Permian	Karroo System	Faulting and subsidence	
280			
Carboniferous		Faulting and subsidence	Pre-Karroo erosion

Based on the geomorphology and tectonics of the post-Karroo faulting in the present area, we here provisionally summarize the time-relationship among the post-Karroo faultings as follows: The faults of the K-trend may date back in origin to an early stage of the Karroo sedimentation and were rejuvenated in the middle Cretaceous time at the close of the post-Gondwana erosion cycle. A main phase of faulting of the R-trend succeeded the close of the African erosion cycle in the early Miocene time and may proclaim the initiation of the extensive Neogene rifting along Lake Malawi, though its embryonic phase may have been related to the formation of the sedimentary basin for the Dinosaur Beds during upper Jurassic to lower Cretaceous time.

Discussion and summary

The Karroo rocks in Malawi were deposited in a series of tectonically controlled basins during the Permian and Triassic (Carter and Bennet, 1973; Shrooder, 1972). It is very difficult to determine the original extent of the Karroo sedimentary basins owing to their structural complexity and sporadic distribution related to the post-Karroo movements, mainly to the major rift-faulting. In this paper, however, it is emphasized that NE-trending faults, the trend of which is designated as the K-trend to represent the typical Karroo-trend, might have controlled the birth of the Karroo sedimentary basin of the Livingstonia area. Along the Ruhuhu depression in Southwest Tanzania across Lake Malawi, is also developed the Karroo System extensively (McKinlay, 1956), which seems to be situated on a northeastern extension of the System in the Livingstonia area. The relationship in space and time between both sedimentary basins is most important when considering the initiation of the K-trending faults.

In this study, it is also emphasized that the major faulting in the Livingstonia area, which formed the present outline of the northern segment of the Malawi Rift Valley, is characterized by NW-trending faults; this trend is designated as R-trend to represent the typical rift-trend. The faulting of the R-trend seems to have postdated that of the K-trend. To account for the formation of the K- and R-trending faults, horizontal tensions in two different directions are postulated: NW-SE for the K-trend and NE-SW for the R-trend, respectively. There must have been a significant change of the stress field during the post-karroo time, though the timing of the change is still questionable. Thatcher (1974) mentioned that the present pattern of the rift-faulting was probably initiated, at the northern end of Lake Malawi, in Upper Jurassic to Lower Cretaceous times, following the break up of the Gondwanaland supercontinent. The change of the stress field may be ascribed to this global event of the breaking up of the continent.

Acknowledgements – The authors are indebted to Professor Emeritus Isao Matsuzawa of Nagoya University for his encouragement. Thanks also are extended to Mr. Mamoru Adachi of Nagoya University for his kindness in critically reading this manuscript and offering constructive suggestions. Field work was much facilitated by Mr. V.H.B.Gondwe of Ministry of Agriculture and Natural Resources of Malawi, Mr.J.H. Dean and Dr. M.J. Crow of Geological Survey Department of Malawi, Mr. Yoshihide Nakai and other staffs of Japan Overseas Cooperation Volunteers, to whom the authors express their deep gratitude. The authors would like to record their sincere thanks to the staffs of the Livingstonia Mission and people in Livingstonia, who gave them warm hospitality during their stay in Livingstonia.

References

COOPER, W.G.G and HABGOOD, G. (1959): The geology of the Livingstonia Coalfield. *Bull. Geol. Surv. Nyasaland,* **11,** 51pp.

BLOOMFIELD, K. and GARSON, M.S. (1965): The geology of the Kirk Range-Lisungwe Valley area. *Bull. Geol. Surv. Malawi,* **17,** 234pp.

CARTER, G.S. and BENNETT, J.D. (1973): The geology and mineral resources of Malawi. *Bull. Geol. Surv. Malawi,* **6,** *62pp.*

DAWSON, A.L. and KIRKPATRICK, I.M. (1968): The geology of the Cape Maclear Peninsula-lower Bwanje Valley area. *Bull. Geol. Surv. Malawi,* **28,** 71pp.

DIXEY, F. (1926): The Dinosaur Beds of Norht Nyasa. *Annu. Rep. Geol. Surv. Nyasaland,* **6.**

DIXEY, F. (1937): The early Cretaceous and Miocene peneplains of Nyasaland and their relation to the Rift Valley. *Geol. Mag.,* **74,** 49-67.

DIXEY, F. (1939): The early Cretaceous valley-floor peneplain of the Lake Nyasa region and its relation to Tertiary rift structure. *Geol. Soc. London Quart. Jour.,* **95,** 75-108.

DIXEY, F. (1956): The East African Rift System. *Bull. Suppl. Colon. Geol. Miner. Res.,* **1,** 77pp.

DRYSDALL, A.R. and KITCHING, J.W. (1963): A re-examination of the Karroo succession and fossil localities of part of the upper Luangwa Valley. *Mem. Geol. Surv. N. Rhodesia,* **1.**

FAIRHEAD, J.D. and GIRDLER, R.W. (1969): How far does the rift system extend through Africa ? *Nature,* **221,** 1018-1020.

HOPKINS, D.A.S. (1973): The geology of the Rumphi-Nkhata Bay area. *Bull. Geol. Surv. Malawi,* **38/39,** 42pp.

KEMP, J. (1975): The geology of the Uzumara area. *Bull. Geol. Surv. Malawi,* **41,** 49pp.

KING, L.C. (1963): *South African scenery,* third edition. Oliver and Boyd, Edinburgh, 308pp.

LISTER, L.A. (1967): Erosion surfaces in Malawi. *Rec. Geol. Surv. Malawi,* **7,** 15-28.

MCCONNELL, R.B. (1972): Geological development of the rift system of eastern Africa. *Geol. Soc. Am. Bull.,* **83,** 2549-2572.

MCCONNELL, R.B. (1974): Evolution of taphrogenic lineaments in continental platforms. *Geol. Rundsch.,* **63,** 389-430.

MCKINLAY, A.C.M. (1956): The Karroo System. *IN: Summary of the Geology of Tanganyika, Part I, Introduction and Stratigraphy, Geol. Surv. Tanganyika, Memoir* **1,** 81-151.

SAKA, Y. (1977): Note on the Karroo System and the probable Dinosaur Beds near the Lion Point, Karonga District, Northern Malawi. *2nd prelim. Rep. Afr. Studies, Nagoya Univ.,* 83-88.

SAKA, Y. and YAIRI, K. (1977a): Sedimentary Structures of the Karroo System in the Livingstonia area, northern Malawi. *2nd Prelim. Rep. Afr. Studies, Nagoya Univ.,* 89-107.

SAKA, Y. and YAIRI, K. (1977b): Karroo System to the west of Karonga, northern Malawi. *2nd Prelim. Rep. Afr. Studies, Nagoya Univ.,* 70-82.

SHRODER, J.F. (1972): Geological history of rocks of post-Basement Complex, rift-faulting, and mineral occurrences. *In: Agnew, S. and Stubbs, M. (Eds.); Malawi in maps.* University of London Press, p.22.

THATCHER, E.C. (1968): The geology of the Dedza area. *Bull. Geol. Surv. Malawi,* **29,** 71pp.

THATCHER, E.C. (1974): The geology of the Nyika area. *Bull. Geol. Surv. Malawi,* **40,** 90pp.

WALSHW, R.D. (1965): The geology of the Ncheu-Balaka area. *Bull. Geol. Surv. Malawi,* **19,** 96pp.

WALTER, M.J. (1972): The geology of the Salima-Mvera Mission area. *Bull. Geol. Surv. Malawi,* **30,** 30pp.

YAIRI, K. (1977): Preliminary account of the lake-floor topography of Lake Malawi in relation to the formation of the Malawi Rift Valley. *2nd Prelim. Rep. Afr. Studies, Nagoya Univ.,* 51-69.

Chromian Phlogopite in the Bushveld Anorthosite, South Africa

Kanenori SUWA and Kazuhiro SUZUKI
Department of Earth Sciences, Faculty of Science, Nagoya University

Introduction

In the course of our study on the Bushveld anorthosite, we found chromian phlogopites in both adcumulate and heteradcumulate layers of the anorthosite from Dwars River Bridge.

As far as we aware, this is the first finding of chromian phlogopite from igneous rock formed in the crustal environment.

Up to now, there are several reports of chromian phlogopites in kimberlite (Rimsaite, 1971), in ultramafic nodules in kimberlites (Carswell, 1975; Dawson and Smith, 1975; Emeleus and Andrews, 1975), in ultramafic nodules in alkaline basalt (Francis, 1976), and in pyroxenite lens in serpentinized lherzolite (Peters, 1968). These rocks containing chromian phlogopite are believed to be of upper mantle origin.

For example, lherzolite nodules containing chromian phlogopite from Nunivak Island, Alaska are believed to have been amphibole-bearing fragments of the upper mantle, that partially melted during their ascent to the surface in the Nunivak basalts of late Tertiary to recent (Francis, 1976); and spinel-free pyroxenite containing chromian phlogopite is found as lenses in the serpentinized lherzolites originated in the upper mantle (Peters, 1968).

In this paper, a phlogopite containing Cr_2O_3 more than 1.0 wt.% is designated as chromian phlogopite.

Bushveld anorthosite

Bushveld anorthosite can be designated as Group I anorthosite, which occurs as layers within stratified basic sheets and lopoliths and is developed under stable cratogenic conditions (Suwa, 1977a, 1977b).

There are two Precambrian events as the basic igneous episodes of the cratons – the earlier episode falling at 2,200±300 m.y. and the later at 1,200±200 m.y. Bushveld Complex, which is one of the former examples, intrudes the Transvaal System at 2,050 m.y. ago.

In Bushveld Complex, anorthosite layers occur in the Critical-, Main-, and Upper-Zones, but no anorthosite layer occurs in the

Fig. 1.
Beautiful alternation of white anorthosite layer (plagioclase adcumulate layer) and black chromite-rich layer (chromite-plagioclase heteradcumulate layer) of anorthosite at Dwars River Bridge, north-eastern part of the Bushveld Complex (Photo by K. Suwa, 8th Mar., 1970).

Basal Zone consisting of ultramafic rocks (Wager and Brown, 1967; Willemse, 1969).

At Dwars River Bridge, Bushveld, anorthosite belonging to the upper part of Critical Zone occurs as beautiful alternation of white anorthosite layer (plagioclase adcumulate layer) and black chromite-rich layer (chromite-plagioclase heteradcumulate layer) as shown in Fig. 1.

The adcumulate layer consists of bytownite with small amounts of clinopyroxene, orthopyroxene, chromite and chromian phlogopite, and the heteradcumulate layer consists of chromite and bytownite with small amounts of clinopyroxene, orthopyroxene and chromian phlogopite (Specimen No. KS-70030818a).

Bytownite grains in the adcumulate layer are developed with their composition plane (010) in subparallel to the cumulate plane, whereas those in the heteradcumulate layer are developed with their composition plane (010) in subperpendicular to the cumulate plane. Grain sizes of bytownite in both layers are obviously different: bytownite in the adcumulate layer is of 1-2mm in length and that in the heteradcumulate layer is of 5–6mm in length. The grain size of chromite in the heteradcumulate layer is 0.02–0.4mm in diameter.

In the adcumulate layer, bytownite primocrystals crystallizing from main liquid accumulate firstly on the cumulate plane and then become to seed for later crystal growth, in which process diffusion between main liquid and pore space liquid plays an important role, and resultant crystal is 1–2mm in length. In the heteradcumulate layer, after the crystallization of chromite, bytownite begins to crystallize from pore space liquid and develops to larger crystal of 5–6mm in length, during this process supercooling effect may play a role.

Bytownite grains in the adcumulate and heteradcumulate layers are twinned according to the albite-Carlsbad law, pericline law, albite law, and Carlsbad law. Frequency percentage of albite-Carlsbad law and Carlsbad law reaches 43% in together.This twinning pattern of the plagioclases clearly indicates the igneous origin of the anorthosite and there is no sign of any metamorphic effect in the later periods (Suwa, 1975, 1977a, 1977b).

Chromian phlogopite

Chromian phlogopites occupy only 1–2 and several vol. % in the adcumulate and heteradcumulate layers respectively.

Under the microscope, chromian phlogopites show strong pleochroism: X=colourless

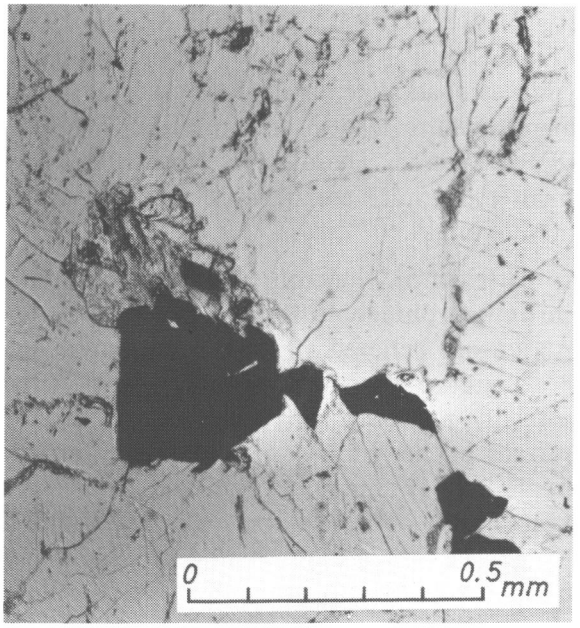

Fig. 2.
Photomicrograph of chromian phlogopite (left upper central) in adcumulate layer of anorthosite (KS-70030818a) at Dwars River Bridge, NE Bushveld Complex. one nicol.

~very pale yellow, Y=Z=light brown and very small optical angle of negative sign. Most of chromian phlogopites occur associated with chromite grains in both adcumulate and heteradcumulate layers. Grain sizes of chromian phlogopites in the adcumulate layer are of 0.05–0.5mm in length and those in the heteradcumulate layer are of 0.05–0.7mm in length (see Figs. 2 and 3).

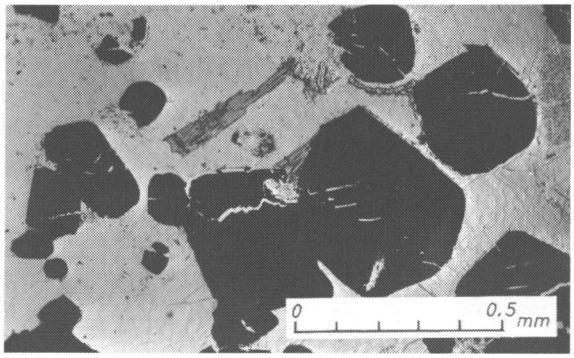

Fig. 3.
Photomicrograph of chromian phlogopite (upper central) in heteradcumulate layer of anorthosite (KS-70030818a) at Dwars River Bridge, NE Bushveld Complex. One nicol.

These chromian phlogopites contain sizable amounts of TiO_2, Cr_2O_3 and FeO, and small amounts of NiO, CaO and Na_2O as shown in Table 1. When we compare chromian phlogopite in the adcumulate layer with that in the heteradcumulate layer, the former is characterized by the enrichment of TiO_2, FeO and K_2O, and the latter is characterized by the enrichment of Al_2O_3, Cr_2O_3 MgO and Na_2O. Similar variation of chemical composition can be recognized also on chromites in both layers as shown in below.

In general, chromium substitutes for octahedral aluminium in small amounts in normal $2M_1$ muscovite. Chromian muscovites are known with as much as 6% Cr_2O_3, and these are called fuchsite or mariposite. Those called mariposite appear to have high SiO_2 and so can be considered as chromian phengites. In Table 1, some examples of chromian muscovites are also shown.

Associated minerals

Bytownite: Zonal structure is found frequently in the bytownite grains. The chemical composition of bytownite in the adcumulate layer by means of EPMA is An 74.3 (71.0–77.0), Ab 24.6 (22.0–27.6), Or 1.1 (0.6–1.4). The chemical composition of bytownite in the heteradcumulate layer varies considerably: the bytownite in narrow zone (0.005–0.02mm in width) surrounding the chromite crystal is more calcic than the bytownite in other main parts. The bytownite in contact directly with chromite is of An 79.1 (75.1–86.8), Ab 20.6 (13.2–24.4), Or 0.3 (0.0–0.5), and the bytownite in main parts is of An 72.7 (69.2–79.2),Ab 26.8 (20.6–30.1) , Or 0.5 (0.2–0.7).

The angular separations in X-ray diffraction patterns of the bytownite in the adcumulate layer are: $2\theta(220) - 2\theta(1\bar{3}1) = 0.995°$, $2\theta(1\bar{3}1) - 2\theta(131) = 2.085°$, $2\theta(131)+2\theta(220)-4\theta(1\bar{3}1) = 1.09°$. Refractive indices of this bytownite are $\alpha_D = 1.565\pm0.001$, $\beta_D = 1.570\pm0.001$, $\gamma_D = 1.575\pm0.001$. These chemical, X-ray, and optical data indicate that the bytownite in the adcumulate layer is of the low-temperature form.

Clinopyroxene: Clinopyroxene in the adcumulate layer is of diopside (Wo 47 En 43 Fs 10) containing Cr_2O_3 (0.81–0.88 wt. %), Al_2O_3 (0.89–1.68 wt.%) and Na_2O (0.18–0.23 wt.%).

Orthopyroxene: Orthopyroxene in the heteradcumulate layer is of bronzite (En 85 Fs 15) containing Cr_2O_3 (0.33–0.50 wt. %), Al_2O_3 (0.82–1.32 wt.%) and CaO (0.42–

Table 1 Chemical compositions of chromian phlogopites (A, B, C), fuchsite (D) and mariposite (E)

	A	B	C	D	E
SiO_2	38.4	38.7	38.92	45.97	56.00
TiO_2	5.48	5.17	0.26	—	—
Al_2O_3	14.3	14.8	17.36	31.67	23.52
Cr_2O_3	1.24	1.42	2.19	4.81	0.78
Fe_2O_3	5.75	4.12	3.77	2.56	3.30
FeO				0.53	0.51
MnO	0.01	0.0	0.05	—	—
NiO	0.10	0.11	—	—	—
MgO	21.6	23.2	23.36	0.31	2.12
CaO	0.08	0.07	0.00	0.15	0.37
Na_2O	0.0	0.10	1.07	1.03	2.72
K_2O	9.40	9.02	8.36	9.07	7.03
H_2O^+	3.78	3.36	—	3.48	3.52
H_2O^-				0.51	
Total	100.1	100.1	95.34	100.09	99.87
Si	5.46	5.43	5.491	6.268	7.421
Al^{IV}	2.39	2.43	2.509	1.732	0.579
Al^{VI}	0.0	0.0	0.379	3.360	3.096
Cr	0.14	0.16	0.245	0.518	0.081
Ti	0.59	0.55	0.027	—	—
Fe^{+3}	0.69	0.48	0.445	0.262	0.330
Fe^{+2}				0.061	0.057
Mn	0.0	0.0	0.006	—	—
Ni	0.01	0.01	—	—	—
Mg	4.57	4.84	4.913	0.063	0.419
Ca	0.01	0.01	0.000	0.022	0.053
Na	0.0	0.02	0.292	0.272	0.700
K	1.71	1.61	1.507	1.578	1.190
Total	15.57	15.54	15.814	14.136	13.926
$\frac{Mg}{Mg+Fe}$	0.87	0.91	0.917	0.16	0.52

A : Chromian phlogopites (average 4) in adcumulate layer of anorthosite (KS-70030818a) from Dwars River Bridge, Bushveld Complex.
B: Chromian phlogopites (average 3) in heteradcumulate layer of anorthosite (KS-70030818a) from Dwars River Bridge, Bushveld Complex.
C: Chromian phlogopites (average 3) in lherzolite nodules from Nunivak Island, Alaska (Francis, 1976).
D: Fuchsite (chrome-muscovite) from Pointe du Boise, Manitoba (Whitmore *et al.*, 1946).
E: Mariposite from Ross Mine, Hislop Township, Ontario (cited in Whitmore *et al.*, 1946).

0.47 wt.%)

Chromite: Chromites in the adcumulate and heteradcumulate layers contain sizable amounts of Al_2O_3 and MgO, and small amounts of TiO_2, MnO, NiO, SiO_2 and CaO. The chemical compositions of chromites in both layers are different each other. When we compare chromite in the adcumulate layer with that in the heteradcumulate layer, the former is characterized by the enrichment of FeO, Fe_2O_3, TiO_2, MnO and CaO, and the latter is characterized by the enrichment of Al_2O_3 and MgO. Cr_2O_3 content of chromites in both layers is same.

Discussion

(1) Chemical composition of chromian phlogopites in the adcumulate layer differs from that of chromian phlogopites in the heteradcumulate layer of the Bushveld anorthosite. Similar variation of chemical composition can be recognized also on chromites in both layers. Therefore, chromian phlogopites are considered to be crystallized primarily in the process of the Bushveld igneous activity.

(2) Chromian phlogopites from the Bushveld anorthosite are characterized by the deficiency of Si and Al in the tetrahedral site and by the enrichment of Ti and K. On the other hand, chromian phlogopites from lherzolite nodules of Nunivak Island in Alaska are characterized by the enrichment of Al, Cr, Mg and Na as shown in Table 1.

Chromium is considered to occupy tetrahedral site and/or octahedral site in the Bushveld chromian phlogopites, and chromium occupies octahedral site in the Nunivak chromian phlogopites.

(3) In the Bushveld anorthosite, chromium prefers to enter into chromite and then into chromian phlogopite, clinopyroxene, orthopyroxene and plagioclase in descending order. In the lherzolite nodules from the Nunivak Island, chromium prefers to enter into chromian spinel and then into chromian clinopyroxene, chromian amphibole, chromian phlogopite and olivine in descending order.

(4) Cr/Al ratios of the chromites in the adcumulate and heteradcumulate layers in the Bushveld anorthosite are 3.1 and 2.4 respectively. Cr/Al ratio, in general, appears to be high in chromian spinel from layered intrusive body and the ratio appears to be low in chromian spinel from ultramafic nodule of upper mantle origin.

For example, Cr/Al ratios of chromites in massive ore of the Stillwater Complex (Stevens, 1944) and in chromitite of the Bushveld Complex(Frankel,1959) are 1.9 and 2.4 respectively; and the ratios of chromian spinels in ultramafic nodules from Ndonyuo Olnchoro, Kenya (Suwa *et al.*, 1975) and from Nunivak Island, Alaska (Francis, 1976) are 0.5.

Cr/Al ratio of chromian spinlel appears to be governed by solid pressure, oxygen partial pressure, temperature and bulk chemical composition of rock concerned.

(5) As far as we aware, most chromian phlogopites have been reported from the rocks of upper mantle origin (Carswell, 1975; Dawson and Smith, 1975; Emeleus and Andrews, 1975; Francis, 1976; Peters, 1968; Rimsaite, 1971). The chromian phlogopite in the Bushveld anorthosite described in this paper is considered to be the first finding of chromian phlogopite from igneous rocks formed in the crustal environment.

Judging from the occurrence, more chromian phlogopites will be found in layered intrusive body, where especially in lower

horizon containing chromite layer.

Acknowledgements – We wish to thank Professor Isao Matsuzawa and Dr. Keiichi Shiraki of Nagoya University and Professor W.J. Verwoerd of the University of Stellenbosch, for their advice and encouragement.

References

Carswell, D.A. (1975): Primary and secondary phlogopites and clinopyroxenes in garnet lherzolite xenoliths. *Phys. Chem. Earth,* **9**, 417–429.

Dawson, J.B. and Smith, J.V. (1975): Chromite-silicate intergrowths in upper-mantle peridotites. *Phys. Chem. Earth,* **9**, 339–350.

Emeleus, C.H. and Andrews, J.R. (1975): Mineralogy and petrology of kimberlite dyke and sheet intrusions and included peridotite xenoliths from south-west Greenland. *Phys. Chem. Earth,* **9**, 179–197.

Francis, D.M. (1976): The origin of amphibole in lherzolite xenoliths from Nunivak Island, Alaska. *Jour. Petrol.,* **17**, 357–378.

Frankel, J.J. (1959): Uvarovite garnet and South African Jade (hydrogrossular) from the Bushveld complex, Transvaal. *Amer. Mineral.,* **44**, 565–591.

Peters, Tj. (1968): Distribution of Mg, Fe, Al, Ca and Na in coexisting olivine, orthopyroxene and clinopyroxene in the Totalp serpentinite (Davos, Switzerland) and in the Alpine metamorphosed Malenco serpentinite (N. Italy). *Contr. Mineral. and Petrol.* ,**18**, 65–75.

Rimsaite, J. (1971): Distribution of major and minor constituents between mica and host ultrabasic rocks, and between zoned mica and zoned spinel. *Contr. Mineral. and Petrol.* ,**33**,259–272.

Stevens, R.E. (1944): Composition of some chromites of the Western Hemisphere. *Amer. Mineral.,* **29**, 1–34.

Suwa, K. (1975): Plagioclases in anorthosites. *1st Prelim. Rep. African Studies, Nagoya Univ.* ,55–59.

Suwa, K. (1977a): Precambrian anorthosites and their plagioclases. *Precambrian Research,* **5** (in press).

Suwa, K. (1977b): Precambrian anorthosites and their plagioclases (Abstract). *2nd Prelim. Rep. African Studies, Nagoya Univ.* ,3–12.

Suwa, K., Yusa, Y., and Kishida, N. (1975): Petrology of peridotite nodules from Ndonyuo Olnchoro, Samburu district, central Kenya. *Phys. Chem. Earth,* **9**, 273–286 (Pergamon Press).

Wager, L.R. and Brown, G.M. (1967): *Layered Igneous rocks.* Oliver and Boyd Ltd., Edinburgh. 588p.

Whitmore, D.R.E., Berry, L.G. and Hawley, J.E. (1946): Chrome micas. *Am. Mineral.* ,**31**, 1–21.

Willemse, J. (1969): The geology of the Bushveld Complex, the largest repository of magmatic ore deposits in the world. *Econ. Geol. Monograph,* No.**4**, 1–22.

Contact Aureole of the North-eastern Part of the Bushveld Igneous Complex, South Africa

Kanenori SUWA and Kazuhiro SUZUKI

Department of Earth Sciences, Faculty of Science, Nagoya University

Introduction

The Bushveld Igneous Complex is a giant among mafic layered intrusions and occupies an area about 67,000 Km^2 in extent. The Complex consists of five adjoining, basin-shaped masses of igneous rocks. The outline of the whole mass is accordingly lobulate.

The total thickness of the exposed layered sequence in the Eastern Transvaal is now placed at 7,500 metres. The rocks range in composition from dunite through peridotite and pyroxenite to norite, gabbro, anorthosite and ferrodiorite in the layered sequence.

There is ample evidence of transgression of the layered sequence to the encircling sedimentary rocks. By taking the Magaliesberg quartzite as a reference horizon, it is clear that for long distances along the strike the Bushveld Igneous Complex adjoins this quartzite, especially in the Western Transvaal. For this reason the Complex has been regarded as a conformable intrusion having a floor. A transgressive relationship, however, is also revealed in many localities (Willemse, 1969).

During intrusion of the Bushveld Igneous Complex at 2,050 m.y. ago, the thermal history of the sedimentary succession of the Transvaal System probably consisted of a rapid temperature increase followed by a temperature maximum and a comparatively long time during which the thick overlying mass of mafic magma crystallized and cooled.

On the Eastern Bushveld, Hall (1908) investigated contact metamorphism in the Pretoria series, Upper sedimentary horizon of the Transvaal System, of the Lydenburg and Zoutpansberg districts as a pioneer. Since Hall, several authors investigated the same problem and recent investigators include Hiemstra and Van Biljon (1959), Schwellnus (1970) and Willemse and Viljoen (1970). Hiemstra and Van Biljon (1959) described contact metamorphic rocks in the area south-east of Steelpoort, Schwellnus (1970) described andalusite and staurolite hornfelses occurring in the north-eastern metamorphic aureole of the Bushveld Igneous Complex and discussed the relationship between these two minerals on the basis of their petrochemical data, and Willemse and Viljoen (1970) described contact metamorphic rocks near Aspiesdoorn and corundum-sillimanite-spinel xenoliths in the north-eastern part of the Bushveld Igneous Complex.

On the Western Bushveld, Hatch (1904) mentioned chiastolite slates to the north of Zeerust. Since Hatch, several authors investigated contact aureole and several surveys were conducted along the chiastolite and andalusite horizons because of the growing economic value of andalusite for refractory purpose, and recently Engelbrecht (1976) described the contact metamorphic rocks in Marico district.

These recent studies include the petrochemical and petrographical data to clarify the physical and chemical conditions during contact metamorphism. No detailed mineralogical data, however, can be found in these

2nd Prelim. Rep. Afr. Studies, Nagoya Univ., 139-153, 1977.

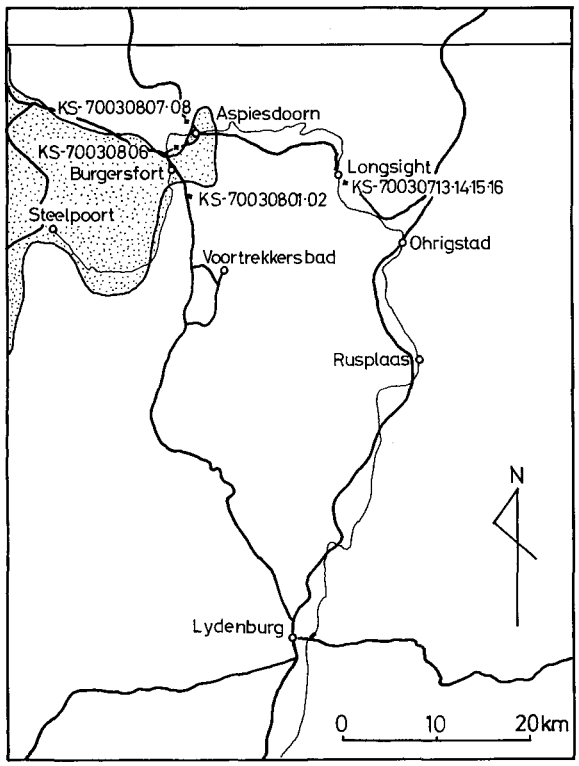

Fig. 1.
Locality map of the north-eastern contact aureole of the Bushveld Complex. Dotted area shows the Bushveld Complex.

recent studies.

In this paper, therefore, we would discuss the contact metamorphism on the basis of mineralogical and petrographical data of the contact metamorphic rocks occurring at the north-eastern contact aureole of the Bushveld Igneous Complex.

Contact metamorphic rocks at Longsight

Studied area is situated in the north-eastern part of the Bushveld Igneous Complex and is shown in Fig. 1. The contact metamorphic rocks can be tentatively divided into two groups, lower grade and higher grade metamorphic rocks. Lower grade metamorphic rocks occur at and around Longsight and higher grade rocks at and around Burgersfort and Aspiesdoorn.

(A) Pelitic-psammitic hornfels at Longsight

Pelitic-psammitic hornfels at Longsight shows clearly graded bedding in the field as well as in the handspecimen as shown in Fig. 2. Even under the microscope, the texture of graded bedding is clearly observed as shown in Fig. 3.

The chemical compositions of pelitic-psammitic hornfels (KS-70030714) at Longsight are shown in Table 1. When we compare the chemical composition of pelitic hornfels with that of psammitic hornfels, the former is higher in Al_2O_3 and FeO and is lower in SiO_2, Fe_2O_3, Na_2O and K_2O.

Psammitic hornfels (KS-70030714-3) consists mainly of quartz, biotite and muscovite with small amounts of garnet, plagioclase, tourmaline, ilmenite and zircon. Grain size of the minerals is very fine-grained as follows: quartz (av. 0.07mm), biotite (av. 0.2mm), muscovite (av. 0.05mm), garnet (av. 0.1mm) and tourmaline (av. 0.05mm). Biotite exhibits sieve texture.

The chemical compositions of the constituent minerals of the psammitic hornfels are shown in Table 2. Garnet is of almandine with spessartine molecule, biotite is lower in TiO_2, muscovite is higher in Na/Na+K ratio,

Table 1 Chemical compositions of pelitic and psammitic hornfels (KS-70030714) at Longsight, north-eastern contact aureole of the Bushveld Complex.

	Pelitic hornfels KS-70030714-4	Semi-pelitic hrnfels KS-70030714-3·4	Psammitic hornfels KS-70030714-3
SiO_2	64. 57	66. 51	69. 55
TiO_2	0. 80	0. 81	0. 66
Al_2O_3	20. 70	20. 20	16. 84
Fe_2O_3	1. 11	1. 45	1. 61
FeO	3. 29	2. 62	2. 28
MnO	0. 09	0. 09	0. 07
MgO	1. 36	1. 27	1. 30
CaO	0. 39	0. 22	0. 31
Na_2O	0. 85	1. 04	1. 38
K_2O	2. 43	2. 88	3. 83
P_2O_5	0. 03	0. 05	0. 05
$H_2O(+)$	4. 24	2. 74	2. 36
$H_2O(-)$	0. 18	0. 14	0. 11
Total	100. 04	100. 02	100. 35

Analyst : K. Suzuki

Table 2 Chemical compositions of garnet, biotite, muscovite and plagioclase in psammitic hornfels (KS-70030714-3) at Longsight, north-eastern contact aureole of the Bushveld Complex.

	Garnet core (av. 6)	Garnet margin (av. 6)	Biotite (av.10)	Muscovite (av. 3)	Plagioclase (av. 7)
SiO_2	36. 1	36. 5	35. 0	45. 3	Ab 86. 0
TiO_2	0. 11	0. 12	1. 58	0. 45	An 13. 7
Al_2O_3	20. 0	20. 0	19. 8	36. 2	Or 0. 2
FeO	28. 6	30. 3	21. 9	0. 83	
MnO	12. 6	10. 4	0. 25	0. 02	
MgO	1. 62	1. 50	8. 04	0. 43	
CaO	0. 69	1. 01	0. 05	0. 01	
Na_2O	0. 00	0. 00	0. 15	1. 52	
K_2O	0. 00	0. 00	8. 51	8. 86	
$H_2O(+)$	0. 00	0. 00	4. 84	6. 30	
Total	99. 7	99. 8	100. 1	99. 9	
Si	2. 98	3. 00	5. 37	6. 08	
Al^{IV}	1. 95	1. 94	2. 63	1. 92	
Al^{VI}	0. 00	0. 00	0. 94	3. 82	
Ti	0. 01	0. 01	0. 18	0. 05	
Fe	1. 98	2. 09	2 80	0. 10	
Mn	0. 88	0. 72	0. 03	0. 00	
Mg	0. 19	0. 18	1. 84	0. 09	
Ca	0. 06	0. 09	0. 01	0. 00	
Na	0. 00	0. 00	0. 04	0. 39	
K	0. 00	0. 00	1. 66	1. 52	

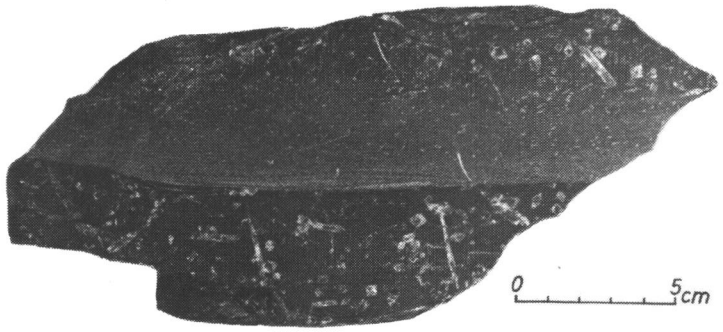

Fig. 2

Graded bedding of pelitic and psammitic hornfels (KS-70030714) at Longsight. Upper half is psammitic-pelitic part, in which psammitic part grades into pelitic part. Lower half is pelitic part with chiastolite porphyroblast. The boundary between upper half and lower half is very sharp.

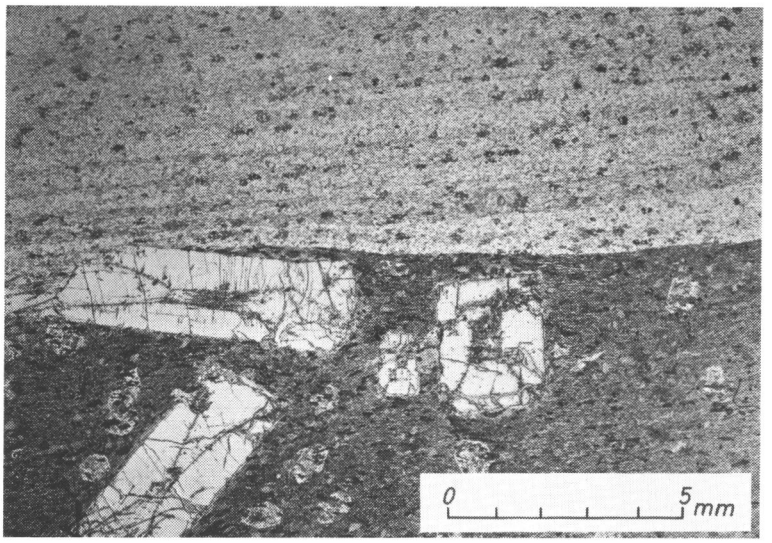

Fig. 3

Microphotograph of the texture of graded bedding of pelitic and psammitic hornfels (KS-70030714) at Longsight. Upper half is psammitic part and lower half is pelitic part with chiastolite porphyroblast. One nicol.

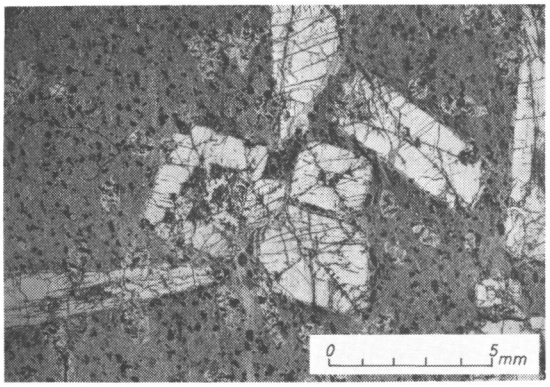

Fig. 4.
Microphotograph of pelitic hornfels (KS-70030714-4) at Longsight. Chiastolite porphyroblasts are studded in very fine-grained groundmass. One nicol.

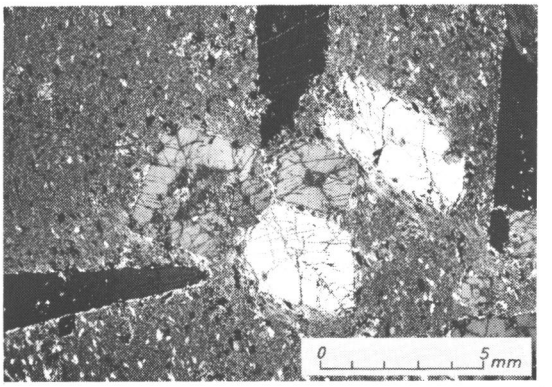

Fig. 5.
Ditto with Fig. 4. Nicols crossed.

Table 3 Chemical compositions of garnet, biotite, muscovite, andalusite and plagioclase in pelitic hornfels (KS-70030714-4) at Longsight, north-eastern contact aureole of the Bushveld Complex.

	Garnet			Biotite	Muscovite	Andalusite	Plagioclase
	core (av. 4)	margin (av. 4)	others (av. 4)	(av. 8)	(av. 3)	(av. 3)	(av. 5)
SiO_2	36. 3	36. 1	36. 0	34. 5	45. 9	36. 2	Ab 87. 8
TiO_2	0. 10	0. 14	0. 12	1. 62	0. 49	0. 01	An 12. 0
Al_2O_3	19. 8	20. 4	19. 9	20. 0	38. 1	63. 6	Or 0. 2
FeO	27. 8	29. 2	28. 0	22. 2	0. 87	0. 25	
MnO	12. 6	11. 4	13. 2	0. 32	0. 06	0. 03	
MgO	1. 61	1. 50	1. 61	7. 99	0. 41	0. 03	
CaO	0. 75	0. 88	0. 67	0. 02	0. 00	0. 00	
Na_2O	0. 00	0. 00	0. 00	0. 21	1. 37	0. 00	
K_2O	0. 00	0. 00	0. 00	8. 52	8. 75	0. 00	
$H_2O(+)$	0. 00	0. 00	0. 00	4. 59	40. 04	0. 00	
Total	99. 0	99. 6	99. 5	100. 0	100. 0	100. 1	
Si	3. 00	2. 98	2. 98	5. 29	6. 00	0. 98	
Al^{IV}	1. 94	1. 98	1. 94	2. 71	2. 00	2. 02	
Al^{VI}	0. 00	0. 00	0. 00	0. 93	3. 87	0. 01	
Ti	0. 01	0. 01	0. 03	0. 19	0. 05	0. 00	
Fe	1. 93	2. 02	1. 94	2. 85	0. 09	0. 01	
Mn	0. 89	0. 79	0. 92	0. 04	0. 01	0. 00	
Mg	0. 20	0. 19	0. 20	1. 83	0. 08	0. 00	
Ca	0. 07	0. 08	0. 06	0. 00	0. 00	0. 00	
Na	0. 00	0. 00	0. 00	0. 06	0. 35	0. 00	
K	0. 00	0. 00	0. 00	1. 67	1. 46	0. 00	

and plagioclase is of sodic oligoclase (An 13.7).

In pelitic hornfels (KS-70030714-4), chiastolite (andalusite) porphyroblasts are studded in very fine-grained groundmass, in which we can recognize two parts: the first is very fine-grained groundmass and the second is oval-shaped clot with 1.5mm in diameter.

Very fine-grained groundmass consists of quartz (av. 0.03mm), biotite (av. 0.2mm), muscovite (av. 0.05mm), garnet (av. 0.1mm), ilmenite (av. 0.05mm), plagioclase, tourmaline, apatite and zircon. Garnet is not poikilitic but euhedral, Z-axial colour of tourmaline is light brown to green, and biotite often exhibits sieve texture and its Z-axial colour is pale brown.

Oval-shaped clot in groundmass consits of fine-grained biotite (av. 0.35mm), quartz (av. 0.07mm), muscovite (av. 0.06mm), tourmaline (av. 0.03mm), plagioclase and garnet. Biotite and muscovite in this clot can grow freely irrespective of the bedding. This clot may be formerly pinnitized cordierite microporphyroblast.

Chiastolite (andalusite) porphyroblasts contain very fine-grained inclusions of quartz, muscovite, biotite, garnet and ilmenite. Figs. 4 and 5 show chiastolite porphyroblasts studded in pelitic hornfels (KS-70030714-4).

The chemical compositions of the constituent minerals of the pelitic hornfels are shown in Table 3. Garnet is of almandine with spessartine molecule, biotite is lower in TiO_2, muscovite is higher in $Na/Na+K$ ratio, andalusite is lower in FeO, and plagioclase is of sodic oligoclase (An 12.0). When we compare Table 3 with Table 2, we can recognize that the chemical compositions of the constituent minerals of the pelitic hornfels are very similar to those of the psammitic hornfels.

Figs. 6 and 7 show long chiastolite porphyroblasts and biotite micro-porphyroblasts studded in a very fine-grained groundmass of pelitic hornfels (KS-70030716).

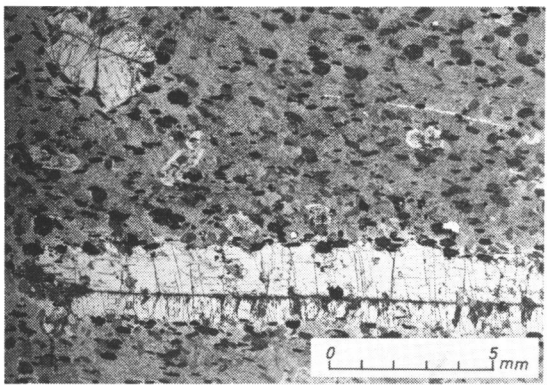

Fig. 6.
Microphotograph of pelitic hornfels (KS-70030716) at Longsight. Long chiastolite porphyroblasts and biotite micro-porphyroblasts are studded in very fine-grained groundmass. One nicol.

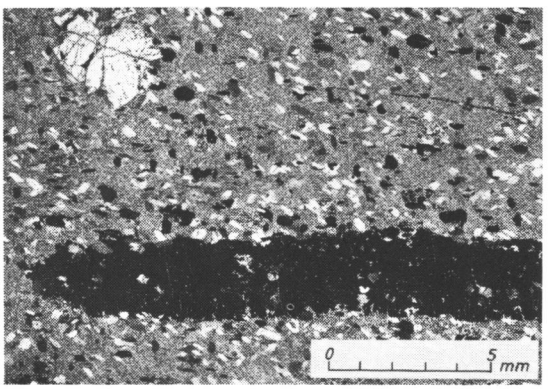

Fig. 7.
Ditto with Fig. 6. Nicols crossed.

(B) Basic hornfels at Longsight

Basic hornfels (KS-70030713) at Longsight consists mainly of actinolite, calcic plagioclase and ilmenite with small amounts of zoisite and calcite. Grain size of very fine-grained actinolite is 0.01 to 0.03 mm and that of fine-grained actinolite is 0.05 to 0.2mm and that of medium-grained actinolite sometimes reaches 0.4 to 0.6mm, and the first two actinolites occupy in majority. Calcic plagioclase is 0.02 to 0.03 mm and sometimes reaches 0.35mm, and we can rarely recognize the plagioclase relict phenocryst (0.8 mm) twinned after albite-Carlsbad law.

Fig.8 shows the microscopic structure of basic hornfels (KS-70030713) at Longsight.

The chemical compositions of the constituent minerals of the basic hornfels are shown in Table 4. Si and Ca of the actinolite reach 7.25 and 1.89 on the basis of 24 (O,OH,F), respectively. Ilmenite is higher in MnO content (2.16%) and calcic plagioclase is of bytownite (An 82).

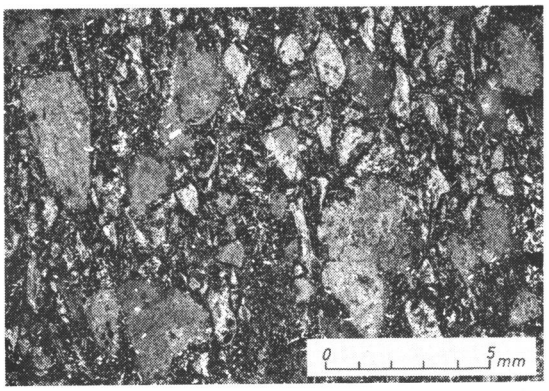

Fig. 8.

Microphotograph of basic hornfels (KS-70030713) at Longsight. All clots and matrix part are mainly composed of fine-grained actionolite and calcic plagioclase. Nicols crossed.

Contact metamorphic rocks at Burgersfort and Aspiesdoorn

(A) Pelitic-psammitic hornfels at Burgersfort

Ptygmatic leucocratic vein is found to occur in pelitic-psammitic hornfels at Burgersfort.

Pelitic hornfels (KS-70030801) at the south of Burgersfort consists mainly of muscovite, quartz, biotite, plagioclase, andalusite and fibrolite with small amounts of ilmenite, tourmaline and apatite. Grain size of the minerals is fine- to medium-grained as follows: muscovite (av. 0.8mm), quartz (av. 0.4mm), biotite (av. 0.6mm), andalusite (av. 3.0mm), plagioclase (av. 0.1mm), fibrolite (individual: 0.1mm, aggregate: 1.0mm), tourmaline (av. 0.2mm) and apatite (av. 0.1mm).

Fig.9 shows fibrolite aggregate and andalusite crystal surrounded by fibrolite aggregate. Muscovite and biotite show sometimes symplectic growth. Biotite contains many zircons showing pleochroic halo. Fibrolite is found to occur as an aggregate replacing biotite and andalusite. Plagioclase shows sometimes zonal structure.

The chemical compositions of the constituent minerals of the pelitic hornfels are shown in Table 5. Biotite is higher in TiO_2, muscovite is lower in Na/Na+K ratio, andalusite is higher in FeO, fibrolite is lower in FeO, and plagioclase is of sodic andesine (An30.8).

Pelitic hornfels (KS-70030802) at the south of Burgersfort consists mainly of muscovite, fibrolite, biotite, quartz, magnetite, titaniferous magnetite, plagioclase and cordierite with small amounts of tourmaline and apatite. Grain size of the minerals is fine- to medium-grained as follows: muscovite (av. 1.5mm), fibrolite (aggregate: av. 2.5mm), biotite (av. 0.6mm), quartz (av. 0.8mm), magnet-

Table 4 Chemical compositions of actinolite, ilmenite and plagioclase in basic hornfels (KS-70030713) at Longsight, northeastern contact aureole of the Bushveld Complex.

	Actinolite (av. 14)	Ilmenite (av. 3)	Plagioclase (av. 8)
SiO_2	48. 9	0. 33	Ab 18
TiO_2	0. 48	52. 3	An 82
Al_2O_3	6. 33	0. 19	Or 0
FeO	15. 9	43. 5	
MnO	0. 34	2. 16	
MgO	12. 4	0. 19	
CaO	11. 9	0. 36	
Na_2O	0. 57	0. 00	
K_2O	0. 14	0. 00	
$H_2O(+)$	3. 11	0. 00	
Total	100. 1	99. 0	
Si	7. 25	0. 02	
Al^{IV}	0. 75	0. 01	
Al^{VI}	0. 36	0. 00	
Ti	0. 05	1. 99	
Fe	1. 97	1. 85	
Mn	0. 04	0. 09	
Mg	2. 73	0. 01	
Ca	1. 89	0. 02	
Na	0. 16	0. 00	
K	0. 03	0. 00	

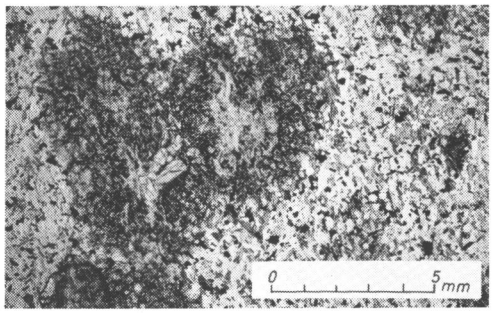

Fig. 9.
Microphotograph of pelitic hornfels (KS-70030801) at the south of Burgersfort. Upper central is fibrolite aggregate and left central is andalusite crystals surrounded by fibrolite aggregate. One nicol.

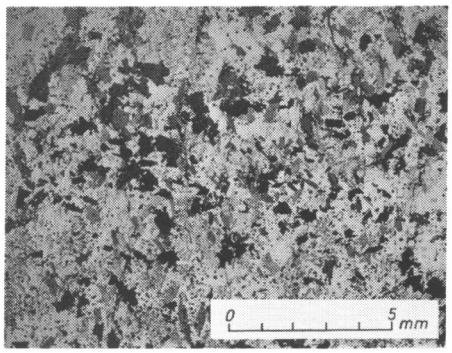

Fig. 10.
Microphotograph of pelitic hornfels (KS-70030802) at the south of Burgersfort. Increase of grain size of the constituent minerals is recognized. One nicol.

Table 5 Chemical compositions of biotite, muscovite, andalusite, fibrolite and plagioclase in pelitic hornfels (KS70030801) at the south of Burgersfort, north-eastern contact aureole of the Bushveld Complex.

	Biotite	Muscovite (av. 2)	Andalusite (av.2)	Fibrolite	Plagioclase (av.6)
SiO_2	35. 6	45. 5	37. 3	37. 3	Ab 68. 8
TiO_2	2. 89	0. 37	0. 09	0. 05	An 30. 8
Al_2O_3	19. 0	36. 7	62. 0	61. 8	Or 0. 4
FeO	22. 8	2. 53	1. 36	0. 47	
MnO	0. 21	0. 03	0. 01	0. 01	
MgO	7. 95	0. 59	0. 03	0. 01	
CaO	0. 03	0. 05	0. 00	0. 01	
Na_2O	0. 12	0. 88	0. 00	0. 00	
K_2O	9. 10	9. 76	0. 00	0. 00	
$H_2O(+)$	2. 32	3. 57	0. 00	0. 00	
Total	100. 2	100. 0	100. 8	99. 9	
Si	5. 37	6. 01	1. 01	1. 01	
Al^{IV}	2. 63	1. 99	0. 00	0. 00	
Al^{VI}	0. 74	3. 73	1. 97	1. 98	
Ti	0. 33	0. 04	0. 00	0. 00	
Fe	2. 87	0. 28	0. 03	0. 00	
Mn	0. 03	0. 00	0. 00	0. 00	
Mg	1. 78	0. 12	0. 00	0. 00	
Ca	0. 01	0. 01	0. 00	0. 00	
Na	0. 04	0. 23	0. 00	0. 00	
K	1. 75	1. 65	0. 00	0. 00	

ite and titaniferous magnetite (av. 0.06mm), plagioclase (av. 0.15mm) and cordierite (av. 0.2mm). Grain size of the higher grade metamorphic rocks (e.g., KS-70030801, 02) shows an increase of about ten times over that of the lower grade metamorphic rocks (e.g., KS-70030714, 16) as shown in Figs. 3 and 10.

Muscovite shows symplectic growth, and biotite shows sometimes symplectic growth and contains many zircons showing pleochroic halo. Fibrolite occurs as an aggregate replacing muscovite and biotite, and twinned cordierite sometimes is found. Plagioclase shows sometimes weakly zonal structure.

Table 6 Chemical compositions of cordierite, biotite, muscovite, magnetite, titaniferous magnetite, and plagioclase in pelitic hornfels (KS-70030802) at the south of Burgersfort, north-eastern contact aureole of the Bushveld Complex.

	Cordierite (av. 3)	Biotite (av. 2)	Muscovite (av. 3)	Magnetite	Titaniferous magnetite	Plagioclase
SiO_2	48. 1	36. 6	45. 5	0. 00	0. 00	Ab 73. 7
TiO_2	0. 06	1. 80	1. 18	0. 27	18. 1	An 25. 9
Al_2O_3	33. 9	21. 2	36. 5	0. 42	0. 45	Or 0. 4
Fe_2O_3	5. 70	16. 3	3. 71	68. 0	25. 2	
FeO				30. 7	55. 3	
MnO	0. 59	0. 23	0. 03	0. 14	0. 47	
MgO	9. 98	12. 4	0. 86	0. 09	0. 12	
CaO	0. 00	0. 00	0. 00	0. 00	0. 06	
Na_2O	0. 54	0. 26	0. 86	0. 00	0. 00	
$K_2O(+)$	0. 00	8. 31	9. 80	0. 00	0. 00	
$H_2O(+)$	1. 22	3. 12	1. 65	0. 00	0. 00	
Total	100. 1	100. 2	100. 1	99. 6	99. 7	
Si	4. 89	5. 34	5. 93	0. 00	0. 00	
Al^{IV}	1. 11	2. 66	2. 07	0. 15	0. 16	
Al^{VI}	2. 96	0. 97	3. 54			
Ti	0. 11	0. 20	0. 12	0. 06	4. 21	
Fe^{+3}	0. 48	1. 98	0. 40	15. 77	5. 87	
Fe^{+2}				7. 91	14. 32	
Mn	0. 05	0. 03	0. 00	0. 04	0. 13	
Mg	1. 52	2. 68	0. 17	0. 04	0. 06	
Ca	0. 00	0. 00	0. 00	0. 00	0. 02	
Na	0. 11	0. 08	0. 22	0. 00	0. 00	
K	0. 00	1. 54	1. 63	0. 00	0. 00	

The chemical compositions of the constituent minerals of the pelitic hornfels are shown in Table 6. As opaque minerals, magnetite and titaniferous magnetite are found to occur. Biotite is lower in TiO_2 and this fact may be due to the absence of ilmenite in this rock. Muscovite is lower in Na/Na+K ratio, Fe/Fe+Mg ratio of cordierite is 0.24, and plagioclase is of calcic oligoclase (An25.9).

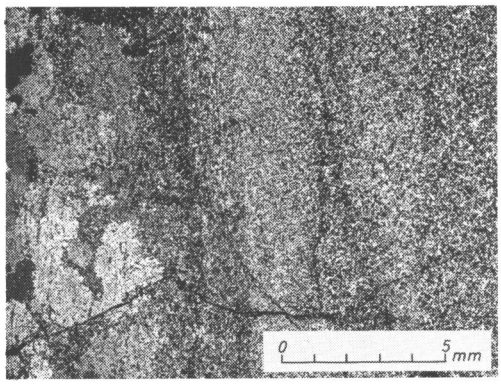

Fig. 11.

Microphotograph of calcareous hornfels (KS-70030808) at Aspiesdoorn. Left part is ilmenite-anorthite-poikiloblastic potassic hastingsite zone, central left part is anorthite-ilmenite-phlogopite-titaniferous salite zone, central part is titaniferous salite zone, central right part is anorthite-salite zone, and right part is clinozoisite-muscovite-salite zone. Nicols crossed.

Table 7 Chemical compositions of plagioclase, potassic hastingsite, ilmenite, titaniferous salite, salite, phlogopite and muscovite in calcareous hornfels (KS-70030808) at Aspiesdoorn, north-eastern contact aureole of the Bushveld Complex.

	Plagioclase	Potassic hastingsite (av. 2)	Ilmenite (av. 3)	Titaniferous salite (av. 7)	Salite	Phlogopite (av. 4)	Muscovite (av. 2)
SiO_2	44. 0	37. 1	0. 30	47. 5	48. 7	33. 8	46. 7
TiO_2	0. 00	1. 82	51. 2	1. 99	0. 30	1. 53	0. 02
Al_2O_3	37. 8	18. 0	0. 20	6. 86	3. 57	19. 0	38. 4
FeO	0. 13	14. 8	45. 3	7. 74	8. 03	14. 0	0. 72
MnO	0. 00	0. 36	3. 73	0. 39	0. 38	0. 25	0. 06
MgO	0. 00	9. 34	0. 19	11. 4	12. 8	16. 3	0. 52
CaO	20. 1	12. 3	0. 20	24. 7	25. 5	0. 19	0. 36
Na_2O	0. 00	0. 57	0. 00	0. 06	0. 03	0. 15	0. 06
K_2O	0. 00	3. 68	0. 00	0. 03	0. 03	8. 24	10. 8
$H_2O(+)$	0. 00	2. 12	0. 00	0. 00	0. 00	6. 59	2. 46
Total	102. 00	100. 1	101. 1	100. 7	99. 3	100. 1	100. 1
Si	0. 99	5. 64	0. 02	1. 78	1. 85	5. 12	6. 04
Al^{IV}	0. 01	2. 36	0. 00	0. 22	0. 15	2. 88	1. 96
Al^{VI}	2. 01	0. 85	0. 01	0. 08	0. 01	0. 51	3. 90
Ti	0. 00	0. 21	1. 93	0. 06	0. 01	0. 18	0. 00
Fe	0. 01	1. 88	1. 90	0. 24	0. 26	1. 78	0. 08
Mn	0. 00	0. 05	0. 16	0. 01	0. 01	0. 03	0. 01
Mg	0. 00	2. 12	0. 01	0. 64	0. 72	3. 68	0. 10
Ca	0. 98	2. 00	0. 01	0. 99	1. 04	0. 03	0. 05
Na	0. 00	0. 17	0. 00	0. 00	0. 00	0. 04	0. 02
K	0. 00	0. 72	0. 00	0. 00	0. 00	1. 70	1. 79

(B) Calcareous hornfels at Aspiesdoorn

Calcareous hornfels (KS-70030808) at Aspiesdoorn shows beautiful zonal banding of green-coloured and chocolate-coloured bands as shown in Fig. 11.

Outermost deep green zone (5mm in width) consists mainly of poikiloblastic potassic hastingsite, anorthite and ilmenite with small amounts of sphene, titaniferous salite, phlogopite, sericite, calcite and clinozoisite. Poikiloblastic potassic hastingsite reaches 1 to 5.5 mm in size and contains inclusions of ilmenite, sphene and anorthite. Size of the other minerals of this deep green zone is about 0.03mm and sometimes reaches 0.1mm.

Outer brownish green zone (2mm in width) consists mainly of titaniferous salite and phlogopite with small amounts of ilmenite, anorthite and sericite. Grain size of the minerals is 0.1 to 0.3mm.

Central outer pale chocolate-coloured zone (2mm in width) consists of titaniferous salite and sericite. Grain size of the minerals is 0.02 to 0.05mm.

Outer central chocolate-coloured zone (2mm in width) consists mainly of salite with small amounts of anorthite and sericite. This zone shows a texture of fine-grained saccharoidal aggregate and grain size of the minerals is 0.03mm in average.

Outer central green zone (3mm in width) consists mainly of salite with small amounts of sericite and zoisite. This zone shows also fine-grained saccharoidal texture of 0.03mm of each grain size.

Central brownish green zone (3mm in width) consists mainly of salite with small amounts of muscovite and clinozoisite. Grain size is 0.03 to 0.1mm.

Inner green zone (15mm in width) consists mainly of salite with small amounts of muscovite and prehnite. Grain size is 0.02 to 0.15mm.

Inner brownish green zone (more than 3mm in width) consists mainly of salite with small amounts of anorthite, sericite, clinozoisite and calcite. Salite exhibits symplectic growth with anorthite and reaches 0.4mm in size. Grain size of the other minerals is 0.03 to 0.1mm.

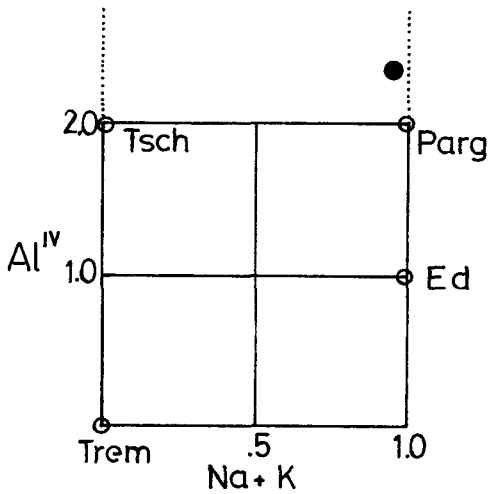

Fig. 12.
Potassic hastingsite in calcareous hornfels (KS-70030808) at Aspiesdoorn.

The chemical compositions of the constituent minerals of the calcareous hornfels are shown in Table 7. Potassic hastingsite is higher in Al_2O_3, K_2O and TiO_2 and the ratio of Fe/Fe+Mg is 0.47. Na+K and Al^{IV} diagram of the potassic hastingsite is shown in Fig. 12. Plagioclase is of anorthite (An 100). Titaniferous salite and salite have a same Fe/Fe+Mg

ratio (0.27), but the former is higher in TiO_2 and Al_2O_3. Ilmenite is rich in MnO, and phlogopite contains considerable amounts of TiO_2 but this amount is lower than that in pelitic hornfels of higher grade part. Muscovite is very low in Na/Na + K ratio, because Na_2O content in this calcareous hornfels is very low and Na_2O concentrates into potassic hastingsite and phlogopite of the outermost zone.

Discussion

(1) Lower grade basic metamorphic rock at Longsight is characterized by the assemblage of actinolite and bytownite (An 82) with zoisite. Around the west of Longsight, actinolite probably becomes unstable in basic metamorphic rocks, and hornblende probably becomes stable instead of actinolite. At present we have, however, no information on the chemical composition of amphibole in the higher grade basic metamorphic rocks.

This actinolite-calcic plagioclase assemblage with zoisite represents a same situation with the low pressure contact metamorphism found in the Kitakami mountains (Seki, 1957 and 1961) and Abukuma Plateau (Shido, 1958).

Plagioclases in the pelitic hornfelses of lower grade group in this area are of sodic oligoclase (An 13±) and those of higher grade group are of calcic oligoclase to sodic andesine (An 26 to 31). Plagioclase in the calcareous hornfels in higher grade group is of anorthite (An 100).

These chemical compositions of plagioclases in this area are plotted in Fig. 13, in which those of plagioclases in contact metamorphic rocks, separately of pelitic and basic compositions, from Kasuga-mura are also shown. Contact metamorphism in Kasuga-mura has been studied by the junior of us (Suzuki, 1975 and 1977).

(2) TiO_2 contents of biotite co-existing with ilmenite in pelitic-psammitic metamorphic rocks increase with increase of metamorphic temperature both in this area and Kasuga-mura as shown in Fig. 14. On the contrary, TiO_2 contents of biotite in pelitic metamorphic rocks without ilmenite are lower in both areas as shown in Fig.14. TiO_2 content of

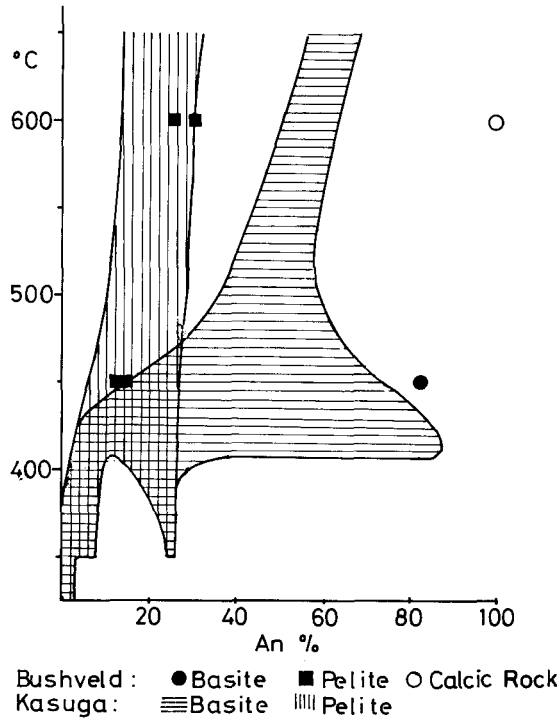

Fig. 13.

Chemical compositions of plagioclases in pelitic, basic, and calcic metamorphic rocks from the northeastern contact aureole of the Bushveld Complex. Vertical hatch and horizontal hatch indicate the chemical compositions of plagioclases in pelitic metamorphic rocks and basic metamorphic rocks from Kasuga-mura, respectively.

phlogopite in ilmenite bearing calcareous hornfels in this area is lower (TiO_2 1.53 %), because of impoverishment of TiO_2 in this rock.

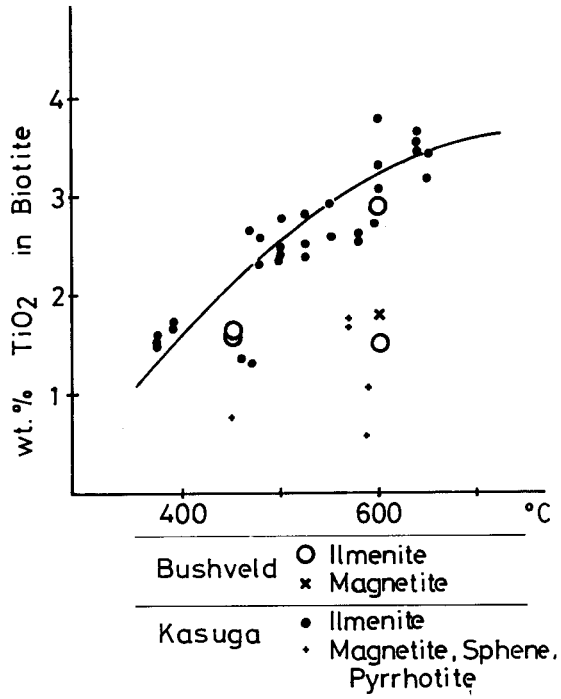

Fig. 14.

Variation of TiO_2 contents of biotite with increase of metamorphic temperature. These biotites coexist with ilmenite or magnetite in metamorphic rocks from the north-eastern contact aureole of the Bushveld Complex and in contact metamorphic rocks from Kasuga-mura.

(3) Andalusite in lower grade pelitic hornfels is richer in Al_2O_3 and MnO and poorer in SiO_2, FeO and TiO_2, on the contrary that in higher grade one is richer in SiO_2, FeO and TiO_2 and poorer in Al_2O_3 and MnO as shown in Tables 3 and 5.

(4) Fig.15 shows the Thompson AFM diagram of the pelitic-psammitic contact metamorphic rocks of this area. Biotite co-existing with cordierite and fibrolite is higher in MgO, and biotites co-existing with garnet and/or andalusite-fibrolite are higher in FeO. Discrimination between the lower grade pelitic-psammitic hornfels and higher grade hornfels, however, is not clear in Fig. 15.

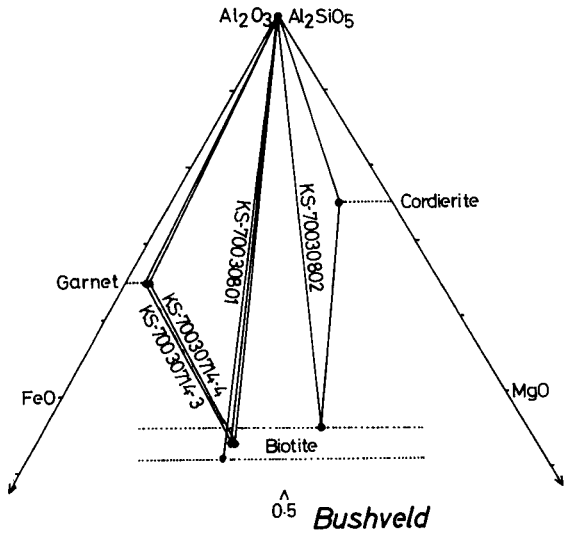

Fig. 15.

Thompson AFM diagram for the contact metamorphic rocks from the north-eastern contact aureole of the Bushveld Complex.

(5) Na/Na+K ratios of muscovite in pelitic-psammitic metamorphic rocks of this area decrease with increase of metamorphic temperature as shown in Fig. 16. This ratio of muscovite in higher grade calcareous hornfels is very low, because of impoverishment of Na_2O in this rock.

(6) Grain size of the higher grade pelitic-psammitic metamorphic rocks shows an increase of about ten times over that of the lower grade pelitic-psammitic rocks as shown in Figs. 3 and 10.

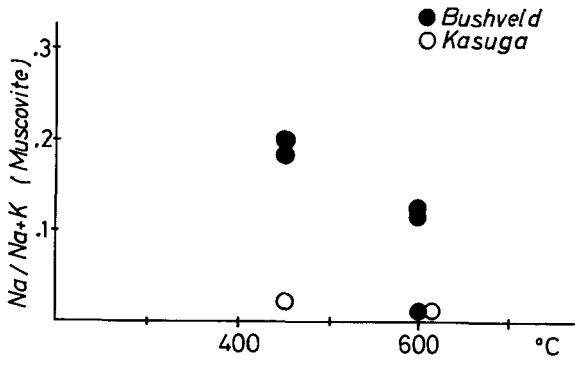

Fig. 16.
Na/Na+K ratios of muscovite with increase of metamorphic temperature. Solid circle represents muscovite from Bushveld and open circle muscovite from Kasuga-mura.

Lower grade pelitic-psammitic hornfels shows clearly graded bedding in the field as well as in the microscope as shown in Figs. 2 and 3. On the other hand, higher grade pelitic-psammitic hornfels contains ptygmatic leucocratic vein.

(7) Potassic hastingsite found in the higher grade calcareous hornfels is rich in Al_2O_3 (18.0%), K_2O (3.68 %) and TiO_2 (1.82 %) and is poor in SiO_2 (37.1%). Na+K and Al^{IV} of the potassic hastingsite reach 0.89 and 2.36 on the basis of 24 (O, OH, F), respectively. Fe/Fe+Mg ratio of the potassic hastingsite is 0.47. This mineral is considered to be a characteristic amphibole in the calcareous hornfels of this area.

Acknowledgements—We would like to express our sincere appreciation to Professor Isao Matsuzawa of Nagoya University and to Professor W.J. Verwoerd of the University of Stellenbosch, for their kind advice and encouragement.

References

ENGELBRECHT, J.P. (1976): Meta-sediments of the Pretoria group in the Enzelsberg area, Marico district. *Trans. Geol. Soc. S. Afr.*, **79**, 61–75.

HALL, A.L. (1908): On contact metamorphism in the Pretoria series of the Lydenburg and Zoutpansberg districts. *Trans. Geol. Soc. S. Afr.*, **11**, 1-24.

HATCH, F.H. (1904): The geology of the Marico District, Transvaal. *Trans. Geol. Soc. S. Afr.*, **7**, 1–6.

HIEMSTRA, S.A. and Van Biljon, W.J. (1959): The geology of the Upper Magaliesberg Stage and the Lower Bushveld Complex in the vicinity of Steelpoort. *Trans. Geol. Soc. S. Afr.*, **62**, 239–255.

SCHWELLNUS, J.S.I. (1970): Andalusite-staurolite relationships in the north-eastern metamorphic aureole of the Bushveld Complex. *Geol. Soc. S. Afr., Spe. Publi.* **1**, 326–335.

SEKI, Y. (1957): Petrological study of hornfelses in the central part of the Median Zone of Kitakami Mountainland, Iwate Prefecture. *Saitama Univ. Sci. Rep., Ser. B*, **2**, 307–361.

SEKI, Y. (1961): Calcareous hornfelses in the Arisu district of the Kitakami mountains, northeastern Japan. *Jap. J. Geol. Geogr.* **32**, 55–78.

SHIDO, F. (1958): Plutonic and metamorphic rocks of the Nakoso and Iritono distircts in the central Abukuma Plateau. *Tokyo Univ. Fac. Sci. J., Sec.* 2, **11**, 131–217.

SUZUKI, K. (1975): On some unusual bands and veins metasomatically developed in the contact aureole in Kasuga-mura, Gifu-ken (in Japanese). *Jour. Geol. Soc. Japan*, **81**, 487–504.

SUZUKI, K. (1977): Local equilibrium during the contact metamorphism of siliceous dolomites in Kasuga-mura, Gifu-ken, Japan. *Contr. Mineral. Petrol.*, (in press).

WILLEMSE, J. (1969): The geology of the Bushveld Igneous Complex, the largest repository of magmatic ore deposits in the world. *Econ. Geol. Monograph, No.* 4, 1–22.

WILLEMSE, J. and VILJOEN, E.A. (1970): The fate of argillaceous material in the gabbroic magma of the Bushveld Complex. *Geol. Soc. S. Afr., Spe. Publi.*, **1**, 336-366.

A Note on the Granitoid Gneisses from the Machakos Area, Kenya

Kunihiko MIYAKAWA* and Kanenori SUWA**

* Department of Earth Scinece, Nagoya Institute of Technology
** Department of Earth Scineces, Faculty of Scinece, Nagoya University

Introduction

Rocks of the crystalline basement complex occupy the greater part of the Machakos district in central Kenya. They consist mainly of metasedimentary rocks of pelitic and psammitic composition and subordinately of basic and calcareous metamorphic rocks. Some of them were affected to a greater or lesser extent by granitization. Regional work done in the area by staffs of the Geological Survey of Kenya resulted in many valuable reports with geological maps (Schoeman, 1948; Dodson, 1953; Baker, 1954; Searle, 1955; Saggerson, 1963; Fairburn, 1963 etc.). According to most of these workers, the crystalline basement rocks were designated as the Basement System and were generally considered to be representative of Archaean rocks in Kenya. On the other hand, Holmes (1951) proposed that eastern and central Kenya, including the Machakos district, constitutes a part of the Mozambique belt. It is probable that rocks referred to the basement consist of rocks of different ages which have been re-affected by the Mozambiquian orogeny of late Precambrian to Cambrian times.

Granitoid gneisses are very abundant in the present area and are one of the most important varieties of gneisses. The main outcrops occur on the Kanzalu range, Kangundo hill, the Mua hills, Mbooni hill, Kalama hill and Momandu hill and at Mitaboni and Opete (Fig. 1). Nevertheless, in the last twenty-five years there has been less information on petrology and geochemistry of metamorphic rocks in east and central Kenya as compared with much information concerning the regional geology. Few chemical analyses of the metamorphic rocks have been made in the past. With a brief description of their petrographical nature, this paper gives the chemistry of the granitoid gneisses.

Geological setting

The western part of the area is covered by the Miocene-Pleistocene volcanics and sediments, which lie on the sub-Miocene peneplain. The surface is fairly flat and is approximately 1500 m above sea level. Meanwhile, in the eastern part the Basement System rocks are widely exposed and form more hilly country varying in height from 1200 m to 2100m. They are considered to be represented by a stratified succession of originally sedimentary rocks which have been transformed into a highly folded metamorphic series. Fairburn (1963) divided them into two rock series :

1. Rocks that have suffered metamorphism with little or no granitization and often more closely resemble sedimentary rocks.
2. Rocks that have been granitized and tend to grade into types that approach granite.

The first rock series comprises metasediments such as biotite gneisses, muscovite-biotite gneisses, muscovite gneisses, quartzites, mica schists, kyanite-staurolite gneisses, hornblende-biotite gneisses, hornblende gneisses, amphibolites, crystalline limestone and so on.

2nd Prelim. Rep. Afr. Studies, Nagoya Univ., 154-160, 1977.

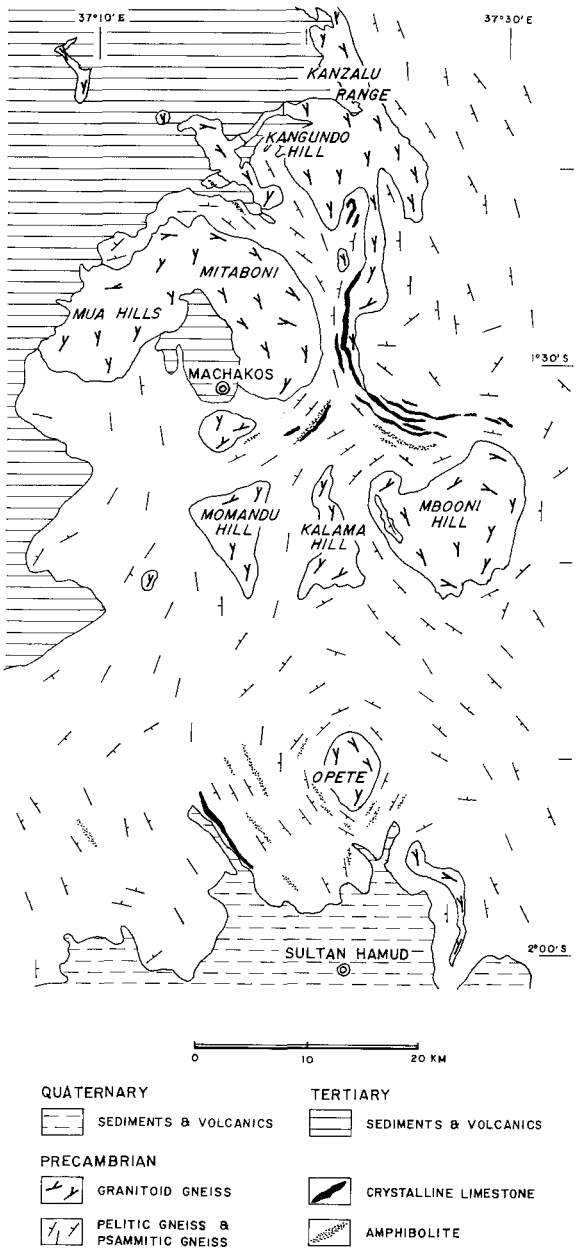

Fig. 1

Simplified geological map of the Machakos area.

The second rock series is a series of granitized sediments, most of which have been designated as migmatites, granitoid gneisses and augen gneisses.

The most common constituents of metamorphic rocks are quartz, plagioclase, potash feldspar, biotite, muscovite and hornblende. Potash feldspar is microcline in many cases. Garnet rich in almandine molecule is often found in basic as well as pelitic metamorphic rocks. In the neighbourhood of Machakos, there is known only one instance of the occurrence of sillimanite (Fairburn, 1963). In the Simba-Kibwezi area about 70 to 120 km south-east of Machakos, however, sillimanite-biotite gneisses with or without cordierite are not uncommon (Saggerson, 1963). Sometimes calcareous and basic rocks contain one or more of tremolite, wollastonite, phlogopite, clinopyroxene and epidote. Sphene is widespread as an accessory mineral. Kyanite and staurolite are found in pelitic gneiss of appropriate composition. The mineral assemblages show that the rocks of the present area have suffered a typical amphibolite-facies metamorphism.

The general structural trend of the Basement System rocks is between north–south and northwest–southeast in concordance with the regional extension of the Mozambique belt. Several dome-like structures appear to be dominant in the area. They cause the disturbance of the general trend shown by the foliation plane of metasediments. The large mass of granitoid gneiss usually forms the core of the dome structure (Baker, 1953; Fairburn, 1963; Biyajima *et al.*, 1975; Biyajima, 1976). The surrounding gneisses have the fairly complete harmony of strike with the boundaries of the granitoid gneisses.

Granitoid gneisses

The term granitoid gneiss has been used for a gneiss having granite composition by Kenyan geologists for a long time. The granitoid gneisses are generally found in the Machakos-Sultan Hamud region and are very similar in appearance to a certain kind of granite because of their homogeneity and poorly developed foliation as well as the similarity of mineralogical composition to granite. Especially in hand specimen, it is not always easy to distinguish the granitoid gneisses from the granitized or metasomatized psammitic gneisses. In this paper, the term granitoid gneiss is applied to the granitic gneisses and allied rocks with a granite-like appearance.

(1) Petrographic description

The granitoid gneisses, irrespective of localities of occurrence, are practically the same in a petrographic character. In outcrop they are usually homogeneous and unbedded. In hand specimen they are generally light-coloured, medium-grained, weakly foliated rocks with a uniform texture. The foliation is caused by parallel arrangement of scattered biotite flakes up to about 2 mm in size. Sometimes it is lacking or indistinct due to the scarcity and the disarrangement of the biotite flakes.

The granitoid gneisses consist predominantly of plagioclase, microcline and quartz with subordinate biotite and muscovite. Sphene, apatite, iron ore and zircon are usually present as accessories. Sericite and chlorite are alteration products and are negligible in amount. Examples of the mode in volume percentages are given in Table 1. Under the microscope microcline is noticeable owing to its well-developed microcline structure. The perthite structure is not so common. It is worthy of notice that microcline often replaces plagioclase and rarely muscovite. Plagioclase is most abundant. It is albite-oligoclase. There characteristically develops the albitized rim up to about 0.1 mm in width surrounding the original plagioclase. Such albitized rim is typically found along the contact with microcline. The plagioclases are generally twinned. The twinning lamellae extend outward to the rim without any disturbance. Quartz is generally granular, sometimes elongated parallel to the foliation. Biotite flakes are often fringed with symplectic muscovite. The biotite is pleochroic from pale yellow to brown. Muscovite occurs as isolated flakes as well as overgrown fringes. It is usually worm-eaten in appearance because of

Table 1 Modes of granitoid gneisses from the Machakos area

	58A	59	63	88A
Quartz	23. 9	20. 8	25. 0	32. 5
Plagioclase	47. 3	44. 8	41. 0	39. 1
Microcline	20. 8	27. 1	28. 2	22. 6
Biotite	7. 1	3. 9	3. 6	4. 9
Muscovite	0. 4	2. 3	1. 8	0. 5
Accessories	0. 5	1. 1	0. 4	0. 4

Table 2 Chemical anlayses and C.I.P.W. norms of granitoid gneisses from the Machakos area

	58 A	63	88 A	123
SiO_2	70. 43	72. 93	74. 94	72. 67
TiO_2	0. 35	0. 19	0. 11	0. 09
Al_2O_3	14. 97	14. 29	12. 85	15. 18
Fe_2O_3	0. 72	0. 78	0. 36	0. 49
FeO	1. 34	0. 55	1. 26	0. 32
MnO	0. 07	0. 06	0. 07	0. 02
MgO	0. 72	0. 38	0. 24	0. 18
CaO	1. 75	1. 35	0. 62	1. 12
Na_2O	4. 86	4. 46	5. 08	6. 75
K_2O	3. 96	4. 33	3. 80	3. 32
P_2O_5	0. 17	0. 10	0. 02	0. 03
H_2O+	0. 63	0. 57	0. 37	0. 26
H_2O-	0. 17	0. 09	0. 05	0. 06
	100. 12	100. 08	99. 77	100. 49
Q	22. 19	27. 20	29. 02	18. 99
Or	23. 37	25. 60	22. 43	19. 59
Ab	41. 10	37. 70	42. 94	57. 09
An	7. 34	6. 06	1. 06	1. 34
C	—	0. 05	—	—
Wo	0. 09	—	0. 81	1. 68
En	1. 80	0. 94	0. 59	0. 45
Fs	1. 37	0. 15	1. 97	0. 07
Mt	1. 04	1. 13	0. 51	0. 72
Il	0. 67	0. 36	0. 21	0. 15
Ap	0. 40	0. 24	0. 03	0. 07

Analyt : K. Miyakawa

its symplectic intergrowth with quartz. Symplectite of muscovite is characteristic of the granitoid gneisses.

(2) Major element geochemistry

Chemical compositions of some granitoid gneisses from the Machakos area are presented in Table 2. There are some similarities among them. The SiO_2 content is somewhat greater than 70%. They have a fairly high content of alkali for a given SiO_2 content and generally contain Na_2O over K_2O. $FeO + Fe_2O_3$, MgO and CaO contents are relatively low. Normative corundum may or may not be present. Its amount is very small even if it appears.

K_2O/Na_2O ratios lie within the range 0.49–1.42.* The average ratio is 0.89,

* The ratios are 0.49, 0.75, 0.81, 0.90, 0.97 and 1.42. The data include two partial analyses of granitoid gneiss in addition to four chemical analyses shown in Table 2. One is 3.77% Na_2O and 5.36% K_2O and the other is 4.94% Na_2O and 4.46% K_2O.

though one of six specimens has an extremely high value of 1.42 as compared with the others. This evidence appears to accord with a general tendency for granitic rocks from the northern part of Africa; Rooke(1970) suggested that average K/Na ratios for acidic rocks of northern Africa are in the range 0.65 – 1.23 (0.58 – 1.10 in K_2O/Na_2O ratio) and are smaller than those of southern Africa (1.56 – 1.96 in K/Na ratio). Particularly, the Machakos granitoid gneisses have a strong resemblance in the average K_2O/Na_2O ratio to Precambrian orogenic granitic rocks from south-east Uganda the average K_2O/Na_2O ratio of which Rooke(1970) estimated to be 0.88. It may awake a further interest in the problems of the crustal development of Precambrian age as

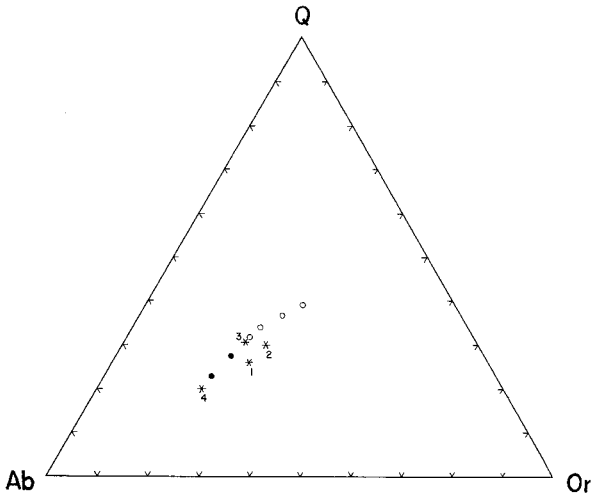

Fig. 2

Normative AB-Or-Q plot of four analyzed granitoid gneisses from the Machakos area. Positions of the isobaric minima (open circles) at water pressures of 0.5, 1, 2 and 3 kilobars and the isobaric eutectics (solid circles) at 5 and 10 Kilobars (after Tuttle and Bowen, 1958; Luth, Jahns and Tuttle, 1964) are included for comparison.

1 : Specimen No. 58A 2 : Specimen No. 63
3 : Specimen No. 88A 4 : Specimen No. 123

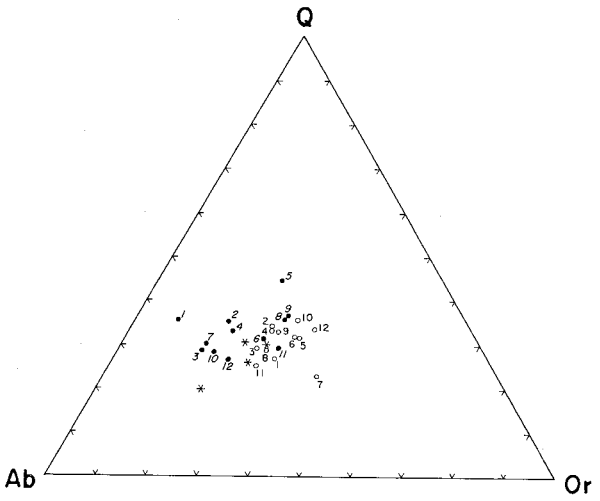

Fig. 3

Average compositions of granites and kindred rock types (open circles) and Precambrian gneisses (solid circles) shown on the normative Ab-Or-Q diagram. Points of four anlayzed granitoid gneisses are shown as in Fig. 2.

Granites and kindred rock types :

1. Average of 7 granites and granitic gneisses from the Aswan Granite Complex, Aswan, Egypt (Rooke, 1970).
2. Average of 24 granitic rocks from the basement complex of northern Somalia (Rooke, 1970).
3. Average of 10 granitic rocks from south-east Uganda (Rooke, 1970).
4. Average of 7 orogenic acid rocks from the basement complex, Luapula, Zambia (Rooke, 1970).
5. Average of 11 granites from Franzfontein, South-West Africa (Rooke, 1970).
6. Average of 14 granites, Chirwa, north-east Rhodesia (Rooke, 1970).
7. Average of 12 granitic rocks form Malawi Basement Complex, Malawi (Rooke, 1970).
8. Average of 61 coarse porphyritic granite from Galway Granite, Eire (Coats and Wilson, 1971).
9. Average of 63 Caledonian granites (Hall, 1972).
10. Average of 198 Variscan granites (Hall, 1972).
11. Average of 5 Alpine granites (Hall, 1972).
12. Average of 72 calc-alkali granites (Nockolds, 1954)

Gneisses :

1. Average of 39 biotite gneisses form the Lewisian complex of N.W. Scotland (Tarney *et al.*, 1972).
2. Average of 18 microcline gneisses from the Lewisian complex of N.W. Scotland (Tarney *et al.*, 1972).
3. Average of 39 gneisses from the Laxfordian complex, Scotland (Tarney *et. al.*, 1972).
4. Average of 22 gneisses from the un-migmatized Laxfordian complex, Outer Hebrides (Tarney *et al.*, 1972).
5. Average of 21 metasedimentary gneisses from the Leverburgh belt, Scotland (Tarney *et al.*, 1972).
6. Average of 18 metasomatized and migmatized Laxfordina complex, Outer Hebrides (Tarney *et al.*, 1972).
7. Average of 41 grey gneisses from East Greenland (Tarney *et al.*, 1972).
8. Average of 3 strongly granitized gneisses from Emeryville, Adirondack, New York, U.S.A. (Engel, 1958).
9. Average of 4 incipiently granitized gneisses from Emeryville, Adirondack, New York, U.S.A. (Engel and Engel, 1958).
10. Average of 6 Uivak I gneisses from Labrador, Canada (Collerson *et al.*, 1976).
11. Average of 8 migmatitic gneisses ($>70\%$ SiO_2) from Labrador, Canada (Collerson *et al.*, 1976).
12. Average of 3 migmatitic gneisses (65-70% SiO_2) from Labrador, Canada (Collerson *et al.*, 1976).

Fig. 3 (continued)

well as of the crustal anatexis in relation to orogeny.

Fig. 2 gives the proportions of normative albite, orthoclase and quartz for the analyzed granitoid gneisses. Positions of the isobaric minimums and eutectics of the system $NaAlSi_3O_8$-$KAlSi_3O_8$-SiO_2-H_2O (Tuttle and Bowen, 1958; Luth, Jahns and Tuttle, 1964) are also plotted on the diagram for comparison. The granitoid gneisses tend to fall near the isobaric minimums and eutectics at higher values of water pressure. The plotted field of the granitoid gneisses partially overlaps that of the alumina-undersaturated rocks, which is shown by Luth *et al.* (1964). However, it comes nearer to the Ab corner of the diagram with respect to the field of the alumina-oversaturated granites (Luth *et al.*, 1964) which has the maximum concentration around the isobaric minimum at a lower water pressure.

Fig. 3 gives orogenic granitic rocks and Precambrian gneisses with about 70% SiO_2 plotted on the normative Ab-Or-Q diagram. The average compositions of these plotted rocks of different areas show a rather limited range of variations and appear to occupy rather distinctive fields for the gneisses and granites. Granitized gneisses and allied rocks have a tendency to fall on part of the gneiss field overlapping with granite field. The granitoid gneisses analyzed also tend to lie within or near the overlap of the two fields. The Machakos granitoid gneisses are comparatively high in normative albite, low in normative quartz and moderate in normative orthoclase. The normative Or/(Q+Or) ratios are fairly restricted, averaging 0.48, whereas the normative Or/(Ab+Or) and Q/(Ab+Q) ratios show a relatively wide range of variations from 0.25 to 0.41. Normative albite tends to decrease with the increase of normative orthoclase and/or quartz.

The origin of the granitoid gneisses may be attributed either to the granitization of supracrustal rocks by alkali metasomatism or to the remobilization of basement rocks by anatexis producing fluid of granitic character at higher water pressures. This question, however, remains still unsettled.

Acknowledgements – We wish to thank Dr. J. Walsh and Mr. S.A. Dodhia of the Mines and Geological Department of Kenya for having afforded full facilities for the field work during our stay in Kenya.

Appendix: Localities of the specimens given Tables 1 and 2.

58A: 2 km north of Opete (Uvete), Kitaingo. 1°50.0′S 37°21.2′E

59 : 1 km north of Opete, Kitaingo. 1°50.5′S 37°21.1′E

63 : Kithangathini 3.5 km south-southeast of Kilungu. 1°49.4′S 37°22.2′E

88A: Kivandini 4 km east-southeast of Machakos. 1°32.0′S 37°18.2′E

123 : The river Ikiwe 5 km south-southwest of Machakos. 1°33.6′S 37°15.4′E

References

Baker, B.H.(1954) : Geology of the southern Machakos district. *Report No.* **27**, *Geol. Surv. Kenya.*

Biyajima, K.(1976) : Petrological study of the Mozambique metamorphic rocks in the Machakos area, Kenya. MS., Dept. Earth Sci., Nagoya Univ.

Biyajima, K., Suwa, K., and Miyakawa, K. (1975) : Mantled gneiss dome in the Mozambique belt around the Machakos area, Kenya. *1st Prelim. Rep. Afr. Studies, Nagoya Univ.*, 6-13.

Coats, J. S. and Wilson, J. R. (1971) : The eastern end of the Galway Granite. *Mineral. Mag.*, **38**, 138-151.

Collerson, K. D., Jesseau, C.W., and Bridgwater, D. (1976) : Crustal development of the Archaean gneiss complex: Eastern Labrador. *In B. F. Windley (Ed.), The Early History of the Earth,* John Wiley & Sons, New York, 237-253.

Dodson, R. G. (1953) : Geology of the south-east Machakos area. *Report No.* **25**, *Geol. Surv. Kenya.*

Engel, A.E.J. and Engel, C.E. (1958) : Progressive metamorphism and granitization of the major paragneiss, northwest Adirondack Mountains, New York : Part I. *Bull. Geol. Soc. Am.*, **69**, 1369-1414.

Fairburn, W. A. (1963) : Geology of the north Machakos—Thika area. *Report No.***59**, *Geol. Surv. Kenya.*

Hall, A (1972) : Regional geochemical variation in the Caledonian and Variscan granites of western Europe. *24th Intern. Geol. Congr., Montreal,* Sect. **2**, 171-180.

Holmes, A. (1951) : The sequence of Precambrian orogenic belts in south and central Africa. *18th Intern. Geol. Congr., London, 1948, Rept.* **14**, 254-269.

Luth, W. C., Jahns, R. H., and Tuttle, O. F. (1964) : The granite system at pressures of 4 to 10 kilobars. *J. Geophys. Res.*, **69**, 759-773.

Nockolds, S. R. (1954) : Average chemical compositions of some igneous rocks. *Bull. Geol. Soc. Am.*, **65**, 1007-1032.

Rooke, J. M. (1970) : Geochemical variations in African granitic rocks, and their structural implications. *In T.N. Clifford and I.G. Gass (Eds.), African Magmatism and Tectonics,* Oliver & Boyd, Edinburgh, 355-417.

Saggerson, E. P. (1963) : Geology of the Simba-Kibwezi area. *Report No.***58**, *Geol. Surv. Kenya*

Schoeman, J. J. (1948) : A geological reconnaissance of the area west of Kitui Township. *Report No.***11**, *Geol. Surv. Kenya.*

Searle, D. L. (1955) : Geology of the Sultan Hamud area. *Report No.***29**, *Geol. Surv. Kenya.*

Tarney, J., Skinner, A. C., and Sheraton, J. W. (1972) : A geochemical comparison of major Archaean gneiss units from Northwest Scotland and East Greenland. *24th Intern. Geol. Congr., Montreal,* Sect. 1, 162-174.

Tuttle, O. F. and Bowen, N. L. (1958) : Origin of granite in the light of experimental studies in the system $NaAlSi_3O_8$-$KAlSi_3O_8$-SiO_2-H_2O. *Geol. Soc. Am. Mem.* **74.**

Major Element Geochemistry of Peridotite Nodules from Samburu District, Kenya (Abstract, 1977)

Ken-ichiro AOKI* and Kanenori SUWA**

* Institute of Mineralogy, Petrology and Economic Geology, Tohoku University
** Department of Earth Sciences, Faculty of Science, Nagoya University

Introduction

Tremendous amounts of soda-rich alkaline to peralkaline volcanic lavas were erupted repeatedly and distributed widely along the Eastern Rift Valley in Kenya, eastern Uganda and northern Tanzania during the Miocene to Recent periods. Mafic rocks, nephelinite, basanite and alkali basalt sometimes contain various types of ultramafic nodules which could have been derived directly from the upper mantle. Recently, much attention has been drawn to these ultramafic nodules. Their mineralogy and petrology have been described by Saggerson (1968), Nixon (1969), Dawson *et al.* (1970), McCall (1970), Walsh (1972), Dawson and Smith (1973), Reid *et al.* (1975), Rhodes and Dawson (1975), Ridley and Dawson (1975), and Suwa *et al.* (1975).

This article gives an account of the major element chemistry of the peridotite nodules in melanephelinites from Ndonyuo Olnchoro and Sasani, Samburu district, about 300 km NNE of Nairobi, Kenya. A discussion of the chemical characteristics of the nodules, believed to represent the uppermost mantle fragments in this region, is included.

Brief petrography

The mode of occurrence and petrology of ultramafic nodules from Ndonyuo Olnchoro and Sasani have been described by Suwa *et al.* (1975); hence only a brief summary on the petrographic features of the peridotite nodules need be given here.

Remarkably fresh ultramafic nodules up to 30 cm in diameter, are sometimes found in Recent small scoria cones consisting of olivine melanephelinite from Samburu district. These rocks can be classified into two distinct groups. The most common group is a suite of peridotites consisting of harzburgite and lherzolite; the other one is a suite of websterites.

The peridotite nodules studied here consist mainly of forsterite, enstatite and chromian spinel associated with traces to small amounts of diopside. They have usually xenomorphic or hypidiomorphic granular texture with grain size ranging from 1 to 10 mm. These rocks belong to the harzburgite–lherzolite series which could be derived directly from the upper mantle (White, 1966; Kuno, 1969).

Chemistry

Fifteen fresh chromian spinel peridotite nodules in olivine melanephelinites from Samburu, Kenya, have been analysed. These rocks have a rather narrow range of major and minor element compositions. Their 100 Mg/Mg + Fe ratios vary from 90.3 to 92.8. It is noteworthy that these peridotites are characterized by very high MgO and low Al_2O_3, total FeO, CaO, Na_2O and K_2O; in general Al_2O_3 and CaO tend to increase slightly with decreasing 100 Mg/Mg + Fe ratio. Combining the modal and chemical data of constituent minerals given by Suwa *et al.* (1975) with the chemical compositions for

Table 1 Average chemical compositions of peridotite nodules

	1	2	3	4	5	6	7	8
SiO_2	43.65 (41.87–46.21)	43.97	42.52	44.62	44.70	43.60	44.9	44.42
TiO_2	0.06 (0.04 – 0.09)	0.07	0.06	0.17	0.13	0.06	0.04	0.15
Al_2O_3	0.83 (0.25 – 1.64)	1.64	0.43	2.29	2.70	1.50	2.12	2.23
Cr_2O_3	0.37 (0.26 – 0.48)	0.49	0.28	0.40	0.36	0.41	0.45	0.33
Fe_2O_3	0.38 (0.21 – 0.63)	0.89	1.04			1.60	1.63	
FeO	6.78 (6.16 – 8.12)	6.03	6.17	8.80	9.21	7.00	6.65	8.86
MnO	0.11 (0.09 – 0.13)	0.13	0.12	0.14	0.13	0.12	0.11	0.14
MgO	46.90 (44.00–48.53)	44.73	47.89	40.87	40.35	43.74	42.25	41.41
NiO	0.33 (0.29 – 0.36)	0.36	0.41			0.29	0.27	
CaO	0.42 (0.09 – 1.48)	1.10	0.58	2.50	1.95	1.49	2.12	2.19
Na_2O	0.13 (0.05 – 0.30)	0.12	0.10	0.17	0.36	0.16	0.14	0.22
K_2O	0.03 (0.02 – 0.04)	0.09	0.03	0.03	0.05	0.03	0.03	0.04
P_2O_5		0.06	0.02	0.01	0.05	0.00		0.02
$\frac{100\,Mg}{Mg + Fe}$	92.1 (90.3 – 92.8)	92.1	92.3	89.2	88.6	90.2	90.3	89.3

1. 15 chromian spinel peridotite nodules from Samburu district, Kenya (Aoki and Suwa, 1977).
2. 8 garnet-bearing peridotite nodules from Lashaine volcano, Tanzania (Rhodes and Dawson, 1975).
3. 8 garnet-free peridotite nodules from Lashaine volcano, Tanzania (Rhodes and Dawson, 1975).
4. 21 peridotite nodules from Itinome-gata, Japan (Kuno and Aoki, 1970; Aoki and Shiba, 1973).
5. 11 chromian spinel peridotite nodules from Hawaii (Kuno, 1969).
6. 55 chromian spinel peridotite nodules from Dreiser Weiher, Germany (Hutchison *et al.*, 1970; Kuno and Aoki, 1970).
7. 130 chromian spinel peridotite nodules from the Central Massif, France (Hutchison *et al.*, 1970).
8. 75 chromian spinel peridotite nodules from alkali basalts (Aoki, 1975).

peridotites, almost all of the peridotites can be classified as Mg-rich harzburgite and only one is Ca-poor lherzolite.

Average compositions of garnet-bearing and garnet-free peridotite nodules from Lashaine volcano, Tanzania (Rhodes and Dawson, 1975), and chromian spinel peridotite nodules from Samburu and other localities are given in Table 1. A comparison of chromian spinel peridotite from Samburu and garnet-bearing and garnet-free peridotites from Lashaine volcano (about 550 km south of Samburu)

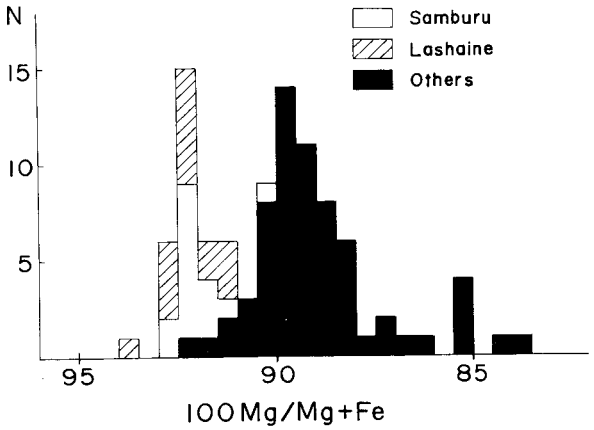

Fig. 1.
Frequency distribution of 100 Mg/Mg + Fe ratio of peridotite nodules. White area, chromian spinel peridotites from Ndonyuo Olnchoro and Sasani, Samburu; hatched area, garnet-bearing and garnet-free peridotites from Lashaine volcano; solid area, chromian spinel peridotite from the other localities (Itinome-gata, Hawaii, Dreiser Weiher, Central Massif in France, and others).

shows no essential chemical difference between them. They are, however, clearly different from those of the other localities; those from Samburu and Lashaine volcano are high in MgO and low in total FeO and CaO. As clearly shown in frequency distributions of the 100 Mg/Mg + Fe ratios of peridotite nodules, peridotites from Samburu and Lashaine volcano and chromian spinel peridotites from the other localities fall in separate fields, with slight overlapping. Most frequent values of the former lie between 91 and 93; in contrast, that of the latter lie between 88.0 and 90.5 (Fig. 1).

According to Rhodes and Dawson (1975) and Suwa *et al.* (1975), peridotite nodules from Lashaine volcano and Samburu have been derived directly from depths of about 150 and 50 to 70 km, respectively. If so, the chemical composition of the lithosphere, which mainly consists of peridotite beneath the M-discontinuity of the Eastern Rift Valley region in the present African Plate, is extremely depleted in fusible oxides such as Al_2O_3, FeO, CaO, Na_2O and K_2O which are important components of basaltic magmas. It is believed that such peridotite could not have produced any kind of basaltic magma.

Geophysical consideration

The presence of a zone of low density upper mantle beneath the Gregory rift valley is suggested by gravity measurement and seismological studies. There are sufficient gravity measurements in the area of the Gregory rift valley to allow a Bouguer gravity anomaly profile to be drawn (Baker and Wohlenberg, 1971). An important observation made by the workers from the University of Newcastle (e.g. Girdler *et al.* 1969) is that superimposed over the general negative Bouguer anomaly of about 100 mgals there is a relatively positive anomaly of 30–60 mgals over the Gregory rift and the presence of a basic intrusion 20 km wide and 20 km deep reaching to within 3 km of the rift floor was postulated. And another important observation made by several workers (e.g. Rodrigues, 1970) was that arrival times at the Nairobi and Addis Ababa stations are delayed by 2–4 seconds for earthquake waves travelling along the rift as compared to those travelling across it. This suggests the presence of a low velocity zone underlying the lithosphere of the rift (Baker and Wohlenberg, 1971).

A zone of low density upper mantle beneath the Gregory rift valley is considered to be composed of the strongly depleted peridotites with high MgO and low Al_2O_3, CaO, Na_2O and K_2O.

References

AOKI, K. (1975) : Petrological model beneath the continental upper mantle. *Marine Sci.*, **7**, 57-63 (in Japanese with English abstract).

AOKI, K. and SHIBA, I (1973) : Pyroxenes from lherzolite inclusions of Itinome-gata, Japan. *Lithos*, **6**, 41-51.

AOKI, K. and SUWA, K. (1977) : Major element geochemistry of peridotite nodules from Samburu district, Kenya. *J. Japan. Assoc. Min. Pet. Econ. Geol.*, **72** (in press).

BAKER, B. H. and WOHLENBERG, J. (1971) : Structure and evolution of the Kenya Rift Valley. *Nature*, **229**, 538-542.

DAWSON, J. B., POWELL, D. C. and RAID, A. M. (1970) : Ultrabasic xenoliths and lava from the Lashaine volcano, northern Tanzania. *J. Petrol.*, **11**, 519-548.

DAWSON, J. B. and SMITH, J. V. (1973) : Alkalic pyroxenite xenoliths from the Lashaine volcano, northern Tanzania. *J. Petrol.*, **14**, 113-131.

GIRDLER, R. W., FAIRHEAD, J. D., SEARLE, R. C., and SOWERBUTTS, W. T. C. (1969): Evolution of rifting in Africa. *Nature*, **222**, 1178-1182.

HUTCHISON, R., PAUL, D. K. and HARRIS, P. G. (1970) : Chemical composition of the upper mantle. *Mineral. Mag.*, **37**, 726-729.

KUNO, H. (1969) : Mafic and ultramafic nodules in basaltic rocks of Hawaii. *Geol. Soc. Am. Mem.* **115**, 189-234.

KUNO, H. and AOKI, K. (1970) : Chemistry of ultramafic nodules and their bearing on the origin of basaltic magmas. *Phys. Earth Planet. Interiors*, **3**, 273-301.

McCALL, G. J. H. (1970) : Gabbroic and ultramafic nodules : high level intracrustal nodular occurrences in alkalic basalts and associated volcanics from Kenya, described and compared with those of Hawaii. *Phys. Earth Planet. Interiors*, **3**, 255-272.

NIXON, P. H. (1969) : Kimberlite volcanoes in East Africa. *50th Ann. Uganda Geol. Survey and Mines Dept.*, 207-225.

REID, A. M., DONALDSON, C. H., BROWN, R. W., RIDLEY, W. I. and DAWSON, J. B. (1975) : Mineral chemistry of peridotite xenoliths from the Lashaine volcano, Tanzania. *Phys. Chem. Earth*, **9**, 525-543.

RHODES, J. M. and DAWSON, J. B. (1975) : Major and trace element chemistry of peridotite inclusions from the Lashaine volcano, Tanzania. *Phys. Chem. Earth*, **9**, 545-557.

RIDLEY, W. I. and DAWSON, J. B. (1975) : Lithophile trace element data bearing on the origin of peridotite xenoliths, ankaramite and carbonatite from Lashaine volcano, N. Tanzania. *Phys. Chem. Earth*, **9**, 559-569.

RODRIGUES, E. B. (1970) : Seismological studies of the East African rift system. A thesis submitted for Ph.D. degree in the Univ. East Africa, pp. 187.

SAGGERSON, E. P. (1968) : Eclogite nodules associated with alkaline olivine basalts, Kenya. *Geol. Rundschau*, **57**, 890-903.

SUWA, K., YUSA, Y. and KISHIDA, N. (1975) : Petrology of peridotite nodules from Ndonyuo Olnchoro, Samburu district, central Kenya. *Phys. Chem. Earth*, **9**, 273-286.

WALSH, J. (1972) : Geology of the Moyale area. *Rep. Geol. Survey Kenya*, No. **89**, 1-33.

WHITE, R. W. (1966) : Ultramafic inclusions in basaltic rocks from Hawaii. *Contrib. Mineral. Petrol.*, **12**, 245-314.

Geology of the Yatta Plateau, Kenya

Motoo FUJITA

Department of Earth Sciences, Faculty of Science, Nagoya University

Introduction

The Yatta Plateau in Kenya (Fig. 1) has been remarked by its hot dispute on the genetical problem since Gregory (1921) observed and discussed it as the pioneer. The Yatta Plateau is extremely long and narrow and is capped with phonolite. The following three theories on its genesis have been presented. (1) The Yatta Plateau phonolite flowed down along an old valley (Gregory, 1921: Walsh, 1963). (2) The phonolite represents the remains of a larger sheet. The destructive erosion of most of an extensive sheet has been carried out by the Athi

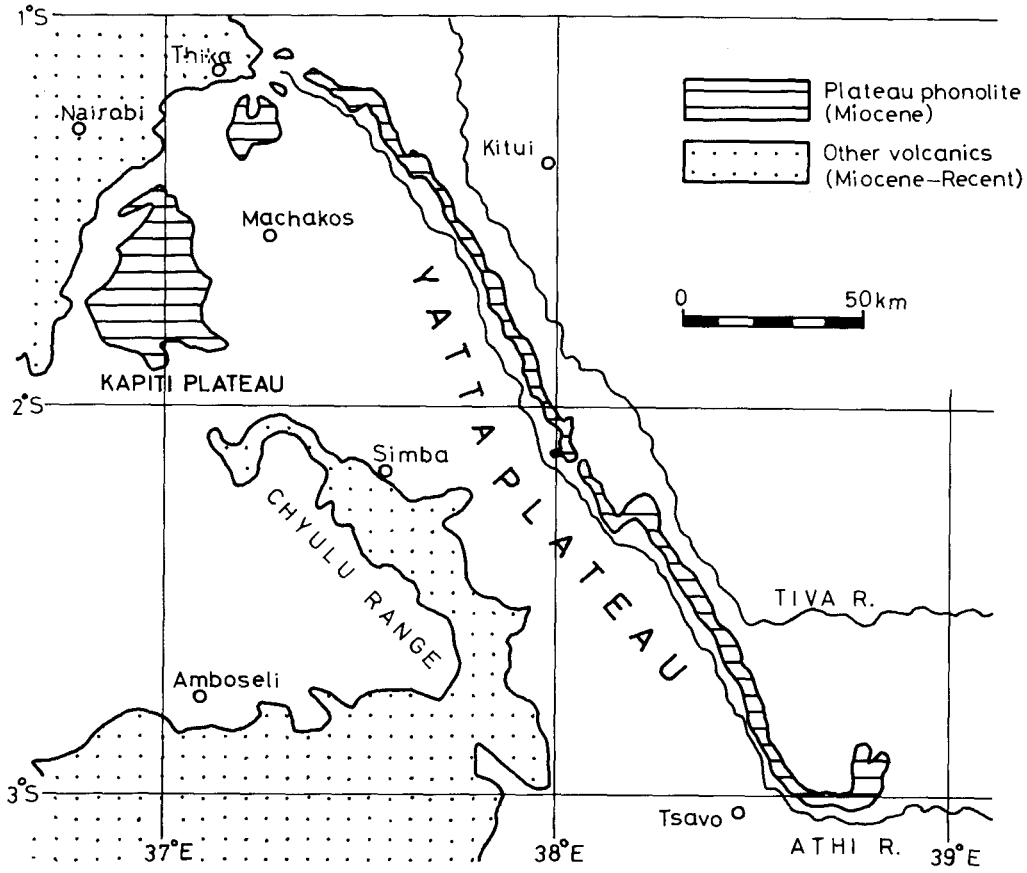

Fig. 1 Index map of the Yatta Plateau.
I investigated the north Yatta Plateau between 1° and 2° south latitude.

2nd Prelim. Rep. Afr. Studies, Nagoya Univ., 165-177, 1977.

and Tiva rivers (Shoeman, 1948: Sanders, 1963). (3) It was given by a lateral flow from the main line of feeding fissures (Dodson, 1953). However, no positive evidences supporting any of above theories have been reported.

According to their suggestion by Professor I.S.Loupekine of the University of Nairobi and Associate Professor K.Suwa of Nagoya University, I began my study on geology and petrology of the Yatta phonolite to elucidate its genetical problem. I carried out the field work in the northern part of the Yatta Plateau for about 60 days when I was studying in the University of Nairobi from September of 1975 to July of 1976.

General Geology

The Yatta Plateau, which is about 300 km in length and is about 3 to 4 km in width, stretches in a south-easterly direction from 01 Doinyo Sapuk to the Galana valley. The altitude of the plateau is about 1,300 m at the northern end and that at the southern end is about 700 m. It has a very flat ridge and average inclination is about 3 m per km. Its relative height compared with the Athi River running on the west of the plateau is about 200 m (Fig. 2). The southern plain of 01 Doinyo Sapuk ("Matuu Plain") situates about 1,500 m above sea level.

The basement of this area is formed by Precambrian metamorphic rocks belonging to the Mozambique belt. These metamorphic rocks show a trend which is striking N20°W to N40°W and dipping westerly 50° to 70°. Of considerable interest is the fact that the stretching direction of the Yatta Plateau and the Athi River is parallel to the trend of the Mozambique belt.

The Yatta Plateau and the Matuu Plain are covered with phonolite which is named as the "Kapiti Phonolite" being of Miocene age (Fairburn, 1963).

Old river deposits are found under the phonolite lava at two points, near Kithimani and Mombasa on the Yatta Plateau, and some round pebbles are also observed among the flow-foot breccias at several points. This is the first finding of the evidence of river deposit before the Yatta phonolite flowed down.

No dykes or plugs that may have been feeders for the phonolite were found in the Mozambiquian basement rocks around the Yatta Plateau and the Matuu Plain.

More geological details on the phonolite lava and old river deposits will be described in below.

Occurrence of Phonolite

The phonolite is a hard, black or dark grey coloured and fine-grained rock with large phenocrysts of anorthoclase and nepheline. The phenocrysts of anorthoclase are columnar in shape, commonly reach 1 to 3 cm in length and occasionally up to 8 cm, and sometimes exhibit penetration twins (Fig. 3). In the field, anorthoclase phenocrysts show a preferred orientation nearly parallel to the stretching direction of the Yatta Plateau. Nepheline phenocrysts are 0.5 to 1 cm in length and are less than anorthoclase phenocrysts in amount.

The distribution map of the phonolite is shown in Fig. 4. Near Nguluni on the Matuu Plain, the phonolite consists of at least two lava horizons, the lower one being over 3 m in thickness and the upper one being about 0.3 m. Around 01 Doinyo Sapuk, however,

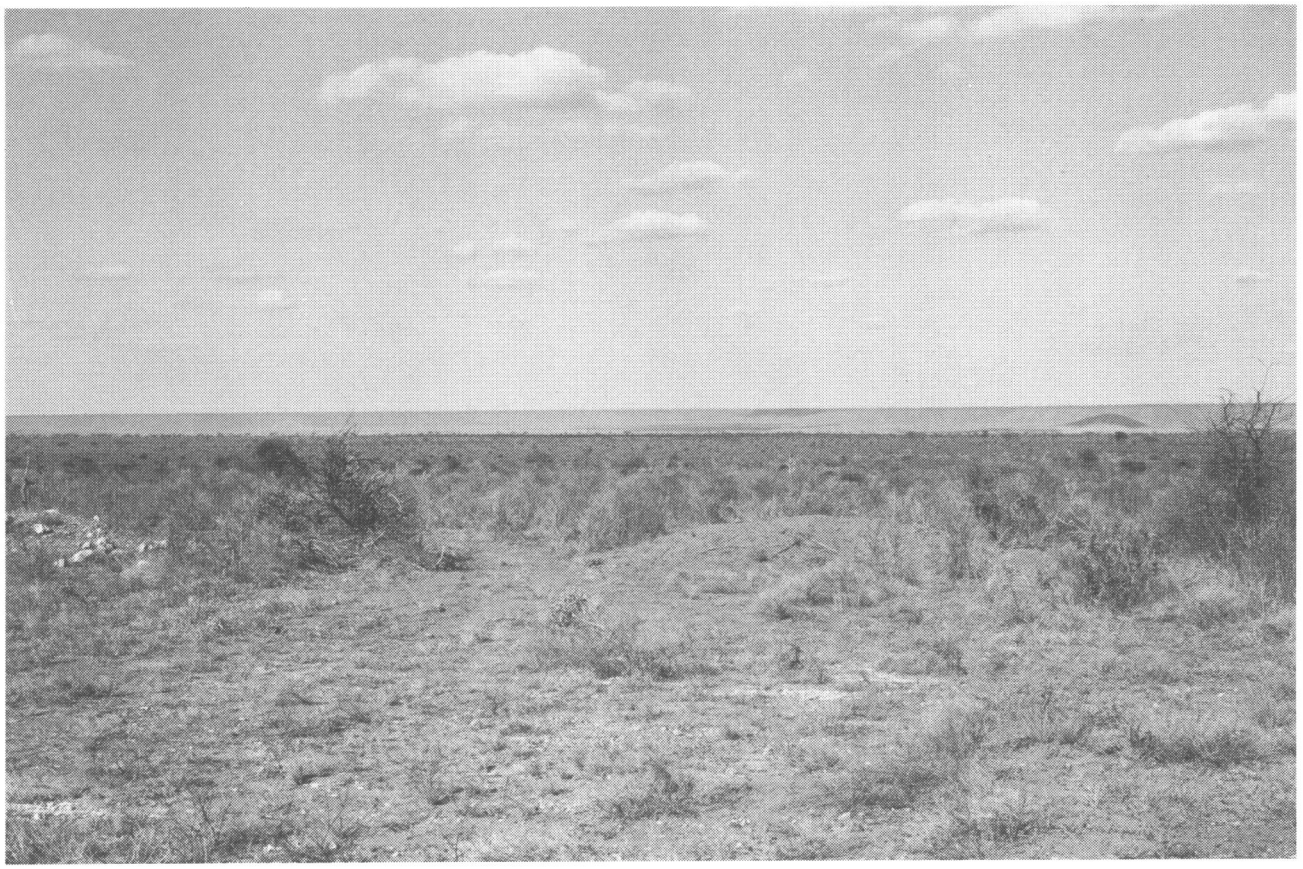

Fig. 2 A vista of the Yatta Plateau near Voi (Photo by K. Suwa).

we can recognize only one phonolite lava horizon and its thickness is slightly variable, e.g., about 2 m, 6 m and 8 m at Kianzabe, Kayata and Fourteen Falls respectively. Flow-foot breccias are observed at every places and are apparently of massive and reddish brown coloured concentrates of small spherical grains with 1 to 2 mm in diameter and sometimes large pieces of phonolite are intermingled among the flow-foot breccia.

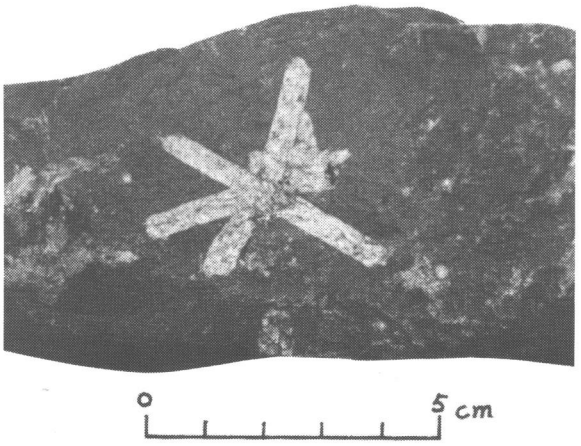

Fig. 3 Penetration twin of anorthoclase phenocryst of phonolite lava (Photo by M.F.).

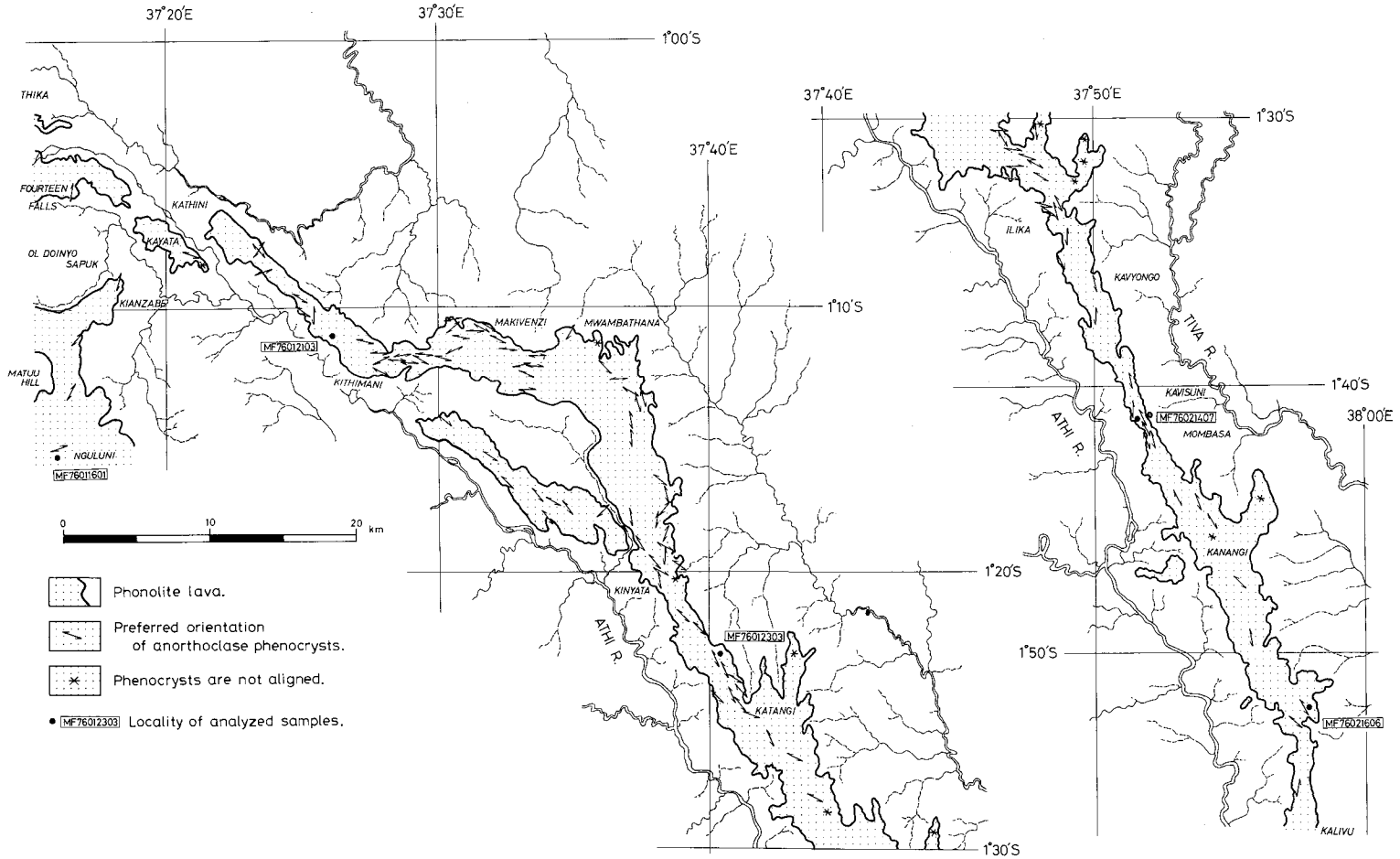

Fig. 4 Orientation of anorthoclase phenocrysts

On the Yatta Plateau, two types of phonolite lava are recognized, i.e., one is a continuous lava flow and the other is a boulder-like lava. The continuous lava flow reaches 10 to 20 m in thickness at the edge of the plateau and extends generally in parallel to the sides of the plateau. Columnar joints are commonly notable, joint blocks are 2 to 5 m in width, and platy joints being 0.2 to 1 m in thickness are sometimes observed at the upper part of lava. No evidence to divide the continuous lava into two or more units was found. Boulder-like lava, about 4 to 8 m in thickness, is widely distributed more than the continuous lava does. Boulder-like lava, however, grades into continuous lava and it is impossible to fix any certain boundary between them. Each boulder being 1 to 2 m in diameter and 30 to 50 cm in thickness is covered with thin weathered material, but the inner features are completely same as those of continuous lava. Preferred orientation of anorthoclase phenocrysts of each boulder is almost parallel to that of the continuous lava in a small area. This fact suggests that these boulders have never moved from their original places. Consequently, it is considered that these boulders were formerly joint blocks of the continuous lava.

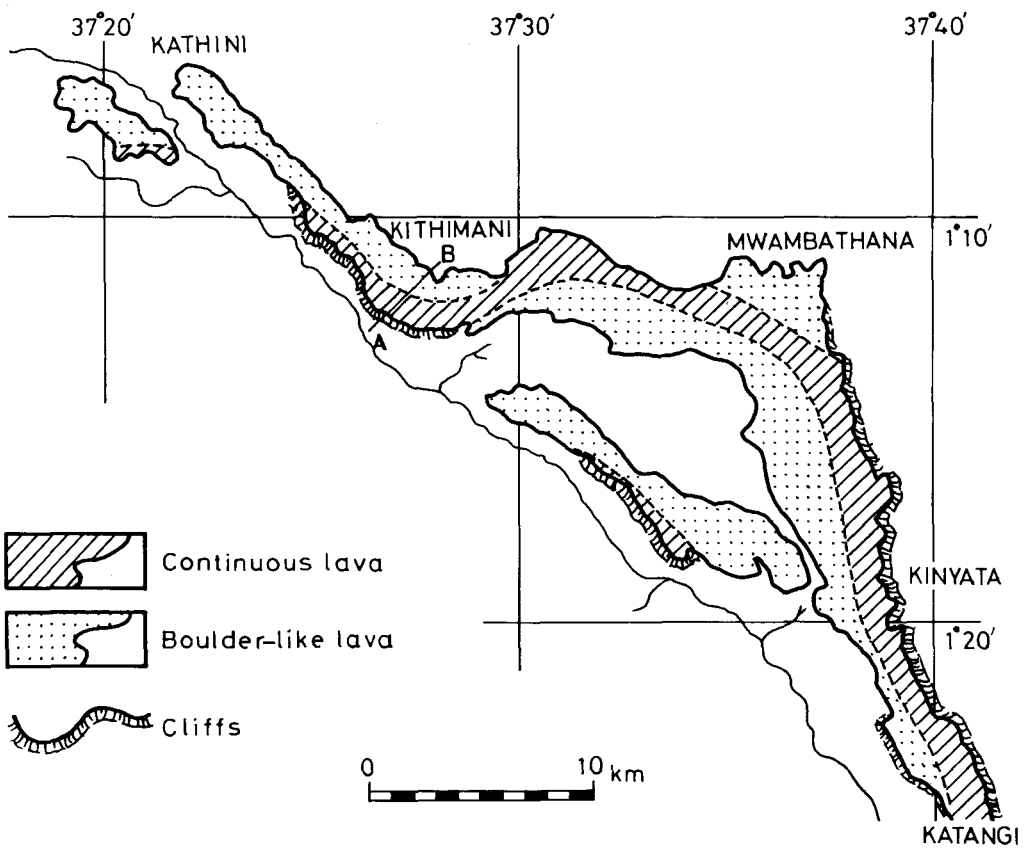

Fig. 5 Distribution map of continuous lava and boulder-like lava.

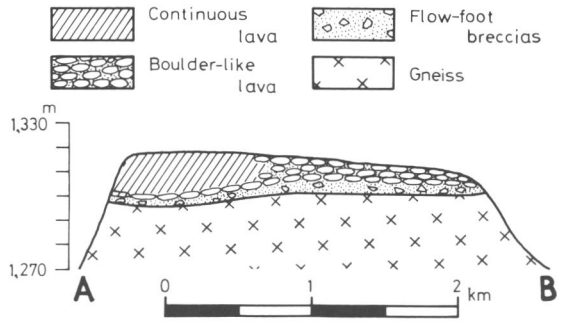

Fig. 6 Sectional diagram of the Yatta Plateau. The location of A-B is shown in Fig.5.

Of considerable interest is the fact that continuous lava flowed down continuously like a river judging from the distribution of continuous lava. Fig. 5 shows the distribution map of the continuous lava in the area between Kathini and Katangi. Northern Kithimani, the continuous lava extends on the west side of the Yatta Plateau, but in the area from Mwambathana to south the continuous lava occurs on the east side and in the area between Kithimani and Mwambathana it crosses the plateau from west to east.

The layer of flow-foot breccia is 2 to 4 m in thickness on the Yatta Plateau and sometimes includes pieces of phonolite, angular and/or rounded pebbles of basement rocks and chips of chalcedony.

Old River Deposits

I found old river deposits between the phonolite lava and the basement rock of the Yatta Plateau. The old river deposit found at the edge of the plateau near Kithimani consists of pebbles and reaches about 2 m in thickness, and occurs between boulder-like lava and the basement rocks. These pebbles are composed of fine-grained quartzite and are 3 to 8 cm in diameter, occasionally up to 15 cm. Their roundness is well and belongs to class "D" by Krumbein's classification (Krumbein, 1941), and their sphericity is also

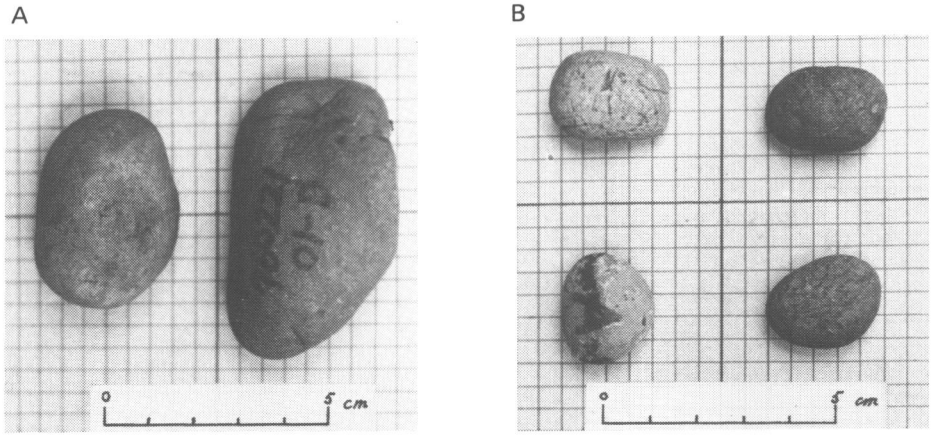

Fig. 7 Pebbles among old river deposit.
A: collected from Kithimani. Roundness "D" by Krumbein's classification.
B: collected from Mombasa. Roundness "E".

not so bad (Fig. 7-A). The old river deposit found at the eastern edge of the plateau near Mombasa consists of pebbles and sands and reaches about 1.5 m in thickness, and rests on the gneissose basement rock. These pebbles are composed of fine-grained quartzite, coarse-grained quartzite, granitic gneiss, pegmatitic quartz and feldspar, and are about 1 to 3 cm in diameter and are smaller than those near Kithimani. Their roundness is best and belongs to class "E", and their sphericity is also well (Fig.7-B). The layer of sands reaching about 40 cm in thickness is found to occur on the layer of pebbles and shows a reverse grading suggesting a positive evidence of river deposit.

In addition, some pebbles are found among flow-foot breccias at several points. These pebbles are composed almost of fine-grained quartzite in the area northern from Katangi. In the area southern from Katangi, however, these pebbles are composed of not only fine-grained quartzite but also coarse-grained quartzite and granitic gneiss. When we compare the size and roundness of quartzite pebbles of the old river deposit, the pebbles occurring in northern part are bigger in size and worse in roundness than those occurring in southern part (Fig. 8).

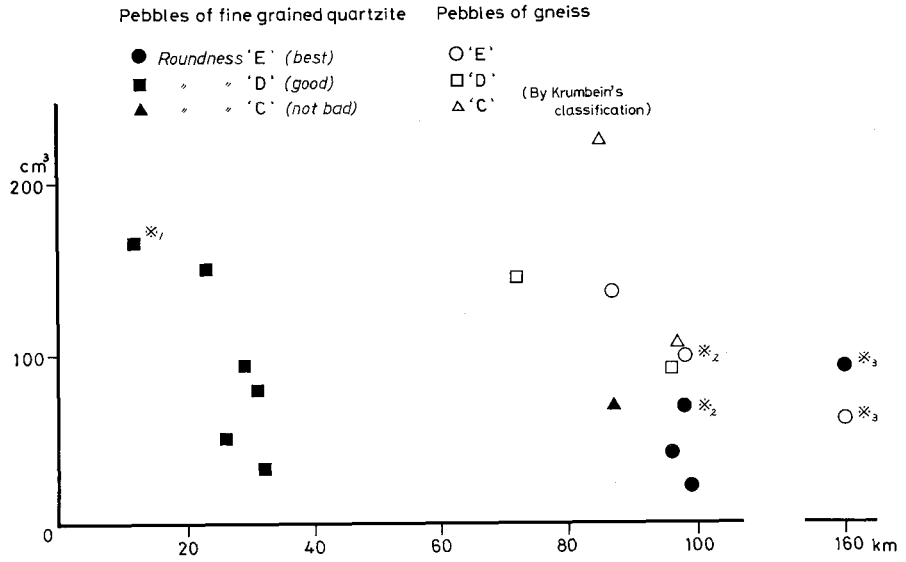

Fig. 8 Roundness and volume of pebbles of old river deposits with respect to the position of the Yatta Plateau. In this figure, distance is recorded from the northern end of the Yatta Plateau.

(*1. near Kithimani. *2. near Mombasa. *3. at Yatta Gap, southern part than this investigated area.)

This old river deposit and pebbles found among flow-foot breccias are considered to be positive evidence for a former river, which was running from north-west to south-east in similar and parallel to the stretching direction of the present Yatta Plateau.

Preferred Orientation of Anorthoclase Phenocrysts

Anorthoclase phenocrysts of the Yatta phonolite show commonly a preferred orientation (Fig. 9). Table 1 and Table 2 show the frequency percentage of the

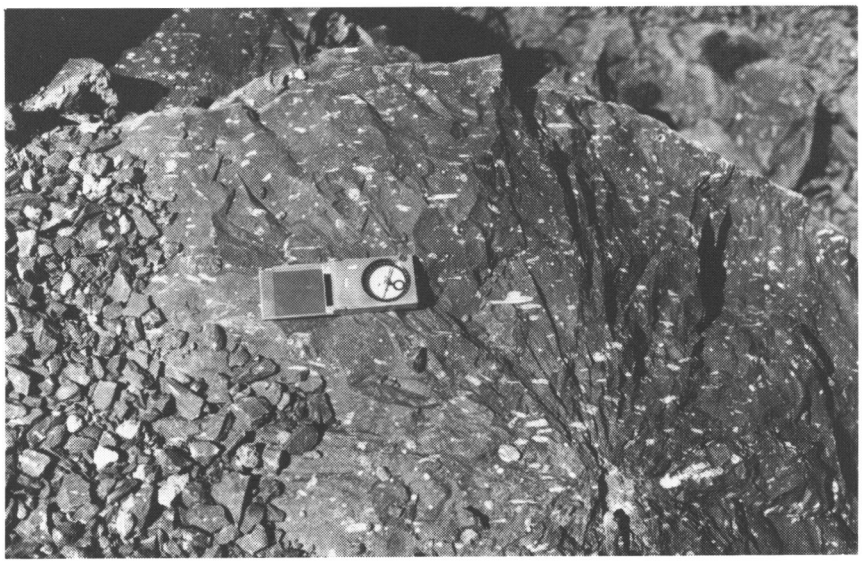

Fig. 9 Outcrop of phonolite lava near Nguluni. Anorthoclase phenocrysts are aligned in a trend of N70°E (Photo by M.F.).

preferred orientation and length of anorthoclase phenocrysts respectively. Irrespective of grain-size of anorthoclase phenocryst, its preferred orientation can be recognized as shown in Table 1. Variations of the preferred orientation of my investigated area are shown in Fig. 4.

On the Matuu Plain near Nguluni, the preferred orientation is about N70°E, but it changes to N30°E to N10°E at northern places of the plain. On the Yatta Plateau it is generally parallel to the stretching direction of the plateau in main areas, except in the northern end area where it is not aligned in parallel to the stretching direction. In the southern Kithimani area, the stretching direction of the plateau slightly bends and two directions of the preferred orientation of the phenocrysts are observed: one is parallel to the bending direction of the plateau and the other is parallel to the stretching direction of the detached area. In the area near Ilika, the stretching direction of the plateau also slightly bends and the preferred orientation becomes also in parallel to the bending direction.

Table 1 The frequency percentage of anorthoclase phenocrysts of the Yatta phonolite at eastern Thika of northern end of the Yatta Plateau.

Orientation	< 20mm in length	Total 10mm <~> 50mm
N85W-85E	2 %	2 %
N75E-85E	3	2
N65E-75E	3	2
N55E-65E	0	2
N45E-55E	4	6
N35E-45E	4	3
N25E-35E	2	4
N15E-25E	4	2
N05E-15E	0	6
N05W-05E	4	3
N05W-15W	2	2
N15W-25W	4	7
N25W-35W	17	17
N35W-45W	15	13
N45W-55W	11	10
N55W-65W	12	8
N65W-75W	8	8
N75W-85W	3	2
Total	99	99

Table 2 The frequency percentage of length of anorthoclase phenocrysts of the Yatta phonolite at eastern Thika of northern end of the Yatta Plateau.

Length	%
< 10 mm	3
10-15	15
15-20	24
20-25	16
25-30	18
30-35	3
35-40	8
40-45	3
45-50	5
50 <	5
Total	100

At the branches of the plateau (e.g., Katangi, Ndunguni and Kathilani), however, any preferred orientation of anorthoclase phenocryst can not be recognized.

Petrography and Petrochemistry of Yatta Phonolite

Every phonolite samples collected from my investigated area show almost same features petrographically. In this section, however, preliminary observation is only described. More detailed petrographical description will be presented in future.

The phenocrysts of anorthoclase reaching about 1.5 cm on average in length show generally a preferred orientation. Phenocrysts of nepheline are about 0.8 cm in diameter, and small black spots having about 1 mm in diameter are also observable.

Microscopically, the anorthoclase phenocrysts show sometimes a combination of pericline and albite twinning and zonal texture (Fig.10). The margin of the anorthoclase is generally corroded. Phenocryst of nepheline is also corroded. Olivine and opaque form micro-phenocysts of 0.8 mm and 0.4 mm in diameter respectively. The olivine is enclosed with brown amphibole (kaersutite?) and opaque, and these parts correspond to black spots with the naked eye. Small laths of felsic minerals are also included in the crystals of olivine. There is a sharp distinction of grain-size between the phenocrysts and groundmass.

The groundmass is fine-grained and holocrystalline, and consists largely of alkali feldspar laths of 0.5 to 0.8 mm in length, and shows a trachytic texture. Nepheline laths occur also as 0.3 to 0.5 mm in length, but its volume is about one fourth of alkali

A

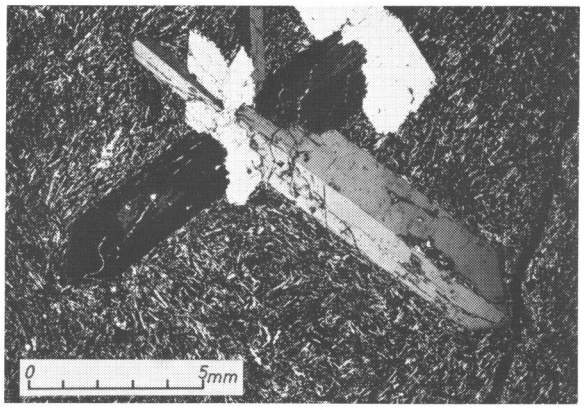

B

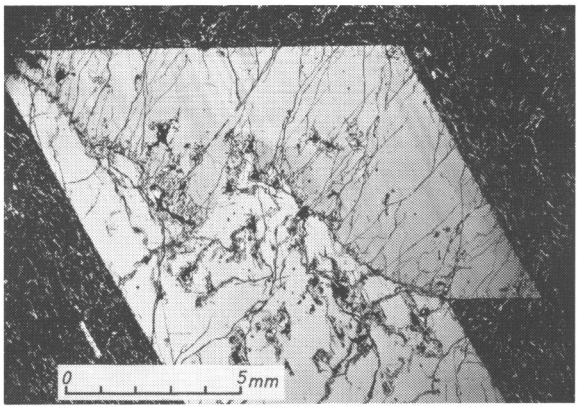

Fig.10 Photomicrograph of the Yatta phonolite (Specimen No. MF76012103). Kithimani, Thika District, Kenya.

A: Penetration twin of anorthoclase phenocryst. Groundmass shows trachytic texture.
B: Anorthoclase phenocryst showing pericline twin.

feldspars. Brown amphibole (kaersutite?), green or colourless aegirine and opaque occur interstitially. Small apatite is recognized as an euhedral form. It is considered that nepheline also fills in the space between laths, for X-ray powder diffraction patterns show strong peaks of nepheline with those of alkali feldspars.

Five phonolite samples from the Yatta Plateau and Matuu Plain were analyzed chemically by Dr. R.Sugisaki of Department of Earth Sciences, Nagoya University. From these five samples, phenocrysts were removed as complete as possible before chemical analysis was performed. In Table 3, the results of analysis and the norms calculated by the method of C.I.P.W. are shown.

All the phonolite collected from the Yatta Plateau show uniformity of composition. They contain about 53–55% SiO_2 and 14–15% total alkalis and they have 24–27% normative Ne and less than 10% Ac in the norm. The result of analysis of the phonolite (MF76011601) collected from the Matuu Plain is roughly similar to that of the Yatta Plateau phonolite. Na_2O content of the phonolite from the Matuu Plain is lower than that of the Yatta phonolite, and CaO contents is higher than the latter. The Matuu Plain phonolite has about 19% Ne, 0.2% 01 and 8.6% Di in the norm, the Yatta phonolites, on the other hand, have about 24–27% Ne, 3–4% 01 and 5–6% Di.

Summary and Discussion

According to my study the following results were obtained:

(1) There are at least two phonolite lava horizons at the southern Matuu Plain, there is, however, only one phonolite lava horizon on the other area of the Yatta Plateau.

(2) Continuous part of the phonolite lava stretches nearly in parallel to the sides of the Yatta Plateau.

Table 3 Chemical data and C.I.P.W. norms of the Yatta phonolite and Matuu phonolite.
(Analyst : R. Sugisaki).

No.	1	2	3	4	5
Sample No.	MF76012103	MF76012303	MF76021407	MF76021606	MF76011601
Locality	Kithimani (Yatta Plat.)	Katangi (〃)	Mombasa (〃)	Kalivu (〃)	Nguluni (Matuu Plain)
SiO_2	52.82 %	54.58 %	53.49 %	52.80 %	53.98 %
TiO_2	0.87	0.84	0.85	0.85	0.84
Al_2O_3	18.86	19.87	18.53	18.64	18.45
Fe_2O_3	2.10	2.47	3.05	3.46	2.88
FeO	3.32	2.91	2.57	2.08	2.66
MnO	0.26	0.27	0.28	0.28	0.28
MgO	1.15	1.31	1.36	1.23	1.14
CaO	1.57	1.57	1.88	1.65	2.50
Na_2O	9.24	8.68	8.60	9.73	7.61
K_2O	5.00	5.49	5.53	5.60	5.46
P_2O_5	0.29	0.26	0.28	0.29	0.31
$H_2O(+)$	2.59	1.91	1.98	1.88	3.30
$H_2O(-)$	1.14	0.77	1.24	1.12	1.50
Total	99.21	100.93	99.64	99.61	100.91
il	1.67	1.67	1.67	1.67	1.67
ap	0.67	0.67	0.67	0.67	0.67
or	29.50	32.28	32.84	32.84	32.28
ab	23.07	28.32	20.45	15.73	29.89
ne	25.00	23.58	23.86	26.71	18.75
ac	6.01	1.39	7.39	10.16	–
ns	0.49	–	–	1.34	–
mt	–	2.78	0.69	–	4.17
di	4.93	4.83	6.23	5.05	8.58
wo	2.44	2.44	3.13	2.55	4.41
en	0.90	1.20	1.51	1.31	2.71
fs	1.58	1.19	1.58	1.19	1.45
ol	4.16	2.73	2.77	2.59	0.17
fo	1.41	1.41	1.34	1.27	0.07
fa	2.75	1.32	1.43	1.32	0.10
$H_2O(+)$	2.59	1.91	1.98	1.88	3.30
$H_2O(-)$	1.14	0.77	1.24	1.12	1.50
Total	99.23	100.93	99.79	99.76	100.98

(3) Anorthoclase phenocrysts of the phonolites align generally in parallel to the sides of the Yatta Plateau.

(4) Old river deposits occur under the Yatta phonolite lava. The old river was running probably from northwest to southeast in similar and parallel to the stretching direction of the Yatta Plateau.

(5) No dyke or plug has been found in the Yatta Plateau.

These results suggest that the Yatta phonolite lava has flowed down along a former river valley from northwest to southeast. This conclusion coincides with the suggestions by Gregory (1921) and Walsh (1963).

The average thickness of the phonolite lava is about 12 m in my investigated area (northern half part of the Yatta Plateau). This thickness is about 10 m in the middle part of the plateau near Ikusa (Walsh, 1963), and is 7.5 to 12 m in the southern part of the plateau near Voi (Sanders, 1963). From these data, total volume of the phonolite lava of the Yatta Plateau is estimated as $10 \pm 2\ km^3$.

Phonolites erupted in Late Miocene age (11-13.5 m.y.) formed several plateaux of Kapiti, Kericho, Kisumu, Uasin Gishu, Kamasia, Laikipia and Yatta in Kenya and are named the Plateau-type phonolite, which is distinguished from Kenya-type or Gwasi-type phonolite occurring at Nairobi, Nakuru, Elgon and others in Kenya (Williams, 1972: Lippard, 1973b).

The Plateau-type phonolite is very unique in the Cenozoic volcanic record in the following points:

(a) Extra-voluminous lava. Total volume of the phonolites in Kenya has been estimated as $25{,}000\ km^3$ by Williams (1972) and $40{,}000–50{,}000\ km^3$ by Lippard (1973b). This amount exceeds that of phonolite lava found elsewhere in the world by several orders of magnitude.

(b) High eruption rate. The Uasin Gishu Plateau is covered with seven phonolite lava horizons and the most voluminous unit (horizon) of them has been estimated as $300 \pm 50\ km^3$ (Lippard, 1973a).

(c) Low viscosity. From the occurrence of phonolite lava constituting the very flat and wide plateaux, low viscosity of the lava is assumed.

(d) Lack of associated rocks. A lack of quantitatively significant associations of basic and intermediate rocks is observed (Williams, 1970).

These points, especially high eruption rate and low viscosity are emphasized by the geological evidences obtained from the Yatta plateau phonolite as shown in this paper.

I will carry out my petrographical and petrological studies with collected samples to clarify the petrogenetic problems of the Yatta phonolite.

Acknowledgements – This investigation was carried out while I was studying in the University of Nairobi from 1975 to 1976 as a resident student sent by the Ministry of Education of Japan. I am greatly indebted to Professor I.S.Loupekine of the University of Nairobi for his kind advice and encouragement and to Associate Professors K.Ishioka and K.Suwa of Nagoya University for their guidance. Many facilities for field work in Kenya were made available by Mr. K.Yairi of Nagoya University and Mr. Y.Yusa of Power Reactor and Nuclear Fuel Development Corporation, to whom I express my deep gratitude.

References

DODSON, R.G., (1953): Geology of the south-east Machakos area. *Report No.25, Geol. Surv. Kenya.*

FAIRBURN, W.A., (1963): Geology of the north Machakos-Thika area. *Report No.59, Geol. Surv. Kenya.*

GREGORY, J.W., (1921): Rift valleys and geology of East Africa. Seeley Service. London.

LIPPARD, S.J., (1973a): Plateau lava flows, Kenya. *Geol. Mag.* 110, 543–549.

LIPPARD, S.J., (1973b): The petrology of phonolites from the Kenya Rift. *Lithos,* 6, 217–234.

SANDERS, L.D., (1963): Geology of the Voi-South Yatta area. *Report No.54, Geol. Surv. Kenya.*

SHOEMAN, J.J., (1948: A geological reconnaissance of the area west of Kitui Township. *Report No.11, Geol. Surv. Kenya.*

WALSH, J., (1963): Geology of the Ikutha area. *Report No.56, Geol. Surv. Kenya.*

WILLIAMS, L.A.J., (1970): The volcanics of the Gregory Rift Valley, East Africa. *Bull. Volcan.,* 34, 439–465.

WILLIAMS, L.A.J., (1972): The Kenya Rift volcanics: a note on volumes and chemical composition. *Tectonophysics,* **15,** 83–96.

Some Petrographical Notes on Phonolite, exposed at the Summit of Uhuru Peak, Mt. Kilimanjaro, Tanzania

Isao SHIIDA and Mitsuo HOSHINO

Department of Geology, College of General Education,
Nagoya University

Introduction

Mt. Kilimanjaro is one of the volcanoes swarming along the Eastern Rift Valley of Kenya and northern Tanzania. Volcanic activity of Kilimanjaro had taken place during Pleistocene age in the form of lava eruption from three main volcanic centres with a number of parasitic centres. Rocks erupted are of typical alkali rock series trending from trachybasalt, through trachyandesite, trachyte and phonolite, to nephelinite (Downie and Wilkinson, 1964). The order of lava eruption and distribution of lavas around Kibo caldera are shown in Fig. 1.

The rock, phonolite, examined in this paper was collected by the senior of us in 1968 from the summit "Uhuru Peak" (Fig. 2). This lava from which the rock was collected forms a part of caldera rim and is designated as Caldera Rim group, which is a product of the last but one activity in later Pleistocene age, as shown in Fig. 1. This rock shows aa-type in appearance.

In the previous works on Kilimanjaro, petrographical description of rocks, especially that exposed at the higher places, was scarcely made, in spite of its importance. It would therefore be worth while describing the rock petrographically in this paper.

Petrography and chemistry of phonolite

Megascopically the rock is grey and scoriatic with large phenocrysts of abundant greyish anorthoclase with subordinate dark greenish ferrosalite and sparsed whitish nepheline. Characteristic short prismatic anorthoclase phenocryst with rhombic cross section is usually less than 5 mm, but sometimes it reaches to 15 mm in length. The proportion of the phenocrysts to the groundmass differes greatly even in one rock specimen.

This rock, in which scattered rhombic anorthoclase phenocrysts are abundant, is designated as "rhomb porphyry" in the field.

Under the microscope, phenocrysts of anorthoclase, ferrosalite, olivine, nepheline and magnetite are recognized (Fig. 3). Dark brown basaltic hornblendes are found occassionally as large phenocrysts. These phenocrysts are scattered through a porous hyalopilitic or hyaline groundmass consisting of brown glass, anorthoclase, ferroaugite, alkali amphibole, apatite and magnetite. Partly variolitic texture showing radial growth of lath-shaped anorthoclase can be observed.

2nd Prelim. Rep. Afr. Studies, Nagoya Univ., 178-183, 1977.

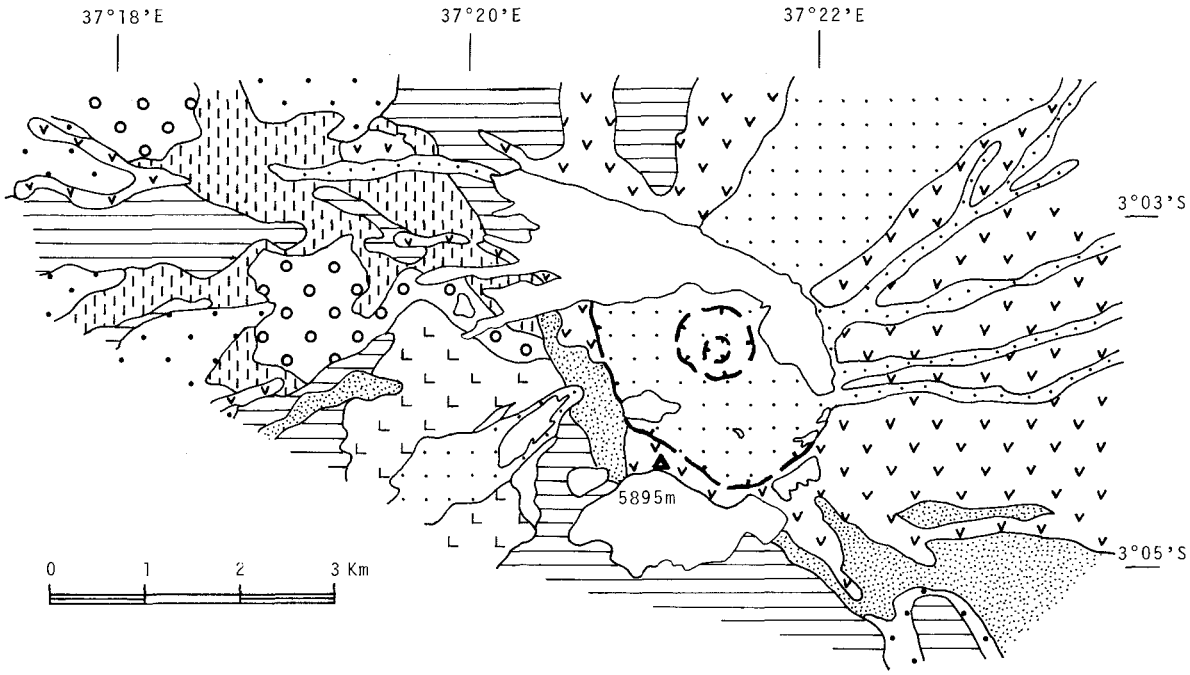

Explanation

Glacier

Inner Crater group (nephelinite) — upper Pleistocene

Caldera Rim group (phonolite) — upper Pleistocene

Small-rhomb Porphyry group (phonolite) — middle Pleistocene

Lent group (phonolite) — middle Pleistocene

Rhomb Porphyry group (trachyte) — middle Pleistocene

Upper Rectangle Porphyry group (trachyandesite) — lower Pleistocene

Upper Trachyandesite group (trachyandesite) — lower Pleistocene

Lower Rectangle Porphyry group (trachyandesite) — lower Pleistocene

Lava Tower Trachyte group (trachyte) — lower Pleistocene

Lower Trachyandesite group (trachyandesite) — lower Pleistocene

Crater

Uhuru Peak

Fig. 1 Geological map of Kibo, Kilimanjaro (after Downie and Wilkinson, 1964).

Modal analyses were made on two thin sections and averaged as shown in Table 1. Only 8.7% of the total volume is occupied by the phenocrysts, and 91.3% by the groundmass. Chemical analysis was performed on the phonolite eliminating the phenocrysts as much as possible. Therefore, this chemical composition roughly represents that of the groundmass of the rock. Table 1 shows the result of chemical analysis and C.I.P.W. norm. Low MgO content, low MgO/(FeO+Fe_2O_3) ratio and high Na_2O content are characteristic of this rock. These chemical and normative data indicate that the rock is typical alkaline rock.

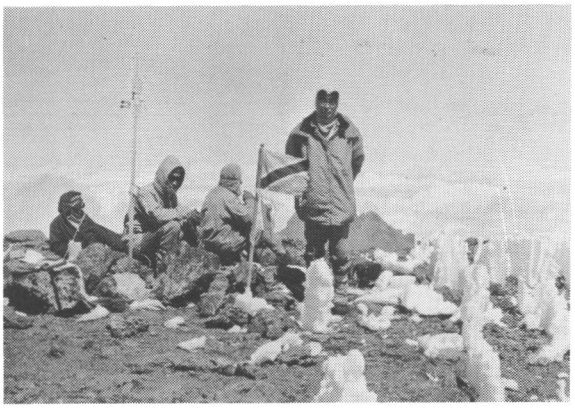

Fig. 2 Exposure of Uhuru Peak, 5895 metres above sea level. Phonolite was collected from the lava flow of the Peak on which the senior author(right) stands up. Mr.Yairi(second from right), Dr.Kurimoto (second from left), Mr.Fata Eli, a guide (left).

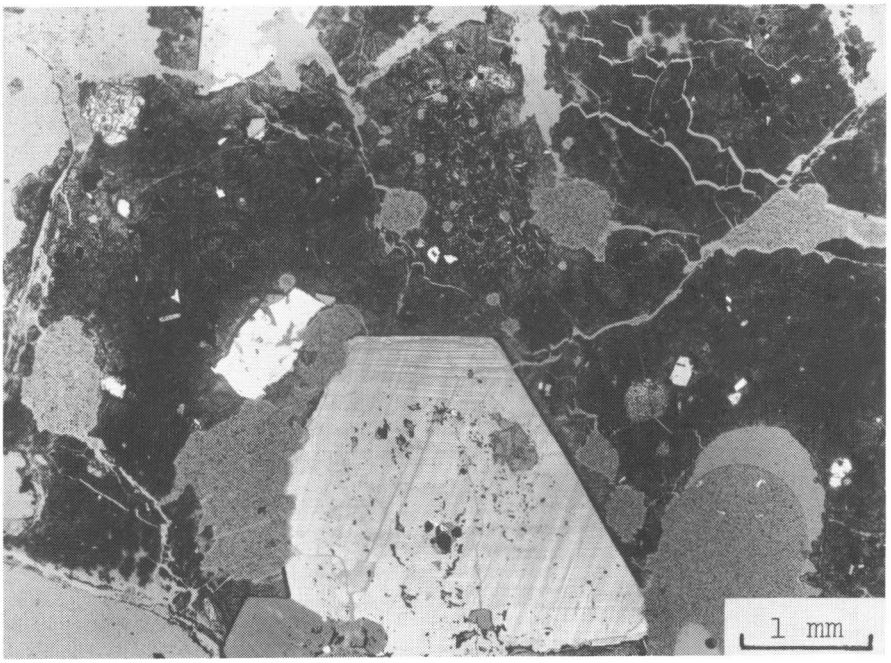

Fig. 3 Photomicrograph of phonolite showing large anorthoclase (bottom), corroded ferrosalite (upper left) and variolitic groundmass (upper centre) in a glassy matrix. Greyish dirty part indicates gas cavity. Nicols half-crossed.

Table 1 Chemical compositions, norms and modes of rocks from Kibo, Kilimanjaro

Oxides wt.%

	I	II
SiO_2	50.26	50.12
TiO_2	1.91	1.24
Al_2O_3	19.84	20.34
Fe_2O_3	5.05	5.96
FeO	4.13	1.88
MnO	0.27	0.23
MgO	0.90	2.14
CaO	5.65	4.23
Na_2O	6.16	8.28
K_2O	2.55	4.19
H_2O (+)	1.94	0.44
H_2O (-)	0.47	0.13
P_2O_5	0.38	0.84
Total	99.51	100.35
$MgO/(FeO + Fe_2O)$	0.10	0.27

C.I.P.W. norms

		I		II	
Q		–		–	
Or	F	15.09	71.96	24.76	54.22
Ab	F	37.92	71.96	23.50	54.22
An	F	18.95	71.96	5.96	54.22
Ne		7.70		25.23	
Hy		–		–	
Wo	Di	2.74	5.26	4.00	7.42
En	Di	1.88	5.26	3.42	7.42
Fs	Di	0.64	5.26	–	7.42
Fo	Ol	0.51	0.69	1.32	1.32
Fa	Ol	0.18	0.69	–	1.32
Mt		7.32		3.22	
Hm		–		3.74	
Il		3.63		2.36	
Ap		0.70		1.99	

Mode

Anorthoclase	6.2	Phenocryst
Ferrosalite	1.1	Phenocryst
Magnetite	0.8	Phenocryst
Olivine (hyalosiderite)	0.2	Phenocryst
Basaltic hornblende	0.2	Phenocryst
Nepheline	0.2	Phenocryst
Glass	36.5	Groundmass
Anorthoclase	31.0	Groundmass
Ferroaugite	13.2	Groundmass
Magnetite	6.4	Groundmass
Alkali amphibole	3.8	Groundmass
Apatite	0.4	Groundmass
Total	100.0	

I. Phonolite (1-68102101c) examined in this paper. Systematic name: phonolitic tephrite. (Analyst: M. Hoshino)

II. Systematic name: latite (K121). Locality: Furtwängler Peak, 0.5km west from Uhuru Peak. Mode is not given. (Downie and Wilkinson, 1972)

Systematic classification of the volcanic rocks based on the three normative parameters, colour index, feldspar ratio and feldspathoid content is adopted by Downie and Wilkinson (1972) to classify the Kilimanjaro volcanic rocks. Accoridng to this classification, the rock examined in this paper belongs to phonolitic tephrite.

Downie and Wilkinson (1972) gave one chemical datum of the volcanic rock, which belongs to the same lava unit from which the rock examined by us was collected. MgO content, $MgO/(FeO + Fe_2O_3)$ ratio, Na_2O content and K_2O content are considerably higher in the rock examined by Downie and Wilkinson than in the rock examined by us (Table 1). This chemical difference is partly due to the inhomogeneity even within a same lava unit and is partly due to the difference of sample preparation: whole rock composition including the phenocrysts or groundmass composition excluding them.

Phenocrysts

Anorthoclase crystal is euhedral and short prismatic. Fine grating twinning on (100) is common. The length varies greatly from 0.5 mm to 15 mm. Large phenocryst often includes rounded nepheline, ferrosalite and brown glass. Optical properties are as follows: α=1.537, β=1.542, γ=1.545, 2V(−)=50°~52°, $r > v$. Despite the zonal structure, remarkable variation of the optic axial angle is not observed within an individual grain. Composition inferred from the optic axial angle gives (Ab+An) 83~84 Or 17~16. The angular difference between $2\theta(\bar{2}01)$ of anorthoclase and $2\theta(10\bar{1}0)$ of quartz as an internal standard (Bowen and Tuttle, 1950) gives the composition (Ab + An) 78 ~ 81 Or 22 ~ 19. This slight discrepancy between the compositional ranges obtained from the optical and X-ray methods may indicate that submicroscopic unmixing of two feldspars, plagioclase and potassium feldspar, has partially taken place. Partial analysis on anorthoclase from the Uhuru Peak is presented by Leedal (1952) as Na_2O 7.8% and K_2O 3.9%. From his data, the chemical composition of the anorthoclase is calculated as Ab68 An10 Or22.

Nepheline exhibits euhedral, short prismatic crystal up to 10 mm in length. This mineral occurs not only as phenocrysts, but also as inclusions in large anorthoclase phenocrysts. Under the microscope, it is optically negative and has refractive indices, ϵ=1.534, ω=1.539, and has poor cleavage. Hamilton and Mackenzie (1960) demonstrated the diagram giving approximate composition of nepheline in the ternary system (nepheline-kalsilite-quartz) from the reflection angles 2θ for $(20\bar{2}2)$ and $(21\bar{3}0)$. According to their diagram, the nepheline examined has a composition Ne76 Ks19 Qz5 for $(20\bar{2}2)$ reflection and Ne79 Ks15 Qz6 for $(21\bar{3}0)$ reflection.

Ferrosalite is euhedral, slender prismatic or short prismatic and rarely corroded. The length varies from 0.2 mm to 10 mm. Optical properties are as follows: α=1.698, β=1.710, γ=1.727, 2V(+)=58°~59°, $r > v$, $c \wedge Z$ on (010)=42°. The colour is pale greenish without sensible pleochroism.

Olivine is not clearly identified to the unaided eyes in the hand specimen, but is prominent under the microscope. It shows corroded form and the size varies from 0.5mm to 1.5 mm. Optical properties are α=1.715, $\gamma-\alpha$=0.039, the latter was determined by means of Berek compensator, 2V(−)=79°, $r > v$. From optical data it's composition is a hyalosiderite variety (Fo60 Fa40). The colour is pale yellowish in thin section.

Basaltic hornblende rarely occurs as

euhedral slender prismatic phenocryst with the length of 1.5 mm. Nearly straight extinction on (010), strong pleochroism: X=pale yellow, Y=reddish brown, Z=dark brown, and 71°(−) of the optic axial angle agree with the optical properties of basaltic hornblende.

Groundmass

Groundmass feldspar is in most cases acicular anorthoclase with 2V around 50° (−), but some mesostatic feldspar showing the 2V ranging from 85°(+) to 90°(+) may be oligoclase. Greenish rounded pyroxene has a 2V ranging from 50°(+) to 55°(+), presumably belongs to ferroaugite variety. Rarely elongated pyroxene shows larger 2V (−) 77° ~ 86°, positive elongation and nearly straight extinction, presumably belongs to eulite variety of orthopyroxene. Amphibole exhibiting a strong pleochroism of deep brown to greenish brown may be alkali variety. Magnetite often occurs as an aggregate of minute grains. Apatite is euhedral and prismatic. Groundmass minerals described above are less than 0.2 mm in size and embedded in pale brownish glass with n=1.521.

The occurrence of anorthoclase both as phenocryst and as groundmass mineral is of special interest. From this study, the phenocrystic anorthoclase was found to be the senior of us expresses his deep thanks. Precise chemical compositions of anorthoclase and associated other minerals are now under study by means of EPMA and will be appeared in a separate paper.

Acknowledgements – Many facilities for field work were made by Mr. L. Michael of the Kilimanjaro Mountain Club, to whom the senior of us expresses his deep thanks. The senior of us expresses his gratitude to Drs. S. Mizutani and H. Kurimoto and Mr. K. Yairi of Nagoya University for co-operation with field work. Dr. K. Suwa of Nagoya University kindly read the manuscript and gave fruitful suggestions, to whom our thanks are also extended.

References

BOWEN, N.L. and TUTTLE, O.F. (1950): The system $NaAlSi_3O_8$-$KAlSi_3O_8$-H_2O. *J. Geol.*, **58**, 489-511.

DOWNIE, C. and WILKINSON, P. (1964): Geological map of Kilimanjaro, 1 : 125,000 (with explanatory notes). *Geol. Surv. Tanganyika.*

—— and —— (1972): The geology of Kilimanjaro. *Dept. Geol., Univ. Sheffield,* 253pp.

HAMILTON, D.L. and MACKENZIE, W.S. (1960): Nepheline solid solution in the system $NaAlSiO_4$-$KAlSiO_4$-SiO_2. *J. Petrology,* **1**, 56-72.

LEEDAL, G.P. (1952): Anorthoclase feldspar crystals from Kibo, Kilimanjaro. *Rec. Geol. Surv. Tanganyika,* **2**, 45-47.

Vermiculite-like Macroscopic Layer Silicates from Kenze Forest and Kioo Forest, Southern Machakos, Kenya

Shigeji MIYAZAKI

Department of Earth Sciences, Faculty of Science, Nagoya University

Introduction

The accumulated field evidence suggests that vermiculite is an alteration product of biotite, and this is supported by numerous experimental studies. Nevertheless there still remains some disagreement about the origin of vermiculite and the process of its formation. Macroscopic vermiculite occurs in four types of host rocks; (1) ultramafic and mafic rocks; (2) gneisses and schists; (3) carbonate rocks; and (4) granitic rocks (Bassett, 1963).

In southern Machakos area about 90 km south-east of Nairobi, vermiculite-like minerals occur at Kioo Forest and Kenze Forest as books in pegmatites and as slips and/or books in vermiculitized biotite masses enclosed with gneisses and schists (Baker, 1954). The clarification of the mineralogical characters of these minerals has been studied in order to contribute toward revealing the origin of vermiculite and the process of its formation.

Mode of occurrence

Vermiculite-like macroscopic layer silicates reported in this paper occur on the slops of Kenze Forest and Kioo Forest about 15 km north of Sultan Hamud Station, Machakos District. The rocks exposed in the area mainly consist of gneisses and schists of Mozambique Metamorphic Belt. The Opete (or Upete) dome filled with granitoid gneiss (Baker, 1954) is 4 km north-east of Kenze Forest and 5 km north of Kioo Forest. The western part of Kenze Forest is composed of biotite gneiss and biotite-muscovite schist which were cut by pegmatites. The metamorphic rocks strike to the NNW direction and dip profoundly to the west.

The rock containing vermiculite-like minerals forms an elongated mass along the strike of the enclosing gneisses and has a length several times as large as its width which is about 5 meters. The 'vermiculite' rock is bounded sharply by gneisses and pegmatites which are inter-tongued each other. The rock chiefly consists of weathered biotite slightly to almost entirely altered into vermiculite-like mineral associated with anthophyllite, hornblende, feldspar and garnet, and has remarkable foliation. Quartz, feldspar and a small amount of apatite are the constituents of pegmatitic veins which cut the 'vermiculite' rock and run parallel to its elongation. There are also a number of vein-like masses over the hill and they chiefly consist of weathered biotite with quartz. The weathered biotite forms books and/or slips about 1 cm in diameter and several mm in thickness. Four specimens (SM760204-10, -11, -12 and -13 from which samples A,B,C and D were separated respectively) were collected from the western wall of the excavation in the 'vermiculite' rock directly hung over by biotite gneiss 2 meters in thickness and covered with a pegmatite several 10 cm in thickness. Very little soil is developed on the surface of the pegmatite whose feldspar has been weathered into kaolinite. Specimen SM76020410 is from

2nd Prelim. Rep. Afr. Studies, Nagoya Univ., 184-193, 1977.

the bottom of the wall and sampling points of specimen SM760204-11, -12 and -13 are 1, 2 and 3 meters upward from the bottom respectively, and besides the latter is from the vicinity of the boundary between the 'vermiculite' rock and the gneiss.

The pegmatite on the northern slop of Kioo Forest contains quartz, kyanite, oligoclase, tourmaline, garnet, biotite and its weathered equivalence with secondary chlorite. This kyanite-bearing pegmatite changes gradually into staurolite-bearing one consisting of quartz and staurolite with accessories of weathered biotite, garnet, ilmenite, hematite and secondary chlorite (Miyakawa and Suwa, 1975). These pegmatites may possibly have some connections with granitoid gneiss of the Opete dome. The Kyanite-bearing pegmatite approximately 2 meters in width is a very irregular body which in some places sends tongues and stringers into surrounding micaceous gneisses and schists (Temperley, 1953). Weathered biotite (sample E separated from specimen SM76020701) forms large books in the pegmatite. Chlorite occurs in crystals from less than 1 mm to 2.5 cm in diameter which are usually found as books and slips associated with vermiculite-like minerals and quartz. Sometimes chlorite surrounds kyanite and garnet crystals and intrudes into cleavage planes of kyanite. Sample F separated from specimen SM76020701 is a book consisting of chlorite layers and interstratified mineral layers associated with quartz, and sample G also separated from specimen SM76020701 forms books composed of chlorite with quartz and without interstratified minerals.

Experimental

Samples A, B, C and D were carefully handpicked to separate weathered biotite. X-ray diffraction patterns of some samples after the separation and light grinding in an agate mortor show very weak reflections of anthophylite and/or hornblende, which are considered to have little or no effect on the subsequent discussion. Some pulverized samples were washed with 1N-$MgCl_2$ solution and boiled in 1N-$CaCl_2$, KCl and NH_4NO_3 solutions to obtain Mg-, Ca-, K- and NH_4-saturated forms respectively Some were also pre-heated at certain temperatures for one hour. The wet chemical analyses were carried out for samples A, B, C and D. KBr pressed disks of samples were prepared to record infrared absorption spectra. Calculated X-ray diffraction data for Reichweite g=1 of biotite/vermiculite interstratified minerals are based on the theory introduced by Kakinoki and Komura (1952) and aplied by Sato (1965).

Results and discussion

Chemical Analyses

Chemical compositions of weathered biotite are listed in Table 1 with values of exchangeable cations. The proportion of ions is calculated on the basis of the anionic composition 22 (O). The water content and the ratio $Fe^{3+}/(Fe^{2+} + Fe^{3+})$ have progressively increased from sample A to D, whereas K_2O content is on the decrease.

All exchangeable Mg^{2+} is allotted to the interlayer site and non-exchangeable Mg^{2+} is assigned to the octahedral position. Both exchangeable and non-exchangeable Ca^{2+}, Na^+ and K^+ are allotted to the interlayer site. Leaving H^+ incorporated in the O^{2-} framework (Barshad and Kishk, 1969) out of consideration, the interlayer and octahedral charges decrease from sample A to D.

Table 1. Chemical analyses and structural formulas of weathering products of biotite

		Sample A	Sample B	Sample C	Sample D
SiO_2		37. 84	37. 97	37. 85	38. 77
TiO_2		2. 22	2. 09	1. 53	1. 68
Al_2O_3		14. 84	15. 27	15. 49	14. 76
Fe_2O_3		9. 42	11. 03	12. 49	12. 00
FeO		4. 91	2. 21	1. 32	0. 29
MnO		0. 14	0. 29	0. 17	0. 14
MgO	(fixed)	15. 99	15. 44	14. 85	12. 67
MgO	(exch.)	0. 84	1. 01	1. 14	1. 81
CaO	(fixed)	0. 78	0. 37	0. 44	0. 39
CaO	(exch.)	0. 06	0. 21	0. 47	0. 52
Na_2O	(fixed)	0. 38	0. 28	0. 33	0. 11
Na_2O	(exch.)	tr.	tr.	tr.	tr.
K_2O	(fixed)	5. 44	4. 15	2. 91	0. 72
K_2O	(exch.)	0. 13	0. 11	0. 09	0. 05
H_2O^+		4. 46	5. 55	5. 76	8. 27
H_2O^-		2. 15	3. 12	4. 49	7. 76
Total		99. 60	99. 10	99. 33	99. 94
		Numbers of ions on the basis of 22(O).			
Si		5. 55 } 8. 00	5. 62 } 8. 00	5. 63 } 8. 00	5. 96 } 8. 00
Al		2. 45 }	2. 38 }	2. 37 }	2. 04 }
Al		0. 12	0. 28	0. 34	0. 63
Ti		0. 25	0. 23	0. 17	0. 19
Fe^{3+}		1. 04	1. 23	1. 40	1. 39
Fe^{2+}		0. 60 } 5. 53	0. 27 } 5. 46	0. 16 } 5. 39	0. 04 } 5. 17
Mn		0. 02	0. 04	0. 02	0. 02
Mg		3. 50	3. 41	3. 30	2. 90
Mg*		0. 18	0. 22	0. 25	0. 41
Ca		0. 13 } 1. 46	0. 09 } 1. 19	0. 14 } 1. 05	0. 15 } 0. 74
Na		0. 11	0. 08	0. 09	0. 03
K		1. 04	0. 80	0. 57	0. 15
H_2O**		1. 23	2. 28	3. 09	6. 21
(OH)		4. 00	4. 00	4. 00	4. 00
$Fe^{3+}/(Fe^{2+}+Fe^{3+})$		0. 63	0. 82	0. 90	0. 97
		Charges on the basis of 22(O).			
Tetrahedral		− 2. 45	− 2. 38	− 2. 37	− 2. 04
Octahedral		+ 0. 72	+ 0. 89	+ 0. 86	+ 0. 74
Interlayer		+ 1. 77	+ 1. 50	+ 1. 44	+ 1. 30
Net		+ 0. 04	+ 0. 01	− 0. 07	± 0. 00

Analyst : K. Suzuki

* : All exchangeable Mg^{2+} is allotted to the interlayer site.

** : No. of water molecules per formula unit, corresponding to total water content less amount required for 4(OH).

Infrared Absorption Spectra

Infrared absorption spectra (Table 2) of samples A, B, C and D are very much similar to each other, having five main absorption bands. Bands with maxima near 3400 cm^{-1} identified as OH stretching vibrations, 1640 cm^{-1} and 690 cm^{-1} which are assigned to OH bending vibrations correspond to hydroxyls involved in hydrogen bonds to surface oxygen and to other loosely adsorbed water molecules (Farmer, 1974; Marel and Beutelspacher, 1976). Si-O stretching vibrations lie near 1000 cm^{-1}. The absorption near 460 cm^{-1} arises principally from in-plane vibrations of the octahedral ions and their adjacent oxygen layers, and these vibrations couple to give modes which are described as M-O stretching or Si-O bending (Farmer, 1964). The ratio of absorbance in Table 2 becomes lesser from sample A to E, which results from the increment of water content. This trend is in accord with the result of chemical analyses. The absorbance ratio of sample E is intermediate between those of samples C and D.

Table 2. Data of infrared absorption spectra of weathering products of biotite

Sample A		Sample B		Sample C		Sample D		Sample E	
Wave number (cm^{-1})	Absorbance ($\log I_o/I$)	Wave number (cm^{-1})	Absorbance ($\log I_o/I$)	Wave number (cm^{-1})	Absorbance ($\log I_o/I$)	Wave number (cm^{-1})	Absorbance ($\log I_o/I$)	Wave number (cm^{-1})	Absorbance ($\log I_o/I$)
3410	$E_1=0.322$	3430	$E_1=0.237$	3420	$E_1=0.285$	3420	$E_1=0.502$	3420	$E_1=0.323$
1640	0.096	1640	0.074	1640	$=0.098$	1640	0.166	1640	0.108
1000	$E_2=1.432$	1010	$E_2=0.821$	1010	$E_2=0.820$	1010	$E_2=0.980$	1015	$E_2=0.709$
690	0.139	690	0.074	690	$=0.094$	685	0.151	690	0.082
460	$E_3=0.764$	465	$E_3=0.485$	465	$E_3=0.503$	470	$E_3=0.561$	470	$E_3=0.435$
$E_2/E_1=4.45$		$E_2/E_1=3.46$		$E_2/E_1=2.88$		$E_2/E_1=1.95$		$E_2/E_1=2.20$	
$E_3/E_1=2.37$		$E_3/E_1=2.05$		$E_3/E_1=1.76$		$E_3/E_1=1.12$		$E_3/E_1=1.35$	

X-ray Diffraction

The b parameter increases with the increment of numbers of octahedral Fe^{2+} and decreases with that of octahedral Fe^{3+} for trioctahedral mica-type layer silicates (Brindley, 1961). This tendency among samples A, B, C and D is shown in Table 3, though it is not much conspicuous. Three basal reflections are recognizable in lower angle region for each air-dried preferred-oriented sample, i.e., the 25–30Å reflection having weak intensity, the 14.5Å reflection and that in the range between 10.2Å and 12.1Å. For some samples, the 14.5Å reflection splits into 16Å and 14Å

by ethylene glycol treatment and, for all samples, it shifts to 14.2–14.3Å by glycerol treatment and to 14.6–14.7Å in wet condition. On the contrary, Mg-saturated samples demean themselves differently; the reflection in the 10.2Å–12.1Å region shifts towards higher angle region, which may be due to the depletion of exchangeable interlayer K^+. Ca- and K-saturated forms of sample A show the 14.9 and 10.3Å reflections, which shift to 15.8 and 10.2Å by ethylene glycol treatment and to 15.2 and 10.2Å in wet condition respectively. Mg-saturated samples A,B,C and D treated with NH_4NO_3 have reflections at 10.3, 10.3, 10.5 and 10.7Å respectively. Mg-vermiculite collapses to 10Å and some sorts of smectite to 14.3–12Å by means of this treatment (Sudo, 1974). The basal spacing of Mg-vermiculite neither expands with glycolation nor swells in wet condition as that of smectite does. Samples A, B, C, D and E have ceased rehydration at 300°C, where sample D has the reflection at a little higher angle region compared with A,B and C. These five samples are identified as interstratified minerals whose components are biotite and vermiculite, associated with vermiculite as a segregated phase in the very same book and/or slip.

Table 3. X-ray diffraction data of weathering products of biotite, and chlorite

Sample A															
Preferred orientation														Random orientation	
Air-dried		EG		GL		RH100		Pre-heated at 300°C		Pre-heated at 450°C		Pre-heated at 600°C		d(Å)	I
d(Å)	I	d(Å)	I	d(Å)	I	d(Å)	I	d(Å)	I	d(Å)	I	d(Å)	I	14.5	s
27	vw													10.2	s
		16.7	w											5.03	vw
		14.2 pt	vw											3.60	w
14.5	m			14.3	m	14.7	m							3.37	s
10.2	s	10.2	s	10.2	s	10.2	m	10.3	vs	10.3	vs	10.2	vs	2.88	w
														2.62	w
(Mg-form)														2.52	w
Air-dried		EG		GL		RH100		Pre-heated at 200°C		Pre-heated at 500°C		AN		2.43	vw
														2.18	w
						26	vw							2.017	m
		16.4	m											1.677	w
14.3 sh	vs	12.8	vw	14.2 sh	vs	14.7 sh	s	14.6	m					1.5351	w
10.5	m	10.5 b	w	11	w	10.3	m	10.8 sh	m	10.0	m	10.3	m	1.440	w
														1.365	vw
														b_o=9.2106	
(Ca-form)															
Air-dried		EG		RH100		Pre-heated at 500°C		Air-dried		EG		RH100		Pre-heated at 500°C	
14.9	vs	15.8	vs	15.2	vs	9.6	m	10.3	vs	10.2	vs	10.2	vs	10.1	vs

Table 3. *(continued)*

Sample B														Random orientation
Preferred orientation														
Air-dried		EG		GL		RH100		Pre-heated at 300°C		Pre-heated at 450°C		Pre-heated at 600°C		
27	vw													14.6 m
														10.6 b m
14.5)sh	m	14.5	m	14.2	m	14.7	w							4.61 vw
10.7 b	m	10.6	m	10.2	m	10.6 b	w	10.3	vs	10.2	vs	10.2	vs	3.40 m
														3.19 m
(Mg-form)														2.62 m
Air-dried		EG		GL		RH100		Pre-heated at 300°C		Pre-heated at 450°C		Pre-heated at 600°C		2.43 vw
														2.17 vw
28.0	vw													2.02 vw
		16.6)pt	m											1.68 vw
14.5	m	14.5	vw	14.3	m	14.7	w	14.4	m					1.5306 w
						12.1	vw							b_o=9.1836
10.9)sh	m	10.6 b	w	11.0)sh	m	10.9 b	vw	10.8	s	10.1	s	10.3	m	

Table 3. *(continued)*

Sample C														Random orientation
Preferred orientation														
Air-dried		EG		GL		RH100		Pre-heated at 300°C		Pre-heated at 450°C		Pre-heated at 600°C		
27	b m	29	vw	26	w	28.	vw	26	vw					27 b w
		16.2	w											14.5 m
14.5	s	14.2	w	14.2	m	14.6	m							12.1 m
12.0	s	12.1	m	11.8	m	12.1	m							4.62 w
		11.3	vw			11.6	vw							3.41 m
								10.2	m	10.1	vs	10.0	vs	2.88 w
														2.63 w
(Mg-form)														2.42 w
Air-dried		EG		GL		RH100		Pre-heated at 200°C		Pre-heated at 500°C		AN		2.03 w
														1.674 w
27	w	30	m	29	vw	29	vw	26	m					1.5300 w
		16.6	m											b_o=9.1800
14.5	m			14.2	m	14.7	w	14.5						
125	m	13	w	12.1	m	12.3 b	w	12.0)sh	m					
										10.0	m	10.5	m	

Table 3. *(continued)*

Sample D

Preferred orientation												Random orientation	
Air-dried		EG		GL		RH100		Pre-heated at 300°C		Pre-heated at 450°C		Pre-heated at 600°C			
28	vw	30	vw	28	vw									27	vw
		16.3	vs											14.5	vs
14.5	vs	14.4	vs	14.3	vs	14.6	vs							12.1	m
12.1	m	12.1	m	11.9	m	12.2	w							7.2	w
								9.9	m	9.8	s	9.8	m	4.80	m
												9.5	w	3.60	s
														3.47	w
(Mg-form)														2.88	s
Air-dried		EG		GL		RH100		Pre-heated at 200°C		Pre-heated at 500°C		AN		2.65	vw
														2.55	vw
28	vw	30	vw	27.	vw									2.39	w
		16.3	vs											1.67	vw
14.4	vs			14.3	vs	14.5	s	14.6	m					1.5301 b	w
12.6 b	w	13.0	vw	12.2	vw			12.5	w					b_o = 9.1806	
										9.6 b	m	10.7	m		

Sample E

Preferred orientation													
Air-dried		EG		Pre-heated at 150°C		Pre-heated at 300°C		Pre-heated at 600°C		(Mg-form) Air-dried		EG		RH100	
25	w	26	w	26	w					26	w			27	w
		16.4	vs												
14.6	vs	14.6	vw	14.5	vs					14.6	m	14.5	m	14.8	m
12.8	w	12.9	vw	12.8	w					12.8	m	12.6	m	12.8	m
						10.2	s	9.8	s						

Sample F

Preferred orientation

Air-dried		EG		GL		RH100	
27	vw	30	vw	29	vw	27	vw
		16.4	vw				
14.3	s	14.4	s	14.3	s	14.3	m
12.7	m	12.6	m	12.6	m	13.0	w
7.9	vw	7.9	w	7.9	vw		
7.1	vs	7.2	vs	7.2	vs	7.1	s
4.74	s	4.74	s	4.74	s	.....	

Sample G

Random orientation

hkl	d(Å)	I	|F|
001	14.18	91	47
002	7.077	100	100
003	4.715	36	92
004	3.540	52	151
005	2.833	12	93
	.....		
007	2.023	3	70
	.....		
060	1.5393		

b_o = 9.2353

d_{001} = 14.155

EG : ethylene glycol treatment. GL : glycerol treatment. AN : NH_4NO_3 treatment.

RH100 : in wet condition. sh : shoulder. b : broad.

Table 4 shows calculated X-ray diffraction data with the probability W_B and P_{VV}, where subscripts B and V mean biotite-like layer and vermiculite-like layer respectively and symbol W_S is defined as the probability of finding S layer at any position and P_{ST} as the transition probability that T layer succeeds S layer. W_B becomes smaller from sample A to D, whereas P_{VV} does not vary in zero value and the segregated phase of vermiculite is produced. W_B may decrease up to 0.5, thus the tendency towards ordered interstratification develops with the increment of the proportion of oxidized structural iron (Gilkes, 1973). Sample E from Kioo pegmatite is similar in characters to samples A,B,C and D, though the occurrence is different. Finally P_{VV} seems to become large to approach the vermiculite point, where $P_{VV}=1$ and $W_B=0$. The schematic characteristics of weathering of biotite to vermiculite via interstratified minerals are shown in Figure 1.

Alternation of Chlorite Layers and Interstratified Biotite/Vermiculite Layers

Sample G is macroscopic chlorite whose X-ray diffraction data are listed in Table 3. The chlorite is identified by means of its diffraction data as $(Mg_{3.9}Fe_{0.7}Al_{1.4})(Si_{2.6}Al_{1.4})O_{10}(OH)_8$ with 0.5 excess Fe^{2+} in the hydroxide sheet (Brindley, 1961; Oinuma et al., 1972). Although octahedral cations are not evenly distributed between the silicate layer and the hydroxide sheet (Shirozu and Momoi, 1972), the chlorite is regarded as a hydrothermal product from biotite and other minerals in the pegmatite.

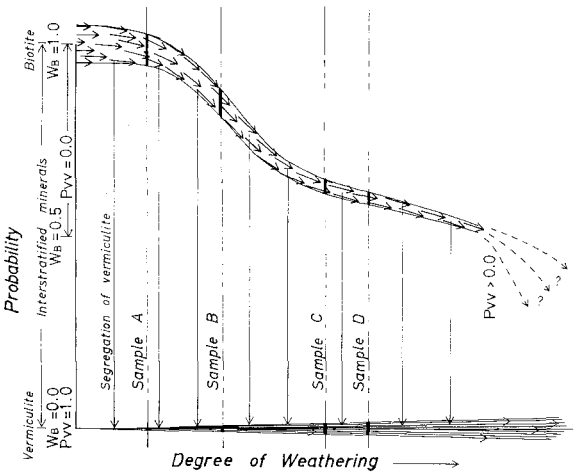

Fig. 1. Schematic characteristics of weathering of biotite to vermiculite via interstratified minerals.

Table 4. Calculated X-ray diffraction data

Biotite	Interstratified minerals					Vermiculite	Correlation between calculated and observed X-ray diffraction data
No. 1	No. 2	No. 3	No. 4	No. 5	No. 6	No. 7	
$W_B=1.00$ $P_{VV}=0.00$	$W_B=0.98$ $P_{VV}=0.00$	$W_B=0.85$ $P_{VV}=0.00$	$W_B=0.63$ $P_{VV}=0.00$	$W_B=0.60$ $P_{VV}=0.00$	$W_B=0.46$ $P_{VV}=0.25$	$W_B=0.00$ $P_{VV}=1.00$	Nos.2 + 7 ≡ Sample A Nos.3 + 7 ≡ Sample B
d(Å) I	d(Å) I	d(Å) I	d(Å) I	d(Å) I	d(Å) I	d(Å) I	Nos.7 + 4 ≡ Sample C Nos.7 + 5 ≡ Sample D
			27.0 w	26.0 m	24.7 m		Nos.7 + 6 ≡ Sample E
						14.6 vs	
	10.2 vs	10.9 s	12.0 s	12.1 s	12.6 s		
10.17 vs							

It is noteworthy that the alternation of chlorite layers and interstratified biotite/vermiculite layers even in a single book of sample F is discernible with the naked eye. It may be deduced that the hydrothermal alteration of biotite to chlorite terminated incompletely and some biotite layers which is now recognized as interstratified mineral layers remained within chloritized books, since it is hardly conceivable that some chlorite layers have altered into interstratified biotite/vermiculite layers.

Summary

Macroscopic crystals of interstratified biotite/vermiculite with some identifying marks of smectite are found in Kenze Forest, southern Machakos, Kenya. Their weathering sequence is characterized as steady increases in water content and in the ratio of Fe^{3+} to Fe^{3+} plus Fe^{2+}, gradual decreases in K_2O content and in the existing probability of biotite-like layers, and the constant zero value of the transition probability that a vermiculite-like layer succeeds another identical one in accord with the increase in the number of vermiculite layers as a segregated phase. Chlorite from Kioo Forest was formed by hydrothermal action. In such a case that the chlorite is an alteration product of biotite, the action left some biotite layers intact which have been preferably weathered within chloritized books.

Acknowledgements – The author wishes to express his sincere thanks to Drs. K. Nagasawa and Y. Tsuzuki for their helpful guidance and constractive criticisms, to Dr. K. Suwa for encouragement, to Mr. K. Suzuki for sparing no labor upon the chemical analyses, and to Dr. M. Sato for affording him every facility for the calculation. Thanks are also due to Prof. I.S. Loupekine for the loan of field equipment and for hospitality. The receipt of the scholarship from the Ministry of Education of Japanese Government is gratefully acknowledged. The calculation has been done with FACOM 230-75 at Nagoya University Computation Center.

References

BAKER, B.H. (1954): Geology of the southern Machakos district. *Geol. Surv. Kenya, Rep. 27.*

BARSHAD, I. and KISHK, F.M. (1969): Chemical composition of soil vermiculite clays as related to their genesis. *Contr. Mineral. Petrol.*, **24**, 136-155.

BASSETT, W.A. (1963): The geology of vermiculite occurrences. *Proc. 10th National Clay Conf.*, 61-69.

BRINDLEY, G.W. (1961): Chlorite minerals. *In: The X-ray identification and crystal structures of clay minerals* (ed. BROWN, G.), 242-296, Mineral. Soc., London.

FARMER, V.C. and RUSSEL, J.D. (1964): The infra-red spectra of layer silicates. *Spectrochimica Acta*, **20**, 1149-1173.

FARMER, V.C. (1974): The layer silicates. *In: The infrared spectra of minerals* (ed. FARMER, V.C.), 331-363. Mineral. Soc., London.

GILKES, R.J. (1973): The alteration products of potassium depleted oxybiotite. *Clays Clay Miner.*, **21**, 303-313.

KAKINOKI, J. and KOMURA, Y. (1952): Intensity of X-ray diffraction by an one-dimensionally disordered crystal. *Jour. Phys. Soc. Japan*, **7**, 30-35.

MAREL, H.W. VAN DER and BEUTEISPACHER, H. (1976): *Atlas of infrared spectroscopy of clay minerals and their admixture.* Elsevier Publ., Amsterdam.

MIYAKAWA, K. and SUWA, K. (1975): An occurrence of staurolite from the Kioo Pegmatite, Machakos District, Kenya. *1st Prelim. Rep. Afr. Studies, Nagoya Univ.,* 52-54.

OINUMA, K. et al. (1972): Triangular diagrams for surveying chemical compositions of chlorites. *Jour. Toyo Univ., Gen. Education,* No. **15,** 1-33.

SATO, M. (1965): Structure of interstratified minerals. *Nature,* **208,** 70-71.

SHIROZU. H. and MOMOI, H. (1972): Synthetic Mg-chlorite in relation to natural chlorite. *Mineral. Jour.,* **6,** 464-476.

SUDO, T. (1974): *Clay mineralogy* (in Japanese). Iwanami Publ., Tokyo.

TEMPERLEY, B.N. (1953): Kyanite in Kenya. *Geol. Surv. Kenya, Mem. 1.*

Palaeomagnetism of South African Kimberlites

Haruaki ITO*, Katsuyasu TOKIEDA*, Kanenori SUWA**
and Shōichi KUME***

* Department of Physics, Shimane University
** Department of Earth Sciences, Faculty of Science, Nagoya University
*** College of General Education, Osaka University

Introduction

Palaeomagnetic survey in Africa has covered an extensive span of geological time over 2,000 m.y. and the pole positions relevant to this continent are subsequently traced back from the middle Precambrian to the Quaternary (McElhinny *et al.*, 1968; Creer, 1970). Throughout these investigations, informations obtained from kimberlites are not many. The formation of kimberlites, however, is featured by its origin at a deeper part of the upper mantle, quick upheaval through the upper mantle and crust and rapid rate of cooling near the surface. Accordingly, remanent magnetization might have been acquired through a short period of time and it would be regarded as thermoremanent magnetization of volcanic rock.

In September 1973, the International Conference on Kimberlite was held in Cape Town. One of us (K. S.) attended the Conference and joined the accompanied field excursion which offered an opportunity to visit several diamond mines in South Africa and to collect oriented samples of kimberlites. This report describes results on the measurements of natural remanent magnetization (NRM) of these rocks.

Collecting sites

Middle Precambrian kimberlites were collected at the Premier mine (25°42′S, 28°32′E), the Montrose pipe (25°46′S, 28°33′E), and the National pipe (25°48′S, 28°33′E). Cretaceous kimberlites were sampled at the Wesselton mine (28°46′S, 24°51′E) and the Koffyfontein mine (29°26′S, 25°00′E). The local geomagnetic field around the sampling sites was approximately D = 343°, I = (−)63° and F = 32,000γ (Hermanus Magnetic Observatory, 1961).

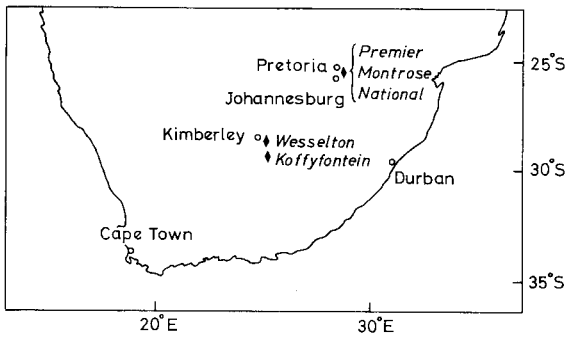

Fig. 1 Sites of kimberlites examined

Geology

Five kimberlite sites in South Africa of different age, mode of emplacement, type and degree of crustal contamination were selected for this palaeomagnetic study. Fig. 1 shows these kimberlite sites.

2nd Prelim. Rep. Afr. Studies, Nagoya Univ., 194-198, 1977.

(1) Premier mine, 38 km east of Pretoria

The kimberlite pipe of the Premier mine contains inclusions of Waterberg quartzite and is cut by a thick sill of post-Waterberg diabase. The geochronologic data give an age of 1,750±10 m.y. and a minimum age of 1,115±15 m.y. (Allsopp *et. al.*, 1967. Recent Rb-Sr age determinations by Barrett and Allsopp (1973) indicate that grey kimberlite is 1,250 m.y. and brown kimberlite may even be as old as 1,400 m.y.

The kimberlite pipe of the Premier mine measures 860 × 400 metres on surface, closing into 820 × 330 metres on the 538 metre level by an average dip of 85 degrees.

Kimberlites have intruded in at least three distinct phases corresponding to the brown, grey and black varieties.

Two samples of grey kimberlite on the 500 metre level were collected for this study.

(2) Montrose pipe, 7 km south of the Premier mine

The Montrose kimberlite pipe measures about 95 metres in diameter and consists of a barren core and a more diamondiferous rim. The kimberlite is intruded into quartzite and shales of the Transvaal System and a diabase sill of post-Transvaal age, and consists of a dark grey kimberlite breccia containing very few large inclusions.

One sample of this kimberlite breccia on the surface level was collected for this study.

(3) National pipe, 11 km south of the Premier mine

The National kimberlite pipe measures 70 metres in diameter and is intruded into the quartzites of the Transvaal System and a diabase sill of post-Transvaal age. The pipe contains the following varieties of unweathered kimberlite: (a) a dark basaltic kimberlite with a glassy matrix, (b) hard, dark grey, basaltic kimberlite, (c) two types of kimberlite breccia with different sizes of inclusions.

One sample of variety (a) on the surface level was collected for this study.

(4) Wesselton mine, 10 km SEE of Kimberley

Wesselton is one of the five major kimberlite pipes in the immediate vicinity of Kimberley. The kimberlites intrude rocks of the Karroo System, which overlies lavas of the Ventersdorp System with intervening quartzite horizons. Ventersdorp System overlies underlying Basement rocks consisting mainly of granitic and amphibolitic gneiss. According to Allsopp and Barrett (1975), the radiometric age of the Wesselton pipe is 84±3 m. y.

The surface area of the pipe is 103,750 m^2. The rocks occupying the pipe can be divided into three groups based on textural and petrographical characteristics.

Group 1 is all non-fragmental varieties of kimberlite, Group 2 is intrusive breccias containing variable amounts of xenolithic material, and Group 3 is volcanic breccias having an agglomeratic or tuffaceous appearance.

Two samples of Groups 1 and 3 kimberlites on the 600 metre level were collected for this study.

(5) Koffyfontein mine, 80 km south of Kimberley

The location of the Koffyfontein, Ebenhaezer and Klipfontein kimberlites along a NW-SE line suggests that their emplacement was controlled by a linear zone of weakness trending in this direction. Both Wagner (1914) and Williams (1932) have suggested that the three occurrences are linked below surface by a kimberlite dyke.

The kimberlites intrude rocks of the Karroo System, which directly overlies Precambrian granite gneiss.

Roughly circular in shape the Koffyfontein pipe has a diameter of about 365 metres. A number of narrow kimberlite dykes (10–50 cms wide), in the wall rock adjacent to the Koffyfontein pipe, strike directly towards Ebenhaezer.

One sample of this narrow kimberlite dyke was collected for this study.

Magnetic measurements

The NRM was measured by an astatic magnetometer. The accuracy of measurements was high but errors on the orientation would be as much as 3° due to the difficulties of collecting samples in mines. After the measurements of NRM, the specimens were subjected to alternating field demagnetization. All of NRM was stable, the directions showing a little change less than 5° in the peak field of 200 Oe. The intensities of magnetization decreased approximately by 30% of the initial values in the same field. It is seen that the magnetizations are also stable on heating up to 300°C. This behaviour is often observed in volcanic rocks which maintain primary thermoremanent magnetization since their formation.

The age of rocks, the results of measurements of RM and the virtual geomagnetic poles calculated from the measurements are summarized in Table 1.

Table 1 Results of measurements and virtual geomagnetic poles

Site	Age	RM After AC demag. in 200 Oe				Magnetization of NRM	Virtual pole	
		Decl.	Incl.	K.	θ_{95}			
Premier	middle P€ 1250 m.y.±	171°	- 3°	589	2.5	7.6 x 10^{-4}emu/cc	171W	62S
		158	- 2	316	2.9	9.0	166W	56S
Montrose	middle P€	193	11	373	2.7	8.2	118W	66S
National	middle P€	185	- 58	1410	2.0	130	147W	26S
Wesselton	Cretaceous 84±3 m.y.	341	- 69	7877	0.9	250	128W	63N
		339	- 73	602	3.7	2.9	136W	56N
Koffyfontein	Cretaceous	347	- 63	899	1.7	13.5	125W	71N

Discussions

Remanent magnetization is proved to be stable to both AC and thermal demagnetization and it is possibly thermoremanent magnetization as suggested by Jones (1968).

(1) Middle Precambrian kimberlites from Premier mine, Montrose pipe and National pipe

The present results show that the magneti-

zation of kimberlites collected from 500 metre level of the Premier mine is directed to (171°, -3°) and (158°, -2°). A 70–80 metre thick post-Waterberg diabase sill cut across the pipe and wall rock between mainly 380 and 450 metre levels and has an overall dip of 15 degrees to the north-east. The effect of the sill has been to metamorphose the kimberlite both above and below, and this metamorphic effect is apparent for a distance of some 25 metres for petrography and of some 200 metres for geochronology from both the upper and lower contacts (Barrett and Allsopp, 1973). The distance between the lower contact of the sill and the 500 metre level of the pipe is about 50 metres and the samples used in this study is considered to be thermally affected by the sill.

Jones (1968) has reported that the mean direction of stable RM of kimberlites collected at 890 feet level of the Premier mine to be 186° and -24° and that the direction of the post-Waterberg diabase sill to be 183° and -3°.

The present results nearly coincide with that of the post-Waterberg sill. This coincidence in the direction of NRM is, therefore, explained by the secondary heating of kimberlite at the time of intrusion of the sill. It is interesting to note that the pole position for the Premier lies close to the upper horizon of the Waterberg succession.

A significant difference in the direction between the Montrose and the National pipes is seen. The RM of the Montrose and that of the National pipes coincide with the upper horizon and the lower horizon of the Waterberg succession, respectively. The direction for the Montrose pipe nearly coincides with that for the Premier mine. According to Jones and McElhinny (1967), the directions of magnetization of the Waterberg succession form three groups and these groups appear to be related to the stratigraphic position of the sites in the succession. Though there has been no trial on the age determination of the Montrose and the National pipes, this result indicates that the kimberlites from the Montrose and the National pipes are classified to the middle Precambrian intrusion and that the Montrose kimberlite may coincide with the Premier kimberlite in age and the National kimberlite may be older than the Premier and the Montrose kimberlites.

(2) Cretaceous kimberlites from Wesselton and Koffyfontein mines

The present results on Wesselton and Koffyfontein kimberlites indicate that the both data coincide each other. Wesselton mine has a same situation with the De Beers mine as one of the five major kimberlite pipes in the immediate vicinity of Kimberley and as a same Cretaceous kimberlite. McFadden (1973) has announced a precise result on the magnetism of the Cretaceous kimberlite of the De Beers mine as stable component alines to D=332° and I = - 73°.

The present results on Wesselton and Koffyfontein kimberlites are in agreement with the direction of the De Beers kimberlite and the virtual pole position is roughly the same as that average value for Cretaceous rock of Africa (Creer, 1970).

Acknowledgements – This work was supported in part by the Grant-in-Aid for Scientific Research of the Ministry of Education, Science and Culture, for which we would like to record our thanks. We are also indebted to Mr. T. Agata of Nagoya University for his kind advice to the ore microscopy.

References

ALLSOPP, H.L., Burger, A. J. and van Zyl, C. (1967): A minimum age for the Premier kimberlite pipe yielded by biotite Rb-Sr measurements, with related galena isotopic data. *Earth Planet. Sci. Lett.,* **3**, 161–166.

ALLSOPP, H.L. and BARRETT, D.R. (1975): Rb-Sr age determinations on South African kimberlite pipes. Phys. *Chem. Earth,* **9**, 605–617.

BARRETT, D.R. and ALLSOPP, H.L. (1973): Rubidium-strontium age determinations of South African kimberlite pipes. *Extended Abstract, Intern. Conf. on Kimberlites, Cape Town,* 23–25.

BROCK, A. and PIPER, J.D.A. (1972): Interpretation of Late Precambrian palaeomagnetic results from Africa. *Geophy. J.R. astr. Soc.,* **28**, 139–146.

CREER, K.M. (1970): Review and interpretation of palaeomagnetic data from the Gondwanic continents. *Proc. 2nd Gondwana Symp. IUGS, Cape Town and Johannesburg,* 55–72.

HERMANUS MAGNETIC OBSERVATORY (1961): Geomagnetic secular variation observations in Southern Africa. Department of Lands, Republic of South Africa.

JONES, D.L. and McELHINNY, M.W. (1967): Stratigraphic interpretation of paleomagnetic measurements on the Waterberg Red Beds of South Africa. *J. Geophy. Res.,* **72**, 4171–4179.

JONES, D.L. (1968): Paleomagnetism of the Premier Mine Kimberlite. *J. Geophys. Res.,* **73**, 6937–6944.

McELHINNY, M. W., BRIDEN, J.C., JONES, D.L. and BROCK, A. (1968): Geological and Geophysical implications of paleomagnetic results from Africa. *Rev. Geophys.,* **6**, 201–238.

McFADDEN, P.L. (1973): A palaeomagnetic study of the De Beers Diamond Mine. *Extended Abstract, Intern. Conf. on Kimberlites, Cape Town,* 221–223.

WAGNER, P.A. (1914): *The diamond fields of Southern Africa.* Transvaal Leader, Johannesburg. Reprinted 1971, Struik (Pty) Ltd., Cape Town. 355 pp.

WILLIAMS, A.F. (1932): *The genesis of the diamond,* 2 vols. Ernest Benn, Ltd., London, 636 pp.

List of publications on African geology

1963 * SUWA, K., Geological excursion of north-east Africa. *Monthly Africa,* **3,** Nos.5-10.
* SUWA, K., Geology of Ethiopia. *Nagoya Jour. Geol.,* **18,** 13-25.

1964 * SUWA, K., Geological excursion of north-east Africa. *Monthly Africa,* **4,** Nos.1 and 3.
* SUWA, K., African Rift Valley. *World Geography,* **13,** 320-322.

1965 * SUWA, K., Geology of Egypt and Sudan. *Nagoya Jour. Geol.,* **20-21,** 34-48.

1966 MATSUZAWA, I., A study on the formation of the African Rift Valley. *Jour. Earth Sci., Nagoya Univ.,* **14,** 89-115.
MIZUTANI, S. and SUWA, K., Orthoquartzitic sand from the Libyan desert, Egypt. *ibid,* 137-149.
SUWA, K., Maximum microcline in Aswan granitic rocks, Egypt. *ibid,* 116-136.
** SUWA, K. and UEMURA, T., Geology of the African Rift Valley and the Olduvai Gorge. *Jour. Afr. Studies,* **3,** 18-48.
* SUWA, K., Precambrian of Africa (I). *Earth Science (Chikyu Kagaku),* **84,** 39-48.

1967 ** MATSUZAWA, I., Some considerations on the formaiton of the African Rift Valley. *Jour. Afr. Studies,* **4,** 1-24.
* SUWA, K., Precambrian of Africa (II). *Earth Science (Chikyu Kagaku),* **21,** 32-44.

1968 ** SUWA, K., Precambrian of African Continent—geology and mineral resources. *Jour. Afr. Studies,* **6,** 25-51.

1969 AOKI, H., Gravity measurements of Rift Valleys in Tanzania. *Jour. Earth Sci., Nagoya Univ.,* **17** (special volume), 169-188.
MATSUZAWA, I., Nagoya University African Rift Valley Expedition(NUARVE) in 1968. *ibid,* 1-10.
MATSUZAWA, I., Formation of the African great rift system. *ibid,* 11-70.
MIYAKAWA, K., SUWA, K., and SHIIDA, I., Metamorphic rocks of the North Pare Mountains, Tanzania. *ibid,* 97-106.
MIZUTANI, S. and YAIRI, K., Tectonic sketch of the Mbeya area, southern Tanzania. *ibid,* 107-124.
SUWA, K., OSAKI, S., OANA, S., SHIIDA, I., and MIYAKAWA, K., Isotope geochemistry and petrology of the Mbeya carbonatite, south-western Tanzania, East Africa. *ibid,* 125-168.
YAIRI, K. and MIZUTANI, S., Fault system of the Tanganyika Rift at the Kigoma area, western Tanzania. *ibid,* 71-96.

1970 * SUWA, K., Six months of geological studies in Africa during 1969-1970. *Gakujutsu-geppo(Monthly Rept. Sci. Research),* **23,** 46-55.

1971 * MATSUZAWA, I., On Africa. *Jour. Afr. Studies,* **11,** 1-8.
* MIYAKAWA, K., Recent trends of African studies in Japan—geology. *ibid,* 9-15.
* SUWA, K., Field studies in Africa—geological researches. *ibid,* 49-58.
* SUWA, K., Earth scientific characteristics of African Rift Valley. *World Geography Seminor,* **5,** 73-91. Daimyodo Pub. Co.

1972 * SUWA, K., African Rift Valley and volcanism. *Geography,* **17,** 7-14.
* SUWA, K. and YAIRI, K., African Rift Valley Research Expedition(2nd). *Gakujutsu-geppo(Monthly Rept. Sci. Research).,* **25,** 548-554.

1973 SUWA, K., OANA, S., WADA, H., and OSAKI, S., Isotope geochemistry and petrology of the African carbonatites. *1 st International Kimberlite Conference, extended abstract,* 297-300.
SUWA, K., YUSA, Y., and KISHIDA, N., Petrology of peridotite nodules from Ndonyuo Olnchoro, Samburu district, central Kenya. *ibid,* 301-304.

1974 ** ADACHI, M., The Mesozoic group near Mombasa, Kenya. *Jour. Afr. Studies,* **14,** 14-20.
* SHIOZAKI, H., Mineral resources of Africa (I). *Nagoya Jour. Geol.,* **30,** 2-10.
** SHIOZAKI, H., Mineral resources and mining affairs of East Africa. *Jour. Afr. Studies,* **14,** 73-81.
** YAIRI, K., En echelon pattern of the East African Rift System. *Jour. Afr. Studies,* **14,** 21-46.

1975 SUWA, K., OANA, S., WADA, H., and OSAKI, S., Isotope geochemistry and petrology of African carbonatites. *Phys. Chem. Earth,* **9,** 735-746(Pergamon Press).

SUWA, K., YUSA, Y., and KISHIDA, N., Petrology of peridotite nodules from Ndonyuo Olnchoro, Samburu district, central Kenya. *ibid,* 273-286(Pergamon Press).

ADACHI, M. and YAIRI, K., Sedimentological notes on the Bukoban orthoquartzite (late Precambrian) around Kisii, Kenya. *1st Prelim. Rep. Afr. Studies, Nagoya Univ.,* 3-5.

ADACHI, M., Sole markings from the Mazeras sandstones (upper Triassic),northwest of Mombasa, Kenya. *ibid,* 17-20.

ADACHI, M. and YAIRI, K., Preliminary report on the carbonatitic clasts in Tertiary sediments from the eastern Kavirondo Rift Valley, Kenya. *ibid,* 26-28.

BIYAJIMA, K., SUWA, K., and MIYAKAWA, K., Mantled gneiss dome in the Mozambique belt around Machakos area, Kenya. *ibid,* 6-13.

KAGAMI, H., Maragori granite in Tanganyika craton. *ibid,* 14-16.

KAGAMI, H., ADACHI, M., YAIRI, K. and MATSUZAWA, I., The rocks constituting the Mozambique belt in the northeast district of Lake Victoria. *ibid,* 6-13.

MIYAKAWA, K. and SUWA, K., An occurrence of staurolite from the Kioo pegmatite, Machakos District, Kenya. *ibid,* 52-54.

SHIBATA, K., Preliminary geochronological study on metamorphic rocks from Taita Hills, southern Kenya. *ibid,* 72-75.

SHIOZAKI, H., Fuchsite from Kibingi, Kenya. *ibid,* 70-71.

SUWA, K., Plagioclases in anorthosites. *ibid,* 55-59.

SUWA, K. and AOKI, K., Reverse pleochroism of phlogopites in kimberlites and their related rocks from South Africa. *ibid,* 60-64.

SUWA, K., YUSA, Y. and KISHIDA, N., Petrology of peridotite nodules from Ndonyuo Olnchoro, Samburu District, central Kenya (abstract). *ibid,* 65-59.

SUWA, K., OANA, S., WADA, H. and OSAKI, S., Isotope geochemistry and petrology of African carbonatites (abstract). *ibid,* 81-84.

UEDA, Y., MATSUZAWA, I. and SUWA, K., Potassium-argon age determinations on the Tanzanian igneous and metamorphic rocks. *ibid,* 76-80.

YAIRI, K., Geometry and mechanics of en echelon faulting with applications to the East African Rift System. *ibid,* 29-38.

YAIRI, K., Fault pattern and crustal extension of the Kavirondo Rift Valley in relation to a bifurcating rift model. *ibid,* 39-43.

YAIRI, K. and KATO, Y., Throw variation of normal faults arranged en echelon. *ibid,* 44-51.

1976 GOTO, T., OHNO, I. and SUMINO, Y., The determination of the elastic constants of natural almandine-pyrope garnet by rectangular parallelepiped resonance method. *Jour. Phys. Earth,* **24,** 149-156.

OHNO, I., Free vibration of a rectangular parallelepiped crystal and its application to determination of elastic constants of orthorhombic crystals. *Jour. Phys. Earth,* **24,** 355-379.

* SUWA, K., Anorthosites and their plagioclases. *Jap. Assoc. Mineral. Petrol. Econ. Geol., Spec. Paper* No.**1**(Progress in Research on Rock Forming Minerals), 215-242.

SUWA, K., Precambrian anorthosites and their plagioclases. *25th Intern. Geol. Cong., Abstract,* Vol.**1,** 21.

* In Japanese

** In Japanese with English abstract